

The fear of the Lord is the beginning of wisdom.

- *Proverbs 1:7*

University of Alberta

Subsurface Behavior of Spilled Fuel in a Permafrost Environment

by

Olumide Iwakun

A thesis submitted to the Faculty of Graduate Studies and Research
in partial fulfillment of the requirements for the degree of

Doctor of Philosophy

in

Geoenvironmental Engineering

Department of Civil and Environmental Engineering

©Olumide Iwakun

Fall 2010

Edmonton, Alberta

Permission is hereby granted to the University of Alberta Libraries to reproduce single copies of this thesis and to lend or sell such copies for private, scholarly or scientific research purposes only.

Where the thesis is converted to, or otherwise made available in digital form, the University of Alberta will advise potential users of the thesis of these terms.

The author reserves all other publication and other rights in association with the copyright in the thesis and, except as herein before provided, neither the thesis nor any substantial portion thereof may be printed or otherwise reproduced in any material form whatsoever without the author's prior written permission.



UNIVERSITY OF
ALBERTA

FACULTY OF GRADUATE STUDIES AND RESEARCH

KILLAM CENTRE FOR ADVANCED STUDIES

2-29 TRIFFO HALL

University of Alberta Library Release

Name of Author: Olumide Iwakun

UofA ID Number: 1068133

Title of Thesis: Subsurface Behavior of Spilled Fuel in a Permafrost Environment

Degree: Doctor of Philosophy

Year Degree Granted: 2010

Permission is hereby granted to the University of Alberta Library to reproduce single copies of this thesis and to lend or sell such copies for private, scholarly or scientific research purposes only. Where the thesis is converted to, or otherwise made available in digital form, the University of Alberta will advise potential users of the thesis of these terms.

The author reserves all other publication and other rights in association with the copyright in the thesis and, except as herein before provided, neither the thesis nor any substantial portion thereof may be printed or otherwise reproduced in any material form whatsoever without the author's prior written permission.

Signature

Date

Personal information on this form is collected under the authority of Section 33(c) of Alberta's **Freedom of Information and Protection of Privacy Act** for authorized purposes including admission and registration; administration of records, scholarships and awards, student services; and university planning and research. Students' personal information may be disclosed to academic and administrative units according to university policy, federal and provincial reporting requirements, data sharing agreements with student governance associations, and to contracted or public health care providers as required. For details on the use and disclosure of this information call the Faculty of Graduate Studies and Research at 492-3499 or see www.ualberta.ca/FOIPP.

05/14/09

EXAMINING COMMITTEE

Dr. Carl Mendoza, Department of Earth and Atmospheric Sciences,
University of Alberta

Dr. David Barnes, Department of Civil and Environmental Engineering,
University of Alaska

Dr. David Sego, Department of Civil and Environmental Engineering,
University of Alberta

Dr. Derek Martin, Department of Civil and Environmental Engineering,
University of Alberta

Dr. Kevin Biggar, Department of Civil and Environmental Engineering,
University of Alberta

Dr. Selma Guigard, Department of Civil and Environmental Engineering,
University of Alberta

DEDICATION

I dedicate this thesis to my mother, Mrs. M. O. Iwakun, and the memory of my late father, Chief K. Iwakun.

ABSTRACT

This dissertation focuses on the subsurface behavior of spilled fuel consisting of diesel and gasoline, which are subsets of light nonaqueous phase liquids (LNAPLs), in a permafrost environment. Particular emphasis is laid on mobile LNAPL in fractured bedrock. The site chosen for this study is the abandoned Colomac gold mine, 220 kilometers northwest of Yellowknife in the Northwest Territories, where over 50,000 liters of spilled fuel occurred between 1990 and 2003. The site is underlain by fractured bedrock with 0 to 4.6 m of overburden soil. The broad objectives of this work involve determination of contamination extent and LNAPL behavior at the site. Other specific objectives include determination of the major geochemical processes and identification of mechanisms influencing LNAPL movement and accumulation at the site.

Both field and laboratory studies were performed to achieve the above-stated objectives. The field study involved site characterization, and the laboratory study involved a top-down freezing experiment using a freezing cell, consisting of parallel glass plates, to evaluate the impact of cyclic freeze-thaw on LNAPL movement. The site characterization efforts showed that the LNAPL contamination is limited to the upper section (~7 m) of the fractured bedrock. The field study showed that water table fluctuations and freezing-induced displacements were active but discontinuous mechanisms contributing to LNAPL migration and accumulation in the formation and monitoring wells at the site.

Analyses of the groundwater suggested ongoing anaerobic biodegradation of the dissolved LNAPL components. Furthermore, the analyses showed that the water was Ca-SO₄ type and the main geochemical processes were gypsum dissolution and carbonate weathering. The analyses underscored the importance of bedrock mineralogical composition on groundwater constituents and geochemical processes.

The laboratory test results involving entrapment of diesel fuel below the water column and admixture of soluble oils with water in the freezing cell showed upward mobility of LNAPL under cyclic freezing, and downward progressive expulsion of the soluble oils ahead of the advancing freezing front. The results corroborated literature findings on cryogenic expulsion ahead of freezing front, and provided new insight into the behavior of trapped LNAPL below the water table when subjected to cyclic freezing.

ACKNOWLEDGEMENTS

Natural Sciences and Engineering Research Council (NSERC) of Canada, the Program for Energy Research and Development (PERD), Indian and Northern Affairs Canada (INAC), and Environment Canada provided funding for this study. I am grateful to my supervisors, Dr. Kevin Biggar and Professor David Segó, for their guidance and support towards the completion of this study. They are the giants whose shoulders I stood throughout the course of my program. Field assistance provided by John Voralek, Dale Van Stempvoort, and Greg Bickerton of Environment Canada is greatly appreciated. I valued the logistic aid provided by Ron Breadmore of INAC in working at the Colomac mine site. Steve Gamble, Christine Hereygers, Jela Burkus, and Todd Carter at the University of Alberta provided invaluable laboratory assistance.

I appreciate the enabling environment provided by my fellow students and the entire staff of the Department of Civil and Environmental Engineering at the University of Alberta. Administrative support by Ms. Sally Petaske, Anita Mueller, Anne Jones and Lorraine Grahn are treasured. I am thankful to Professor Gerhard Reuter with his family for his assistance and guidance throughout the course of my program.

Furthermore, I give the outermost thanks to GOD, the grand creator of heaven and earth for keeping me from my mother's womb until this present moment. I thank my mother, Mrs. M.O. Iwakun, for her unwavering support, love, and prayers. Daddy, I wish you are around but GOD knows best. Thank you. I am grateful to my Sisters, "Mosunmola, Dr. Omotebi and Ebunola" with her husband Segun Ogungbesan, for their encouragement, sacrifice and support. My sincere gratitude also goes to my Aunt, Dr. Funmi Omotayo with her family for her benevolence, advice, and encouragement.

TABLE OF CONTENTS

EXAMINING COMMITTEE

DEDICATION

ABSTRACT

ACKNOWLEDGEMENTS

TABLE OF CONTENTS

LIST OF TABLES

LIST OF FIGURES

LIST OF ACRONYMS

DEFINITION OF TERMS

1	INTRODUCTION	1
1.1	Background	1
1.2	Site History	10
1.3	Research Objectives.....	12
1.4	Scope of Work	13
1.5	Organization of Dissertation.....	13
	References.....	17
2	FUEL CONTAMINANT CHARACTERIZATION IN A PERMAFROST FRACTURED BEDROCK AT THE COLOMAC MINE SITE	25
2.1	Introduction	25
2.2	Field Activities.....	28
2.3	Results and Discussion.....	31
	2.3.1 <i>Manual monitoring of water levels</i>	31
	2.3.2 <i>Manual monitoring of depth to ice</i>	31
	2.3.3 <i>Measured ground temperatures</i>	34
	2.3.4 <i>Hydraulic testing of fractured bedrock</i>	36
	2.3.5 <i>LNAPL monitoring in wells</i>	36
	2.3.6 <i>Groundwater chemistry</i>	38
2.4	Conclusions	40
	References.....	57
3	BEHAVIOR OF SPILLED PETROLEUM HYDROCARBONS AT THE COLOMAC MINE SITE, NWT	59
3.1	Introduction	59
3.2	Field Work	62
3.3	Product Recovery Method	65
3.4	Temperature Monitoring	66
3.5	Results and Discussion.....	67
	3.5.1 <i>LNAPL monitoring in wells</i>	67
	3.5.2 <i>Temperature profile</i>	68
	3.5.3 <i>Free product recovery</i>	70
	3.5.4 <i>LNAPL mobilization mechanisms</i>	71
	3.5.5 <i>Conceptual model of LNAPL movement</i>	74
3.6	Conclusions	78
	References.....	96

4	ESTIMATION OF ACTUAL LNAPL THICKNESS IN A FUEL CONTAMINATED ARCTIC MINE SITE.....	99
4.1	Introduction	99
4.2	Fieldwork	103
4.3	Methodology	106
4.4	Results and Discussion.....	108
4.5	Conclusions	111
	References.....	123
5	GROUNDWATER GEOCHEMICAL CHARACTERIZATION AT THE COLOMAC MINE SITE.....	127
5.1	Introduction	127
5.2	Site description.....	127
5.3	Methodology	128
5.4	Results and Discussion.....	132
5.5	Conclusions	140
	References.....	158
6	INFLUENCE OF CYCLIC FREEZING ON THE MOBILIZATION OF LNAPL AND SOLUBLE OIL IN A POROUS MEDIA	160
6.1	Introduction	160
6.2	Methodology	164
6.2.1	<i>Freezing cell</i>	164
6.2.2	<i>Setup</i>	165
6.2.3	<i>Cell-infilling</i>	165
6.2.4	<i>Cell-placement</i>	166
6.2.5	<i>Testing</i>	167
6.2.6	<i>Test series</i>	167
6.3	Results and Discussion.....	168
6.4	Conclusions	175
	References.....	186
7	SUMMARY CONCLUSIONS AND RECOMMENDATIONS	190
7.1	Summary Conclusions	190
7.1.1	<i>Contributions</i>	193
7.1.2	<i>Project limitations</i>	194
7.2	Recommendations.....	194
7.2.1	<i>Remediation</i>	194
7.2.2	<i>Natural attenuation</i>	196
7.2.3	<i>Further assessments</i>	197
7.2.4	<i>Future directions</i>	197
	References.....	198
	APPENDIX A: PACKER TEST PROCEDURE AND SAMPLE DATA.....	200
	APPENDIX B: ELEVATION DATA AND SAMPLE CALCULATION FOR WATER TABLE CORRECTION	215
	APPENDIX C: UPDATED THERMISTOR PROFILE ACROSS THE SITE	228
	APPENDIX D: MEASURED GROUNDWATER CONSTITUENTS.....	240
	APPENDIX E: SELECTED IMAGES OF THE BEDROCK CORES AND WELL-BORE IMAGES	271
	APPENDIX F: SAMPLE CALCULATIONS AND PHREEQC DATA FILES	283
	APPENDIX G: SAMPLE IMAGES FROM LABORATORY TESTS	295

APPENDIX H: LNAPL RECOVERY IN PERMAFROST FRACTURED BEDROCK AT THE COLOMAC MINE SITE, NWT	303
---	------------

LIST OF TABLES

Table 2.1 Apparent free product thickness in wells during 2005/06 study	42
Table 2.2 Readings from flow through cell 23/24 August 2005	42
Table 3.1 Measured apparent LNAPL thickness in monitoring wells for 2005/06 study. The blank cells indicate no measurable product or inaccessible well.....	80
Table 3.2 Summary of product recovery data in June 2006.	81
Table 3.3 Summary of the thermal regime at the Colomac mine site.	81
Table 4.1 Drill log for selected monitoring wells (MWs).....	112
Table 4.2 Apparent LNAPL thickness of selected monitoring wells from 2005 to 2007.	112
Table 4.3 Data obtained using the method described by Hughes et al. (1988).....	113
Table 5.1 Summary of parameters used for the inverse modeling.....	142
Table 6.1 Characteristics of the fuel and soluble oil used for the experiment.....	177

LIST OF FIGURES

Figure 1.1 Conceptual model for the transport of light nonaqueous phase liquid (LNAPL) in fractured media. Time t_1 represents the initial time of LNAPL release corresponding to time of elevated water table for this scenario. Time t_2 represents the time of lowered water table, and time t_3 represents the time when the water table rebounded to initial level at t_1	15
Figure 1.2 Conceptual model of DNAPL transport in fractured media.	15
Figure 1.3 Layout of the mine site before demolition of the structures.	16
Figure 1.4 A site map of Colomac mine, reduced to show details of site investigation. The map shows the spatial locations of the installed monitoring wells, thermistor boreholes, and some of the initial measures taken to mitigate the movement of free product to Steeves Lake before commencement of this study in 2005 (Iwakun and Biggar, 2008).	16
Figure 1.5 A site model showing the approximate location, volume, and date of historical spillage at the site. Most spills at the site were Arctic diesel but not all were accounted for (modified after EBA, 2001).	17
Figure 2.1 Map showing location of Colomac mine site, 220 km northwest of Yellowknife in the Northwest Territories (modified after Smith and Burgess, 2001).	43
Figure 2.2 North to south trending bedrock outcrop with 3 main sets of fractures: (1) sub vertical fractures, parallel to foliation that includes “slaty cleavage” – includes most of the exposed surfaces shown in this picture; (2) sub-horizontal fractures; (3) sub-vertical fractures that are approximately perpendicular to 1&2.	44
Figure 2.3 Simplified site model showing the approximate locations of historical fuel spillage (modified after EBA, 2001).	44
Figure 2.4 Site map showing spatial location of the monitoring wells and thermistor-boreholes.	45
Figure 2.5 Ground elevation contour before overburden removal at the tank farm area.	45
Figure 2.6 Inferred groundwater contours for August 17, 2005.	46
Figure 2.7 Water table and well bottom elevations for (a) monitoring wells farthest upslope and (b) wells at mid-slope.	47
Figure 2.8 Water table and well bottom elevations for (a) monitoring wells near the edge of Steeves Lake, and (b) wells near warehouse.	48
Figure 2.9 Conceptual model of hydrogeological settings at the Colomac mine site to illustrate well-water behavior discussed in Figure 2.10.	49

Figure 2.10 Summary of the behavior of water within the monitoring wells at the Colomac mine site.	50
Figure 2.11 Temperature versus time and depth from thermistors (a) from well 22 (adjacent to warehouse), December 05 to June 06, and (b) adjacent to well 29 (along lakeshoreline to north), April to December, 2006.	51
Figure 2.12 Temperature versus time and depth from thermistor adjacent to well 31 (along lakeshoreline to south), April to December 2006.	52
Figure 2.13 Transmissivity calculated from packer tests for wells around warehouse. (Values reported as 1.0 E-09 are transmissivities that were too low to measure with the apparatus used).	52
Figure 2.14 Measured LNAPL thicknesses (in meters) for August 06, 2006.	53
Figure 2.15 Results of analyses of LNAPL from different wells around the tank farm and warehouse.	53
Figure 2.16 Isopleths of dissolved F1 fraction (in mg/L) for August 2005.	54
Figure 2.17 Isopleths of measured sulfate concentration (in mg/L) for August 2005.	54
Figure 2.18 Inorganic groundwater concentrations in MW 14 during the summer of 2005: (a) Ions less than 25 mg/L; (b) Major ions greater than 25 mg/L.	55
Figure 2.19 Isopleths of dissolved iron concentrations (in mg/L) for August 2005.	56
Figure 2.20 Interpreted isopleths for distribution of total volatile fatty acids (acetate + propionate + butyrate + pyruvate in mg/L) detected in monitoring wells in August 2005.	56
Figure 3.1 Location of Colomac mine site, 220 km northwest of Yellowknife, NWT.	82
Figure 3.2 Simplified site-map showing the historical spilled fuel at Colomac mine.	82
Figure 3.3 Simplified site-map showing spatial location of the monitoring wells and the thermistor – boreholes.	83
Figure 3.4 Groundwater contour inferred for August 6, 2006. The bull-eye seen around MW 26 may be associated with inadequate data to bound the measured groundwater elevation at that time.	84
Figure 3.5 Samples of borehole images for monitoring wells 4, 11, 27, and 30. More fractures were observed in the upper section of the bedrock than at depth. Not all the monitoring wells contained water all year round (e.g., MWs 11 and 27). MW 11 had free product sitting atop ice in early spring, while MW 27 seem not to intersect water-bearing fractures. Nevertheless, they all had measurable amount of free product.	85
Figure 3.6 Summary of product recovery test procedure and later activities aimed at evaluating the need for product recovery system at the site.	86

Figure 3.7 Hypothetical results for the product recovery test (modified after Testa and Winegardner, 2000). The point of inflection (p) corresponds to the LNAPL entry point, and its vertical distance to the constant LNAPL depth is used to estimate formation LNAPL thickness.....	87
Figure 3.8 Measured apparent LNAPL thickness for August 06, 2006.	87
Figure 3.9 Well-probe data for monitoring wells (MWs) 17 and 26 at the site.	88
Figure 3.10 Well-probe data for monitoring well (MW) 12 at the site.	89
Figure 3.11 Temperature profile with (a) time and (b) depth in one of the dedicated thermistor strings “T10” adjacent to MW 12.....	90
Figure 3.12 Graphical representation of data from the product recovery test for MW 26 in June 2006.....	91
Figure 3.13 Graphical representation of data from the product recovery test for MW 12 in December 2006.....	91
Figure 3.14 Conceptual fracture pattern at the site showing: (a) bedrock elevation with the inferred fracture pattern based on site characterization efforts, and (b) conceptual subsurface fracture distribution at the site.	92
Figure 3.15 Conceptual surficial model at the Colomac mine site, highlighting the importance of fracture network and distribution on the movement of the spilled fuel.	93
Figure 3.16 Conceptual model of LNAPL movement during (a) the winter period after fresh spill when the water table is low, and (b) in the spring/summer when the spill source is removed or contained and the water table is elevated.....	94
Figure 3.17 Summary of subsurface behavior of LNAPL in porous media including fractured bedrock.....	95
Figure 4.1 Fuel spill history at Colomac mine site. Shown on the map are the quantity spilled (when known), the location, and the date of spillage.	114
Figure 4.2 Site layout showing the relative location of the installed monitoring wells (MWs).....	115
Figure 4.3 Transmissivity distribution at the site showing that the upper sections of the bedrock are more transmissive and that the mean transmissivity may be less than 10-9 m ² /s assigned to test sections that were too tight to test due to equipment limitations.....	115
Figure 4.4 Core samples retrieved from one of the newly installed MWs (MW 38) at the site. The cores shown above are from the upper 4 m of the bedrock. The fracture pattern ranged from vertical to horizontal. The upper section of the bedrock is highly fractured with a rock quality designation (RQD) of less than 50% in many cases.	116

Figure 4.5 Illustration of actual LNAPL thickness in the formation as often construed in the literature (modified after Weiner, 2000).....	116
Figure 4.6 Sample of graphical results using Yaniga's method to estimate actual LNAPL thickness in the formation (modified after Hampton et al., 1990).	117
Figure 4.7 Sample of graphical results using Gruszczenski's method to estimate actual LNAPL thickness in the formation (modified after Gruszczenski, 1987).....	117
Figure 4.8 Sample of graphical results using Hughes et al. (1988) method to estimate actual LNAPL thickness in the formation (modified after Hughes et al., 1988).	118
Figure 4.9 Sample of borehole image snapshots from Well-Vu camera. Characteristically stained sections of the MW are rife in the upper section of the bedrock. The image shown above is for MW 26. Accumulated LNAPL in the MW came from the contaminated upper section (~ 7 m) of the bedrock.	118
Figure 4.10 Rose diagram summarizing the azimuths and inclinations of fractures from bedrock core samples at the Colomac mine site. The azimuths are inferred from bedrock outcrops.....	119
Figure 4.11 Stereonet the bedrock fractures. The data point density contour shows that the fractures are generally sub-vertical and sub-horizontal, and oriented northwest.....	119
Figure 4.12 Sample of graphical results using modified Gruszczenski method.....	120
Figure 4.13 Conceptual geological section of subsurface contamination at the Colomac mine site.	120
Figure 4.14 Analysis of product thickness estimation in MW 12.	121
Figure 4.15 Analysis of product thickness estimation in MW 26.	121
Figure 4.16 Analysis of product thickness estimation in MW 30.	122
Figure 4.17 Analysis of product thickness estimation in MW 17.	122
Figure 4.18 Monthly average temperature profile for thermistor probe near MW 9 at the warehouse area.....	123
Figure 5.1 Spill history at the abandoned Colomac mine site showing the quantity spilled, relative locations and spill date.	143
Figure 5.2 Site layout showing the relative locations of the installed monitoring wells (MWs) and thermistor strings with some implemented remedial strategy at the Colomac mine site.	143
Figure 5.3 Piper plot interpretation summary (modified after Hounslow, 1995).....	144
Figure 5.4 Piper plot of major ions in selected MWs at the Colomac mine site.	145
Figure 5.5 The A part shows the Stiff diagram of selected MW samples for June 2007; the polygon shapes are similar for most of the MWs, implying common groundwater	

source. B shows the ratios of bicarbonate to silica in most monitoring wells at the site.....	146
Figure 5.6 Subdivisions of the site based on pre-existing facilities before demolition. The general groundwater flow at the site is northwest.....	147
Figure 5.7 Kruskal-Wallis non-parametric test results for (A) Total Dissolved Solids (TDS) and (B) total measured alkalinity at the site.	148
Figure 5.8 Kruskal-Wallis non-parametric test results for (A) sulfate and (B) dissolved iron concentrations at the site.....	149
Figure 5.9 Trends of selected ions in MW 4 and MW 15 at the Tank farm and Steeves Lake areas respectively.	150
Figure 5.10 The thermal profile from thermistor strings nearest the MWS. T09 is near MW04 and T02 is adjacent to MW 15.	151
Figure 5.11 Summary of saturation indexes for major mineral phases at the site (A), and the sulfate concentration profile with depth (B).	152
Figure 5.12 Summary of inverse model analyses using PHREEQC. A-C-E are models without dissolvable oxygen phase, while models B-D-F are those with dissolvable oxygen phase. Mineral phases for each model are summarized in Table 5.1.	153
Figure 5.13 Summary of (A) BTEX and (B) benzene concentrations at the site. The benzene concentrations are generally above the CCME limits except the powerhouse area.	154
Figure 5.14 Summary of (A) Ethylbenzene and (B) Toluene concentrations at the site.	155
Figure 5.15 Selected dissolved metal concentrations at the site. Apart from aluminum, nickel, and iron, most of the dissolved metals have concentrations that are generally less than CCME guideline values with some few outliers.	156
Figure 5.16 Summary of Kruskal-Wallis test results for (A) aluminum, and (B) nickel: The site has high background aluminum concentration and there is no statistical difference in the means of its values. However, nickel has significant concentrations above the background and requires further investigation.	157
Figure 6.1 Fabricated freezing cell used for the experiment.....	177
Figure 6.2 Setup of the laboratory system showing (a) freezing cell placement in the environmental chamber, and (b) schematic layout of the setup.	178
Figure 6.3 Thermal propagation for the control experiment, (a) Snapshots of freezing progression in the cell; (b) temperature profile.....	179
Figure 6.4 Comparison of laboratory and field thermal profile: (a) Frost penetration profile for the control experiment, and (b) sample of temperature profile in MW 15 at the Colomac mine site.	180

Figure 6.5 Freezing-test results using diesel subjected to freeze-thaw cycles. (a) Temperature profile; (b) profile for thermal propagation rates.....	181
Figure 6.6 Frost penetration profile for freezing test with diesel (Figure 5): (a) Snapshots of upward displacement of diesel at the start of freezing and after thawing; (b) Plots of cumulative LNAPL displacement and frost penetration for each freeze-thaw cycle.	182
Figure 6.7 Illustration of freezing induced displacement that takes place during water nucleation process as ice is formed. For LNAPL-water system, suction induced during the phase change of water causes upward mobilization of entrapped LNAPL below the water table. For dissolved organics, the nucleation process causes forward exclusion of the organics from freezing water ahead of freezing front. ..	183
Figure 6.8 Profile of thermal propagation for freezing test using Mobilcut-102 soluble oil: (a) Snapshots of the observed progressive cryogenic expulsion; (b) temperature profile for the test.....	184
Figure 6.9 Condensed plot of freezing test using Mobilcut-102 soluble oil, showing the freezing and exclusion fronts, thermal propagation rates and the thermal gradient.	185
Figure 6.10 Snapshots of the observed micro-fissures in freezing test from a freezing cell under prolonged freezing with fluorescein-water only.....	186

LIST OF ACRONYMS

BE	Bedrock Elevation
BTEX	Benzene, Toluene, Ethylbenzene, Xylene
CCME	Canadian Council of Ministers of the Environment
CSO	Contaminated Site Office
DNAPL	Dense Nonaqueous Phase Liquid
DO	Dissolved Oxygen
DTP	Depth to Product
DTW	Depth to Water
EPA	Environmental Protection Agency
EPM	Equivalent Porous Media
FO	Faint Odor
GCFID	Gas Chromatography with Flame Ionization Detector
GE	Ground Elevation
GWE	Groundwater Elevation
IC	Ion Chromatography
ICPMS	Inductively Coupled Plasma Mass Spectroscopy
ILSB	Indin Lake Supracrustal Belt
INAC	Indian and Northern Affairs Canada
L	Liters
LNAPL	Light Nonaqueous Phase Liquid
MW	Monitoring Well
NAPL	Nonaqueous Phase Liquid
NWT	Northwest Territories
ORP	Oxydation Reduction Potential
PHC	Petroleum Hydrocarbon
PT	Product Thickness
RTD	Resistance Temperature Detector
TDS	Total Disolved Solids
TEA	Terminal Electron Acceptor
VFA	Volatile Fatty Acids
WT	Water Table

DEFINITION OF TERMS

Capillary Fringe: - Saturated zone above the water table where the water is held by capillary action. Its thickness may be less than the total capillary rise due to heterogeneity of the porous media.

Desorption: - This is the release of a sorbed substance from a solid back into the surrounding liquid or gas in the porous media. It is the reverse of adsorption.

Formation: - In this study, formation refers to in situ geologic material, which includes soil, bedrock, and fill soil.

Fracture Intensity: - Number of fractures per unit length along a bedrock feature or sample line.

Free phase product: - This denotes separate phase LNAPL consisting of diesel and/or gasoline in this study. The term is used interchangeably with free product, product, and loosely as mobile LNAPL. Within the monitoring well, it is commonly referred to as LNAPL. In general, free phase product means separate phase material with saturations above the residual saturation points or levels of a contaminant. By this definition, free product can be mobile or trapped within the formation.

Ground Ice: - Ice formed below 0°C in the formation, which may occur as structured ice or unstructured large bodies of ice. Structured ice includes segregated ice, reticulate ice, inclusions of ice crystals, and intrusive ice. Unstructured ice includes ice wedges, ice beds, and pingo cores.

Hardening Temperature: - This is defined as the lowest limiting temperature of a material below which it hardens and ceases to pour. The term is synonymous with pour point and used interchangeably as such in this study.

Light Nonaqueous Phase Liquid (LNAPL): - Petroleum hydrocarbons (PHCs) that are mostly immiscible with water with specific gravity (S.G.) below that of water (e.g., 1) at ambient temperature. LNAPL exists in two forms as mobile and immobile phases.

Mobile LNAPL: - This denotes a continuous free phase product that can flow under a hydraulic gradient. Furthermore, due to seasonal, temporal, and spatial fluctuations of residual saturation of LNAPL in the formation, mobile LNAPL at one location may switch to residual LNAPL at the same location but different time.

Permafrost: - A ground or formation that remains at or below 0°C for two or more consecutive years. The ground or formation may consist of soil, rock, ice, or organic material. Permafrost is subdivided based on percent coverage of the underlying land area into continuous (90 - 100%), discontinuous (50 - 90%), sporadic permafrost (10 - 50%), and isolated patches (<10%).

Residual Phase Product: - This denotes a separate phase material (i.e., LNAPL) in the formation with saturations below a contaminant residual saturation point. This term is used interchangeably with residual product, and residual LNAPL. Residual product may be bonded with the porous media and held by capillary suction.

Residual Saturation: - The limiting saturation point, below which a fluid becomes discontinuous and immobilized by capillary suction. Thus, the fluid will not drain by gravity. The fluid may be air, water, or nonaqueous phase liquid (NAPL).

Retention Capacity: The amount of fluid a porous media can retain, in which fluid drainage by gravity will not occur. It is often measured in terms of volumetric fluid content in the porous media. This term is used interchangeably with residual saturation in this study.

Rock Quality Designation (RQD): - Sum of core pieces greater than 4 inches divided by the total length of core.

Talik: - Unfrozen zone beneath permafrost.

1 INTRODUCTION

1.1 Background

The demand for petroleum is increasing due to industrialization and urbanization. Transportation and storage of this fuel have led to higher incidence of spillage, with deleterious effects on the environment and living organisms. Existing legislation on fuel spillage requires the determination of the extent of contamination, risk assessment, and remediation to site-specific cleanup goals. Key to these requirements is site characterization to determine the extent, fate, and behavior of the spilled fuel in the environment. There are different types of petroleum hydrocarbons broadly categorized based on their density behavior with respect to water into light and dense nonaqueous phase liquids (i.e., LNAPLs and DNAPLs). Much literature exists on the subsurface behavior of LNAPL and DNAPL for porous media in temperate and warmer temperate (or tropical) regions. However, there is limited understanding of their subsurface behavior in colder temperate regions that overlap with permafrost environments. Thus, this study will focus on subsurface behavior and remediation of spilled fuel in a permafrost environment with particular emphasis on LNAPL in fractured bedrock.

Several studies have focused on the behavior of spilled fuel in permafrost environments. Biggar et al. (1998) showed that permafrost might not be an effective barrier to migration of petroleum hydrocarbons (PHCs), and corroborated by the findings of Chuvilin et al. (2001a), and McCarthy et al. (2004). Studies on the impacts of freezing and frozen environments on dissolved and free phase PHC in soils have proposed different mechanisms influencing the migration of PHC. These include the exclusion of solutes as water freezes, gravity drainage, capillary suction, advection, hydrodynamic dispersion (i.e., dispersion and diffusion), and surface forces of the mineral skeleton (Konrad and Seto, 1991; Biggar et

al., 1998; Chuvilin et al., 2001a; Barnes and Chuvilin, 2009). As water freezes, rearrangement of the molecular structure from trigonal to hexagonal form during nucleation causes volume expansion of the ice. Accompanied with the nucleation process is the rejection and concentration of solutes in the unfrozen water, which is termed solute exclusion. Given that solute exclusion can occur in the absence of freezing (Beier et al., 2007), the term “cryogenic expulsion” is adopted in this study as coined by Barnes and Chuvilin (2009) because it properly describes solute rejection and concentration below 0°C during freezing. Laboratory studies on freezing soils demonstrated that the established concept of cryogenic expulsion for dissolved ions as water freezes might be applicable for dissolved PHCs (Konrad and Seto, 1991; Tumeo and Davidson, 1993; Chuvilin et al., 2001a and 2001b; Barnes et al., 2004). Field studies by Motenko et al. (2003) corroborated such conclusion, but that of Overduin (1998) did not observe dissolved PHC exclusion. Cryogenic expulsion is dependent on freezing rate, initial solution concentration, types of solute, mineral surface, and crystallographic orientation of ground ice (Konrad and Seto, 1991; Overduin, 1998). Barnes et al (2004) suggested physical displacement of free product from pore spaces in addition to cryogenic expulsion as water expands during freezing. The equilibrium concentration of solutes in water depends on the solutes’ solubility, fractional composition in a mixture of substances, temperature, and geochemistry of the water (i.e., phase equilibrium). Thus, secondary to cryogenic expulsion, “cryogenic chemical deposition” defined as precipitation of a solute (or dissolved substance) out of solution when its concentration is above its equilibrium concentration or solubility limit (Cailleux, 1964) may occur.

Biggar and Neufeld (1996) suggested capillary movement of diesel due to the formation of micro channels in a column of soil subjected to cyclic freezing. Chuvilin et al. (2001a) showed that oil composition, soil temperature, and types of mineral surface affect the spreadability and

movement of oil in frozen ground. Of the surfaces tested, including sand, silt, clay, and ice, spilled fuel had the least spreadability in ice, due to the latter's high oil wetting angles, and most spreadability occurred in sand due to sand's low wetting angle. Weathering of spilled fuel coupled with decreasing temperatures leads to increase in its density and viscosity, thereby limiting spreadability (Wilson and Mackay, 1987; Mawhinney, 1979). Experiments conducted in salinized soil by Chuvilin and Miklyaeva (2003) showed decreased penetration in salinized frozen soil in comparison to un-salinized frozen soil due to decreased free porosity and formation of microcracks. They postulated that salinized frozen soils are less vulnerable to freezing embrittlement. Their results also suggested that capillary transfer through micropores and channels is the dominant mechanism of oil penetration in frozen soil.

In unsaturated frozen soil, there may be extensive lateral migration and deeper penetration along preferential flow paths depending on ice distribution in the formation (Barnes and Chuvilin, 2009). Networks of LNAPL saturated macropores in the formation in the active layer after thaw enhances lateral migration of mobile LNAPL (Dyke and Eggindon, 1990; Chamberlain et al., 1997). According to Barnes and Chuvilin (2009), both lateral and downward migration of LNAPL may be enhanced in the active layer subjected to freeze-thaw cycles.

Catalan and Dullien (1995) performed a laboratory experiments with sand of varying homogeneity and permeability and found that due to water table (WT) fluctuations, LNAPL trapping as isolated blobs below the groundwater may occur. Subsequent lowering of the WT may remobilize the isolated blobs on contact with the LNAPL layer above the WT. However, LNAPL films above the dewatered zone may flow by gravity drainage (though a very slow process) and accumulate atop the water table.

A laboratory investigation by Dobson et al. (2007) on the effect of water table fluctuation on PHC dissolution and biodegradation using

silica sand showed that water table fluctuations enhance biodegradation and dissolution of LNAPL components, increase LNAPL migration down-gradient and along the vertical extent, and cause entrapment of LNAPL below the water table. In fractured bedrock, the foliation and fissures control LNAPL migration from the source zone (McCrorry, 1997; David et al., 1999) rather than the groundwater flow direction. Inverse correlations were observed at contaminated sites between LNAPL thickness in a monitoring well and water table elevations (Iwakun et al., 2008b; Hostettler et al., 2000).

In an experiment, Lenhard et al. (1993) showed that entrapment of LNAPL below the water table is reproducible due to cyclic water table fluctuations. Aral and Liao (2002) developed a numerical model to evaluate the impacts of water table fluctuations on LNAPL thickness in monitoring wells, and used it to predict LNAPL response due to water table fluctuations in the field and the laboratory.

Field studies by Steffy et al. (1995) suggested that LNAPL in monitoring wells and in the formation might never be in equilibrium because of a time lag between LNAPL pore pressure increase and accumulation in the monitoring well. Thus, water table fluctuations will influence migration, distribution, and recovery of LNAPL in the formation. The areal flow model used by Parker et al. (1991) to simulate a site over a period of three years suggested that LNAPL recovery and spreading rates decreased with water table fluctuations, and that hydraulic gradient influences lateral spreading of LNAPL when in contact with the water table.

Figure 1.1 shows a conceptual model of LNAPL migration in a soil underlain by fractured bedrock. The conceptual model is for illustration purpose only. Coexisting with released LNAPL in the unsaturated zone are air and water. LNAPL is the wetting phase with respect to air in a system involving only air and LNAPL, but when water is involved, LNAPL is the non-wetting phase (Weiner, 2000). Above the capillary fringe,

water is at irreducible saturation and essentially immobile. Thus, in the unsaturated zone, LNAPL spill will displace the air in the soil matrix because it is preferentially wetting with respect to the air, penetrate smaller pores, and partition onto the soil. Upon release (at t_1), the LNAPL will tend to spread into smaller pores via capillary transfer in the unsaturated zone and drain from larger pores (Weiner, 2000). This accounts for why residual LNAPL saturations in fine-grained soils are greater than coarse-grained soils. The capillary transfer of the LNAPL into the soil also creates an inverted cone-shaped contamination zone. At depth, LNAPL will continue downward migration if residual saturation is exceeded at that location and mass loss due to capillary transfer and partitioning onto the environmental media is replenished from a continuous LNAPL source. The penetration rate of LNAPL is a function of media type and the nature of the LNAPL (Mercer and Cohen, 1990; Simantiraki et al., 2009). The penetration rate diminishes with decrease in soil grain size, aquifer permeability, and LNAPL density. Additionally, increase in LNAPL viscosity, interfacial tension, and partition coefficients in the porous media decrease the rate of LNAPL penetration. Heterogeneity of the porous media may also enhance lateral migration of the LNAPL (Newel et al., 1995; Barnes and Chuvilin, 2009). Downward migration of the LNAPL will continue if the LNAPL builds up enough pressure head to overcome the entry capillary pressure of the porous media at depth.

The pressure head build-up is mostly dependent on the connectivity of the LNAPL column with the source (Sharp, 2001). The LNAPL leaves behind residual saturation as it advances through the media. If the spilled amount is small (e.g., less than the retention capacity of the porous media between the release point and the leading edge of the LNAPL), it will partition into the soil and remain essentially immobile. For large spills of LNAPL, sufficient LNAPL pressure head build-up will enhance downward migration of the LNAPL. On reaching the capillary

fringe, the LNAPL will spread atop it and may skew in the direction of prevailing groundwater flow. Large accumulation of LNAPL atop the capillary fringe may collapse it and depress the water table until the LNAPL weight balances the upthrust and entry pressure of the pore matrix. Lateral migration of the LNAPL atop the water table will continue until it reaches residual saturation level. The saturation level reached is at quasi-steady state because it changes seasonally and is dependent on the wetting history of the porous media. Seasonal or anthropogenic lowering of the water table (at t_2) will enhance further downward migration. If sufficient LNAPL head is built to overcome the entry capillary pressure of the fractures, LNAPL will penetrate the fractures, and there may be lateral spreading of the LNAPL along the bedrock surface and within the interconnected fractures. In the course of vertical migration and lateral spreading, sorbing onto the soil matrix and fracture wall will occur for some of the LNAPL, and some may diffuse across the fracture wall, and partition into the water and air pockets in the formation.

Diffusion across the fracture wall and sorption into the soil matrix retards the LNAPL plume, but constitutes a major problem from a remediation perspective because of the time dependent desorption into the groundwater following source removal.

According to Farr et al. (1990), LNAPL will coexist with the formation fluid (i.e., water and air). Thus, at maximum saturation, irreducible saturation of other fluids may be present. However, the degree of saturation will be dependent on the site history, quantity of LNAPL released, properties of the media, and fluids present. Subsequent elevation of the water table (at t_3) will cause LNAPL remobilization and entrapment below the water table, and may enhance its lateral migration (Weiner, 2000).

Dense nonaqueous phase liquid (DNAPL) consists of heavy fuel oils, chlorinated hydrocarbons, and polyaromatic hydrocarbons. DNAPL is denser than water but has varying viscosity below and above one

centipoise (cp). Chlorinated DNAPLs often have viscosity in the range of 0.6 to 0.9 cp at room temperature; thus, have greater penetration when spilled in porous media due to low flow resistance. However, the DNAPLs with viscosity above 1 cp flow slowly through the media. DNAPLs have higher residual saturation in the saturated zone as opposed to LNAPLs whose residual saturation occurs in the unsaturated zone above the water table. Trapping of LNAPLs also occurs below the water table as discussed above. Figure 1.2 illustrates the conceptual model of DNAPL migration.

The migration mechanisms of DNAPL differ from that of LNAPL in that while LNAPL accumulates atop the water table when spilled in a sufficient amount to penetrate the unsaturated zone, DNAPL actually displaces water in the formation below the water table because of its greater density. DNAPL migrates to a greater depth, and is much less dependent on water table fluctuation. DNAPLs often penetrate through successive layers of aquifers and aquitards up to 1000 meters below the surface (Feenstra et al., 1996). Physical experiments of DNAPL migration through a partially saturated fracture by Schwille (1988) showed that fracture roughness causes more residual entrapment and pathway fingering (or channeling) of the DNAPL in comparison to its behavior in a smooth fracture wall. Numerical studies of DNAPL migration through a rough-walled fracture showed that the aperture size, matrix entry pressure or capillary pressure, and density of DNAPL controls its migration, as does the interconnectivity and nature of the fractures (Kueper and McWhorter, 1996; Esposito and Thompson, 1999; Slough et al., 1999; and Heise, 1999). Like most fluids, DNAPL follows the path of least resistance (i.e., zones with larger apertures, and dependent on the wettability of the aperture to DNAPL). Thus, subsurface DNAPL migration studies often use discrete flow models.

There are extensive reviews of groundwater flow and solute transport in fractured media in temperate and warmer temperate regions

(Bear et al., 1993; US NRC, 1996; Lapcevic et al., 1999; Berkowitz, 2002, and Neuman, 2005). Governing factors for groundwater flow in fractured bedrock are fracture density, orientation, effective aperture widths, interconnectivity of the fractures, and the nature of the bedrock material (Witherspoon et al., 1980; Lapcevic et al., 1999). Primary porosity is the void fraction in rock matrices and secondary porosity is that due to fracturing. It should be noted that porous media is any solid or semi-solid material that contains interconnected pores, voids, or openings, which can permit continuous flow of fluid. Thus, by definition, an interconnected fractured media may be classified as a porous medium when it permits continuous flow of fluid, and forms the basis of equivalent porous media (EPM) concept for fracture flow.

Types of flow models in fractured media include continuum, discrete, and dual porosity. Continuum models assume pertinence of EPM concept for flow through a system. The EPM concept assumes the properties of individual fractures are insignificant in comparison to large regions of the system, and continuum mechanics developed for porous media applies. Discrete fracture models assume that discrete fractures govern flow through the system, and that contributions from rock matrices are insignificant. In dual porosity models, discrete and rock matrix properties govern flow through a system. The choice of model used to develop a conceptual model of a site is dependent on fracture density, bedrock geology, and observed flow patterns in the field. Fate and transport mechanisms in fractured media include advection, dispersion, capillary suction, gravity drainage, diffusion into rock matrices, biological decay of dissolved constituents, and geochemical processes (Lapcevic et al., 1999). However, the main transport mechanisms are advection and diffusion. Geochemical processes include oxidation-reduction reactions, precipitation-dissolution, and adsorption-desorption. However, studies are lacking on the effects of freezing on these mechanisms in fractured media.

Panday (1990), and Zukowski and Tumeo (1991) developed numerical models for solute (dissolved PHC) transport in freezing and frozen soils. However, testing of the developed models has not been verified in the field. In fractured media, different numerical models exist for solute transport without a permafrost module. The basic concepts of these numerical models are speculative and field data do not adequately support the input parameters of the models (Parker, 2007). Even stochastic methods employed in recent models do not accurately represent real systems, and the predictive capabilities of these models are generally poor. Lack of field data to calibrate the model adequately complicates its applicability. Any attempt to develop a numerical model for fractured media with a permafrost module will require determination of the influence of freezing in the media. Additionally, failures of remedial strategies for spilled fuel in permafrost environment suggest knowledge of its subsurface behavior is inadequate (Iwakun et al., 2010).

Thus, a field study to understand the behavior of spilled fuel in a permafrost bedrock environment is necessary to improve understanding of its subsurface behavior and factors influencing LNAPL migration in fractured media. To this end, this research initiates a field study with the aim of gaining insight into the subsurface behavior of spilled fuel in a permafrost bedrock environment and the factors influencing LNAPL migration in fractured media. Coupled with this field study is a laboratory experiment, aimed at evaluating some of the proposed mechanisms from the field study. The chosen site for the field study is the abandoned Colomac mine site because it provided a unique opportunity to study fuel contamination in a discontinuous permafrost fractured bedrock environment. The following section presents a brief history of the site before and after the commencement of the field study.

1.2 Site History

The Colomac mine site is approximately 220 km northwest of Yellowknife in a discontinuous permafrost environment, surrounded by lakes. The mine was an open pit gold mine that operated between 1990 and 1997. The mine became insolvent in 1999 resulting in its closure and abandonment. At present, the Contaminants and Remediation Directorate, also known as Contaminated Site Office (CSO), of Indian and Northern Affairs Canada (INAC) is responsible for remediating the site. The site has between 0 and 4.6 meters of overburden soil made up of sand, gravel, and peat. Underlying the site is fractured bedrock identified as metamorphosed siliceous sedimentary rock formed in close contact with metavolcanic rock (Hearn, 1990; Shelton et al., 2000). Although reports from other consultants that have worked at the site referred to the bedrock as greywacke (i.e., EBA, 2001; SEACOR, 2007), in this study, the bedrock will be referred to as metavolcanic sedimentary rock in agreement with the description of Shelton et al. (2000) and Hearn (1990). Remediation of different areas of the site is ongoing but this study focuses on the tank farm area where fuel spills have occurred (Figure 1.3). Shown in Figure 1.4 are the locations of the existing and newly installed monitoring wells (MWs) at the site.

There was an electric generator in the southwest corner of the warehouse building providing a year-round source of heat. Arctic diesel (P40 and P50) and gasoline were stored in tanks at the site. At the tank farm area, nine diesel tanks, each with a capacity of 4.36 million liters (L), were stored inside a bermed area lined with plastic membrane. Associated with the tank farm were systems of distribution pipes, including a buried pipeline to the powerhouse. Many smaller fuel tanks associated with generators and building heating systems were located around the site. Lubricating oil, grease, and other solvents were stored in the mechanical workshop inside the warehouse building. Beneath the

mechanical section in the warehouse were drainage channels and collection systems.

Approximately 24 reported spills at the site between 1990 and 2003 involved only diesel and gasoline, which are LNAPLs. Shown in Figure 1.5 are the approximate locations, volume, and time of fuel spills at the site. These spills were associated with accidental releases during transportation, pipe bursts, and tank leakage. Two major spills that occurred include 18,000-liter spill in February of 1990 and 27,300-liter spill in February of 1997. After the first major spill in 1990, seepage of LNAPL occurred along the shoreline of Steeves Lake adjacent to the site, which suggested that the plastic membrane liner beneath the tank farm was compromised. Thus, the mine authority and the CSO took some measures before the commencement of this study to mitigate migration of the spilled fuel. These include:

- Installation of a five-meter deep interceptor trench lined with corrugated pipe at the west berm of the tank farm in late 1990, as indicated in Figure 1.4;
- Placement of a skirted boom with an absorbent pads along the shoreline of Steeves Lake, as shown in Figure 1.4 when PHC sheen was observed in 1990/1991;
- Site characterization, including installation of monitoring wells across the site, in 2000. The spatial location of the monitoring wells is shown in Figure 1.4;
- Decommissioning of existing site fuel tanks and replacement of smaller capacity fuel tanks with double-walled steel tanks referred to as Enviro-Tanks in 2000;
- Cleaning and demolishing of the main diesel tanks, coupled with purging of the underground piping system in 2004;
- Replacement of the interceptor trench with a frozen soil barrier in 2004 to contain down-gradient migration of free product; and

- Removal and biopile treatment of contaminated overburden soil from the tank farm area in 2005.

Despite these measures, free product was observed in many of the monitoring wells across the site, and there was observable LNAPL seepage and a PHC sheen appearance along the shoreline of the lake in the summer. The limited effectiveness of these measures demonstrated inadequate knowledge of the distribution and movement of subsurface spilled fuel at the site. This research is part of multifaceted studies at the site to understand the subsurface behavior of the spilled fuel. Work elements involve collaborative efforts by the University of Alberta's Geotechnical Center, Environment Canada, and the Contaminants and Remediation Directorate of Indian and Northern Affairs Canada.

1.3 Research Objectives

In light of the discussion above, the main objectives of this research work are:

1. Determine the vertical and spatial extent of LNAPL contamination at the Colomac mine site.
2. Study and identify mechanisms contributing to LNAPL migration and accumulation at the site.
3. Determine the active geochemical processes at the site.
4. Develop a conceptual model and propose a remedial strategy to cleanup LNAPL contamination at the site.

The research questions that need answers in this research are:

- a. What are the impacts of cyclic freeze-thaw and water table fluctuations on the accumulation and migration of LNAPL in fractured media?
- b. What factors influence the behavior of LNAPL in permafrost environment?

- c. Is there reliable evidence of natural attenuation of dissolved hydrocarbons at the site?
- d. What can be done to optimize recovery of LNAPL at the site?

The hypotheses to test include:

- a) Has the LNAPL penetrated the bedrock fissures at the site, and not limited between the soil and bedrock interface?
- b) Will the freezing water in the bedrock fissures contribute to LNAPL accumulation in the monitoring wells?
- c) Is natural attenuation a viable and reliable process to mitigate the dissolved PHC contamination in groundwater at the site?

1.4 Scope of Work

Understanding the subsurface behavior of spilled fuel in freezing and frozen soils including fractured media is critical in developing a conceptual model to guide an effective and a timely cleanup of PHC-contaminated sites in permafrost environments. This research work is comprised of both field and laboratory studies to achieve this understanding. Studies presented in this thesis will be limited to the behavior of spilled fuel at the site, with particular emphasis on mobile LNAPL in the fractured bedrock. Site characterization will be limited to the areas where historical fuel spills occurred adjacent to Steeves Lake. Furthermore, this work also precludes implementation and pilot scale study of any remedial strategy at the site; sediment and surface water sampling at Steeves Lake; and analyses of the overburden soil.

1.5 Organization of Dissertation

This dissertation is written in paper format consisting of six main chapters. The breakdown of the chapters includes two published peer reviewed journal papers, two published peer reviewed conference papers, and two manuscripts submitted for journal publication. Chapter 2

lays the groundwork studies involving site characterization. The work elements include groundwater sampling, hydraulic tests, and thermal regime monitoring. It answers questions on the viability of natural attenuation at the site and offers improved understanding of the contamination extent, groundwater conditions, and thermal regime at the site. Chapter 3 describes the behavior of spilled fuel at the site and identifies factors influencing its behavior from site characterization efforts presented in Chapter 2. It answers question on what can be done to optimize recovery of LNAPL at the site and presents conceptual models of LNAPL movement at the site.

Additional efforts taken to determine both the vertical and spatial extent of contamination are discussed in Chapter 4. The chapter includes analyses in estimating the amount of recoverable fuel at the site. Additionally, Chapter 4 proposes the main mechanisms contributing to LNAPL migration and accumulation at the site. It answers the question on whether the LNAPL contamination has penetrated the bedrock fissures, and presents a refined conceptual model of the site. Chapter 5 presents the groundwater analyses aimed at determining the active geochemical processes at the site, and evaluation of compliance of the measured groundwater constituents to the Canadian Council of Ministers of the Environment (CCME) guidelines for the protection of freshwater aquatic life.

Chapter 6 presents the laboratory evaluation of the viability of some of the postulated mechanisms contributing to LNAPL migration and accumulation at the site from Chapters 4 and 5. The chapter discusses the importance of freezing-induced LNAPL displacements due to cyclic freeze-thaw. There are many instances of cross referencing and citations in this thesis because it is a collation of published and submitted manuscripts. The seventh chapter provides summary conclusions of the findings and the direction for future work.

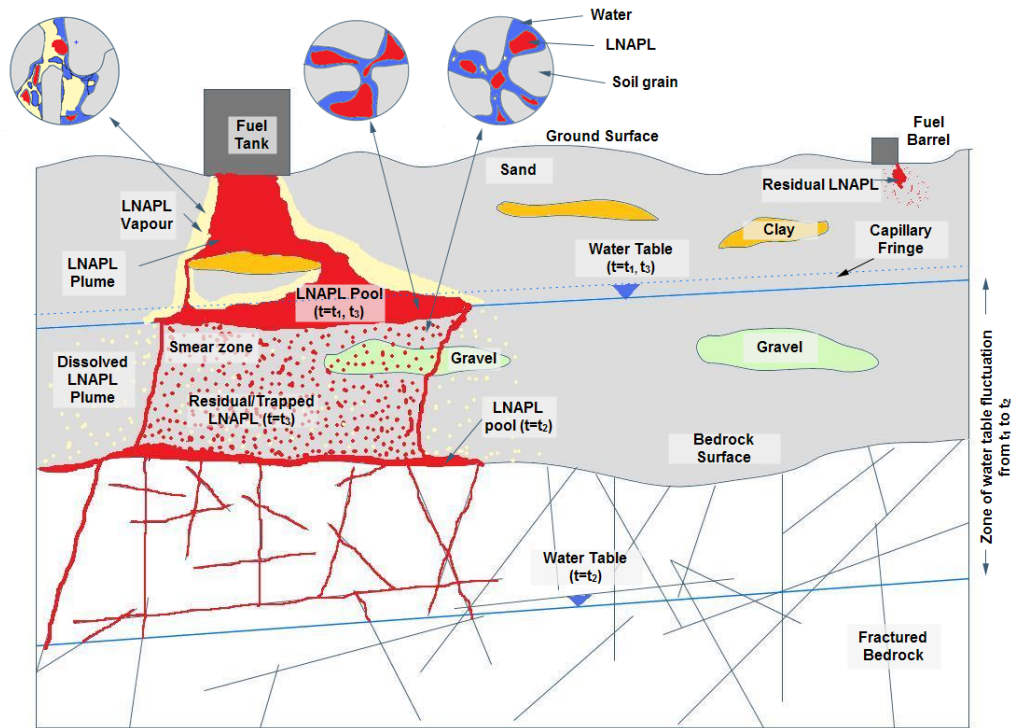


Figure 1.1 Conceptual model for the transport of light nonaqueous phase liquid (LNAPL) in fractured media. Time t_1 represents the initial time of LNAPL release corresponding to time of elevated water table for this scenario. Time t_2 represents the time of lowered water table, and time t_3 represents the time when the water table rebounded to initial level at t_1 .

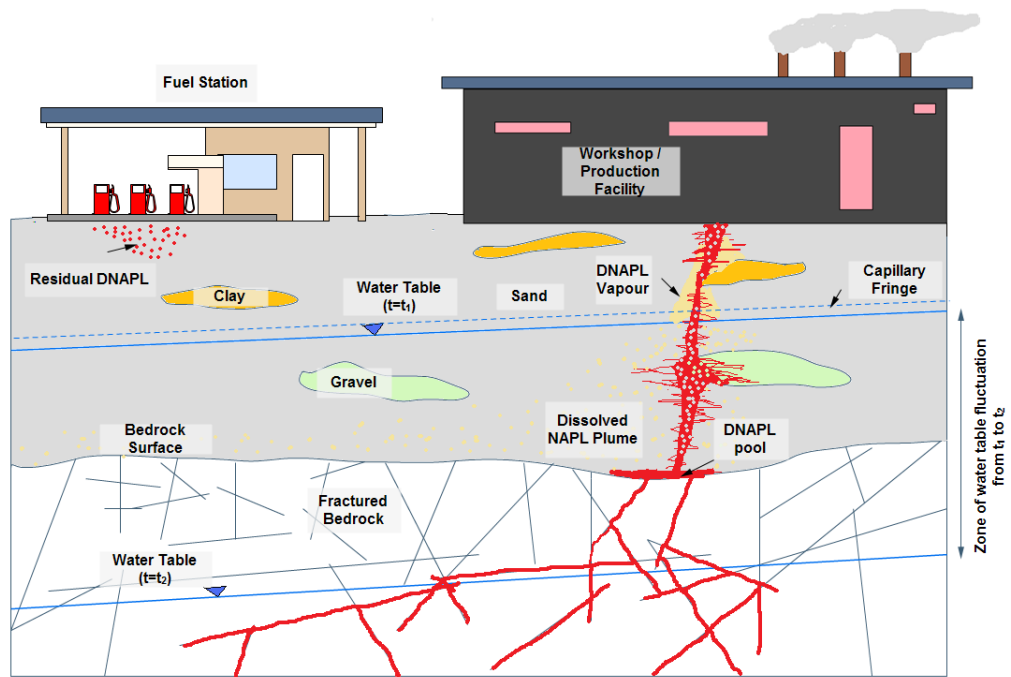


Figure 1.2 Conceptual model of DNAPL transport in fractured media.



Figure 1.3 Layout of the mine site before demolition of the structures.

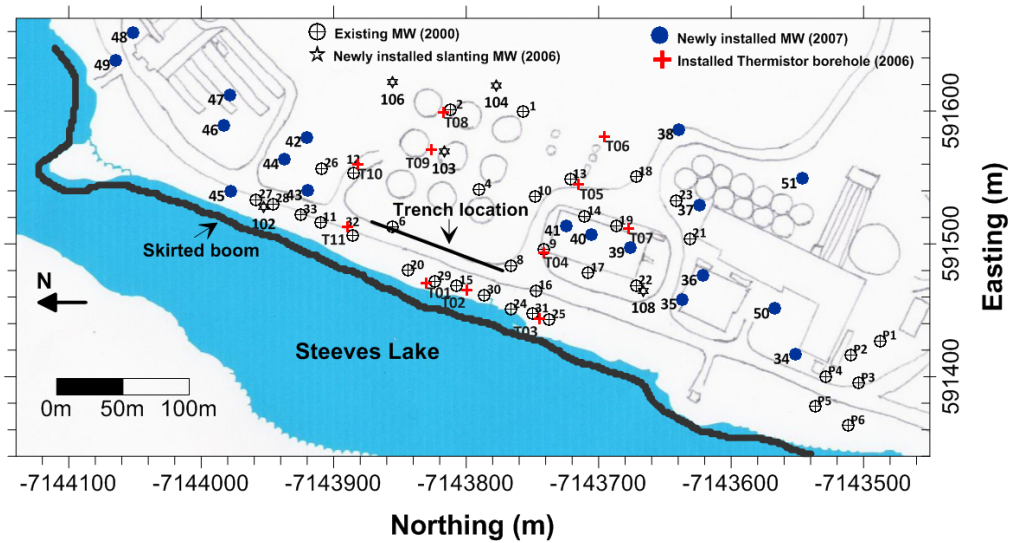


Figure 1.4 A site map of Colomac mine, reduced to show details of site investigation. The map shows the spatial locations of the installed monitoring wells, thermistor boreholes, and some of the initial measures taken to mitigate the movement of free product to Steeves Lake before commencement of this study in 2005 (Iwakun and Biggar, 2008).

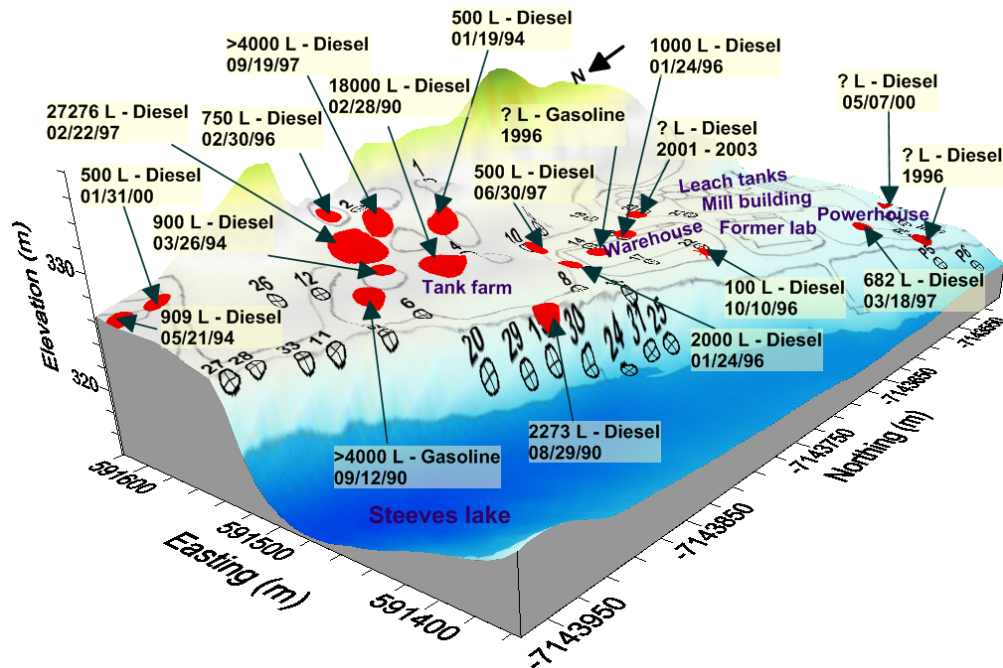


Figure 1.5 A site model showing the approximate location, volume, and date of historical spillage at the site. Most spills at the site were Arctic diesel but not all were accounted for (modified after EBA, 2001).

References

- API - American Petroleum Institute, 1989. A Guide to the Assessment and Remediation of Underground Petroleum Releases, Second Edition, API Publication 1628, Washington, D.C.
- Aral, M.M., Liao, B., 2002. Effect of groundwater table fluctuations on LNAPL thickness in monitoring wells. *Environmental Geology*, 45: 151-161.
- Barnes, D.L., Chuvlin, E., 2009. Migration of petroleum in permafrost-affected regions. *Permafrost soils*, R. Margesin (Ed). *Soil biology*, 16: 263-278. Springer, Germany.
- Barnes, D.L., Wolfe, S.M., Filler, D.M., 2004. Equilibrium of petroleum hydrocarbons in freezing ground. *United Kingdom. Polar Record* 214: 245-251.
- Bear, J. 1993. Modeling flow and contaminant transport in fractured rock. In: Bear, J., Tsang, C., and de Marsily, G. (Eds), *Flow and*

contaminant transport in fractured rock. Academic Press, Inc., Academic Press, Inc., pp. 1-37.

- Beier, N., Seago, D., Donahue, R., Biggar, K., 2007. Laboratory investigation of freeze separation of saline mine waste. *Cold Regions Science and Technology*, 48(3): 239-247.
- Berkowitz, B., 2002. Characterizing flow and transport in fractured geologic media: a review. *Advances in Water Resources*, 25(8): 861-884.
- Biggar, K.W., Haidar, S., Nahir, M., Jarrett, P.M., 1998. Site investigations of fuel spill migration into permafrost. *Journal of Cold Regions Engineering*, 12:84-104.
- Biggar, K.W., Neufeld, J.C.R., 1996. Vertical migration of diesel into silty sand subject to cyclic freeze-thaw. In: Carlson, R. (editor). *Proceedings of the Eighth International Conference on Cold Regions Engineering*. Fairbanks: American Society of Civil Engineers, pp. 116-127.
- Cailleux, A. 1964. 'Genese possible de depots chimiques par congelation (possible origins of chemical depositions through congelation; in French),' *Societee Geologiques France*, 1, 11-12. *Canadian Journal of Earth Sciences*, 20:978-986.
- Catalan, L.J.J., Dullien, F.A.L., 1995. Application of gravity drainage to the recovery of residual LNAPL in homogeneous and lensed sand packs. *Journal of Contaminant Hydrogeology*, 18: 279-306.
- Chamberlain, E.J., Erickson, A.E., Benson, C.H., 1997. Frost resistance of cover and liner materials for landfills and hazardous waste sites. Hanover, NH: Cold Regions Research and Engineering Laboratory (CRREL Special Report 97-29).
- Chuvilin, E.M., Mikiyaeva, E.S., 2003. Investigation of the influence of salinity and cryogenic structure in the dispersion of oil and oil products in frozen soils. *Cold Regions Science and Technology*, 37: 89-95.

- Chuvilin, E.M., Miklyaeva, E.S., Kozlova, E.V., Instanes, A., 2001b. Experimental study of freezing soils contaminated by oil. In: Kim, S., and D. Jung (editors). Proceedings of the 7th International Symposium on Thermal Engineering and Sciences for Cold Regions. Seoul, Korea, pp. 145-149.
- Chuvilin, E.M., Naletova, N.S., Miklyaeva, E.C., Kozlova, E.V., Istanes, A., 2001a. Factors affecting the spreadability and transportation of oil in regions of frozen ground. *Polar Record*, 37 (202): 229-238.
- David, T.W., Michener, S.R., Dolan, T.I., Cavagrotti, R.R., 1999. An integrated approach to the characterization and remediation of gasoline in a fractured, sedimentary bedrock setting. Proceedings of the 1999 petroleum hydrocarbons and organic chemicals in ground water; prevention, detection, and remediation conference and exposition, pp. 316-330.
- Dobson, R., Scroth, M.H., Zeyer, J., 2007. Effect of water table fluctuation on dissolution of a multi-component light nonaqueous phase liquid, *Journal of Contaminant Hydrogeology*, 94: 235-248.
- Dyke, L.D., Egginton, P.A., 1990. Influence of ice lens fabric on the hydraulic conductivity of thawing soil. *Collection Nordicana*, 54: 137-141.
- EBA - Engineering Consultants Ltd., 2001. Hydrocarbon assessment, Lakefront, and waste oil areas, Colomac Mine, NWT. Report to Deton 'Cho Corporation. Yellowknife, NWT, 37 p., and appendices.
- Esposito, S.I., Thomson, N.R., 1999. Two-phase flow and transport in a single fracture-porous medium system. *Journal of Contaminant Hydrology*, 37:319-341.
- Farr, A.M., Houghtalen, R.J., McWhorter, D.B., 1990. Volume estimation of light nonaqueous phase liquids in porous media, *Ground Water*, 28(1): 48-56.
- Feenstra, S., Cherry, J. A., Parker, B.L., 1996. Conceptual Models for the Behavior of Dense Nonaqueous Phase Liquids (DNAPLs) in the

- Subsurface. In: Pankow, J.F., and Cherry, J.A. (Eds), Dense Chlorinated Solvents and other DNAPLs in Groundwater. Waterloo Press, Waterloo Press, 53-88.
- Hearn, K., 1990. The Colomac deposit. Geological Survey of Canada Open File Report 2168, pp. 84–89.
- Heise, M.D., 1999. Simulation of coupled aqueous and nonaqueous phase flow and transport in a fracture. Unpublished M.Sc. Thesis. Department of Earth and Atmospheric Science, University of Alberta, Edmonton, Alberta, 114 p.
- Hostettler, F.D., Rostad, C.E., Kvenvolden, K.A., Delin, G.N, Putnam, L.D., Kolak, J.J., Chaplin, B.P., Schaap, B.D., 2001. Hydrologic Setting and Geochemical Characterization of Free-Phase Hydrocarbons in the Alluvial Aquifer at Mandan, North Dakota, Report: USGS/WRD/WRI-01-4108, 128p.
- Iwakun, O., Biggar, K., 2007. Behavior of spilled petroleum hydrocarbon at Colomac mine site, NWT. Proceedings of 60th Canadian Geotechnical Conference and the 8th Joint CGS/IAH-CNC Groundwater Conference, Ottawa, pp 2106-2114.
- Iwakun, O., Biggar, K., 2008. Characterization of Fuel Spill Plumes in Fractured Rock at a Permafrost Site: Colomac Mine, NWT. Progress report submitted to Indian and Northern Affairs Commission (INAC), Yellowknife.
- Iwakun, O., Biggar, K., Sego, D., 2008b. Influence of temperature and groundwater fluctuation on LNAPL migration at Colomac mine site. Proceedings of Ninth international conference on permafrost. Kaine, D. L., and Hinkel, K. M., (Eds), 1: 815-820.
- Iwakun, O., Biggar, K., Van Stempvoort, D., Bickerton, G., Voralek, J., 2008a. Fuel contamination characterization in permafrost fractured bedrock at the Colomac mine site, NWT. Cold Regions Science and Technology, 53(1): 56-74.

- Konrad, J.M., Seto, J.T.C., 1991. Freezing of a clayey silt contaminated with an organic solvent. *Journal of Contaminant Hydrology*, 8 (3-4): 335-356.
- Kueper, B.H., McWhorter, D.B., 1996. Physics Governing the Migration of Dense Nonaqueous Phase Liquids (DNAPLs) in Fractured Media. In: Pankow, J.F., and Cherry, J.A. (Eds), *Dense Chlorinated Solvents and other DNAPLs in Groundwater*. Waterloo Press, Waterloo Press, 89-128.
- Lapcevic, P.A., Novakowski, K. S., Sudicky, E. A., 1999. Groundwater flow and solute transport in fractured media. In: *The Handbook of Groundwater Engineering*. J. W. Delleur (Ed.), Chap.17, pp. 17-39.
- Lenhard, R.J., Johnson, T.G., Parker, J.C., 1993. Experimental observations of nonaqueous-phase liquid subsurface movement *Journal of Contaminant Hydrology*, 12: 79-101.
- Mawhinney, J.R., 1979. An Investigation into the occurrence and development of groundwater in permafrost regions. Unpublished M.eng. report, Civil Engineering Department, University of Alberta. Edmonton, Alberta. 65 p.
- McCarthy, K., Walker, L., Vigoren, L., 2004. Subsurface fate of spilled petroleum hydrocarbon in continuous permafrost. *Cold Regions Science and Technology*, 38: 43-54.
- McCrorry, T.A., 1997. Fracture control of free-product migration at an emergency response, Blue Ridge, Georgia. *Abstracts with Programs - Geological Society of America*, 29(6): 386-387.
- Mercer, J.W., Cohen, R.M., 1990. A review of immiscible fluids in the subsurface: Properties, models, characterization, and remediation, *Journal of Contaminant Hydrology*, 6: 107-163.
- Motenko, R.G., Ershov, E.D., Chuvilin, E.M., Miklyaeva, E.S., Zhuravlev, I.I., 2003. Heat and mass transfer in freezing soils contaminated by oil. In *Proceedings of the Eighth International Conference on Permafrost*. Zurich, Switzerland, July 21-25. Edited by M. Phillips,

- S.M. Springman, and L.U. Arenson. A.A. Balkema, Vol. 2, pp. 795-799.
- Neuman, S.P., 2005. Trends, prospects, and challenges in quantifying flow and transport through fractured rocks. *Hydrogeology Journal*, 13: 124-147.
- Overduin, P.P., 1998. Soil moisture and soil water solutes during freeze-back at Lake Levinson-Lessing, Taymyr Peninsula, and Siberia. Unpublished M.Sc. thesis. Department of Geography, York University, Toronto, Ontario, 113 p.
- Panday, S.M., 1990. Soil and groundwater contamination by petroleum products in frozen soils. Unpublished PhD thesis. Department of Civil and Environmental Engineering, Washington State University. Pullman, Washington, 257 p.
- Parker, B.L., 2007. Investigating contaminated sites on fractured bedrock using DFN approach. Proc. Of EPA/NGWA Fractured Rock Conference: State of the Science and Measuring Success in Remediation, Portland, ME.
- Parker, J.C., Katyal, A.K., Zhu, I.L., 1991. Free product recovery with fluctuating water tables. *Ground Water Management*, 5: 291-305.
- Schwille, F., 1988. Dense chlorinated solvents in porous and fracture media: Model experiments. Lewis Publishers, Inc., Lewis Publishers.
- SEACOR Environmental Inc., 2007. Environmental investigations of former Colomac mine, Draft report submitted to the Department of Indian Affairs and Northern Development (DIAND) Canada, Yellowknife, 115 p.
- Sharp, T.L.M., 2001. LNAPL migration and trapping in heterogeneous porous media. Unpublished M.Sc. thesis in the Department of Earth and Atmospheric Sciences, University of Alberta, Edmonton, Alberta. 130 p.

- Shelton, K. L., Costello, C.S., van Hees, E.H., 2000. Contrasting styles of Achaean greenstone gold deposition: Colomac gold mine, Canadian Northwest Territories. *Journal of Geochemical Exploration*, 69 – 70: 303 – 307.
- Simantiraki, F., Aivalioti, M., Gidarakos, E., 2009. Implementation of an image analysis technique to determine LNAPL infiltration and distribution in unsaturated porous media. *Desalination*, 248: 705-715.
- Slough, K.J., Sudicky, E.A., Forsyth, P.A., 1999. Importance of rock matrix entry pressure on DNAPL migration in fractured geologic materials. *Ground Water*, 37(2): 237-244.
- Steffy, D.A., Johnston, C.D., Barry, D.A., 1995. A field study of the vertical immiscible displacement of LNAPL associated with a fluctuating water table. *Groundwater Quality: Remediation and Protection*, 49-57.
- Tumeo, M.A., Davidson, B., 1993. Hydrocarbon exclusion from ground water during freezing. *Journal of Environmental Engineering-ASCE*, 119(4): 715-724.
- U.S. National Research Council, 1996. *Rock Fractures and Fluid Flow: Contemporary Understanding and Applications*. National Academy of Sciences, 551 p. (see chap. 6, Field scale flow and transport models: p. 301-403).
- Weiner, E.R., 2000. *Applications of environmental chemistry: A practical guide for environmental professionals*. CRC press LLC, Florida.
- Wilson, D.G., Mackay, D., 1987. The behavior of oil in freezing situations. Unpublished report of Environmental Protection Directorate, River Road Environmental Technology, Ottawa. 78p
- Witherspoon, P.A., Wang, J.S.Y., Iwai, K., Gale, J.E., 1980. Validity of cubic law for fluid flow in a deformable rock fracture. *Water Resources Research*, 16(6): 1016-1024.

Zukowski, M.D., Tumeo, M.A., 1991. Modeling solute transport in ground water at or near freezing. *Ground Water*, 29(1): 21-25.

2 FUEL CONTAMINANT CHARACTERIZATION IN A PERMAFROST FRACTURED BEDROCK AT THE COLOMAC MINE SITE¹

2.1 Introduction

In Canada's north, contaminant characterization is complicated by the presence of permafrost and remote site logistics, among other issues. This paper summarizes the progress of a study being conducted into the behavior of fuel contamination in permafrost fractured bedrock at the abandoned Colomac gold mine site shown in Figure 2.1, approximately 220 km northwest of Yellowknife in the Northwest Territories (NWT). The site was an open pit gold mine that operated between 1990 and 1997. The site was abandoned and is currently the responsibility of the Contaminants and Remediation Directorate of Indian and Northern Affairs Canada (INAC) for the site cleanup and mitigation of potential environmental impacts.

The site has between 0.2 to 4.6 m overburden over fractured bedrock. The overburden consists of mainly sand and gravel till with some peat near the shoreline of the lake. The bedrock is a metamorphosed siliceous and slaty sedimentary rock formed in close contact with metavolcanic rock, fractured, and strongly foliated (Hearn, 1990; Shelton et al., 2000). Blasting operations to level the area during construction may have induced fractures in the bedrock surface and near blast faces. The geometric relationships and interconnectivity of the various bedrock fractures have the potential to produce a complex flow system at the site and may lead to seemingly unusual responses in the existing monitoring network. Outcrops at the site appear to be generally

¹ A version of this chapter has been published.

Iwakun, O., Biggar, K., Van Stempvoort, D., Bickerton, G., Voralek, J., 2008a. Fuel contamination characterization in permafrost fractured bedrock at the Colomac mine site, NWT. *Cold Regions Science and Technology*, 53(1):56-74.

massive and competent except near occasional site-scale linear features (e.g. shear zone) where the outcrops appear highly fractured and weathered. Previous work by Van Stempvoort et al. (2006) and examination of the bedrock outcrops showed that the fractures are near vertical and sub-horizontal as shown in Figure 2.2.

There were approximately 24 reported releases of petroleum hydrocarbons (PHCs), mostly diesel fuel, in and around the main tank farm area from 1999 to 2003 as shown in Figure 2.3 (EBA, 2001; CSO, 2004). Two major fuel spillages include 18,000 L and 27,276 L in 1990 and 1997, respectively, as shown in Figure 2.3, some of which leaked out of the tank farm because of a damaged plastic membrane liner. No pooled PHC product was identified during attempted recovery of spilled fuel on both occasions. PHC sheen was noted along portions of shoreline on Steeves Lake after the 1990 spillage (EBA, 2001). Subsequent investigation revealed the presence of free phase PHC, often referred to as light nonaqueous phase liquid (LNAPL) in this paper, atop the supra-permafrost water table.

A five meter deep interceptor trench was excavated to the base of the fill/top of bedrock along the west berm of the tank farm between the tank farm and the lake (Figure 2.4) after the initial release in 1990, to mitigate the PHC migration. Though the trench intercepted some LNAPL flow, it did not capture all of it; some continued to flow towards the lake. A continuous skirted boom was also installed along the lake's shoreline in the early 1990s. Oil absorbent pads were used within the skirted boom, which were periodically collected, treated, and incinerated on site.

The active seepage observed at the lake's shoreline (Figure 2.4) led to the installation of monitoring wells (MWs) throughout the site as shown in Figure 2.4 to monitor the thickness and distribution free product in the subsurface (EBA, 2001). The wells were percussion drilled using a diamond drill-bit, unscreened and cased through the overburden, leaving the rock exposed beneath the casing. Monitoring in 2000 showed

an average LNAPL thickness of 1.5 m over the impacted area with the highest thickness being 15.4 m in one of the MWs in the tank farm area (MW 11). Later assessment of the LNAPL within the fractured bedrock in 2001 (URS, 2002) showed lower average LNAPL thickness of 0.4 m with a maximum thickness of 1.6 m in one well. The assessment concluded that the majority of the spilled fuel had dissipated and that PHC seepage being observed along the lakeshoreline at that time was the remnant of the spills. From the evaluation of fracture density in the bedrock, it was inferred by URS (2002) that there was little PHC in the fractures, and it was held by capillary tension, thus immobile. However, recent studies showed that though permafrost may impede water movement, it might not completely curtail flow of PHCs as LNAPL (Biggar et al., 1998; McCarthy et al., 2003). URS (2002) also assessed the mobility and recoverability of LNAPL in the formation using the BIOVENT computer program, and concluded that LNAPL in the formation is fundamentally immobile and its recovery via conventional pumping would not be possible.

Recent measures at the site to mitigate the PHC seepage and reduce source concentration included the removal and treatment of contaminated overburden from the tank farm area in 2004-05 using an on-site biopile, and the construction of a frozen soil barrier. In the fall and winter of 2004-05, a trench was blasted and excavated into the bedrock between the tank farm and the lake to a depth of 5m (e.g., between MW 6 and MW 8 shown in Figure 2.4). The trench was lined with a geomembrane, backfilled with layers of saturated soil and allowed to freeze, thereby creating a frozen soil barrier. Sumps were placed at each end of the barrier for monitoring and removal of free product and water. Significant volumes of water were removed from the sumps in 2005. Despite these measures, LNAPL was still being observed in some of the wells downgradient of the barrier.

Complicating the understanding of the distribution and movement of the PHCs is the presence of an electric generator in the southwest corner of the warehouse that generates heat causing a large thaw bulb in the permafrost bedrock. This influences the local thermal regime and may affect the contaminant migration. Therefore, a study of the thermal regime of the site, hydraulic conductivity of the fractured bedrock, its interconnectivity, and groundwater flow pattern was necessary to understand and mitigate contaminant movement to Steeves Lake. It was also necessary to understand the current distribution of both free product and dissolved PHC contamination, as well as the distribution of other dissolved chemicals to evaluate potential for natural attenuation as a remedial strategy at this complex site. This chapter presents the results to achieve this understanding with inputs from National Water Research Institute (NWRI) scientists from Environment Canada.

2.2 Field Activities

The field study presented in this paper commenced in June 2005 after the review of relevant information on previous work done at this site. The study's field activities include monitoring the depths to free-phase PHC, water, and ice in existing monitoring wells, temperature profile measurement with thermistor cables, groundwater sampling, and geochemical analysis, and the measurement of bedrock permeability using borehole hydraulic tests. The depths to free product, water, and ice in the wells were measured to understand the groundwater flow regime, active layer thickness fluctuation, temporal and spatial variation of the water and apparent thickness of free product. When the depth to refusal in the well bottom was less than the installed MW depth, it was inferred that ice extended to the bottom of the MW (often confirmed by the presence of ice crystals on the bailer and/or interface meter). The depth to the ice in each well provided a means of estimating the active layer

thickness during the thawing season over a greater extent of the site than could be monitored with the limited number of thermistor cables.

Vertical profiling of bedrock permeability was conducted in August and September of 2005 using constant-head test in collaboration with NWRI scientists. This test approach uses inflatable packers to isolate sections of the bedrock in the borehole. The isolated well-water was allowed to equilibrate in pressure to measure initial head using a calibrated transducer attached to the packers. Water was then injected into the well under pressure to bring about a two to three millivolts change in the transducer reading. The head in the well was then allowed to come into equilibrium with the injected water. Maintaining a constant pressure in the MW, the volume of injected water was measured versus time, which was then used to calculate the transmissivity, equivalent permeability, and the average fracture width in that zone. The full procedure and some of the data generated for the packer test are in Appendix A.

Dedicated bailers were used for weekly sampling of a number of the wells between June and August, 2005 in collaboration with NWRI scientists and INAC staff, to investigate temporal changes in inorganic groundwater chemistry. In late August 2005, a more detailed sampling program was undertaken involving both sampling at discrete intervals using a peristaltic pump and packer assembly, as well as sampling near the water table surface using dedicated tubing with a peristaltic pump. In June and September 2006, the wells without free product and those with a thin film of free product were either sampled using a peristaltic pump (depth to water < 8 m) or a submersible pump (depth to water > 8 m). The samples were analyzed for the Canadian Council of Ministers for the Environment (CCME) F1 hydrocarbon fraction (nC₆ to nC₁₀), other volatile organic compounds, inorganic ions, and volatile fatty acids. For some of the wells, a flow through cell was used to measure groundwater pH, dissolved oxygen (DO) and oxidation reduction potentials (ORP). The ORP

and volatile fatty acids were measured during the August 2005 sampling only.

In December 2005, thermistor cables with 8 sensors each were installed in three existing MWs (19, 22 and 27) to a depth of approximately 15 m. Samples of LNAPL (Light Nonaqueous Phase Liquid) were taken for analysis from MWs #9, 12, and 17 during the same sampling event. In April 2006, three 75mm diameter boreholes were drilled along the shoreline of Steeves Lake and dedicated thermistor cables were installed (T-01 to T-03). In June 2006, eight additional boreholes were drilled and thermistor cables were installed (T-04 to T-11). These boreholes were backfilled with bentonite after thermistor cable installation. Five inclined monitoring wells were also installed in June 2006. The five inclined wells are denoted with a prefix of MW (i.e. MW 106). The new inclined monitoring wells are at approximately 35° to the vertical and ranged between approximately 15 m and 22 m in length (i.e. as measured on the incline). MW 104 and 106 are east of the tank farm to monitor background concentrations: MW 103 is at the centre of the tank farm area, MW107 is northwest of the tank farm area, and MW108 is at the southwest corner of the warehouse.

The ground elevation of the site before the removal of overburden in the tank farm area is shown in Figure 2.5. The overburden was approximately 0.2 m thick on the east extent of the area, thickening to approximately 3 m westwards. North of the tank farm area, there is a deepening of the bedrock surface leading to increase in the overburden thickness. The overburden includes rock fill placed to level the site for the mine operations. Close to the edge of the lake there is a steep drop in ground elevation of approximately 3-4 m.

2.3 Results and Discussion

2.3.1 Manual monitoring of water levels

The measured depth to water in each monitoring well was used to produce elevation contours of the water table. It is recognized that such contour plots may not be a true representation of flow in fractured bedrock; however they do lend insight into the general patterns of flow. A sample of the groundwater elevation contours for August 2005 is shown in Figure 2.6. The groundwater elevation was corrected for the measured apparent free product in the monitoring wells where observed. A sample calculation with some of the elevation data used for the plot is shown in Appendix B. The general flow direction is westwards towards Steeves Lake. Other contour plots from June to September (not shown) are in agreement with increased hydraulic gradient around the tank farm area.

2.3.2 Manual monitoring of depth to ice

It was necessary to develop an understanding of the thermal regime to better understand the supra-permafrost water flow characteristics to provide insight into the thickness of the water during thaw as well as the direction of flow and hydraulic gradients. The depths to the well bottom (DTBs), reported as bottom elevation (BE), indicated the depth to ice when the measured depths were less than the known depths of the MWs. Additionally, the DTBs also provided insight on the active layer prior to installation of dedicated thermistor strings at the site. These data were not recorded prior to June 2005, so measurements were taken at 7-14 day intervals from mid-June until mid-September 2005 but less frequently from September 2005 through 2006.

Figure 2.7 and Figure 2.8 show the depths to the water table (or groundwater elevation), and depths to well refusal (or BE) along four areas of the site over time. Figure 2.7a is from wells at the east side of the tank farm, farthest from the lake. Figure 2.7b is from wells midway

between the lake and the upslope edge of the study site. Figure 2.8a is from wells along the shoreline of the lake, and Figure 2.8b is from wells adjacent to the warehouse.

Furthest from the lake, Figure 2.7a shows a gradual deepening of the active layer; however the water table surface remains nearly constant except MW 2, where the water drops a similar amount as the ice in late August. The temporary rise in depth to well bottom for MWs 1 and 2 is interpreted to have been rafting and jamming of ice within the water column in the borehole, which subsequently melted. Due to non-uniformity and constrictions in the borehole, ice may be blocked at constricted regions in the well, and additional water recharge from the surface will result in a perched water condition in the monitoring well. Later borings at the site showed that perched existed above isolated patches of permafrost in the formation as illustrated in Figure 2.9. With time, as the ground warms up, the ice locked in the constricted regions is gradually melted and the perched water table is released. Comparison of water surface and ground-ice elevations infers the development and presence of perched water table conditions at the upslope region of the site (Figure 2.9 and Figure 2.10). Groundwater elevation in MW 18 is nearly constant and it does not decrease as the ice clog in the well melts. Through the summer of 2005, the depth of the active layer increased from approximately 3 m to 9 m over the monitoring period, and the change in water thickness ranged from approximately 2 m to 6 m, depending on the MW.

At mid-slope shown in Figure 2.7b, thaw depths in MWs 8 and 12 gradually increased to a depth of approximately 7-10 m through September, 2005; however the depth to well bottom in well 26 dropped rapidly in August to approximately 21 m, which is the bottom of the borehole. In this region the water thickness in early June, 2005 was only approximately 1 m for MWs 8 and 12, thickening to 5-7 m in September, 2005. MW 26, which is relatively close to MW 12 (approximately 25 m)

had deeper thaw (~5 m in June, and 10 m in September) indicative of a significantly different thermal and possibly flow regime over the short separation distance, even though there was no vegetation and similar soil cover at each well. There was also a rapid drop in the water depth in MW 26 in August when the depth to ice also dropped rapidly, suggesting the possible exposure of a drainage zone within the well that had been ice blocked. This behavior was also observed in the 2006 groundwater profile shown in Figure 2.7b but less pronounced, likely because of fewer monitoring data.

In Figure 2.8a adjacent to the lake, MWs 29 and 30 (in the central portion of the monitoring zone) were thawed over their entire depth (~10 m) by early July, 2005, but their water table depth changed little. MW 24, to the south, did not thaw through until September, 2005. Each well along the shoreline displayed a rapid drop in depth to the well bottom over a short period, indicative of an ice plug over a portion of the well with an unfrozen zone beneath. The lower thawed zone is corroborated by thermistor string data, discussed in the following section. This would indicate that a talik extends inland from the lake beneath the active layer as illustrated in Figure 2.9.

Based on the monitoring of water and ice in the MWs adjacent to the warehouse (Figure 2.8b), it is apparent that there is a deep thaw bulb beneath the warehouse, especially at the southwest corner of the building where a generator is situated. MW 19 was thawed over its entire depth for the duration of monitoring. In MW 14 the depth to refusal dropped to the bottom of the borehole in late June. MW 9, close to the warehouse, thawed slowly over the entire summer to a depth of approximately 11 m in September and over its entire depth in December 2005. In 2006, thaw in MW 9 was much more rapid and the well was thawed over its entire depth of 21m by August. The deep thaw bulb beneath the warehouse (Figure 2.9) and its close proximity to the lake may provide a pathway for

water migration year round; however there are inadequate data to verify this.

Figure 2.10 summarizes the observed behavior of water in the monitoring wells. It should be noted that if the perched water condition extend to the permeable formation adjacent to the water-perched section of the monitoring well, the water would not drain off. Thus, perched water conditions in some of the wells suggest development of perched groundwater condition in the adjacent formation between June and September of the year. This perched water condition was not elicited in some of the wells in which the drop in bottom ice elevation was not accompanied by significant change in water table elevation (Figure 2.10). However, when the surrounding formation adjacent to the water-perched section of the monitoring well is impermeable or clogged by ice, the perched water condition due to either ice rafting in the wells or freezing over only the upper portion of the well may be localized and not representative of the water table condition in the formation.

2.3.3 Measured ground temperatures

The site is located in the discontinuous permafrost zone between Norman Wells and Yellowknife at latitude 64°12'N in the Northwest Territories. This region is densely marked with standing water bodies with unfrozen thaw bulb beneath them. Thus, the permafrost table at the site will vary considerably and be dependent on nearness to water bodies, surface cover, anthropogenic factors and the local climatic condition. Temperature profiles from the thermistor string installed in MW 22 at the southwest corner of the warehouse are shown in Figure 2.11a. Adjacent to the warehouse, freezing progressed to a depth of approximately 9 m. The thermistor at 8.8 m depth remained slightly below 0°C from 26 April until 5 June, 2006, and the thermistors at depths of 11.8 meters and 14.8 m remained above 0°C throughout the winter. The depth of the talik (or thaw bulb) beneath the warehouses is unknown, however based on the

data from the thermistors in MWs 22, 19, and 27; it is known to be more than 21 m deep.

Data from some of the installed thermistors along the shoreline are shown in Figure 2.11 and Figure 2.12. The updated thermistor data temperature profiles across the site are shown in Appendix C. In the spring of 2006, the temperature profile in T-01 near MW 29 (Figure 2.11b) was above 0°C below a depth of approximately 6 m, and was frozen above that depth until mid-May, which corroborates the measured depths to ice in MW 29 in 2005. The thermistor data from T-03, adjacent to MW 31 (Figure 2.12), showed that the ground remained below 0°C from near the surface to depths of approximately 6-8 m until June. The region south of MW 30 is covered with an organic mat which insulates the rock, slowing warming, whereas the region around MW 29 has no vegetative cover. This explains the much later thaw-out in MW 24 observed in 2005 (Figure 2.8a). No data are available to discern the depth to the bottom of the talik. However, as the ground warms up, differences between the depth of the 0°C isotherm measured by the thermistors and the depth to ice in the well are expected because ice in the formation will thaw faster than that in the well due to lower latent heat required for melting in the formation.

The frozen depth temperature profile correlates with frozen water in the well in the late winter and early spring. Away from the lake (east side of tank farm) the depth to ice increases from spring to fall, but the water table does not drop significantly, thus the zone of water flow thickens throughout the thaw season up to 6 m upslope and 10 m at mid-slope.

The lateral extent of the talik beneath the lake and its effect on the thermal profile at the site are unknown. Adjacent to the lake the bedrock freezes seasonally at the top, but remains thawed at depth. Between the tank farm and warehouse at the site where some of the spills have

occurred, the behavior varies. At the warehouse, the heat generated causes a local thaw bulb, most felt in MW 19, 22, and 14. This may imply hydraulic interconnectivity of these wells because water in the surrounding wells including MW 9 and 17 is frozen at depth.

2.3.4 Hydraulic testing of fractured bedrock

Calculated hydraulic transmissivities from packer tests conducted in August and September, 2005 in selected wells are shown in Figure 2.13. Testing of deep well profiles was achieved only in thawed monitoring wells. Transmissivity generally varied between 3×10^{-4} and 6×10^{-7} m²/s (equivalent to hydraulic conductivities of approximately 5×10^{-4} and 1×10^{-6} m/s for the 0.57 m packer interval). A few zones at the powerhouse area had values approximately one order of magnitude higher than that specified above. This may indicate a few larger fissures near the rock surface, but data are inadequate to make definitive conclusions. Values shown as 1×10^{-9} m²/s were in rock too tight to accurately measure any flow into the formation. In general, transmissivity varied from borehole to borehole, with no strong spatial relationship.

Based on the hydraulic testing results and outcrop observations, the bedrock at the site is currently characterized as generally competent rock of low permeability with localized fractures or fracture zones of moderate to high permeability

2.3.5 LNAPL monitoring in wells

LNAPL of PHCs was detected atop the water in many of the wells in previous studies (EBA, 2001; URS, 2002; and Biogenie, 2004). However, based on the ongoing study, wells with measurable LNAPL are divided into three categories; those with continuous, often, and periodic free product as shown in Table 2.1. Monitoring wells with measurable free product all year round are categorized as continuous, those with free product in many instances are categorized under often, and those with

measurable sheen of free product intermittently are grouped under periodic.

Distribution of apparent LNAPL thickness distribution for August, 2006 is shown in Figure 2.14. The distribution pattern of LNAPL in the wells is similar to the fuel spillage on the site. The actual distribution and mode of free product movement at the site is uncertain. It had been speculated in previous studies at the site that the flow was predominantly within the overburden fill or atop the bedrock surface, and that there should be little flow in the fissures in the bedrock. Investigations in 2005 and 2006 have shown that though the monitoring well casings were "seated" into the bedrock, the seal between the casing and the bedrock is loose in some wells, which would have allowed free product to flow down into the well from the bedrock surface. There is, however, evidence that the fissures in the bedrock, at least in some locations, contain significant free product. MWs 12 and 26, for example, had free product thicknesses of 0.04 m and 0.15 m in June 2005 when the water depths were 1.6 and 2.7 m, respectively. In December 2005, the product thickness in MWs 12 and 26 had increased to 5.01 m and 3.68 m with depths to water of 12.9 m and 12.4 m respectively as shown in Table 2.1. Since all of the contaminated overburden was removed during the summer of 2005 and treated in a biopile, this behavior indicates that as the water table dropped in this region, free product drained from the fissures into the borehole. These data imply that at least portions of the bedrock contain significant free product and that transport within the fissures may be occurring over portions of the site.

In December of 2005, samples of LNAPL from MWs 9, 12, and 17 were analyzed for their chemical composition, shown in Figure 2.15. The benzene concentration was below the reliable detection limit in all the samples, implying that the relative fraction of benzene to other compounds is low, possibly due to preferential dissolution and biodegradation of benzene. The figure also shows that the CCME fractions

F1 (nC₆ to nC₁₀), F2 (nC₁₀ to nC₁₆), and F3 (nC₁₆ to nC₃₄) are essentially the same for all wells, suggesting that the PHCs in the tank farm area (MW 12) and the warehouse (MWs 9 and 17) are from the same source. It is notable, however, that the toluene, ethylbenzene, and xylenes are approximately one-half order of magnitude less in MW 12. This may imply that some spillage of lighter fuel hydrocarbons, possibly gasoline, may have occurred around the warehouse. This is possible, since the gasoline storage area and refueling pad was close to the north end of the warehouse as shown in Figure 2.4. Visual examination of the free product showed that the product around the warehouse was dark and nearly opaque whereas the product in MW 12 was clear and slightly amber in color. It may be that the free product around the warehouse was contaminated by other lubricants, solvents or hydraulic oils being used in the area where vehicle maintenance was carried out, whereas the product in MW 12 was likely pure fuel. Moreover, the dark appearance of the product around the warehouse may be due to weathering.

2.3.6 Groundwater chemistry

In late August 2005 selected wells were sampled using a flow through cell measuring pH, dissolved oxygen (DO), and oxidation-reduction potential (ORP) by NWRI scientists. The results shown in Table 2.2 indicate that DO in the impacted area was generally less than 0.5 mg/L, which coupled with the negative ORP readings indicate that reducing conditions dominate the groundwater at the impacted area.

Most of the wells at the site had been impacted with free product at one time or other, thus, obtaining reliable dissolved hydrocarbon concentration data is challenging. Given that some of the dissolved hydrocarbon concentrations reported in this paper may have been affected by the presence of LNAPL droplets/emulsions, it is still useful to examine trends in the data. All wells sampled contained measurable volatile hydrocarbon CCME F1 fraction (nC₆ to nC₁₀), and concentrations

ranged from 0-25 mg/L. Interpreted concentration isopleths for the dissolved CCME F1 fraction are shown in Figure 2.16. Note that this and other contour maps included in this report are intended to illustrate spatial distribution of various properties, not to imply that actual patterns of these properties/parameters in the fractured rock are smooth contours. The highest concentrations are currently north and south of the tank farm, where observed free product occurred. In the immediate vicinity of the former tank farm where free product is no longer observed the dissolved concentrations have also decreased.

Interpreted isopleths of the spatial distribution of sulfate in August 2005 shown in Figure 2.17 indicate higher values east of the site and around monitoring well 13. Sulfate concentrations are lower at the impacted zone relative to the background concentrations and lowest furthest down-gradient adjacent to the lake. The sulfate may be derived from oxidation of sulfide minerals that are present in the fractured rock in the vadose zone above the water table. Preliminary analysis of data trends from June through September suggests springtime sulfate recharge in the upper region of the water table; therefore, sulfate mixing is likely to underestimate the extent of sulfate reduction at the site. Figure 2.18 shows concentrations versus time for a number of inorganic chemical parameters from MW14 adjacent to the warehouse. The water is dominated by calcium, sulfate, and bicarbonate, with minor concentrations of magnesium, sodium, potassium iron (II), manganese (IV), and chloride (Appendix D). Temporal fluctuations in calcium were generally mimicked by changes in sulfate. Iron (II) and manganese (IV) had background concentrations in the range of 1-2 mg/L; however elevated concentrations of dissolved iron were measured in the centre of the contaminated area as shown in Figure 2.19.

Samples obtained during the August 2005 sampling event were also analyzed for volatile fatty acids (VFA: acetate, butyrate, propionate, pyruvate) by the NWRI scientists, which are possibly the metabolites of

microbial degradation of PHCs. The results provided in Figure 2.20 show enriched VFA concentrations in the regions with the highest CCME F1 concentrations. This provides further evidence of ongoing biodegradation of hydrocarbons at the site, particularly in the former tank farm area.

The depleted sulfate and increased dissolved iron at the central portion of the impacted area suggest that anaerobic biodegradation of the dissolved hydrocarbons is ongoing. Because the changes in sulfate concentrations are much larger than those in iron, it appears that sulfate reduction is the dominant electron accepting process. However precipitation of iron sulfides in response to the release of sulfide associated with sulfate reduction would also deplete the dissolved iron, so quantification of the contribution of each process is not possible based on the currently available information. Stable isotope analyses by Van Stempvoort et al. (2006) provided further evidence that sulfate reduction may be an important electron accepting process, indicating that the sulfate in MWs near Steeves Lake is relatively enriched in ^{34}S and ^{18}O , as would be expected if sulfate reduction were occurring due to biological processes along the inferred groundwater flow path. A summary of measured groundwater constituents are shown in Appendix D.

2.4 Conclusions

Characterization of spilled fuel in fractured bedrock in a permafrost environment is complex and highly variable. In this study, improved understanding of the behavior of spilled fuel was gained by monitoring water table, depths to ice and product thickness, thermal regime, hydraulic testing, and sampling for groundwater constituents. The measured water table and depth to ice suggests the development of perched groundwater conditions in some of the monitoring wells east of the warehouse and tank farm area due to ice bridging in some of the wells in the spring until the ice had completely melted in late summer. The measured ground temperatures showed that a thaw bulb beneath the

lake extended into wells along the lakeshoreline, and the active layer extended below 10 m over most of the site.

Hydraulic testing of the fractured bedrock indicated transmissivities between 3×10^{-4} and 1×10^{-7} m²/s, with some subsurface zones too impervious to test. The transmissivity varied from borehole to borehole and no spatial correlation was identified.

The measured apparent LNAPL thickness showed spatial and temporal variation. Some wells (i.e. MW 12 and 26 north of the tank farm) had measurable LNAPL year round because they were located where most of the fuel spills occurred, while others showed periodic free product. Increased LNAPL thickness was observed in some of the wells in response to decline in water table in the winter period especially in December of the monitoring year. This suggests that significant volume of mobile LNAPL persists in the fractured bedrock at the site.

The water chemistry suggests that active anaerobic biodegradation with sulfate and iron as the main terminal electron acceptors is ongoing. However, further investigation is required to determine the biodegradation rate and capacity.

Table 2.1 Apparent free product thickness in wells during 2005/06 study

Well	7/23/00	6/23/05	7/21/05	8/11/05	9/12/05	12/12/05	6/15/06	7/6/06	8/6/06
Continuous free product (cm)									
8		2	3	3	6.3		2	2	2
9	51	11	3	16	14	67	76.5	15	17
12	189	4	7	6.5	7.5	501	21.5	1	2
14	3	5	2	1		0.5	51	9	8
15		2	3	14	9.4	9	6.6	8	6.5
17	296	51	26	28	13.8	13.8	47	5	4.5
19	9	9	6	7.5	2.9	3	28.6	21	20.5
26	280	15	7	2	25	368	231.9	26	25
30		3	2	12	6.8	3		18	15.5
Often free product (cm)									
23		8	4	4.5	3.7				
28		13		11	9	8	5.9		
Periodic free product									
10	12				3			1	
13								1	
16					0.5	1.5			
18	226						0.2		
21				2.2	5.2				3.5
29	12	3		4	4.5	4			

Table 2.2 Readings from flow through cell 23/24 August 2005

Well	Temperature (°C)	pH	DO (mg/L)	ORP (mV)
2	7.9	7.5	8.2	-20
4	9.4	6.5	0.4	-85
6	5.4	6.9	0.2	-79
8	4.9	6.6	0.6	-76
10	5.3	7.6	0.2	-136
13	6.3	7.4	0.2	-133
18	7.0	8.2	0.3	-180
20	6.0	6.4	2.0	-57
29	5.4	5.9	0.5	-60

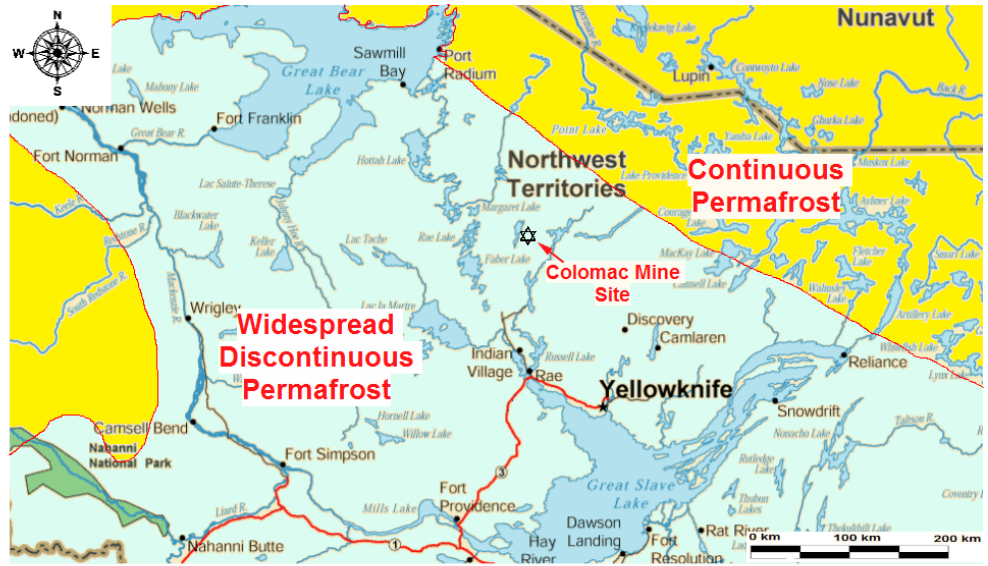


Figure 2.1 Map showing location of Colomac mine site, 220 km northwest of Yellowknife in the Northwest Territories (modified after Smith and Burgess, 2001).



Figure 2.2 North to south trending bedrock outcrop with 3 main sets of fractures: (1) sub vertical fractures, parallel to foliation that includes “slaty cleavage” – includes most of the exposed surfaces shown in this picture; (2) sub-horizontal fractures; (3) sub-vertical fractures that are approximately perpendicular to 1&2.

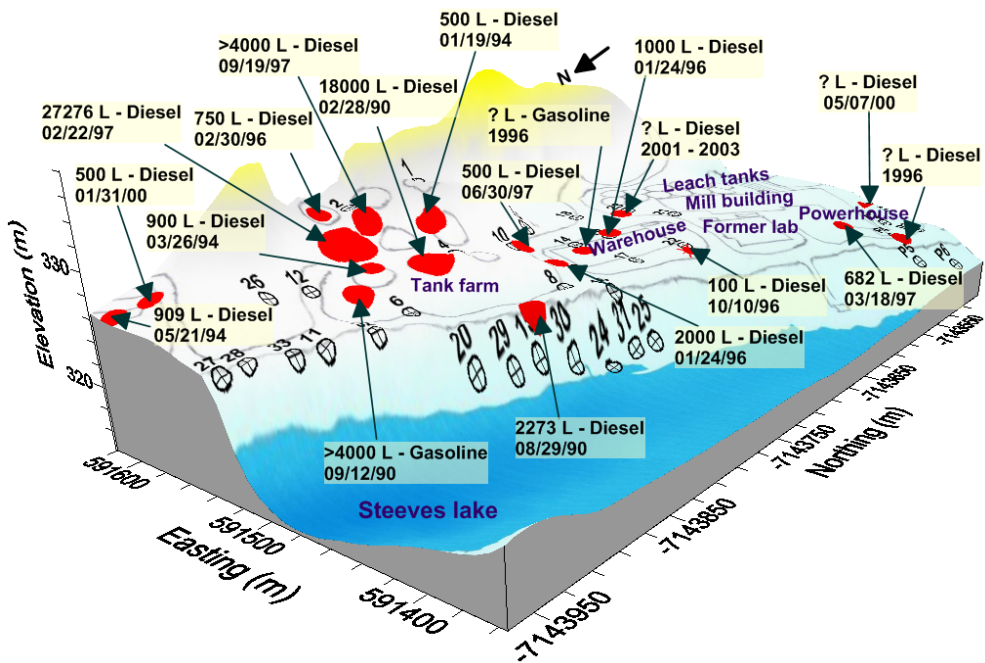


Figure 2.3 Simplified site model showing the approximate locations of historical fuel spillage (modified after EBA, 2001).

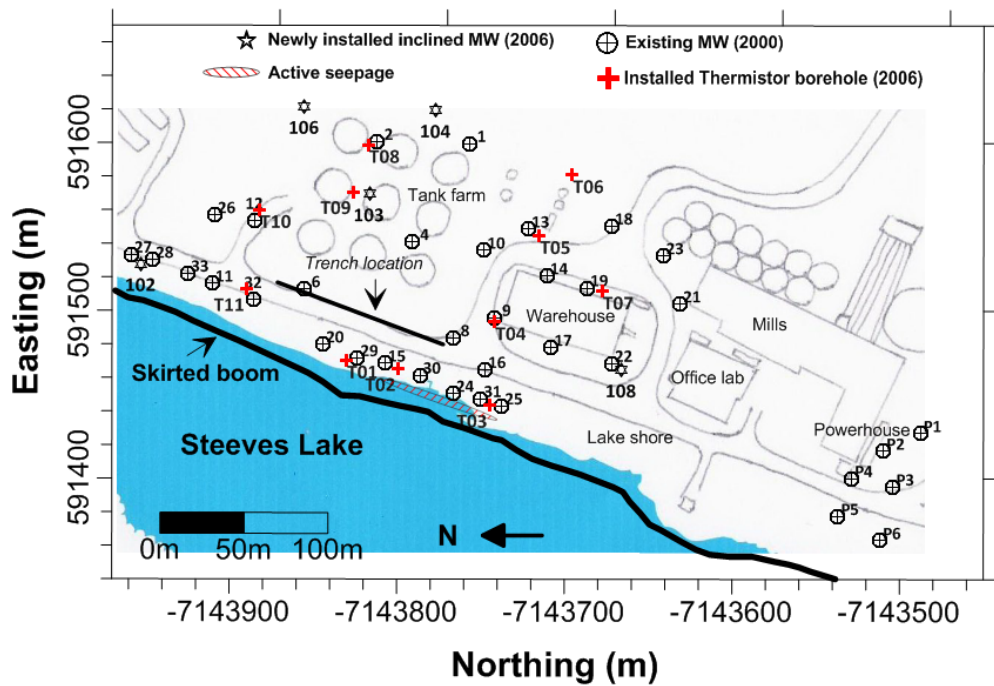


Figure 2.4 Site map showing spatial location of the monitoring wells and thermistor-boreholes.

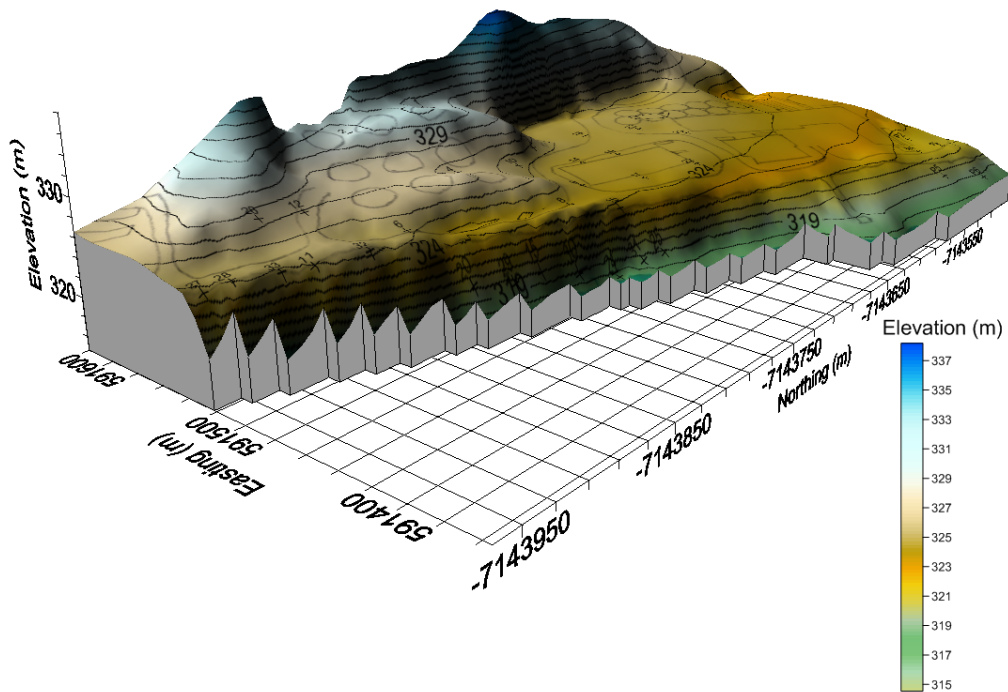


Figure 2.5 Ground elevation contour before overburden removal at the tank farm area.

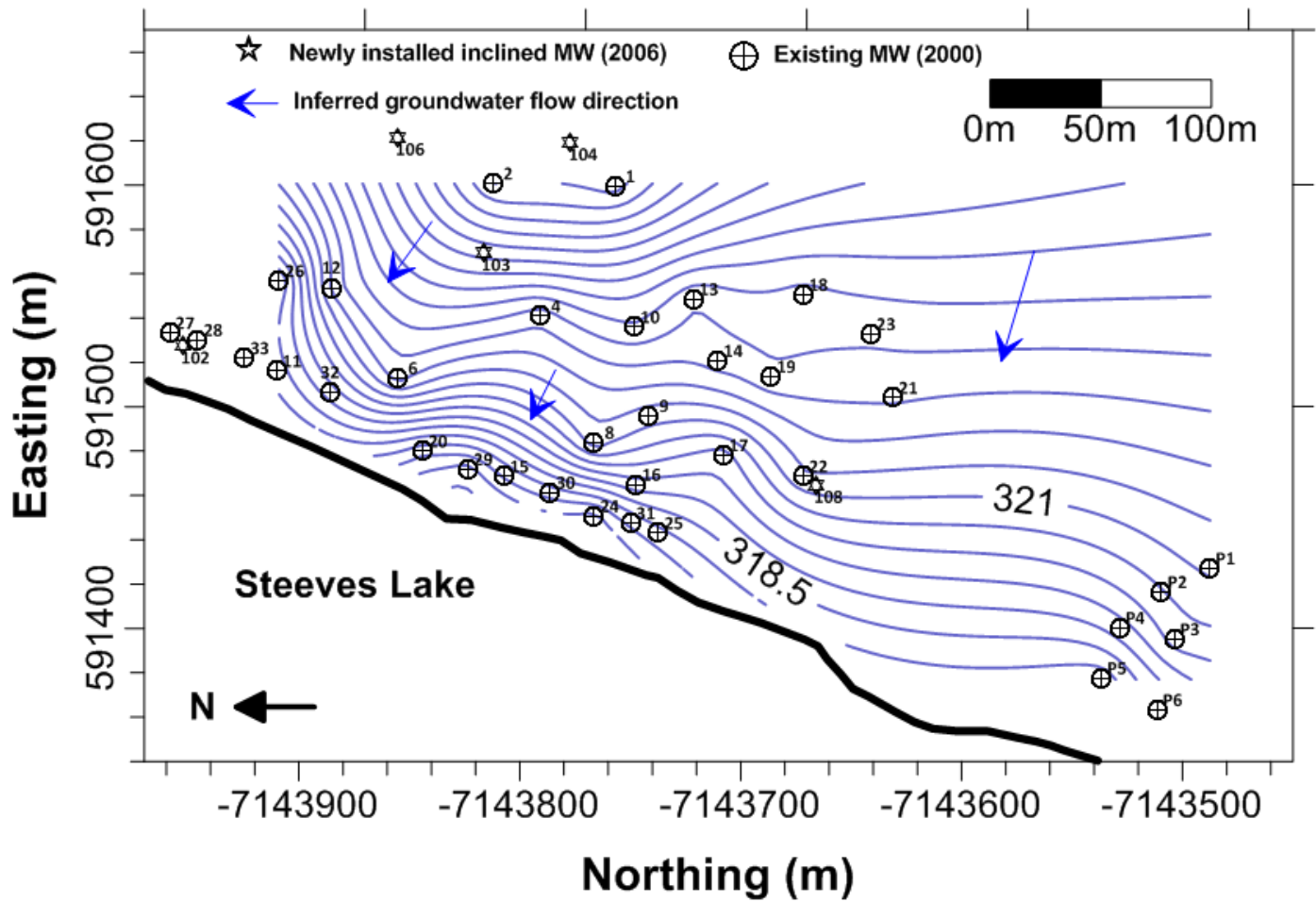


Figure 2.6 Inferred groundwater contours for August 17, 2005.

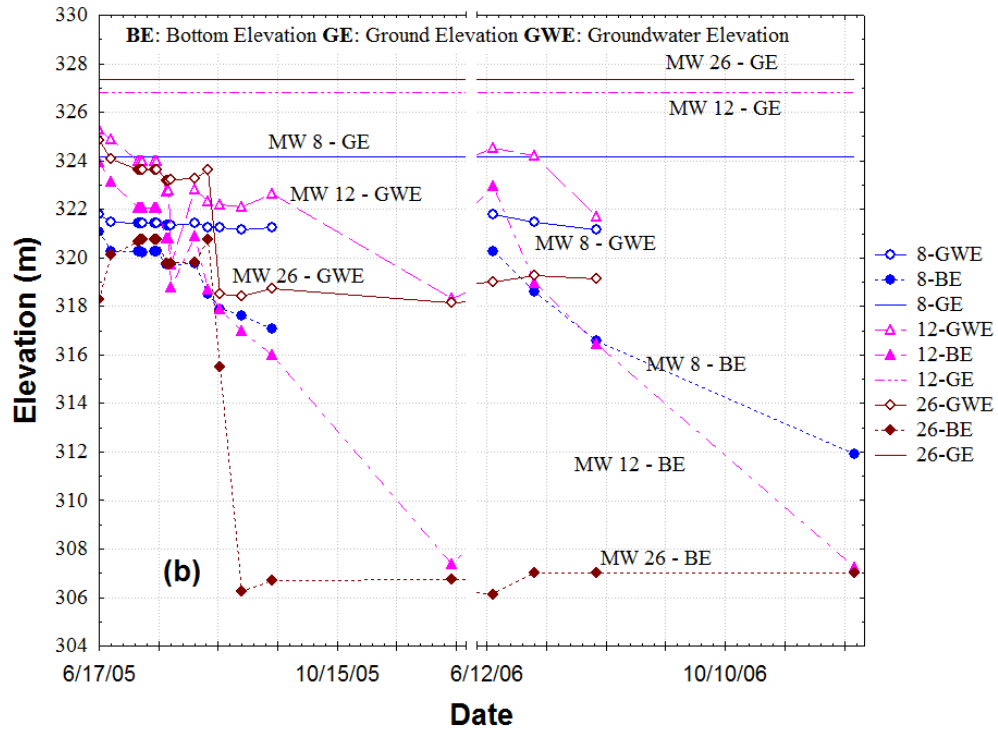
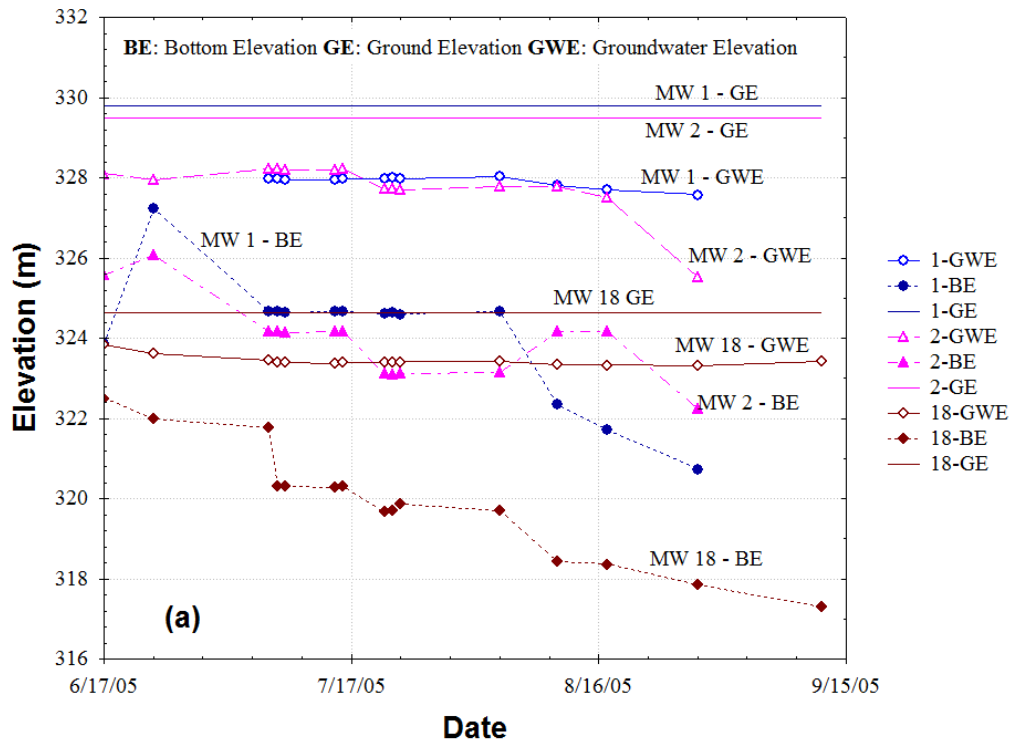


Figure 2.7 Water table and well bottom elevations for (a) monitoring wells farthest upslope and (b) wells at mid-slope.

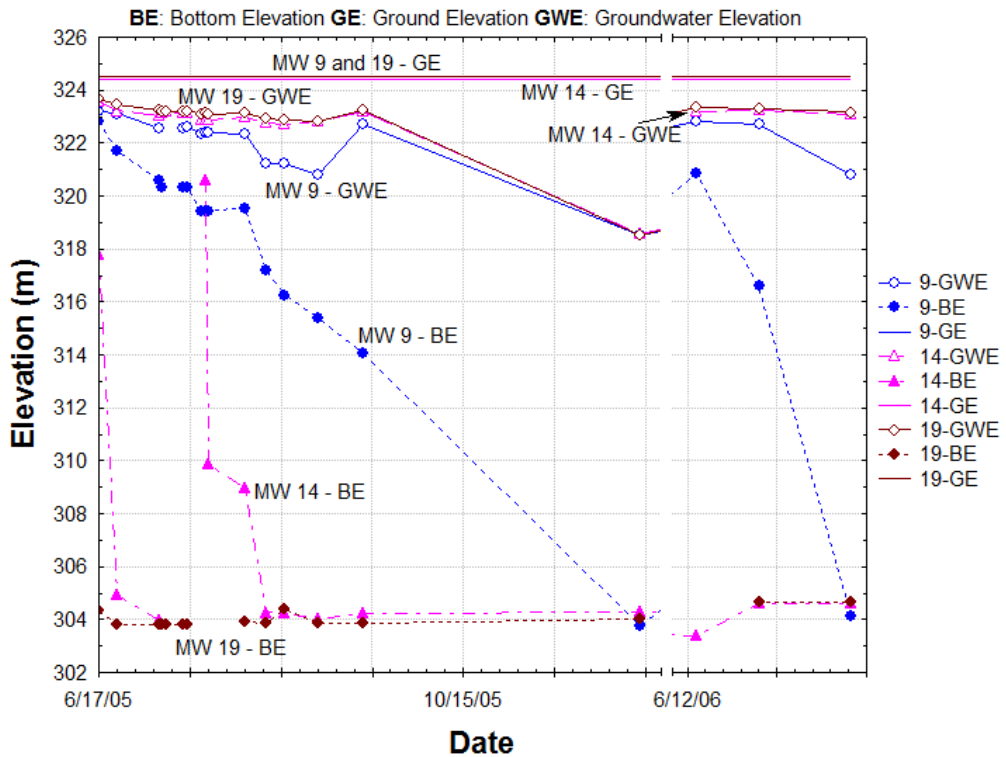
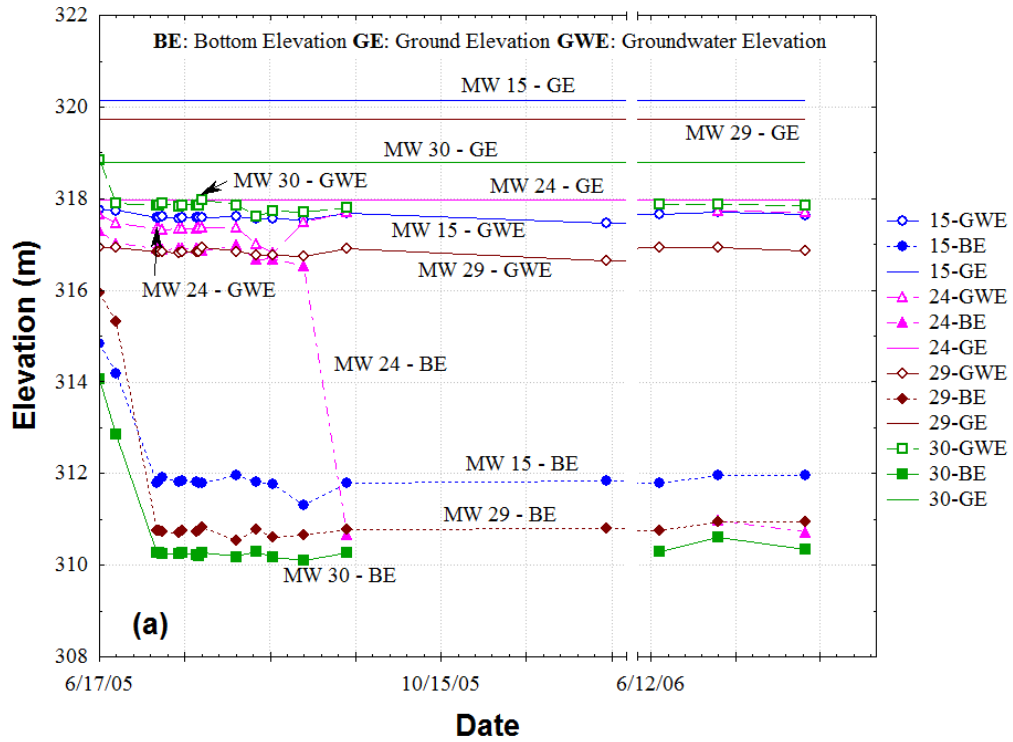


Figure 2.8 Water table and well bottom elevations for (a) monitoring wells near the edge of Steeves Lake, and (b) wells near warehouse.

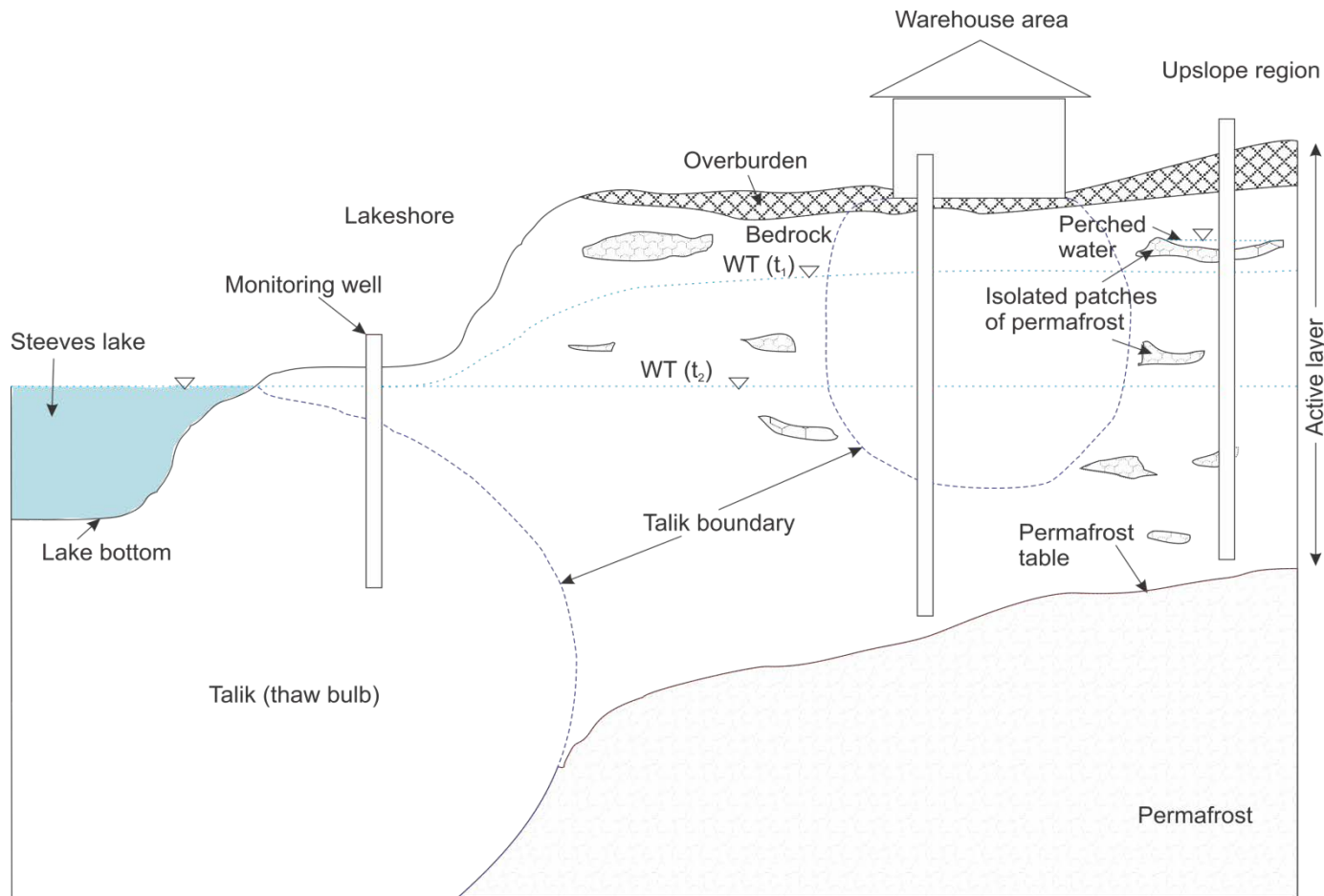
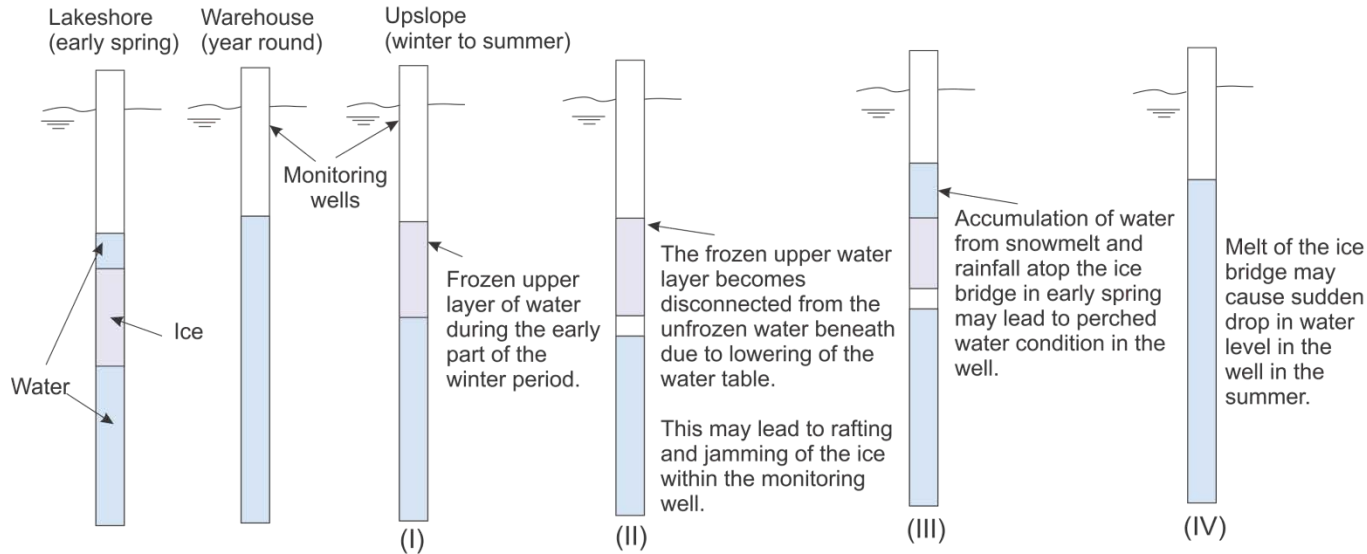


Figure 2.9 Conceptual model of hydrogeological settings at the Colomac mine site to illustrate well-water behavior discussed in Figure 2.10.



Notes:

The water table elevation in the monitoring wells (MWs) at the lakeshore underwent little change from early spring through the summer period but the MWs had a sudden change in their measured depths to bottom (DTBs) as shown in Figure 2.8a. The inferred reason for the sudden change in the DTBs was the presence of an ice-plug within the MW in early spring before melting in the summer period.

At the warehouse, the MWs were mostly thawed all year round. The local heat generated in the building via heating by an electric generator at its southwest corner coupled with lowered water table in the winter period accounted for this behavior.

Some of the MWs at the upslope region at the site showed peculiar behavior as illustrated from (I) to (IV). During the early part of the winter period, the upper section of the water inside the MW is frozen as depicted in (I). The continued lowering of the water table may cause the frozen upper section of the water inside the MW to be disconnected from the unfrozen water at depth as shown in (II). This may lead to rafting and jamming of ice within the MW.

In early spring, water recharge from snowmelt and rainfall may cause accumulation of water above the ice bridged section in the MW, which may lead to perched water condition inside the well as shown in (III). It should be noted that if the perched water condition extend to the permeable formation surrounding the MW, the accumulated water atop the ice-bridge will not drain off. Complete melt of the ice-bridge in the MW in late spring or summer period may cause sudden drop in the water level inside the MW as shown in (IV).

Figure 2.10 Summary of the behavior of water within the monitoring wells at the Colomac mine site.

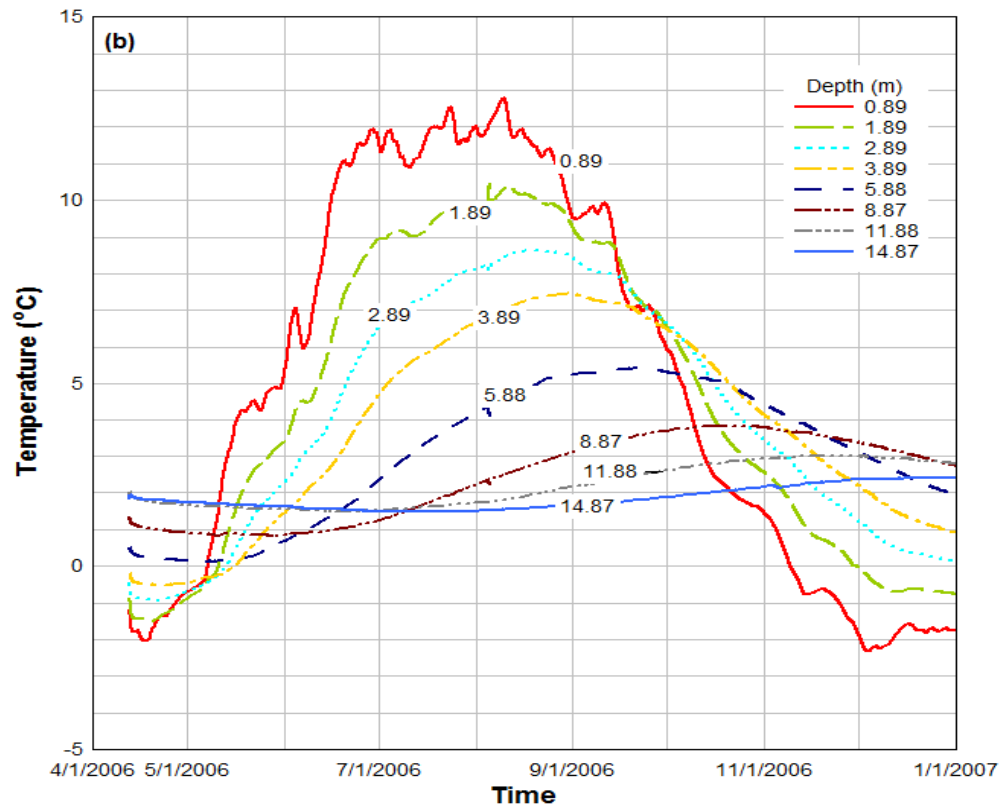
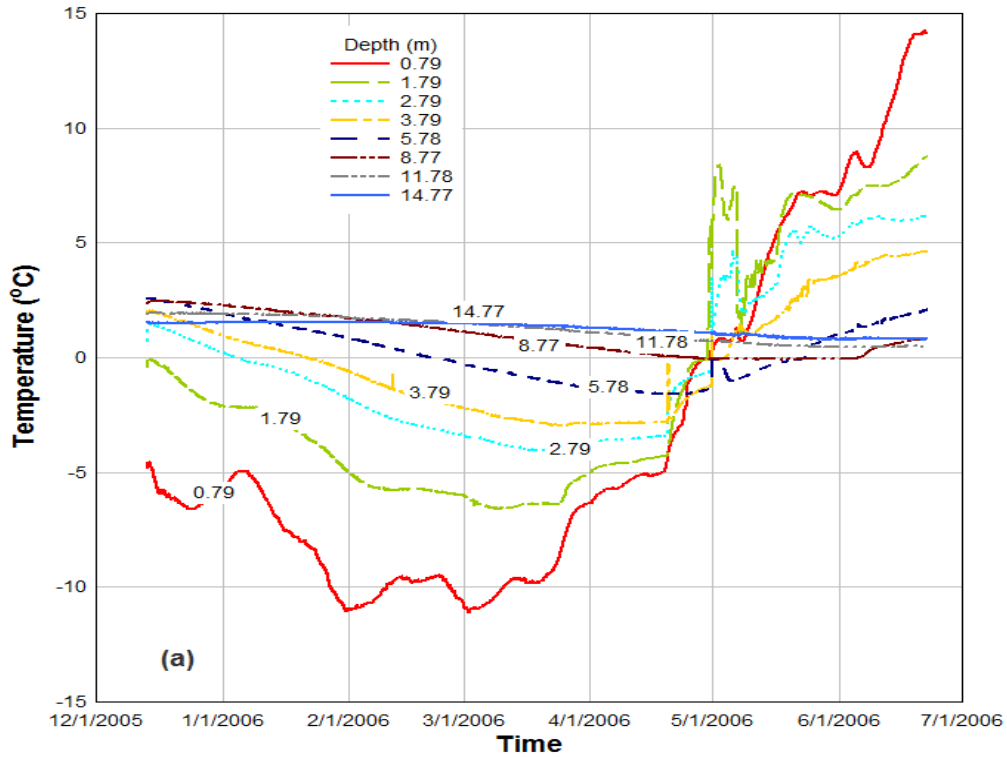


Figure 2.11 Temperature versus time and depth from thermistors (a) from well 22 (adjacent to warehouse), December 05 to June 06, and (b) adjacent to well 29 (along lakeshoreline to north), April to December, 2006.

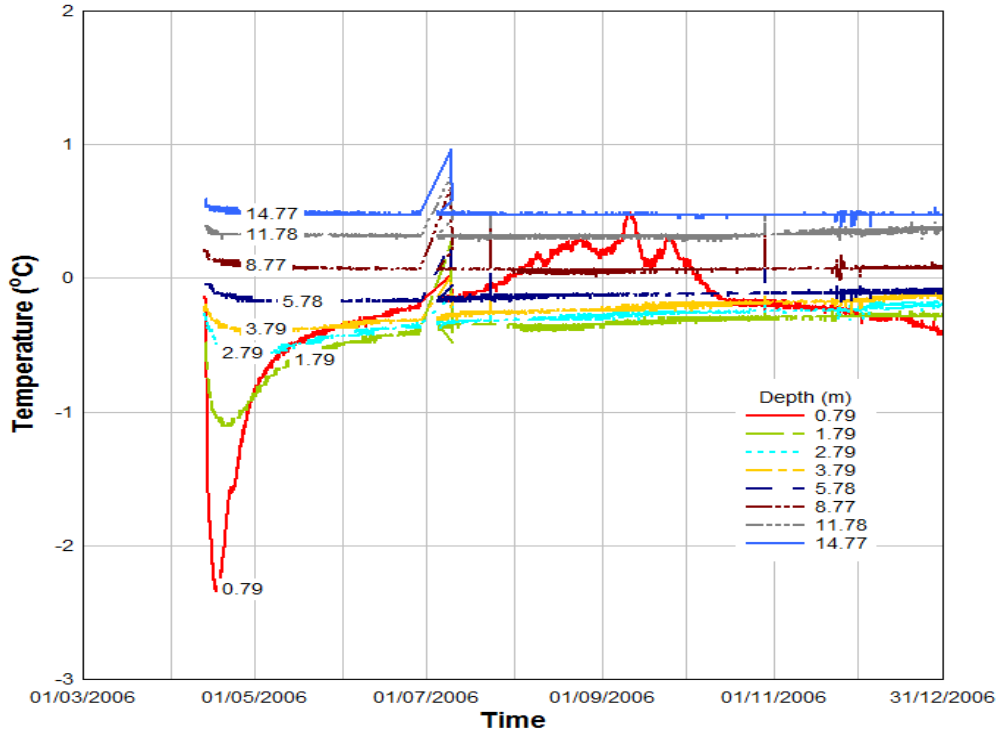


Figure 2.12 Temperature versus time and depth from thermistor adjacent to well 31 (along lakeshoreline to south), April to December 2006.

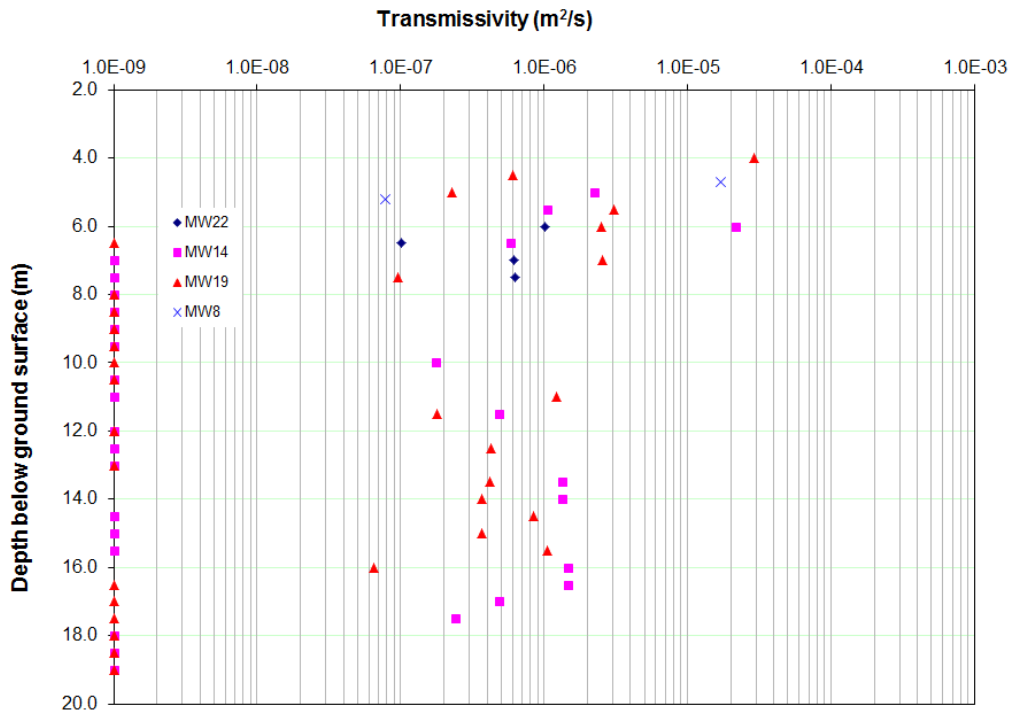


Figure 2.13 Transmissivity calculated from packer tests for wells around warehouse. (Values reported as 1.0 E-09 are transmissivities that were too low to measure with the apparatus used).

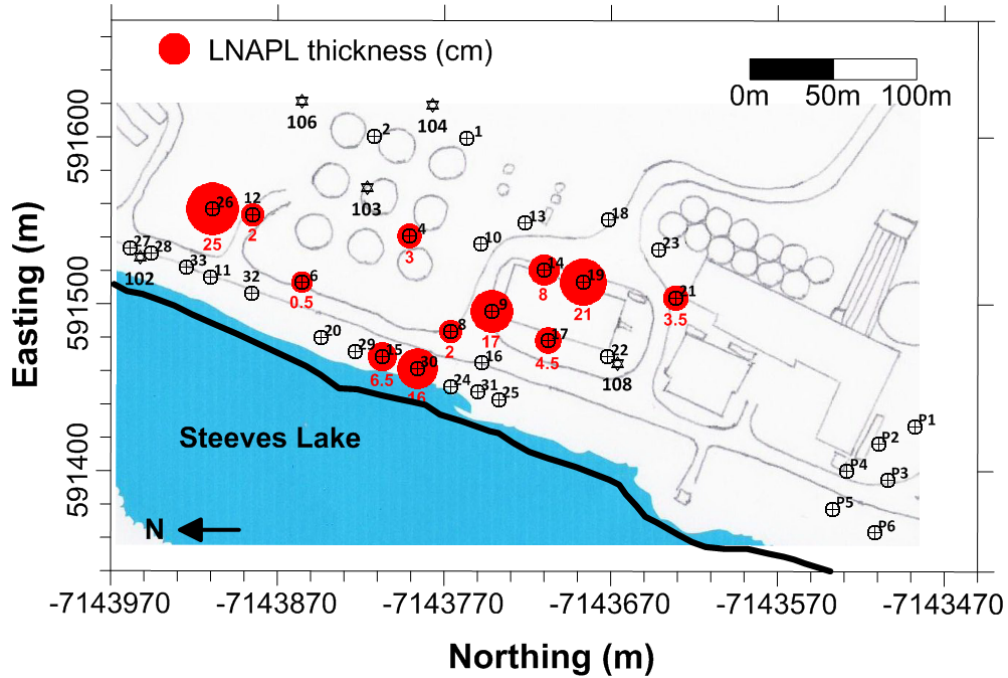


Figure 2.14 Measured LNAPL thicknesses (in meters) for August 06, 2006.

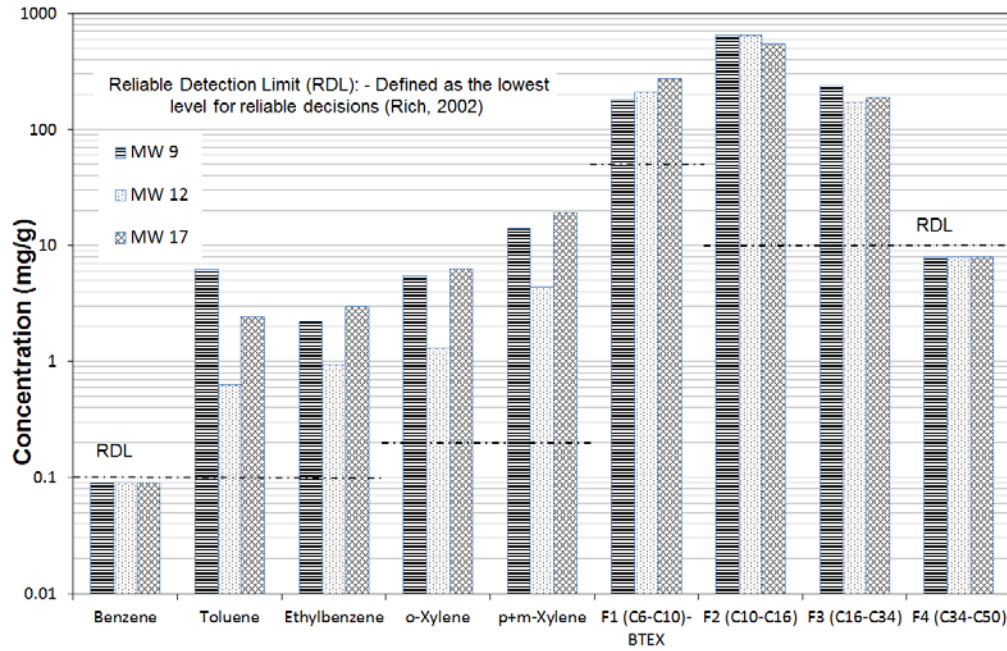


Figure 2.15 Results of analyses of LNAPL from different wells around the tank farm and warehouse.

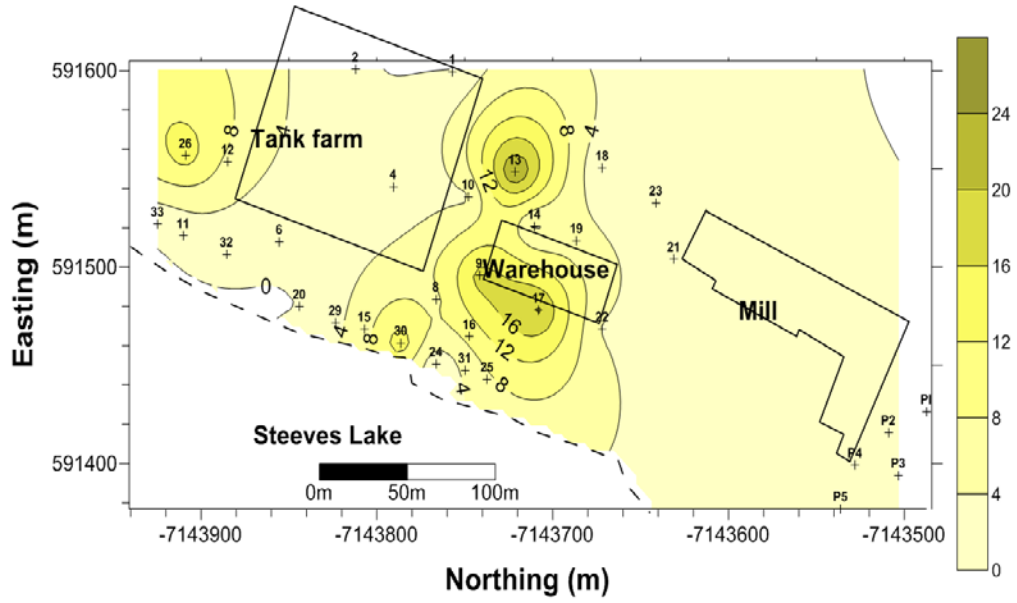


Figure 2.16 Isopleths of dissolved F1 fraction (in mg/L) for August 2005.

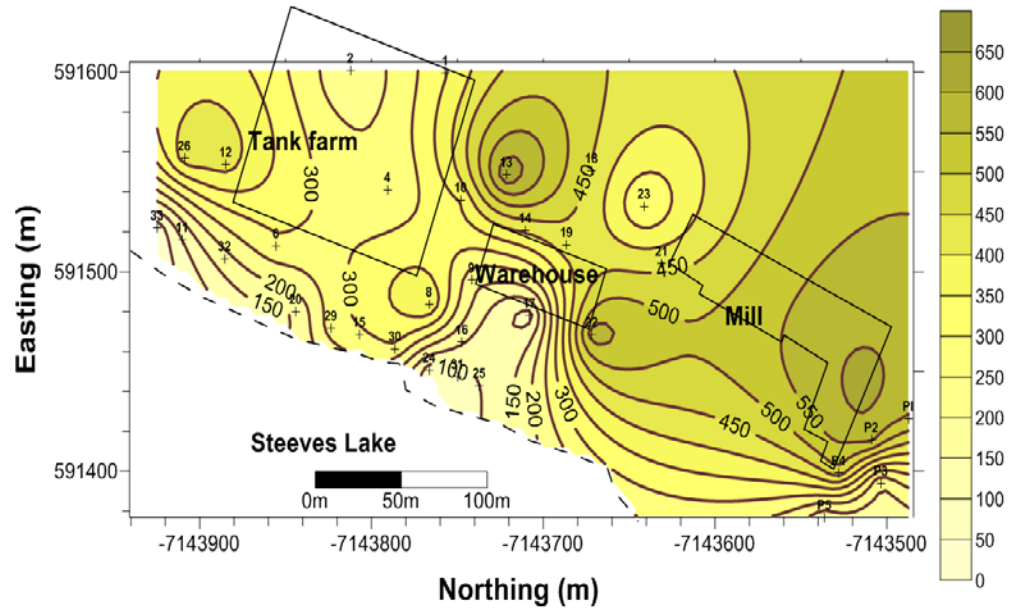


Figure 2.17 Isopleths of measured sulfate concentration (in mg/L) for August 2005.

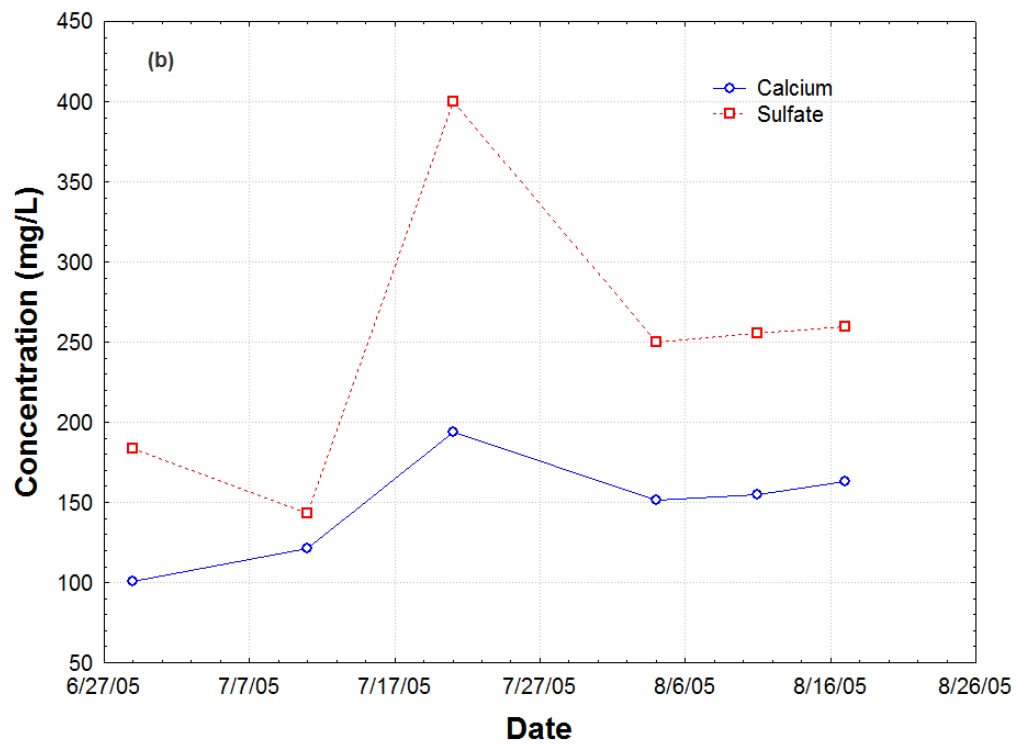
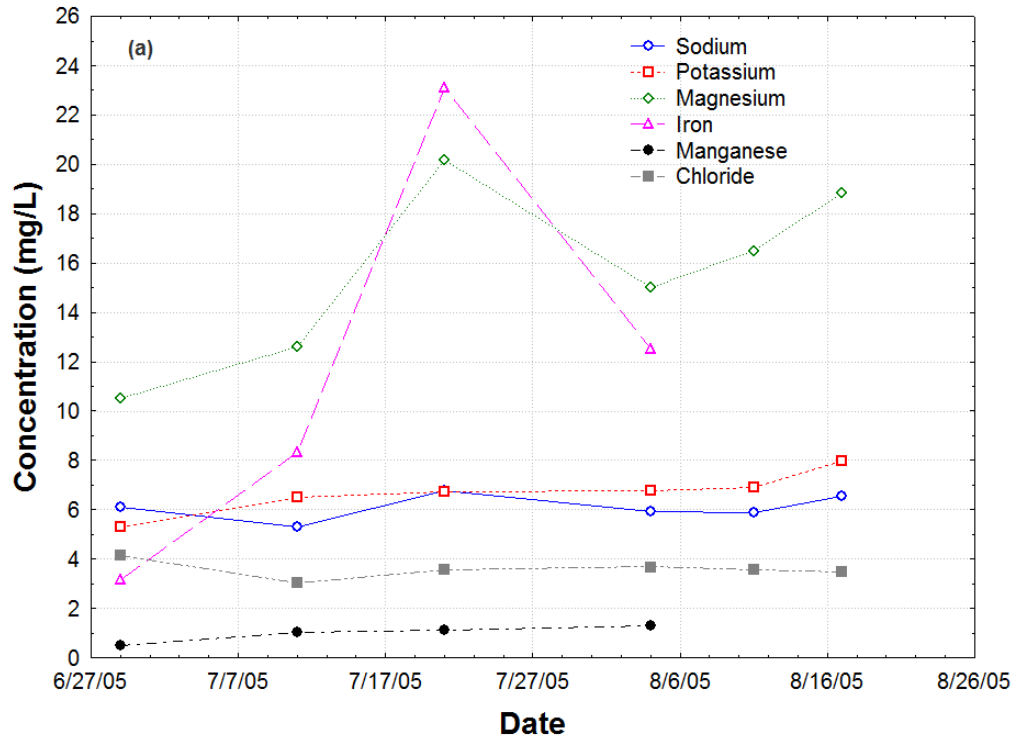


Figure 2.18 Inorganic groundwater concentrations in MW 14 during the summer of 2005: (a) Ions less than 25 mg/L; (b) Major ions greater than 25 mg/L.

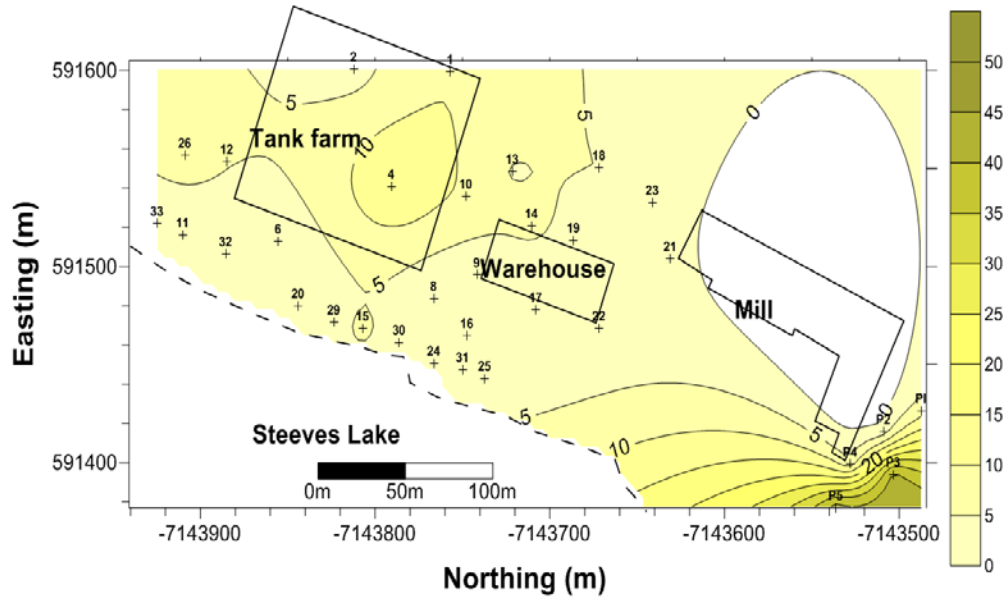


Figure 2.19 Isopleths of dissolved iron concentrations (in mg/L) for August 2005.

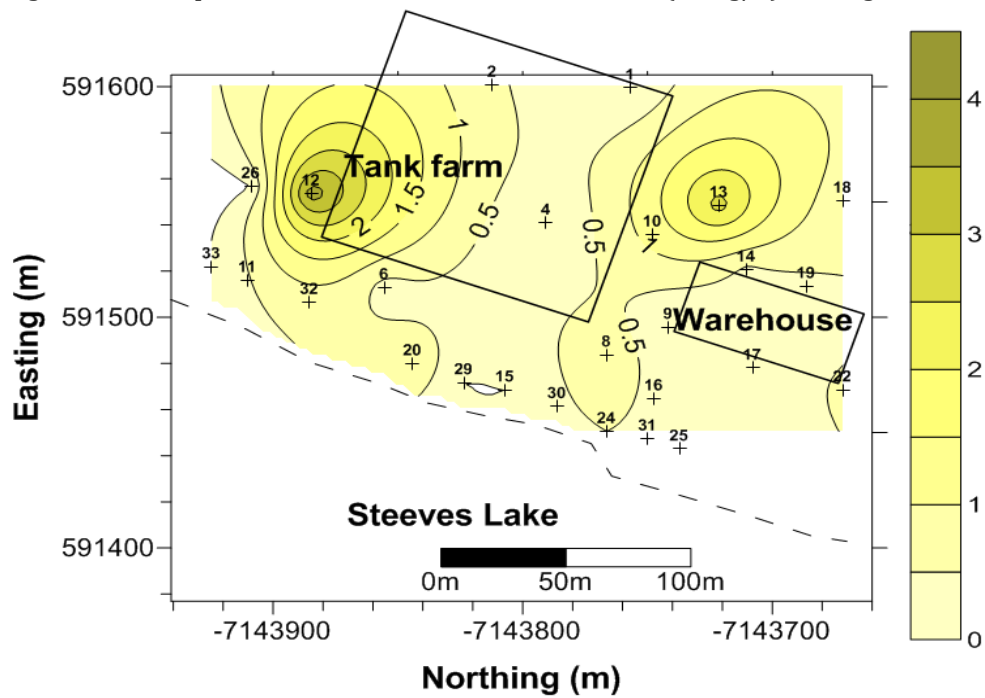


Figure 2.20 Interpreted isopleths for distribution of total volatile fatty acids (acetate + propionate + butyrate + pyruvate in mg/L) detected in monitoring wells in August 2005.

References

- Biggar, K.W., Haidar, S., Nahir, M., Jarrett, P.M., 1998. Site investigations of fuel spill migration into permafrost. *Journal of Cold Regions Engineering*, 12: 84– 104
- Biogenie S.R.D.C. Inc. 2004. Hydrocarbon contamination management. Phase I report – proposed remedial action plan. Report for Tli Cho Logistics and Northern Affairs Canada. 47 p. and appendices.
- CSO – Contaminated Site Office, 2004. Colomac remediation plan. Water license MV2000L2-0018, Indian and Northern Affairs Canada. Yellowknife.
- EBA Engineering Consultants Ltd., 2001. Hydrocarbon assessment, Lakefront and waste oil areas, Colomac Mine, NWT. Report to Deton 'Cho Corporation. Yellowknife, NT. 37 p. and appendices.
- Hearn, K., 1990. The Colomac deposit. Geological Survey of Canada Open File Report 2168, pp. 84–89.
- Konrad, J.M., Morgenstern, N.R., 1980. A mechanistic theory of ice lens formation in fine-grained soils. *Canadian Geotechnical Journal*, 17(4): 473-486.
- McCarthy, K., Walker, L., Vigoren, L., 2004. Subsurface fate of spilled petroleum hydrocarbon in continuous permafrost. *Cold Regions Science and Technology*, 38: 43-54.
- Rich, D.W., 2002. Relational management and display of site environmental data. CRC Press, Florida.
- Schluep, M., Gälli, R., Imboden, D.M. and Zeyer, J. 2002. Dynamic equilibrium dissolution of complex nonaqueous phase liquid mixtures into the aqueous phase. *Environmental Toxicology and Chemistry*, 21: 1350–1358.
- Shelton, K. L., Costello, C.S., van Hees, E.H., 2000. Contrasting styles of Achaean greenstone gold deposition: Colomac gold mine, Canadian

Northwest Territories. *Journal of Geochemical Exploration*, 69 – 70: 303 – 307.

Smith, S., Burgess, M., 2001. The sensitivity of Canadian permafrost to climate warming. Terrain sciences division, Geological Survey of Canada, <http://cgc.rncan.gc.ca/permafrost/pdf/wkshpsensitivity_poster2.pdf> (last accessed June, 2010).

URS Norecol Dames and Moore Inc., 2002. Assessment of hydrocarbons within fractured bedrock at the lakefront and waste oil areas and development of a remedial action plan, Colomac Mine, NWT. Report for Public Works & Government Services Canada. Vancouver, BC., 21 p. and appendices.

Van Stempvoort D., Biggar, K.W., Iwakun, O., Bickerton, G., Voralek, J., 2006. Characterization of Fuel Spill Plumes in Fractured Rock at a Permafrost Site: Colomac Mine, NWT. 2005/2006 Program Progress Report, April 2006, National Water Research Institute and University of Alberta.

Williams, P.J., 1967. Unfrozen water in frozen soils. *Publications of the Norwegian Geotechnical Institute*, 72: 37-48.

3 BEHAVIOR OF SPILLED PETROLEUM HYDROCARBONS AT THE COLOMAC MINE SITE, NWT²

3.1 Introduction

In permafrost environments in Northern Canada where different mining activities occur, spillage of petroleum hydrocarbons (PHCs) from fuel stored in the site is common. Presence of permafrost and deep and long seasonal freezing complicate characterization and cleanup of such contamination. This paper describes the contaminant characterization efforts at the abandoned Colomac mine site, which is approximately 220 km northwest of Yellowknife in the Northwest Territories (NWT) (Figure 3.1), and focuses on the behavior of spilled PHCs at the site. The site was an open pit gold mine that operated between 1990 and 1997. The mine was abandoned and is currently the responsibility of the Contaminants and Remediation Directorate (CARD) of Indian and Northern Affairs Canada (INAC) to mitigate and cleanup the potential environmental impacts.

The site is underlain by strongly foliated bedrock that is composed of metamorphosed siliceous and slaty units (Hearn, 1990). Blasting operations to level the area during construction may have induced fractures in the bedrock surface and near blast faces. The fracture pattern at the site is complex (Chapter 2). Bedrock outcrops at the site appear to be generally massive with localized weathered and fractured surface. Three major fracture sets were identified at the site, which include a sub-horizontal fracture set and two sub-vertical sets (Chapter 2). The overburden was approximately 0.2 m thick at the east extent of the site, thickening to approximately 4.6 m west of the site. Most of the

² A version of this chapter has been published.

Iwakun, O., Biggar, K., 2007. Behavior of spilled petroleum hydrocarbon at Colomac mine site, NWT. Proceedings of 60th Canadian Geotechnical Conference and the 8th Joint CGS/IAH-CNC Groundwater Conference, Ottawa, pp. 2106-2114.

overburden was rock fill that had been placed to level the site for the mine operations. Close to the edge of the lake there is a steep drop in ground elevation of approximately three to four meters. The structure of the bedrock may influence the migration of free phase PHCs, as light nonaqueous phase liquid (LNAPL), in the subsurface. The fault zones and bedding planes may be disconnected at different stratigraphic units in the subsurface, thus causing local flow or focused infiltration in some areas.

Between 1990 and 2003, there were approximately 24 reported releases of PHCs in and around the main tank farm area as shown in Figure 3.2 (EBA, 2001). Two major fuel spillages include 18,000 L and 27,276 L in 1990 and 1997 respectively as shown in Figure 3.2. Most of the spillage occurred in the storage tanks at the tank farm due to leakage of the tank and subsequent migration into the subsurface due to a damaged plastic membrane liner. No pooled free product was identified during attempted recovery of spilled fuel on both occasions. PHC sheen was noted along portions of shoreline on Steeves Lake after the 1990 spillage (EBA, 2001). Subsequent investigation revealed the presence of free product atop the supra-permafrost water table.

A five-meter deep interceptor trench was excavated to the base of the fill/top of bedrock along the west berm of the tank farm between the tank farm and the lake after the initial release in 1990, to mitigate the PHC migration. Though the trench intercepted some free product flow, another portion continued to flow towards the lake. A continuous skirted boom was also installed along the Lake's shoreline in the early 1990s. Oil adsorbent pads were used within the skirted boom and were periodically collected, treated and incinerated on site.

The active seepage observed at the lake's shoreline led to the installation of monitoring wells (MWs) throughout the site as shown in Figure 3.3 to monitor the thickness and distribution of the free product or free product in the subsurface (EBA, 2001). The MWs were cased through the overburden, leaving the rock exposed beneath the casing. Monitoring

in 2000 (EBA, 2001) showed an average LNAPL thickness of 1.5 m over the impacted area with the highest thickness being 15.4 m in one of the MWs (MW 11) in the tank farm area. Later assessment of the LNAPL within the fractured bedrock in 2001 (URS, 2002) showed lower average LNAPL thickness of 0.4 m with a maximum thickness of 1.6 m in one well. The assessment concluded that the majority of the spilled fuel had dissipated and that PHC seepage being observed along the lakeshoreline at that time was the remnant of the spills. From the evaluation of fracture density in the bedrock, it was inferred by URS (2002) that only small amounts of PHCs in the fractures exist and held by capillary tension, thus, immobile. However, recent studies showed that though permafrost may impede water movement, it might not completely curtail flow of PHCs as LNAPL (Biggar et al., 1998; McCarthy et al., 2003).

Additional measures taken at the site to mitigate the LNAPL migration and reduction of source concentration included the removal and treatment of contaminated overburden from the tank farm area in 2004-05 using on-site biopile treatment, and the construction of a frozen soil interception barrier. A frozen core trench was installed in the fall of 2004 through the winter of 2005 between MW #6 and #8 (Figure 3.3) to a depth of 5 m. The trench was lined with a geo-membrane, backfilled with layers of saturated soil and allowed to freeze, thereby creating a frozen soil barrier. Sumps were placed at each end of the wall for monitoring and removal of free product and water. Significant volumes of water were removed from the sumps in 2005. From 2000 to date, there was periodic free product removal from the wells. However, there was no data on the amount of free product recovered from the wells from when recovery started until the current recovery efforts. Despite these measures, free product seepage persisted at the site.

The understanding of the distribution and mobility of spilled fuel at the site is further complicated by the presence of a heated warehouse southwest of the tank farm, which has generated a large thaw bulb in the

permafrost bedrock. This influences the local thermal regime and may affect the contaminant migration. Therefore, a study of the thermal regime of the site, hydraulic conductivity of the fractured bedrock, its interconnectivity, and the groundwater flow pattern is necessary to understand and mitigate contaminant movement to Steeves Lake. It is also necessary to understand the current distribution of both free product and dissolved PHC contamination, as well as the distribution of other dissolved chemicals to evaluate the potential for natural attenuation as a remedial strategy at this complex site. However, due to multifaceted components involved in the characterization of this site, this paper is focused primarily on the LNAPL distribution and behavior at this site, which is a component of the joint study by the University of Alberta Geotechnical Centre and Environment Canada to achieve this understanding.

3.2 Field Work

Since commencement of this study in June 2005, several steps have been taken towards characterizing this site. Some of the steps taken include:

- Monitoring of depths to free product, water, and bottom ice in existing monitoring wells (MWs);
- Thermistor string installation and drilling of additional MWs;
- Groundwater sampling;
- Bedrock coring;
- Borehole imaging; and
- Hydraulic testing of existing MWs.

Some of these activities have been discussed in Chapter 2 and will be excluded from discussion in this paper. However, highlights of previous and ongoing field activities are summarized below including inferences drawn from previous activities.

A. Depths to water and refusal (i.e., well bottoms) were manually monitored using interface probe to determine the groundwater flow pattern, seasonal fluctuation, and impacts of seasonal freezing and thawing on the groundwater regime. Bottom ice in monitoring wells (MWs) was inferred where depths to refusal were less than the recorded bored depth of the MW. Whenever the MW bottom was equal to the recorded depth, permafrost absence or MW bottom above the permafrost table was inferred. Based on the results of these measurements, the inferred flow direction of the groundwater was westward as shown in Figure 3.4. However, ice bridging was noticed in some instances causing pooling of water above the bridged zone in the thaw season, thus, leading to perched groundwater condition. Beneath the bridged section, it is possible for groundwater to flow. Initially, it was unknown if the perched groundwater condition was a local phenomenon in the MW or occurs more widely in the formation. Furthermore, borings at the site showed that perched groundwater condition occurred in the formation around the tank farm area due to pooling of water atop isolated patches of permafrost as illustrated in Chapter 2.

B. Depths to free product were measured along with the depths to water and well bottom to determine the apparent distribution of mobile LNAPL in the formation, which is crucial for LNAPL recovery and remediation of the site. The measured apparent free product thicknesses in some of the MWs are shown in Table 3.1. Measured thicknesses were higher in monitoring wells 12, 17 and 26. The free product thicknesses in MW 12 and 26 increased in the winter but appeared stagnant in the summer. It should be noted that Table 3.1 does not incorporate periodic removal of free product because removed free product volumes were not consistently measured at the site.

C. Solinst Levelloggers and barologgers were installed in some selected wells (i.e. monitoring wells P1, P3, P5, 1, 15, and 28) to measure the

temporal groundwater and temperature fluctuation. The results were corroborated by manual measurements at the site.

D. Eleven boreholes were drilled between April and June 2006. These boreholes had dedicated thermistor strings installed in them. The locations of the thermistor strings are shown in Figure 3.3. Additional MWs were installed in June 2006 and March - April 2007. These MWs were installed to obtain additional information to characterize the site and gain more insight on LNAPL behavior at the site. The MWs installed in March - April 2007 were designated as recovery wells, and were drilled by rotary coring. Approximately 1.5 m lengths of bedrock core were obtained for each trip-in. The preliminary examination of the bedrock cores suggests that near vertical, sub-vertical and sub-horizontal fissures are the dominant fractures, and hydrocarbon impact is limited to the upper 7 m of the bedrock.

E. Hydraulic tests using sets of packers spaced at 0.57 m were performed in selected MWs (i.e., P1-P6, 8, 14, 19, and 22) to determine transmissivities at discrete intervals. The tests were conducted in collaboration with National Water Research Institute (NWRI) scientists from Environment Canada. The hydraulic test method is given in Appendix A. The test results suggested that the upper 7 m of the bedrock are fractured with transmissivity varying from 3×10^{-4} to 6×10^{-7} m²/s, with higher values near the bedrock surface. This amounted to hydraulic conductivities of approximately 5×10^{-4} and 1×10^{-6} m/s for the 0.57 m packer interval assuming horizontal flow. However, the transmissivity varied from borehole to borehole, with no strong spatial relationship (Chapter 2).

F. In September 2006, a Well-Vu borehole camera system was deployed to the site and used for borehole imaging. The aim of the borehole imaging was to identify zones of major fractures, correlate the observed fractures with the hydraulic test results, and possibly observe locations of seepage of petroleum hydrocarbon within each MW. A sample of the

image obtained is shown in Figure 3.5 with notes on the observed fracture pattern. Though the camera system is compact and easy to deploy, images are poor within oil-smear zones due to reflection of light. Moreover, given the method of drilling of most of the wells (percussion hammer drilling), the identified major fractured zones cannot be correlated to the transmissive zones due to spalling and damage around the fractures at the borehole wall. The borehole imaging cannot give indications of fracture interconnectivity nor how deep the observed fractures extend into the bedrock. The observed fractures may be artifacts of well scarring associated with the drilling.

G. Product recovery test involving removal of free product from the MWs and monitoring its recharge into the MW over time was conducted in the MWs that had historical thick LNAPL layers (i.e. MWs 12, 17, and 26). The test was conducted to evaluate the feasibility of removal of free product from the site and its behavior underground. The test procedure is discussed in the next section.

H. Inorganic and organic constituents of the groundwater were sampled periodically using dedicated bailers and peristaltic pump. The samples were analyzed in the laboratory to determine the extent of contamination, active geochemical processes, and geochemical indicators for natural attenuation assessment. The groundwater geochemistry is discussed in Chapter 5. The background geochemistry presented in Chapter 2 identified metabolic by-products of fuel biodegradation such as volatile fatty acid in the groundwater samples. The geochemistry suggested that the groundwater was undergoing anaerobic reduction with sulfate and iron as the main terminal electron acceptors (TEA).

3.3 Product Recovery Method

An overview of the recovery test method and the intended usage of the results are summarized in Figure 3.6. After dipping the MW using an interface probe, only the free product is bailed out using a modified bailer

system. In the modified bailer, the intake was shifted to the top of the bailer and additional weight was added to its bottom so that it can submerge deep enough to allow for free product skimming. When the apparent free product thickness in the MW is less than 4 cm, the MW is allowed to sit for 2, 5, 30 ... minutes as shown in Figure 3.6, and the depth to product (DTP) and depth to water (DTW) are plotted over time (Figure 3.7). After plotting the data, the distance between the LNAPL depth and the point of inflection, which corresponds to the free product entry point, is determined and used to estimate the amount of LNAPL in the formation as shown in Figure 3.7 (Testa and Winegardner, 2000). From the DTP and DTW, the product thickness (PT) is determined and used to compute average recovery or recharge rate to desired recovery efficiency. EPA – Environmental Protection Agency (1996) published a guideline document that contains application of this method including sample calculations and other methods in evaluating recoverability of free product.

3.4 Temperature Monitoring

To understand the influence of the thermal regime on contaminant distribution, Solinst level loggers, barologgers, and thermistor strings were initially installed in some of the wells to corroborate the monitored depths to water and bottom-ice at the site between June-2005 to April-2006 as discussed in Chapter 2. Between April and June 2006, new boreholes with dedicated thermistor strings were installed across the site as shown in Figure 3.3. Each thermistor string consists of eight sensors at specific depths with battery operated data logger. The boreholes were backfilled with bentonite pellets and water after installation. Laboratory sensitivity testing of the thermistor strings found that the readings from the thermistor strings are within $\pm 0.2^{\circ}\text{C}$ of actual melting point of ice at 0°C .

3.5 Results and Discussion

This section will be limited to the analyses of activities related to LNAPL behavior at the site. The section is sub-divided into five sections: namely, LNAPL monitoring, temperature profile, free product recovery, LNAPL mobilization mechanisms, and conceptual model of LNAPL movement.

3.5.1 LNAPL monitoring in wells

Measured product thicknesses in selected wells are shown in Table 3.1. In some instances product thickness increased, in other instances it decreased, and in some instances it remained nearly the same, showing that the distribution of product in the fissured rock is very complex. Wells #12, 17 and 26 had the highest apparent thickness of free product in 2005/06 as shown in Table 3.1. Apparent LNAPL thickness in MW 12 increased in the winter of 2005/06 period. MW 26 also showed similar pattern to MW 12, but the observed LNAPL layer in December 2006 was much thinner than in Dec 2005, which may be attributed to the ongoing recovery of free product as discussed in the paragraph below. MW 17 did not seem to follow a seasonal pattern, varying inconsistently from 3 cm to 140 cm.

In June (2006), over 37 liters of free product were removed from MWs 9, 12, 17, and 26 combined as shown in Table 3.2. The distribution of the measured LNAPL in the MWs (for August, 2006) as shown in Figure 3.8 suggests some of the MWs have recharged (i.e., MWs 26, 17, and 9) after free product recovery in June. Figure 3.8 also shows that the distribution of free product across the site is spatially variable, so the actual distribution and mode of free product movement at the site requires further investigation. Previous studies had speculated that the flow of LNAPL was predominantly within the overburden fill or atop the bedrock surface, and that there should be little flow in the fissures in the bedrock (URS, 2002). Site inspection in 2005 and 2006 showed that some

of the well casings used to maintain the well opening through the overburden were loose (Chapter 2). Monitoring well logs by EBA (2001) showed that the well casings were secured to at least 0.4 m into the bedrock. Thus, the loosening of the well casing implied that the seal between the casing and the bedrock was compromised in some of the MWs, which might have allowed free product to flow down into the MW from the bedrock surface. However, there is evidence that the fissures in the bedrock in some locations contain significant free product.

Shown in Figure 3.9 and Figure 3.10 are the measured groundwater elevations and product thicknesses in selected MWs at the site. MWs 12 and 26, for example, had free product thicknesses of 5 and 18 cm in June 2005 when the depths to water were 1.6 m and 2.7 m, respectively. In December 2005 when the water depths were 13.6 m and 13.3 m, the product thickness in MWs 12 and 26 had increased to 501 cm and 368 cm, respectively (Figure 3.9 and Figure 3.10). Because the contaminated overburden had been removed during the summer of 2005, this increased thickness of free product in December indicated that as the water table dropped in this region, there was free product drainage from fissures around the MWs. These data also imply that portions of the bedrock likely contain significant free product, and transport within the fissures may be occurring over portions of the site. In December 2006, MWs 12 and 17 had free product thicknesses of 209 cm and 140 cm, respectively, whereas, MW 26 had only 21 cm of product at the same time (Table 3.1). The decreased LNAPL thickness in MW 26 in December of 2006 compared to that of 2005 might be attributed to free product recovery from this well between September and December in 2006.

3.5.2 Temperature profile

Rising and falling of the water table occurred in the spring and winter period respectively as discussed in Chapter 2. Shown in Figure 3.11 is the temperature profile in MW 12 north of the tank farm area

where most of the fuel spill occurred. Other temperature profiles from the installed thermistor strings at the site are included in Appendix C. Discussion of temperature profile presented in Chapter 2 relates to the groundwater regime at the site. In summary, the thermistors locations with a talik (or thaw bulb) beneath them, and those with the active layer extending below 14.8 m are summarized in Table 3.3. Thermistor string T03 near MW 13 upslope of the site was frozen at 11.8 m depth all year round (Appendix C), in essence, supporting the conceptual model of hydrogeological settings presented in Chapter 2.

The thermistor data show that the maximum temperatures with depth are later in the year with increasing depth. This resulted in complete reversal of peak temperature at depth from the spring through the winter period except T03 near MW 31 at the shoreline of Steeves Lake. This time delay in maximum temperature is due to thermal conductivity and volumetric specific heat effects. As the surface temperature increases in the spring, the ground temperature near the surface starts to rise, however at depth, the freezing front progresses downward at a slower rate due to the mass of cold rock above. Similarly, as winter approaches, the surface temperature decreases, and the ground temperature gradually decrease from the surface downward but the thaw front at depth still progresses downward at a slow rate due to the heat contained in the rock mass above.

The temperature profile in T03 (Appendix C) is nearly constant with time due to vegetative organic mat cover over the ground surface in this region. The vegetative cover extended over most of the shoreline of Steeves Lake. The vegetative mat insulates the ground and prevents thermal penetration due to its very low thermal conductivity

when dry in the summer. It also contains a significant amount of ice so has a high latent heat component which retards thaw in the spring.

Having established in Chapter 2 that the upper section of the bedrock is highly fractured and contamination is limited to the upper fractured section of the bedrock (see Chapter 4), it seems the fuel contamination at this site is limited to the active layer of thermal fluctuations at the site. According Barnes and Chuvilin (2009), cyclic freeze thaw may promote downgradient of LNAPL and influence the distribution of disconnected petroleum blobs. Biggar and Neufeld (1996) postulated that fissures induced during freezing may enhance downward migration in a porous media subjected to cyclic-freeze thaw. This study postulates that this mechanism plays a role in mobilizing LNAPL at the site, and Chapter 6 explores the feasibility of occurrence of this mechanism.

3.5.3 Free product recovery

In June 2006, product recovery test was performed on MWs 9, 12, 17, and 26. Approximately 24 liters of LNAPL were recovered from MW 26. Much smaller volumes of LNAPL were recovered from MW 9, 12, and 17 (i.e., 7.6, 4.6, and 1.4 liters respectively). In June 2006, the LNAPL layer in MW 12 was very thin so little recovery was possible and the hypothesized plot shown in Figure 3.7 could not be generated. The product recovery response over time in MW 26 in June 2006 is shown in Figure 3.12. The data for MWs 9, 12, and 19 are shown in Table 3.2. The results showed that no measurable recharge of LNAPL into the MWs occurred over the test period. The insignificant free product recharge may be due to either one or a combination of the following. (1) Slow recharge rate, (2) the mechanism transporting the free product into the MW was not active at the time, (3) the free product was locked (or trapped) within the fractured bedrock, or (4) the cumulative removal of

free product and removal of overburden have greatly reduced the free product within the vicinity of these MWs in the bedrock.

The LNAPL recharge rate to the MWs may be slow if the LNAPL is locked in by capillary suction in the unsaturated zone in the bedrock as suggested by URS (2002). LNAPL may have smeared the upper section of the bedrock due to water table fluctuations over time, thus, becoming less mobile.

In December 2006, there was little LNAPL in MW 26 as shown in Table 3.1, so no product recovery testing could be conducted. A recovery test performed in MW 12 at that time (Figure 3.13) showed no measurable recharge into the well over two days, in agreement with previous tests. This suggests that free product mobility is very limited, and/or that possibly the volume of free product remaining in the formation is small, or the underlying mechanisms mobilizing free product at the site are inactive. A coring program was conducted in March – April 2007 and the analyses of the bedrock cores suggest that across the site, the petroleum impacted zone is limited to the upper section of the bedrock (as discussed in Chapter 5 of this thesis).

3.5.4 LNAPL mobilization mechanisms

Observations of sheen and seepage of LNAPL at the shoreline of Steeves Lake at the site were always in response to high precipitation event and when the water table is elevated. Thus, the seepage of LNAPL at these locations may be attributed to remobilization of trapped LNAPL at the upper section of the fractured bedrock due to the rising water table. Additionally, the LNAPL seepage may result from remobilization of accumulated LNAPL along local depressions on the bedrock surface. The remobilization may also be from mobile LNAPL in the bedrock fissures ensuing from local LNAPL spills along the shoreline of Steeves Lake (as shown in Figure 3.2), or the result of LNAPL migration from more distant spill zones along discrete fractures in the bedrock.

Since the extent of fissuring in the bedrock is uncertain, URS (2002) and EBA (2001) postulated that most of the LNAPL flow across the site might be limited to the overburden/bedrock interface and the highly fissured upper section of the bedrock respectively. Inspection of the MWs casing in September 2006 using a borehole camera where possible showed that some casings in the MWs were not well sealed into the bedrock as previously discussed. Exhumation of one MW casing confirmed this. Thus, pooling and leakage of LNAPL around the casing was possible. Seasonal groundwater fluctuation and time averaged release of this LNAPL around the well casing may have been an active mechanisms contributing to seasonal variation of LNAPL in the MWs. In the winter period, the water table is lowered across the site. This water table decrease may allow perched or accumulated mobile LNAPL around the MW casing and unsaturated zone to drain into it, thereby increasing the thickness of pooled LNAPL in the MW. The pooled LNAPL in the MW will also not recharge if the hydraulic head difference between the well and the formation is not sufficient to drive mobile LNAPL from the formation into the MW. In the summer period, the increase in water table at the site may force any product pooled during winter back into the formation where possible, thereby leaving less LNAPL in the MW.

Other studies in the literature (i.e., Hardisty et al., 2003; Kemblowski and Chiang, 1990; Weiner, 2000) support the impact of groundwater fluctuation on LNAPL behavior described in the preceding paragraph. Studies have shown that fluctuations of the groundwater elevation may affect the LNAPL thickness measured in a monitoring well (Blake and Hall, 1984; Kemblowski and Chiang, 1990; Yaniga, 1984). Gradual decline in the water table may increase the volume of mobile LNAPL and increase the apparent LNAPL thickness in MW due to drainage from unsaturated zone (Weiner, 2000; Hardisty et al., 2003). According to Kemblowski and Chiang (1990), preferential flow through the well, especially in low permeability formation may increase apparent

LNAPL thickness in monitoring well during decline of the water table. Rising water table may cause reduction in apparent LNAPL thickness in the MW due to compression of capillary fringe in porous media (Weiner, 2000). Rising water table can also push LNAPL back into the formation and enhance lateral migrations in directions controlled by fracture network geometry rather than hydraulic gradient, and cause entrapment of LNAPL below the water table (Weiner, 2000, Hardisty et al., 2004; Kemblowski and Chiang, 1990). In summary, literature findings on the impacts of water table fluctuation on LNAPL transport showed that groundwater fluctuation may result in the following:

- Enhance migration of mobile LNAPL into areas not previously contaminated or areas with low LNAPL saturation ,
- Enhance entrapment of LNAPL in the formation with reduction in mobile LNAPL,
- Enhance dissolution, biodegradation and volatilization of LNAPL due to increase in LNAPL contact area with the formation and water.

Different measures have been taken to remove LNAPL from the site as discussed in Chapter 2. Thus, the cumulative removal of LNAPL from the MWs and overburden at the tank farm may have reduced the amount of mobile LNAPL in the formation because according to Weiner (2000), up to 40% of spilled LNAPL volume may be immobilized in the formation. The amount of immobile LNAPL in the formation may now be larger than the mobile component. Measured decreases in maximum LNAPL thicknesses in MWs since June 2005 supports this notion. Therefore, the observed LNAPL thickness may be from the mobile and localized free product in the formation, some of which may be trapped in the bedrock fissures. Thus, long-term dissolved contamination may occur as the residual component goes into solution after the removal of mobile components. Free product in the formation may be mobilized towards the

MWs over time due to effects of alternate freeze and thawing in the active layer, water table fluctuations. This mechanism has been proposed in literature case histories (Barnes et al, 2004; Biggar and Neufeld, 1996; Biggar et al, 1998; McCarthy et al, 2003), but is not well understood, thus, further investigations are required.

In this study, the inferred mechanisms contributing to LNAPL migration and accumulation are water table fluctuations and freezing-induced displacement associated with cyclic freeze-thaw. The impact of water table fluctuations on the mobility of LNAPL is well established in the literature as discussed in this section. However, that of freezing induced displacement requires further research, which formed the rationale for conducting the laboratory experiment presented in Chapter 6 to evaluate the feasibility of this mechanism.

3.5.5 Conceptual model of LNAPL movement

The fuel spill history showed that most of the spills occurred during the winter period (Figure 3.2), which may influence its subsurface behavior. According to URS (2001), the strikes of the bedrock fissures are oriented near parallel to the shoreline of the adjacent Steeves Lake, and the dip is very steep (e.g., almost 90° to the horizontal). Further characterization of the site showed that other fracture sets ranging from horizontal to near vertical exist at the site. A conceptualized fracture pattern of the bedrock is shown in Figure 3.14 overlaying the contour of bedrock topography. Vector overlay for the natural gradient of the bedrock surface (Figure 3.15) suggests that the LNAPL movement could not have been limited to the overburden/bedrock interface as previously suggested by URS (2002), but that the fracture pattern influenced the movement of the LNAPL at the site, and may account for LNAPL contamination north of the tank farm area. Moreover, initial blasting operations associated with site preparation before installation of the

storage tanks at the tank farm area may have induced a very complex fracture network that is difficult to capture or represent.

The potential LNAPL movement is illustrated with the conceptual model shown in Figure 3.16. Fuel spilled in the winter will be absorbed by the snow cover, saturate and penetrate the snow and the underlying unsaturated portion of the ground surface under gravitational force provided enough LNAPL thickness is developed at the surface to overcome entry capillary pressure of the largest pore size of the subsurface. For LNAPL movement to take place, its saturation must be greater than the residual saturation or retention capacity of the media. Thus, some LNAPL will be trapped by capillary suction in the unsaturated zone along the migration pathway. When the LNAPL reaches the frozen water saturated region (also referred to as frozen plane), it may spread laterally atop the saturated zone depending on the surface's type, ice content and temperature (Chuvilin et al., 2001). Cold temperatures and weathering of the LNAPL increases its viscosity and density thereby reducing its mobility. Increased penetration of LNAPL atop the frozen saturated zone may occur due to creeping effect of columns of LNAPL in the formation (e.g., regelation). The LNAPL will follow the gradient of the saturated zone and may travel further away from the source of contamination. This may leave patches of LNAPL along local zones of depression at the soil-bedrock interface before reaching residual saturation level. This may explain why no pool of LNAPL was encountered after the first major spill in 1990 because the bedrock and depth to saturated zone at the source region are slightly elevated as shown in Figure 3.15.

Decreased groundwater elevation is often observed in the winter period because recharges are less than discharges due to lack of rainfall and due to continued groundwater extraction for anthropogenic and natural purposes. At the tank farm area, the groundwater decreased as much as eight meters in the winter, extending up to 13 meters below the

surface, thus, LNAPL might have penetrated to depths in excess of 10 m and migrated significant distances from the source zone. This seasonal decline in groundwater elevation may also enhance gravity drainage and remobilization of isolated blobs of LNAPL in individual fissures and those initially trapped below the water table in the vadose zone from previous spills.

In the spring, meltwater and early rainfall lead to a supra-permafrost groundwater condition. Thus, the resulting surface runoff may enhance LNAPL migration downgradient of any pooled location atop the bedrock surface towards Steeves Lake. A transient rise in the water table may also cause smearing of LNAPL into the previously uncontaminated vadose zone and possibly lead to more trapping of LNAPL by capillary suction. The transient thrust of groundwater flow may cause drift of LNAPL to Steeves Lake. Since the fracture orientation and effective aperture width controls the flow of water, there is a propensity for channelization of flow. This implies that LNAPL may be observed at considerable distances from the source zone along a definite path missed during the site investigation. This may explain why LNAPL is observed adjacent to Steeves Lake, and further north of the tank farm area by the camp. New MWs #47, #48, #49 by the camp showed no evidence of hydrocarbon contamination (Table A1.8), though hydrocarbon sheen was observed in MW 46 in September 2007.

Progression of the thaw front as the ground warms up from early spring through summer may open up micro cracks in the frozen saturated region above the bedrock surface, which may serve as conduit for vertical penetration of any pooled LNAPL. However, since the contamination source and overburden soil had been removed, this may not be an active mechanism contributing to LNAPL movement at the site at present. It should also be noted that from the thermal profile (Appendix C) at the site, two thermal progressions occur. In the spring through fall seasons, the ground warms from the top down simultaneously with advancing

freezing front from the bottom up until equilibrium is reached and vice versa in the winter period. Thus, lateral migration of spilled LNAPL in the summer, which is trapped below advancing freezing front in the winter period, may be enhanced. Subsurface abrupt movement of the LNAPL may also ensue in a discontinuous fashion when the two progressing freezing and thawing fronts meet..

Increases in subsurface temperature enhance weathering of the LNAPL and increase in LNAPL solubility in water. Thus, in the fall seasons, an increased dissolved organic concentration is expected in the groundwater. Though evidence of LNAPL weathering and preferential dissolution were reported in Chapter 2 at the Colomac mine site, there was no evidence of increased organic concentrations in the summer since no winter groundwater sampling took place. Moreover, the LNAPL will flow atop the capillary zone of the water table and follow the natural gradient of the groundwater along the prevailing fracture network in the bedrock, provided sufficient LNAPL thickness is established to overcome capillary forces in the formation. Temperature increases also decrease the capillary pressure thereby releasing some of the LNAPL trapped by capillary suction. This may be significant because of the observed sheen of LNAPL at the shoreline of Steeves Lake. Advective movement of LNAPL in the fracture network should be slower than water movement through the same fissure and due to processes such as adsorption, weathering, and matrix diffusion, its movement may be further retarded.

Shown in Figure 3.17 is a summary of subsurface behavior of LNAPL in the formation. LNAPL behavior is grouped under fresh and existing spill. In a temperate environment, the behavior of LNAPL is well documented in the literature (Mercer and Cohen, 1990; Weiner, 2000). The differences in LNAPL subsurface behavior between temperate and permafrost regions are the cyclic freezing and thawing, and the presence of ground ice. This Chapter discussed some of these differences, and

further discussions on the feasibility of some of the highlighted mechanisms in Figure 3.17 are given in Chapter 6.

3.6 Conclusions

In this study, improved understanding of the subsurface behavior of LNAPL at the site was gained by monitoring LNAPL thickness variation in MWs with time, and performing free product recovery test in the MWs. The distribution of mobile LNAPL that was observed in MWs across the site is erratic. The measured data obtained from the field study suggest water table fluctuations coupled with freezing-induced displacement are the main mechanisms contributing to LNAPL migration and accumulation at the site. These mechanisms are active but discontinuous due to their seasonal nature. The apparent LNAPL thicknesses in the monitoring wells at the tank farm area where most of the fuel spills occurred increased with decreasing water elevation but decreased with rising water table. Additionally, seepage of LNAPL at the shoreline of Steeves Lake was observed in response to precipitation event and water table elevation, suggesting that rising water table may enhance migration of LNAPL through discrete fractures as discussed by Hardisty et al. (2003, and 2004).

Furthermore, this study presents a conceptual model of the subsurface behavior of LNAPL at the site. The observed behavior of the influence of water table fluctuations is supported by existing literature studies (i.e., Kemblowski and Chiang, 1990; Mercer and Cohen, 1990; Hardisty et al., 1998; Weiner, 2000; Hardisty et al., 2004; and Dobson et al., 2007). Additionally, the impacts of freezing induced displacement associated with a permafrost environment is also supported by existing literature studies (i.e., Barnes et al., 2004, Chuvilin et al., 2003; and Biggar et al., 1998). However, further studies are required (as discussed in Chapter 6) to evaluate some of the inferred freezing induced processes.

This study also showed that LNAPL contamination is not limited to the bedrock and soil interface, and that significant LNAPL contamination abounds in the fractured upper section of the bedrock. Additionally, the product recovery test data showed that a standby free product recovery system using only the skimmer pump may not be efficient because of very slow recharge of LNAPL into the MWs.

Table 3.1 Measured apparent LNAPL thickness in monitoring wells for 2005/06 study. The blank cells indicate no measurable product or inaccessible well.

Well	7/23/00	6/23/05	7/24/05	8/11/05	9/12/05	12/12/05	6/15/06	7/6/06	8/6/06	12/14/06
Continuous free product (cm)										
8		2.0	3.0	3.0	6.3		2.0	2.0	2.0	
9	51.0	11.0	3.0	16.0	14.0	67.0	76.5	15.0	17.0	2.0
12	189.0	4.0	7.0	6.5	7.5	501.0	21.5	1.0	2.0	209.0
14	3.0	5.0	2.0	1.0		0.5	51.0	9.0	8.0	13.0
15		2.0	3.0	14.0	9.4	9.0	6.6	8.0	6.5	6.0
17	296.0	51.0	26.0	28.0	13.8	13.8	47.0	5.0	4.5	140.0
19	9.0	9.0	6.0	7.5	2.9	3.0	28.6	21.0	20.5	6.0
26	280.0	15.0	7.0	2.0	25.0	368.0	231.9	26.0	25.0	21.0
30		3.0	2.0	12.0	6.8	3.0		18.0	15.5	
Often free product (cm)										
23		8.0	4.0	4.5	3.7					
28		13.0		11.0	9.0	8.0	5.9			0.5
Periodic free product										
10	12.0				3.0			1.0		
13								1.0		
16					0.5	1.5				
18	226.0						0.2			
21				2.2	5.2				3.5	
29	12.0	3.0		4.0	4.5	4.0				

Table 3.2 Summary of product recovery data in June 2006.

Well ID	Date	Time	ΔT	DTP (m)	DTW (m)	DTB (m)	PT (m)	WC (m)	PPV (L)
17	6/18/06			5.39	5.85	5.85	0.47	0.00	
	6/18/06	11:18 AM	00:00.0	5.42	5.82	5.82	0.40	0.00	1.15
	6/18/06	11:59 AM	0:41:00	5.55	5.72	5.72	0.17	0.00	1.75
	6/18/06	12:33 PM	1:15:00	5.59	5.60	5.61	0.01	0.01	1.67
	6/18/06	1:36 PM	2:18:00	5.51	5.55	5.62	0.04	0.07	0.00
	6/18/06	2:34 PM	3:16:00	5.51	5.55	5.55	0.04	0.00	0.00
	6/19/06	11:58 AM	24:40:00	5.50	5.53	5.53	0.03	0.00	0.00
	6/20/06	11:02 AM	47:44:00	5.52	5.52	5.52	0.00	0.00	0.00
6/22/06	9:16 PM	105:58:00	5.54	5.56	5.56	0.02	0.00	0.00	
9	6/19/06			2.54	3.33	4.62	0.79	1.30	
	6/19/06	10:30 AM	00:00.0	3.25	3.31	4.62	0.06	1.31	7.01
	6/19/06	11:05 AM	0:35:00	3.31	3.31	4.62	0.00	1.31	0.55
	6/19/06	11:35 AM	1:05:00	3.29	3.31	4.62	0.01	1.31	0.00
	6/19/06	12:05 PM	1:35:00	3.28	3.29	4.65	0.01	1.35	0.00
	6/20/06	10:58 AM	24:28:00	2.84	2.92	4.76	0.08	1.84	0.00
	6/20/06	8:18 PM	33:48:00	2.80	2.89	4.80	0.09	1.91	0.00
	6/21/06	2:46 PM	52:16:00	2.73	2.83	4.86	0.11	2.03	0.00
6/22/06	9:08 AM	70:38:00	2.71	2.79	5.06	0.08	2.28	0.00	
12	6/19/06			3.28	3.45	4.85	0.16	1.40	
	6/19/06	2:38 PM	00:00.0	3.47	3.50	4.89	0.03	1.39	1.34
	6/19/06	3:21 PM	0:43:00	3.48	3.51	4.90	0.03	1.40	0.00
	6/20/06	8:15 AM	17:37:00	3.54	3.56	4.99	0.02	1.43	0.00
	6/20/06	10:45 AM	20:07:00	3.59	3.61	4.97	0.02	1.36	0.00
	6/20/06	8:10 PM	29:32:00	3.71	3.75	5.10	0.04	1.35	0.00
	6/21/06	3:00 PM	48:22:00	3.93	3.94	5.24	0.02	1.30	0.00
	6/22/06	4:00 PM	73:22:00	4.18	4.20	5.24	0.02	1.04	0.00
26	6/20/06			8.91	11.00	21.80	2.10	10.80	
	6/20/06	10:04 AM	00:00.0	10.25	10.27	21.40	0.03	11.13	24.00
	6/20/06	10:34 AM	0:30:00	9.72	9.77	21.40	0.05	11.63	0.00
	6/20/06	11:08 AM	1:04:00	9.55	9.60	21.40	0.05	11.80	0.00
	6/20/06	1:34 PM	3:30:00	9.42	9.50	21.40	0.08	11.90	0.00
	6/20/06	7:35 PM	9:31:00	9.41	9.48	21.40	0.08	11.92	0.00
	6/21/06	2:55 PM	28:51:00	9.40	9.46	21.40	0.07	11.94	0.00
	6/22/06	3:08 PM	53:04:00	9.40	9.48	21.40	0.07	11.93	0.00

DTP Depth to product PT Product thickness
 DTW Depth to water WC Water column length
 DTB Depth to bottom PPV Purged product volume

Table 3.3 Summary of the thermal regime at the Colomac mine site.

Areas with deep talik			Areas with active layer deeper than 14.8 m depth	
Thermistor ID	Nearest monitoring well (MW)	Interval thawed (m)	Thermistor ID	Nearest monitoring well (MW)
T01	MW 29	5.8 – 14.9	T04	MW 9
T02	MW 15	8.8 – 14.8	T08	MW 2
T03	MW 31	8.8 – 14.8	T09	MW 103
T07	MW 19	5.8 – 14.8	T10	MW12
T11	MW 32	14.8		
Areas with permafrost at depth and active layer less than 14.8 m depth				
T05	MW 13	< 12 m	Permafrost at 12 m	

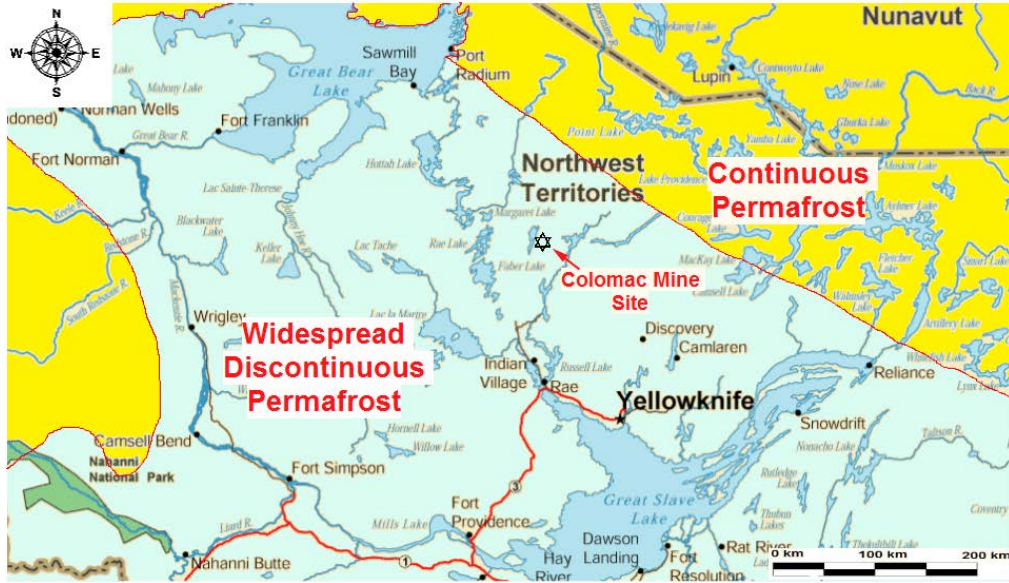


Figure 3.1 Location of Colomac mine site, 220 km northwest of Yellowknife, NWT.

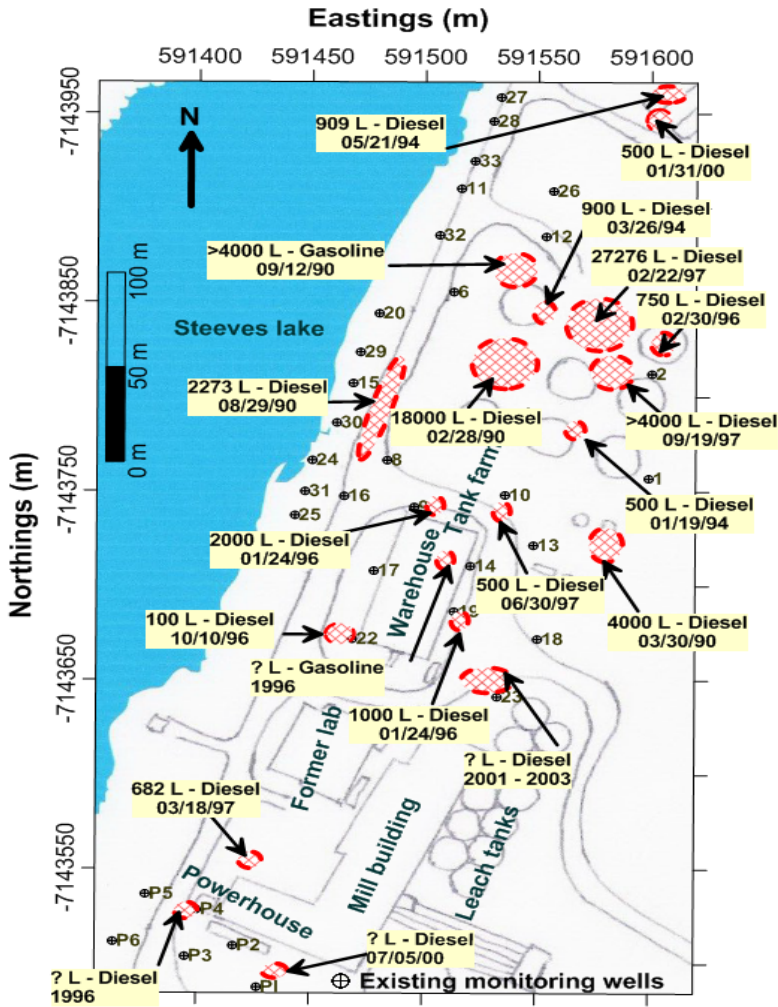


Figure 3.2 Simplified site-map showing the historical spilled fuel at Colomac mine.

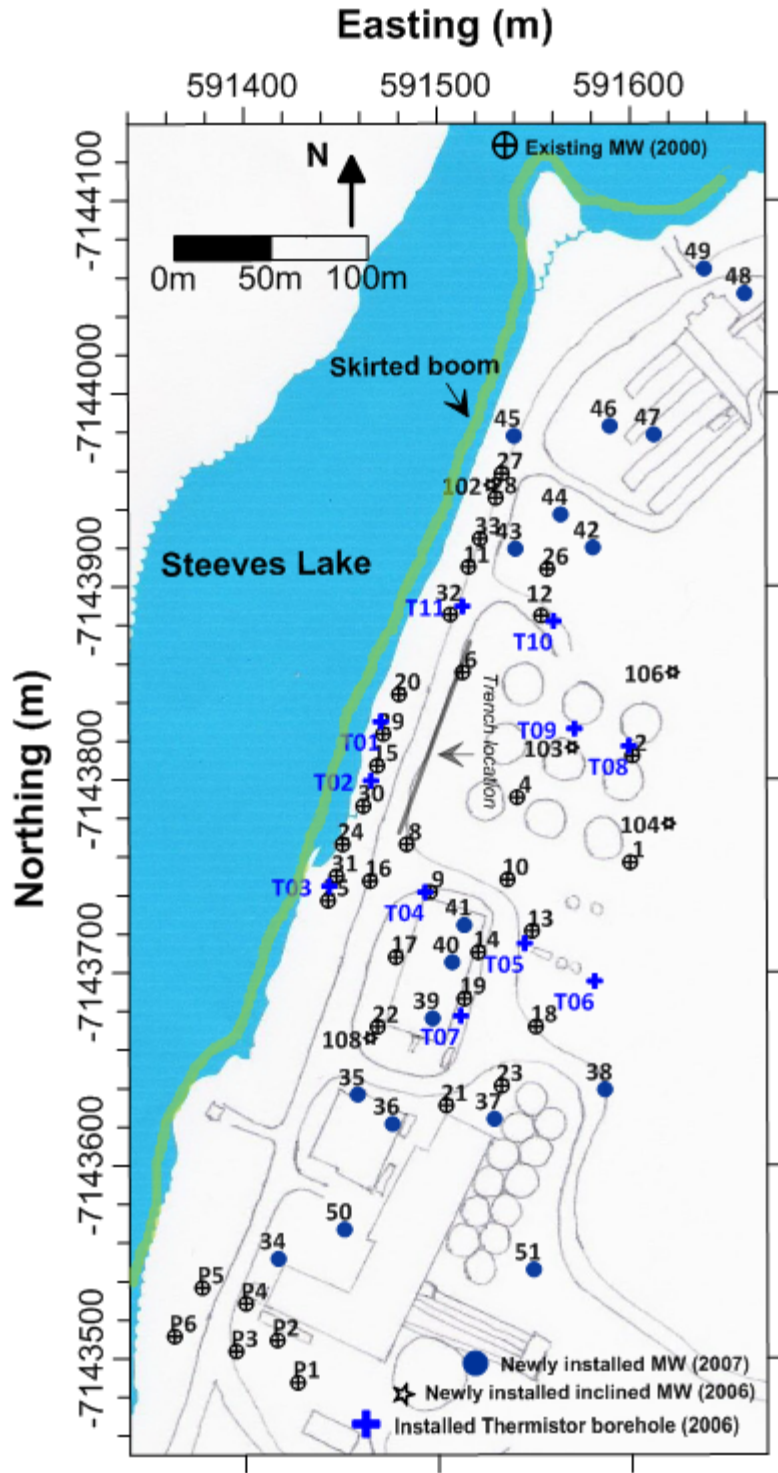


Figure 3.3 Simplified site-map showing spatial location of the monitoring wells and the thermistor - boreholes.

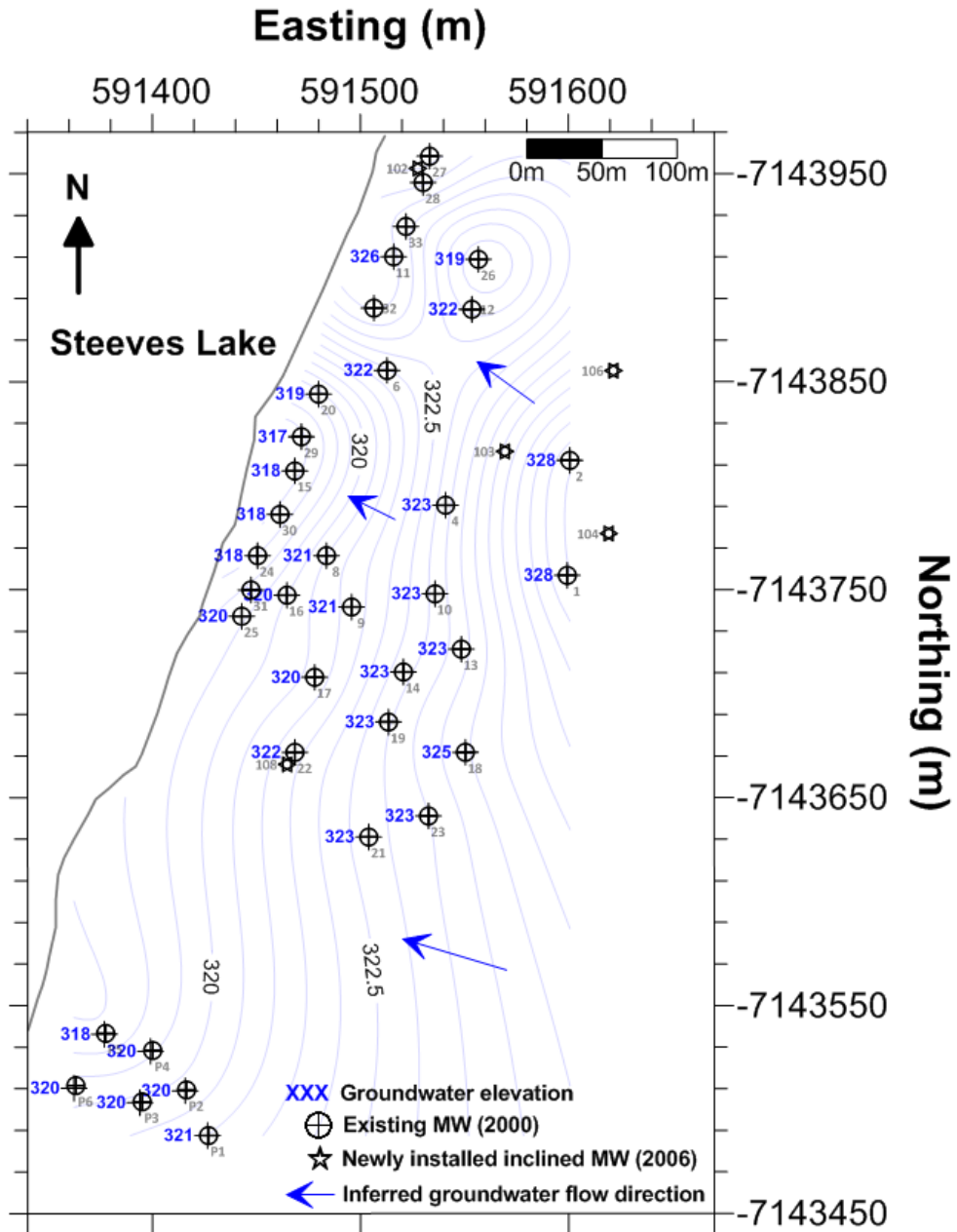


Figure 3.4 Groundwater contour inferred for August 6, 2006. The bull-eye seen around MW 26 may be associated with inadequate data to bound the measured groundwater elevation at that time.

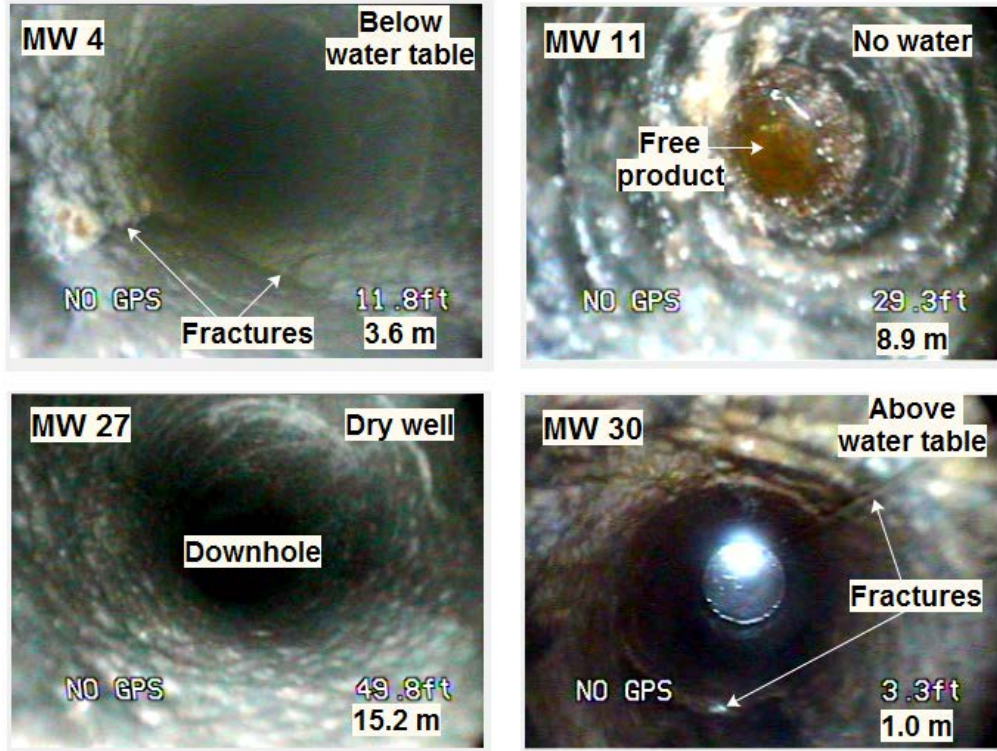


Figure 3.5 Samples of borehole images for monitoring wells 4, 11, 27, and 30. More fractures were observed in the upper section of the bedrock than at depth. Not all the monitoring wells contained water all year round (e.g., MWs 11 and 27). MW 11 had free product sitting atop ice in early spring, while MW 27 seem not to intersect water-bearing fractures. Nevertheless, they all had measurable amount of free product.

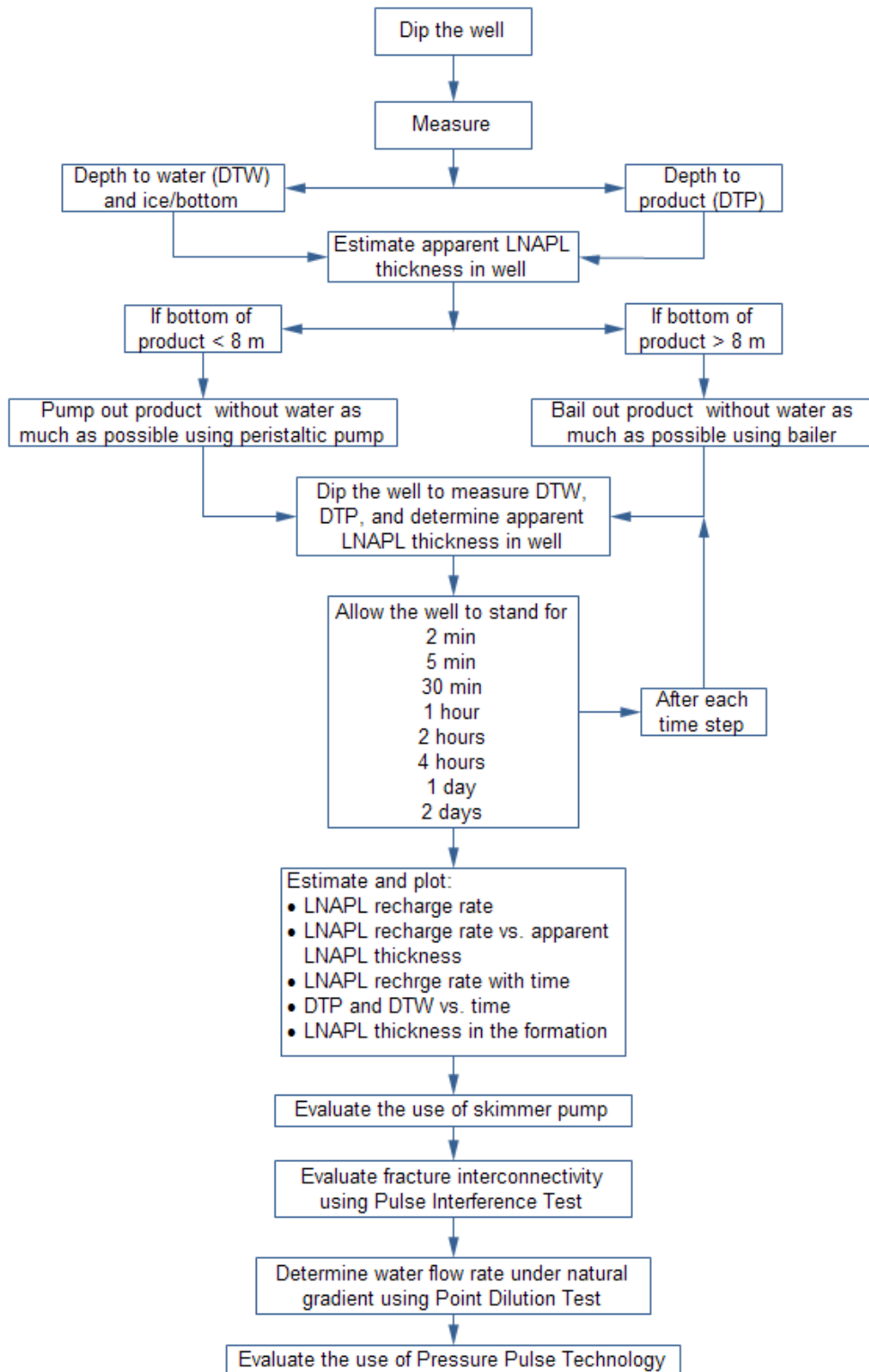


Figure 3.6 Summary of product recovery test procedure and later activities aimed at evaluating the need for product recovery system at the site.

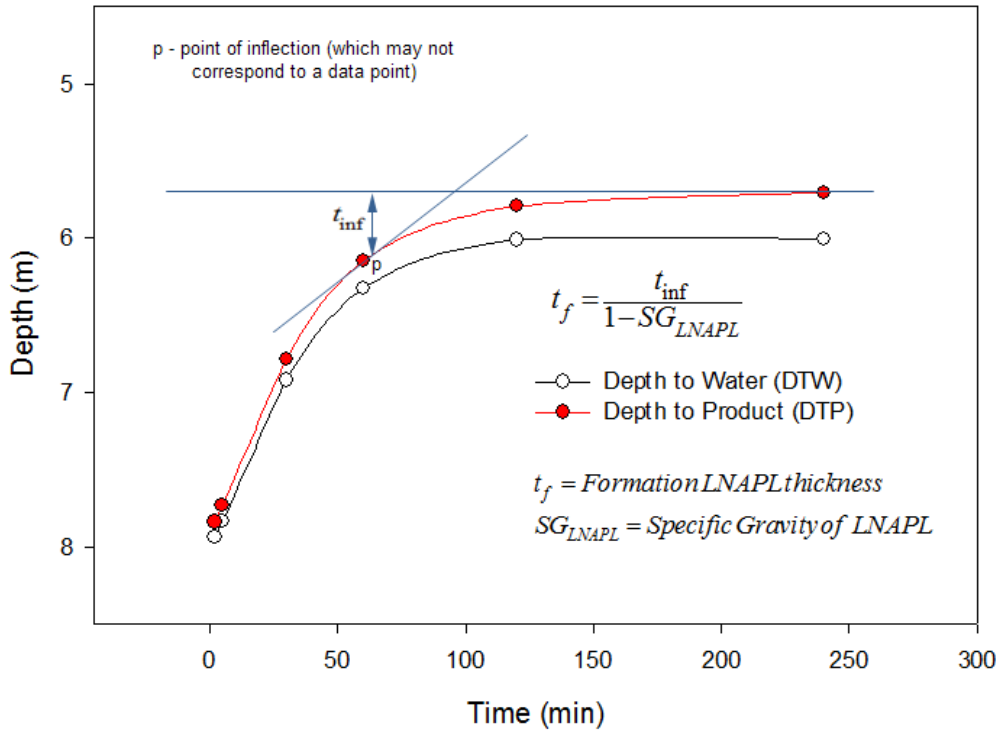


Figure 3.7 Hypothetical results for the product recovery test (modified after Testa and Winegardner, 2000). The point of inflection (p) corresponds to the LNAPL entry point, and its vertical distance to the constant LNAPL depth is used to estimate formation LNAPL thickness.

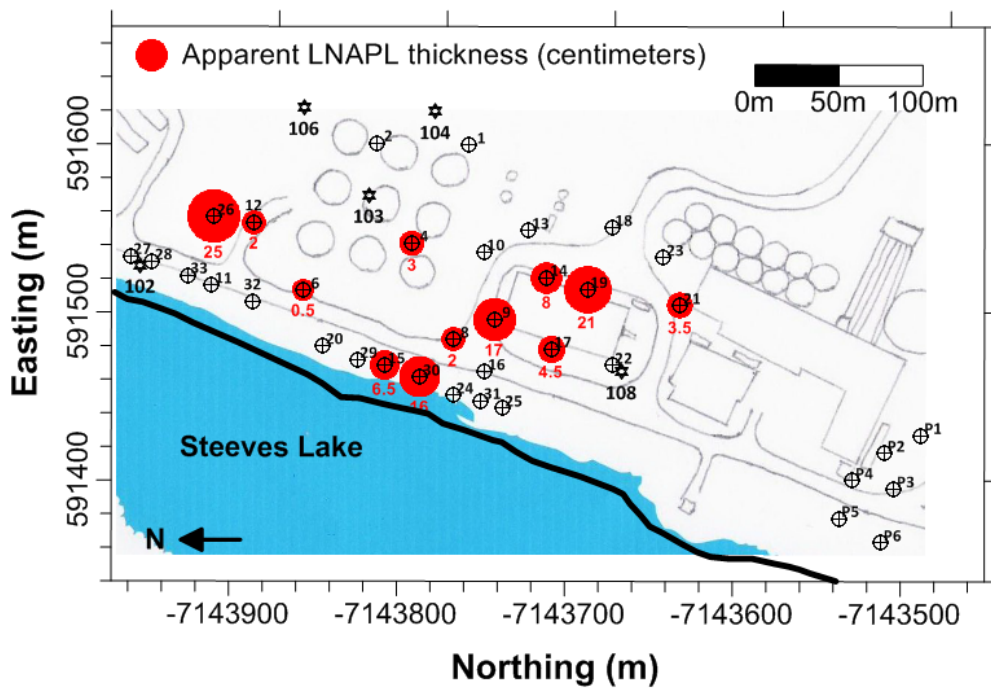


Figure 3.8 Measured apparent LNAPL thickness for August 06, 2006.

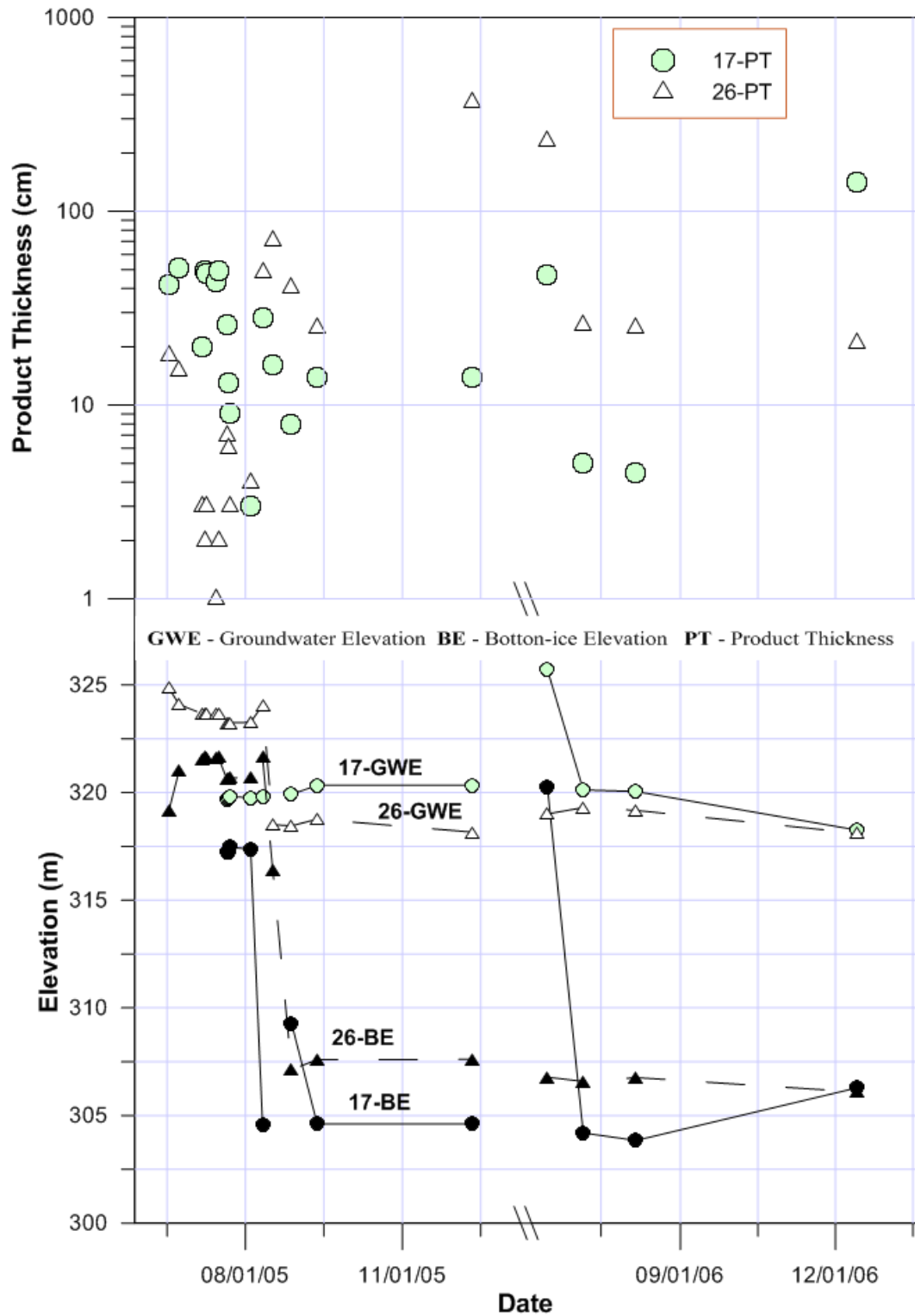


Figure 3.9 Well-probe data for monitoring wells (MWs) 17 and 26 at the site.

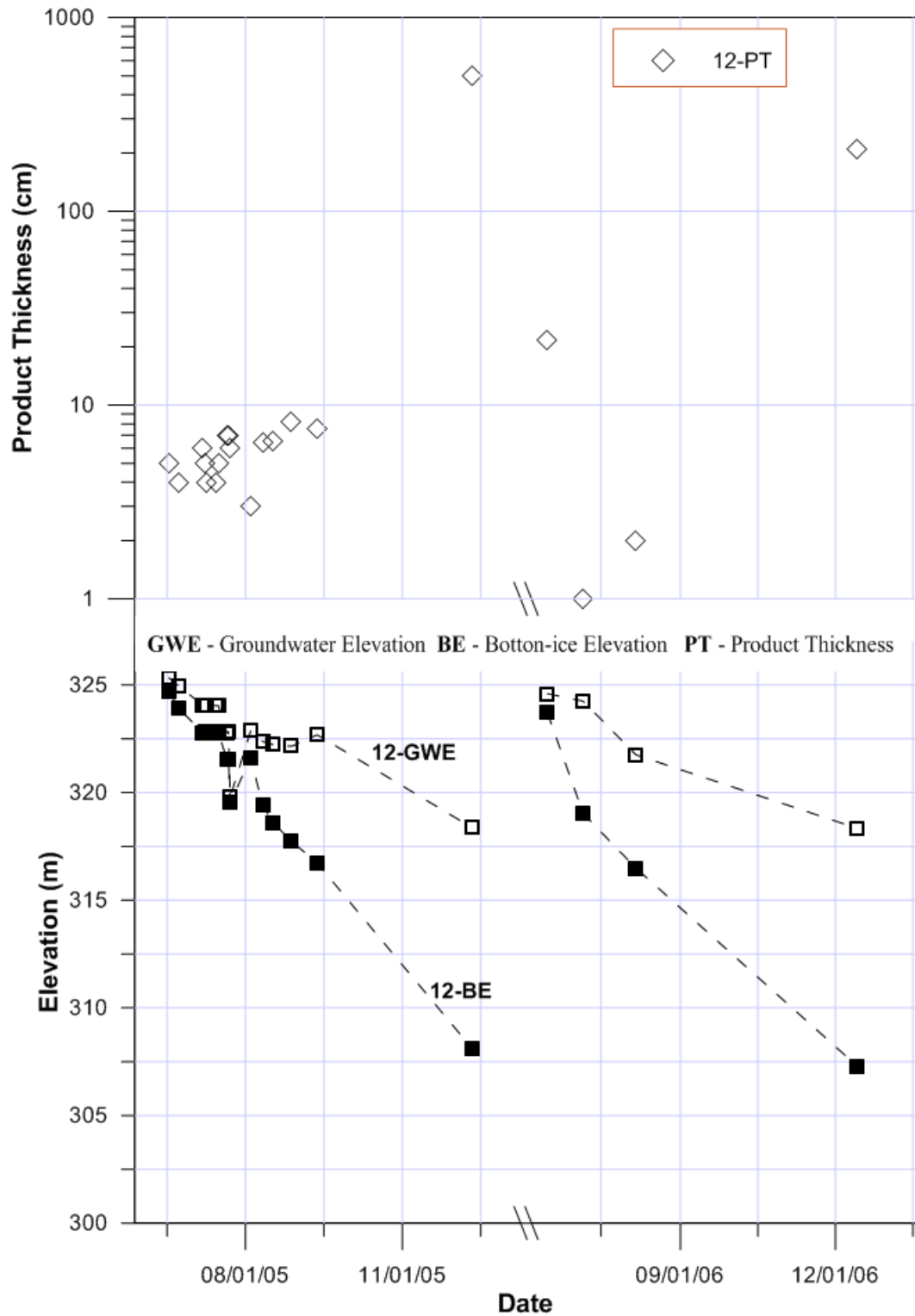


Figure 3.10 Well-probe data for monitoring well (MW) 12 at the site.

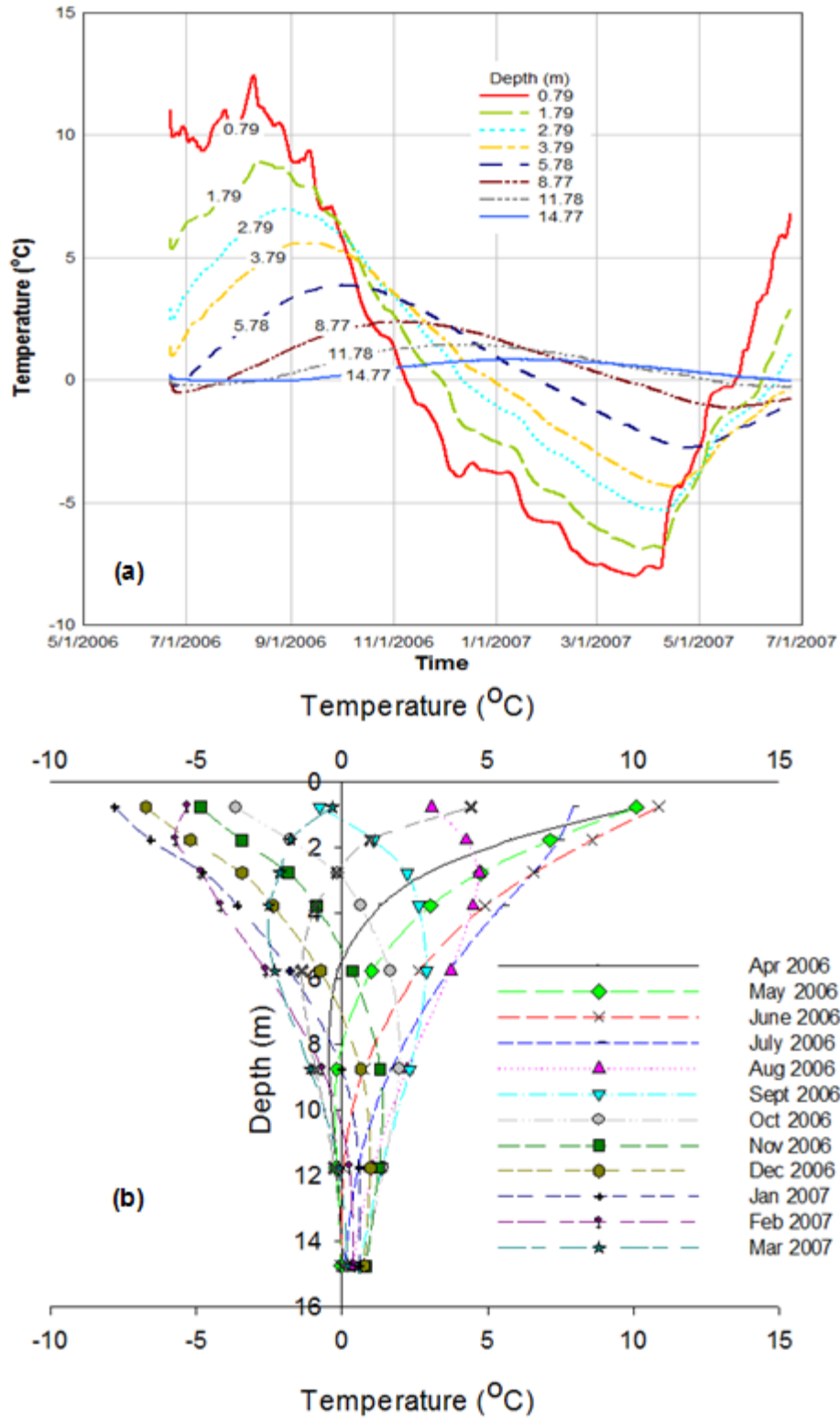


Figure 3.11 Temperature profile with (a) time and (b) depth in one of the dedicated thermistor strings “T10” adjacent to MW 12.

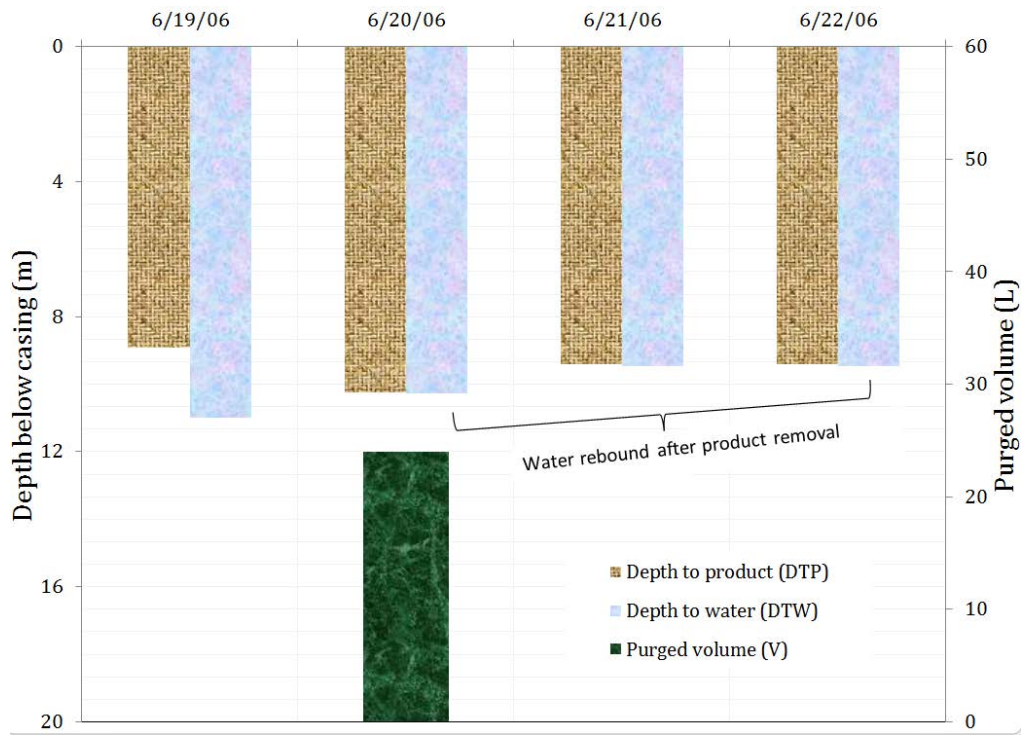


Figure 3.12 Graphical representation of data from the product recovery test for MW 26 in June 2006.

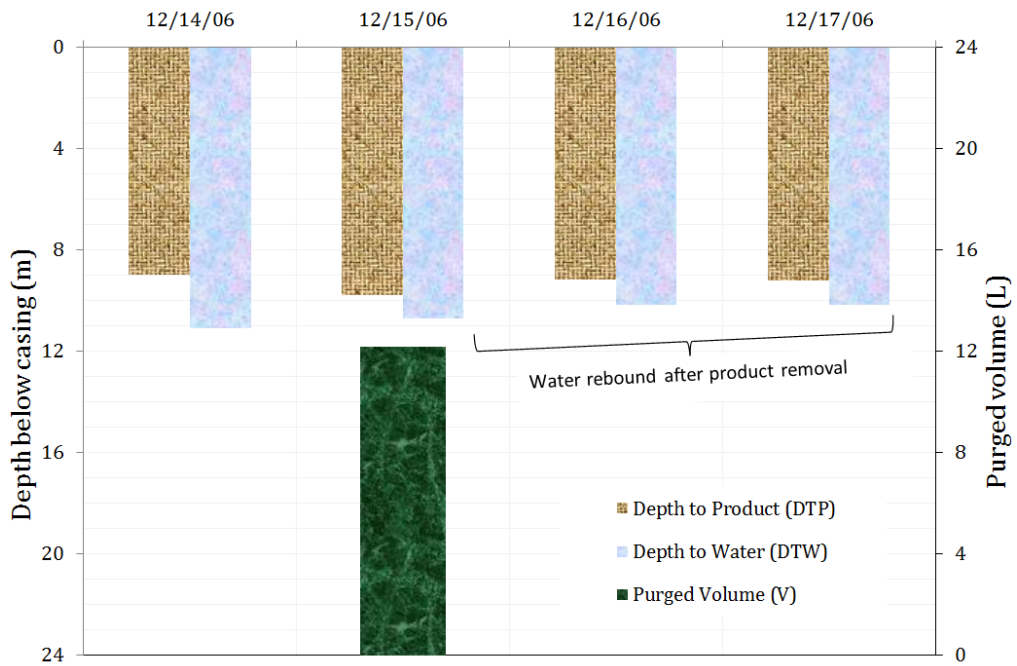


Figure 3.13 Graphical representation of data from the product recovery test for MW 12 in December 2006.

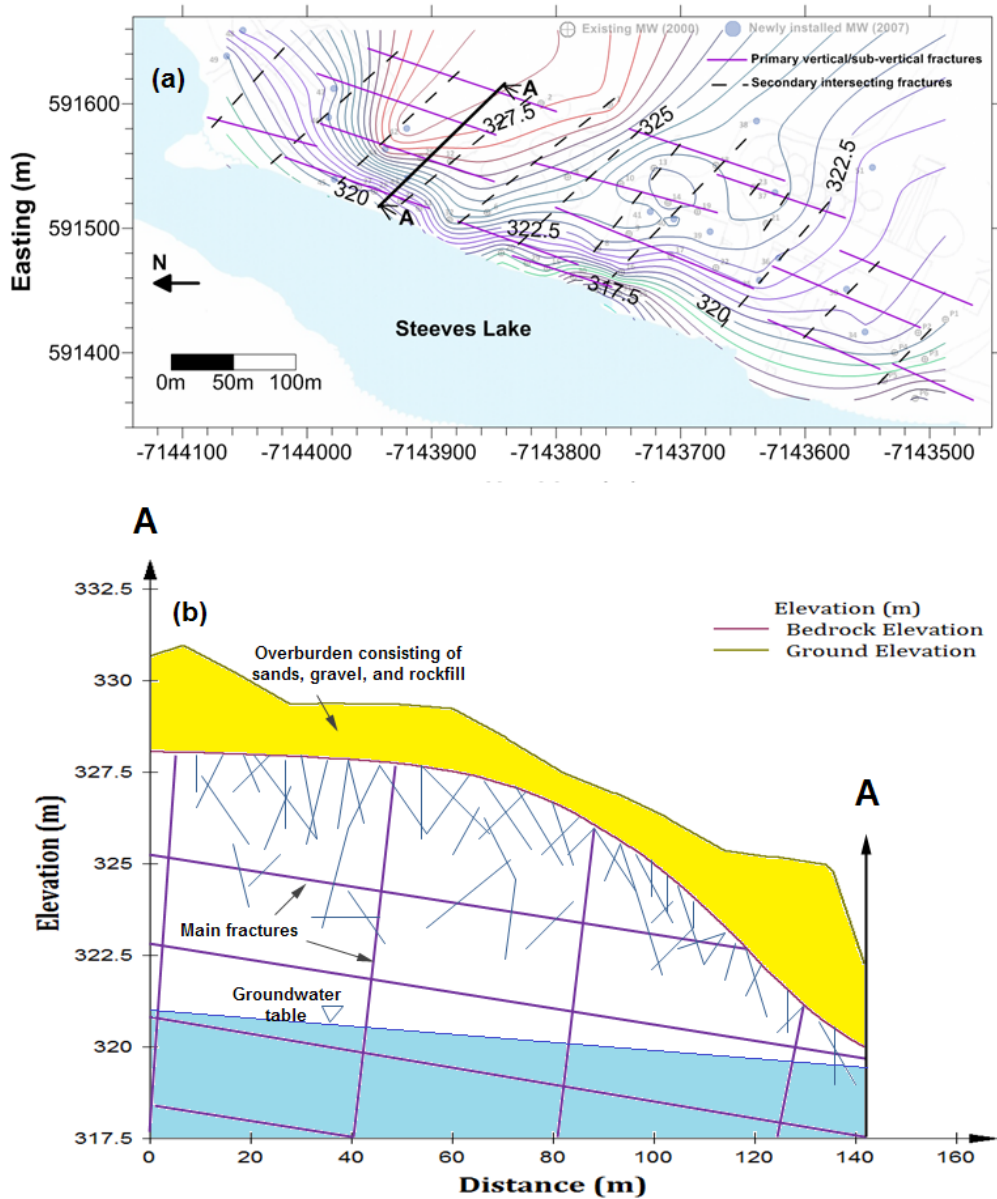


Figure 3.14 Conceptual fracture pattern at the site showing: (a) bedrock elevation with the inferred fracture pattern based on site characterization efforts, and (b) conceptual subsurface fracture distribution at the site.

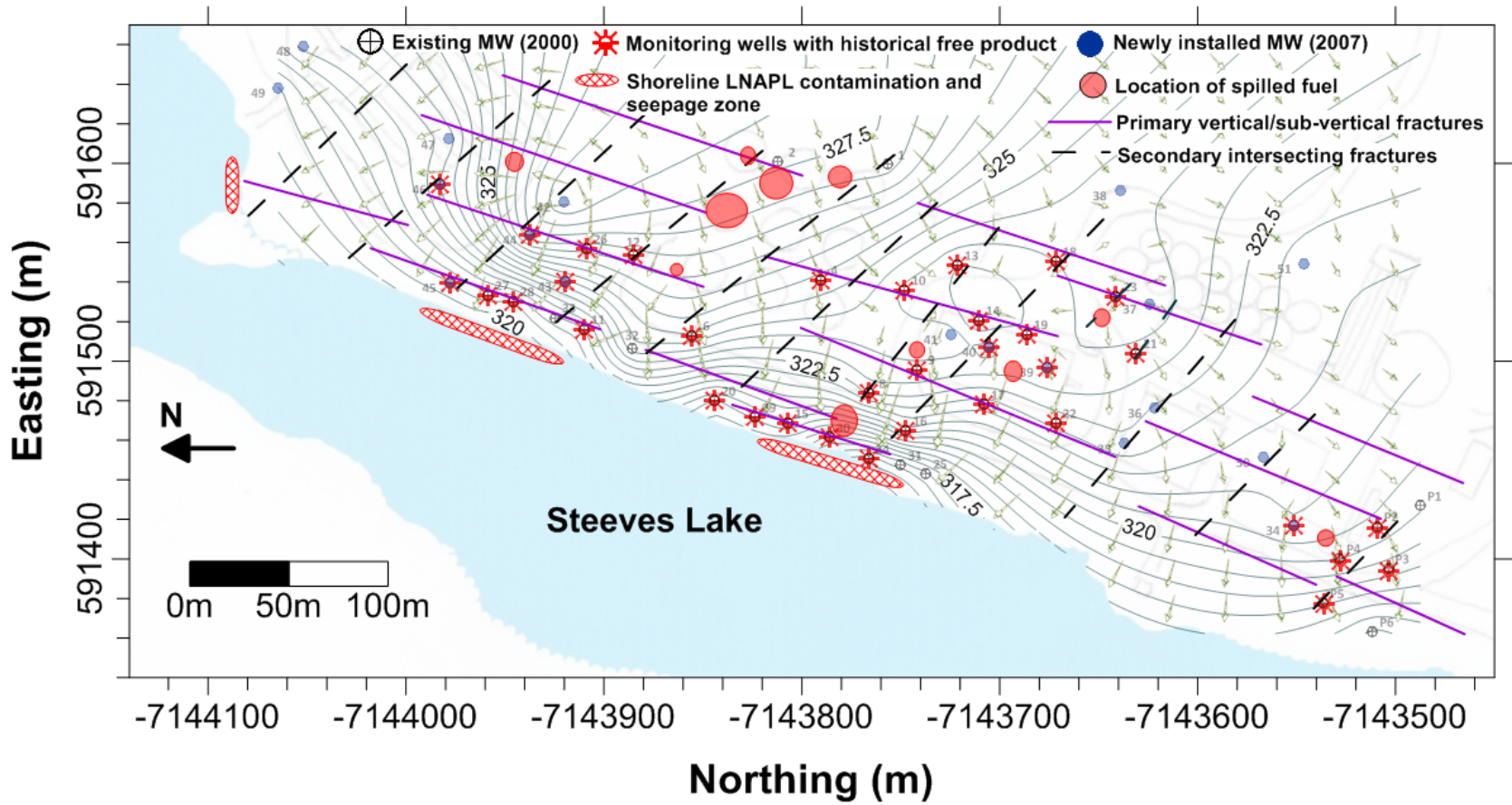


Figure 3.15 Conceptual surficial model at the Colomac mine site, highlighting the importance of fracture network and distribution on the movement of the spilled fuel.

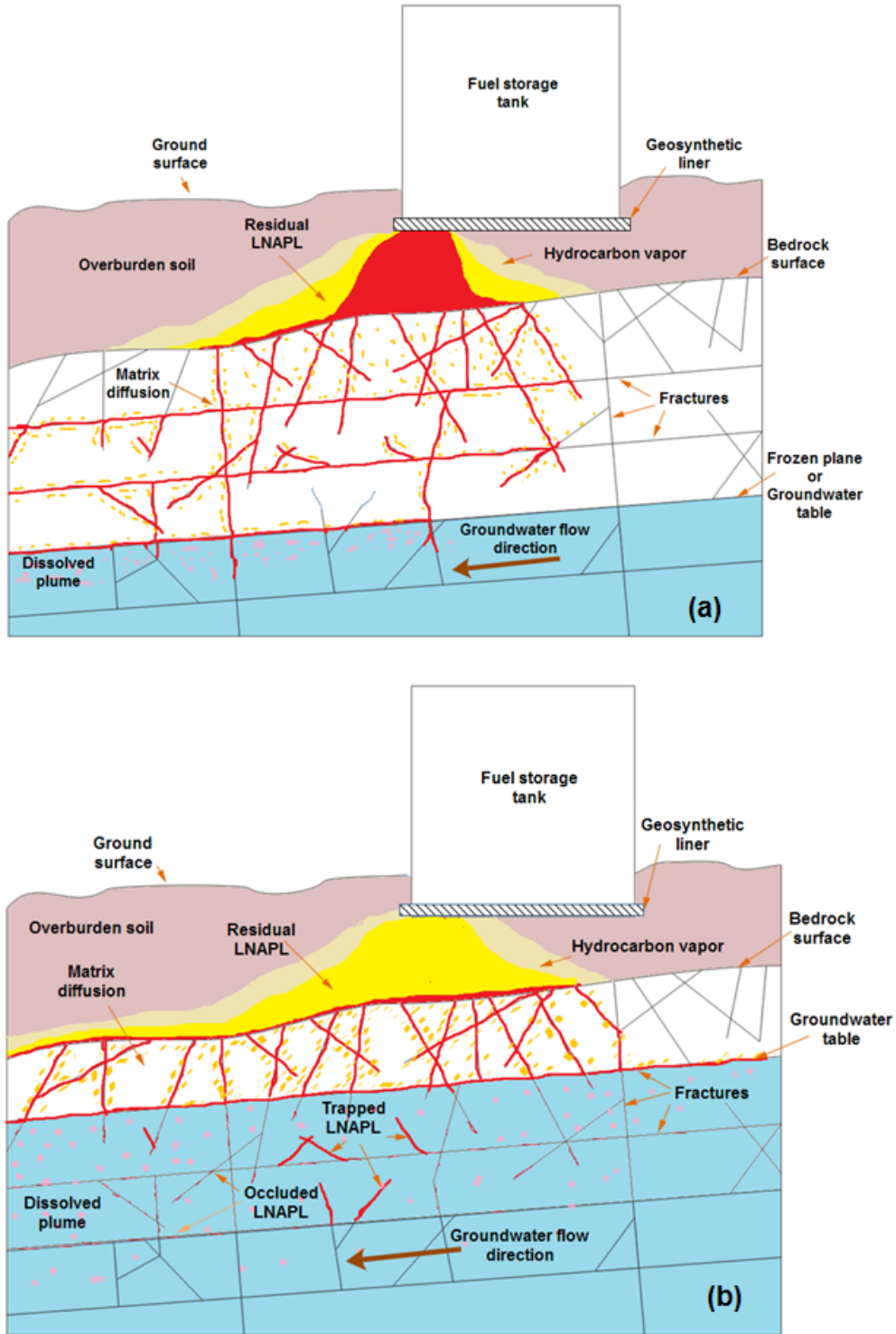


Figure 3.16 Conceptual model of LNAPL movement during (a) the winter period after fresh spill when the water table is low, and (b) in the spring/summer when the spill source is removed or contained and the water table is elevated.

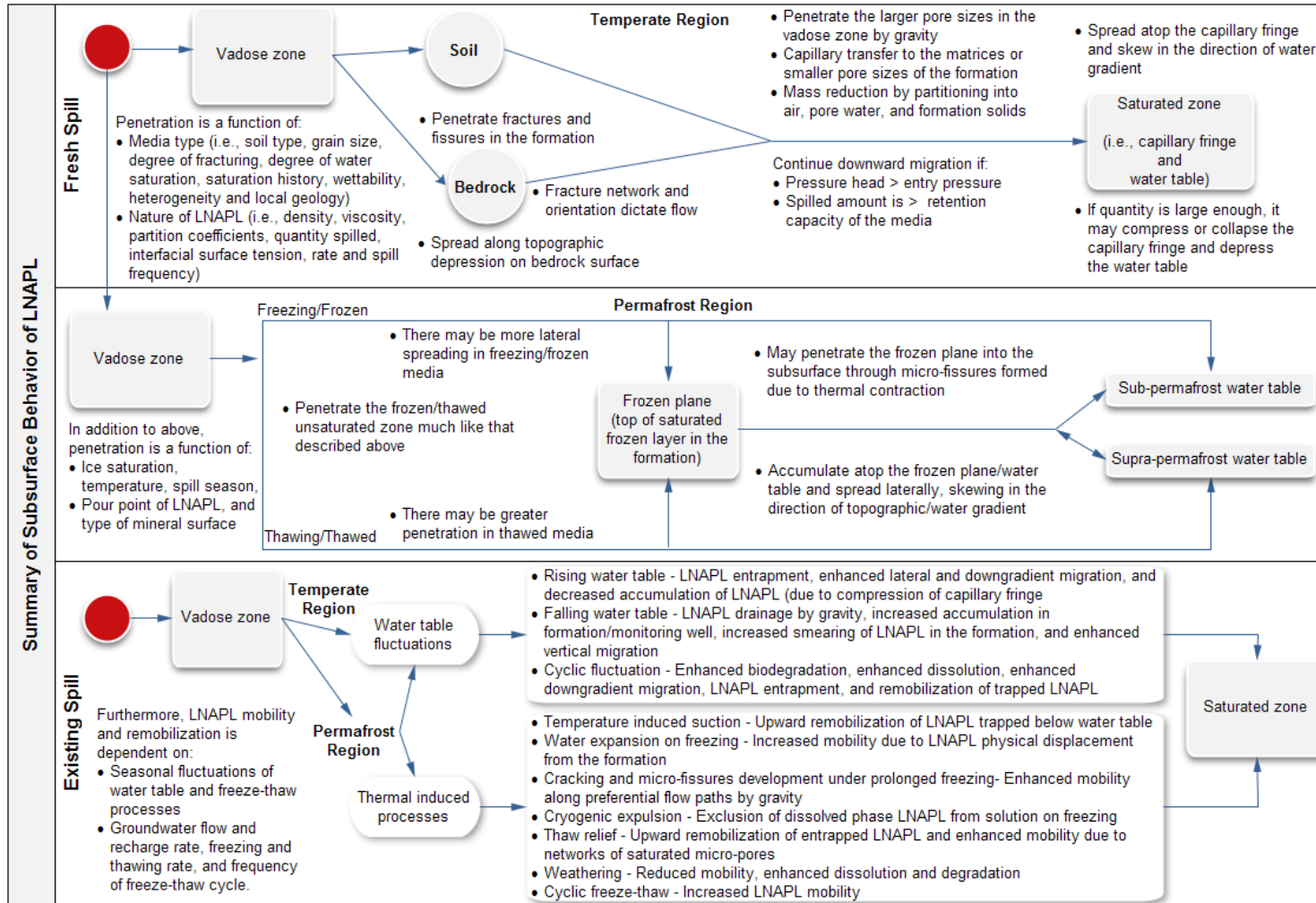


Figure 3.17 Summary of subsurface behavior of LNAPL in porous media including fractured bedrock.

References

- Barnes, D.L., Wolfe, S.M., Filler, D.M., 2004. Equilibrium of petroleum hydrocarbons in freezing ground. United Kingdom. *Polar Record*, 214: 245-251.
- Barnes, D.L., Wolfe, S.M., Filler, D.M., 2004. Equilibrium of petroleum hydrocarbons in freezing ground. United Kingdom. *Polar Record*, 214: 245-251.
- Biggar, K.W., Haidar, S., Nahir, M., Jarrett, P.M., 1998. Site investigations of fuel spill migration into permafrost. *Journal of Cold Regions Engineering*, 12: 84- 104
- Biggar, K.W., Neufeld, J.C.R., 1996. Vertical migration of diesel into silty sand subject to cyclic freeze-thaw. In: Carlson, R. (editor). *Proceedings of the Eighth International Conference on Cold Regions Engineering*. Fairbanks: American Society of Civil Engineers: 116-127.
- Blake, S.B. and Hall, R.A., 1984. Monitoring petroleum spills with wells: Some problems and solutions. *Proc. 4th Natl. Syrup. on Aquifer Restoration and Groundwater Monitoring*. Natl. Water Works Assoc., Columbus, Ohio, pp. 305-310.
- Chuvilin, E.M., Mikiyaeva, E.S., 2003. Investigation of the influence of salinity and cryogenic structure in the dispersion of oil and oil products in frozen soils. *Cold Regions Science and Technology*, 37: 89-95.
- Chuvilin, E.M., Naletova, N.S., Miklyaeva, E.C., Kozlova, E.V., Istanes, A., 2001. Factors affecting the spreadability and transportation of oil in regions of frozen ground. *Polar Record*, 37 (202): 229-238.
- Dobson, R., Scroth, M.H., Zeyer, J., 2007. Effect of water table fluctuation on dissolution of a multi-component light nonaqueous phase liquid, *Journal of Contaminant Hydrogeology*, 94: 235-248.
- EBA Engineering Consultants Ltd., 2001. Hydrocarbon assessment, Lakefront and waste oil areas, Colomac Mine, NWT. Report to Deton 'Cho Corporation. Yellowknife, NT. 37 p. and appendices.

- EPA – Environmental Protection Agency, 1996. How to effectively recover free product at leaking underground storage tank sites: A guide for state regulators. EPA 510-R-96-001, <www.epa.gov/oust/pubs/fprg.htm>, [last assessed in May 2010].
- Hardisty, P.E., Roher, J., Dottridge, J., 2004. LNAPL Behavior in Fractured Rock: Implications for Characterization and Remediation, U.S. EPA/NGWA Fractured Rock Conference: State of the Science and Measuring Success in Remediation, Portland Maine, pp 129-134.
- Hardisty, P.E., Wheeler, H.S., Birks, D., Dottridge, J., 2003. Characterisation of LNAPL in Fractured Rock, Quarterly Journal, Engineering Geology and Hydrogeology, 36: 343-354.
- Hardisty, P.E., Wheeler, H.S., Johnson, P.M., Bracken, R.A., 1998. Behavior of Light Immiscible Liquid Contaminants in Fractured Aquifers. Geotechnique, 48(6): 747-760.
- Hearn, K., 1990. The Colomac deposit. Geological Survey of Canada Open File Report 2168, pp. 84-89.
- Kemblowski, M.W., Chiang, C.Y., 1990. Hydrocarbon thickness fluctuations in monitoring wells. Ground Water, 28(2): 244-252.
- Lenhard, R.J., Parker, J.C. 1990. Estimation of Free Hydrocarbon Volume from Fluid Levels in Monitoring Wells. Ground Water, 28(1): 57-67.
- McCarthy, K., Walker, L., Vigoren, L., 2004. Subsurface fate of spilled petroleum hydrocarbon in continuous permafrost. Cold Regions Science and Technology, 38: 43-54.
- Mercer, J.W., Cohen, R.M., 1990. A review of immiscible fluids in the subsurface: properties, models, characterization and remediation. Journal of Contaminant Hydrology, 6: 107-163.
- Testa, S.M., Winegardner, D.L., 2000. Restoration of contaminated aquifers. 2nd Ed., Lewis Publishers, CRC Press LLC, Washington.
- URS Norecol Dames and Moore Inc., 2002. Assessment of hydrocarbons within fractured bedrock at the lakefront and waste oil areas and development of a remedial action plan, Colomac Mine, NWT. Report

for Public Works & Government Services Canada. Vancouver, BC. 21 p.
and appendices.

Weiner, E.R., 2000. Applications of environmental chemistry: A practical
guide for environmental professionals. CRC Press LLC, Florida.

Yaniga, P.M. Mulry, J., 1984. Accelerated aquifer restoration: In situ applied
techniques for enhanced free product recovery/adsorbed
hydrocarbon reduction via bioreclamation. In: Proceedings of
Petroleum Hydrocarbons and Organic Chemicals in Ground Water.
Natl. Water Well Assoc., Worthington, Ohio, pp. 421--440.

4 ESTIMATION OF ACTUAL LNAPL THICKNESS IN A FUEL CONTAMINATED ARCTIC MINE SITE³

4.1 Introduction

More than 99% of spilled fuel in contaminated environments remains as trapped immobile or mobile free product in both the vadose and saturated zones of the subsurface (Weiner, 2000). Estimating the amount of free product remaining in such an environment is crucial to an effective remedial strategy. This study involves estimating the actual thickness of light nonaqueous phase liquid (LNAPL) hydrocarbon from measured apparent thicknesses in monitoring wells (MWs). This is done using a direct field approach at the Colomac mine site in the Northwest Territories (NWT). Chapter 2 discussed characterization efforts at the site in details. The site has 0–4.6 m of overburden soil over fractured bedrock. Steeves Lake is adjacent to the fuel-impacted zone. The overburden soil consists of sand and gravel until with some peat along the bank of the lake (Chapter 2). Between 1990 and 2003, approximately 24 spills of diesel fuel and some gasoline were reported at the site, as shown in Figure 4.1 (EBA, 2001, Biogenie, 2004). These were the result of leaks in stored fuel tanks and releases during transportation at the site. The major spills include 18,000 L in February 1990 and 27,300 L in February 1997.

Figure 4.2 shows the layout of the site, which can be divided into four areas, namely: tank farm, warehouse, Steeves Lake shoreline and powerhouse. More than 43 monitoring wells (MWs) were installed in 2000 using a diamond percussion hammer drill, and an additional 23 MWs were installed between 2005 and 2007 using a percussion rotary drill. The MWs were cased through the overburden soil up to 1 m into the bedrock. The annulus between the casings and the formation was backfilled with bentonite

³ A version of this chapter has been published. Iwakun, O., Biggar, K.W., Segó, D., 2010. Estimation of actual LNAPL thickness in a fuel-contaminated mine site. *Cold Regions Science and Technology*, 60:212-220.

pellets and flushed with water. The MWs were not screened below the casing. Table 4.1 shows a summary of the MW logs for selected MWs (EBA, 2001). The depths at which fractures were noted and fuel odors detected were referred to as fracture and product depths respectively (Table 4.1). The MW-logs showed detectable strong odor of fuel in the overburden soils and up to nine meters into the fractured bedrock. In MW 12 and 26, a faint odor (FO) of spilled fuel was observed more than 9 m into the bedrock. The well-logs also showed that the upper section of the bedrock is highly fractured, and that the fracture density decreased significantly with depth. Hydraulic test results (obtained in collaboration with scientists from Environment Canada) at the site (Figure 4.3) corroborated the MW-log data and rock cores examined in subsequent drilling by SEACOR (2007) shown in Figure 4.4. Thus, apart from the localized fractured zone in the upper section of the bedrock, it appears competent.

Chapters 2 and 3 described remedial measures implemented at the site. These include LNAPL recovery from MWs, the construction of a frozen core interceptor trench to mitigate free product migration to the adjacent lake, and the removal of overburden soil at the tank farm area and its biopile treatment on site. Despite these measures, LNAPL has persisted at the site.

The LNAPL thickness measured in MWs does not truly represent what is in the formation. Factors influencing apparent LNAPL thickness may include water table fluctuations, freezing-induced displacement, media texture, and the availability of free product in the formation (Weiner, 2000; Dippenaar et al., 2005; Chapter 3; Barnes et al., 2004). A depressed water table may enhance drainage of LNAPL in the vadose zone and remobilization into the MW of LNAPL trapped in a previously saturated zone. However, an elevated water table may push LNAPL back into the formation and entrap LNAPL below the water table (Catalan and Dullien, 1995; Aral and Liao, 2002; Chapter 3). In permafrost environments, water expansion due to freezing may cause the physical displacement of mobile petroleum hydrocarbon (PHC) from soil matrixes and enhance LNAPL accumulation.

Capillary suction in a formation will exert upward pull on LNAPL in the formation, thereby increasing its thickness and subsequent drain into the MW. This explains why LNAPL is thicker in finer formations thus, accumulated LNAPL in MWs is also dependent on its availability in a formation (Weiner, 2000). Thus, LNAPL thickness in a monitoring well is not representative and in disequilibrium with LNAPL thickness in the formation. This accounts for why measured LNAPL thickness in a monitoring well is often referred to as “apparent LNAPL thickness”. This disequilibrium is due to fluctuations in the LNAPL and water interface in the formation. Kemblowski and Chiang (1990) postulated that differences in the residual LNAPL saturation below and above the water table, and preferential flow through the monitoring wells account for LNAPL thickness variation in the formation.

The actual LNAPL thickness in a formation is often construed as a uniform saturated mobile LNAPL layer in the formation as illustrated in Figure 4.5. Methods often employed to measure the actual LNAPL thickness in the formation are direct and indirect methods (Saleem et al., 2004). The direct methods include excavation, use of geophysical probe, soil sampling, and bail down test. The indirect methods include theoretical correlations and empirical correlations based on laboratory experiments. The indirect methods assume that: (1) the formation is homogeneous; (2) There exist a uniform saturated LNAPL layer in the formation; and (3) that the MW and the surrounding formation are in equilibrium (Liao and Aral, 1999; Saleem, 2004; and Dippenaar et al., 2005). These assumptions have resulted in large uncertainty in using the indirect methods. Besides, the indirect methods are mostly incorrect due to natural heterogeneity and static disequilibrium in the formation (Hampton and Miller, 1988; Liao and Aral, 1999; and Dippenaar et al., 2005). According to Wagner et al. (1989), such analytical approach may lead to over estimation of spilled volume, and no indirect method can be trusted in the field without further validation.

The direct method commonly employed in the field is the bailout (or baildown) test because it is quicker, gives smaller value than apparent LNAPL thickness from the MW, and easier to perform than other direct methods (Hampton et al., 1990). The bail down test involve (1) bailing of free product from the MW; (2) measuring and plotting of depths to free product and water over time; and (3) interpreting and inferring the product thickness. However, controversy exists in the literature on the interpretation of data obtained from the bail down test because there is no established basis for why or how they work (Hampton et al., 1990; Testa and Winegardner, 2000). Huntley et al. (2000) argued that a “true LNAPL thickness” determination using bailout test has no theoretical basis, but provide useful information on LNAPL mobility in the formation under the prevailing hydraulic condition.

Figure 4.6 to Figure 4.8 illustrate some of the discrepancies in the interpretation of bailout test. Yaniga (1982) and Yaniga and Demko (1983) presented a graphical interpretation of the bailout test without any other justifications than correlation with measured values in the field using other approaches (Figure 4.6). Gruszczenski (1987) described another graphical interpretation of the bailout test based on the assumption that pendular water is negligible, fluid phases are independent of each other, and assume enough time has passed for equilibrium to occur (Figure 4.7). Furthermore, Hughes et al. (1988) discussed another graphical interpretation based on the assumption that the initial surface of the product is the same as that in the formation, neglects LNAPL flow from the capillary fringe above the LNAPL, and assume enough time has passed for equilibrium to occur (Figure 4.8). All the afore-mentioned methods of graphical interpretations are based on direct empirical comparisons of measured and interpreted LNAPL thicknesses in contaminated aquifers. Testa and Wingardner (2000) provide further discussion on these methods. The main disadvantages of the bailout test are:

- a. Neglects the effect of groundwater fluctuation on LNAPL thickness because the measurements taken are snapshots in time that do not consider fluctuation in LNAPL thickness;
- b. Neglects situations where the LNAPL in MW is not derived wholly or partly from the adjacent formation;
- c. Assumes the MW is in equilibrium with the formation; and
- d. It is developed for porous media and may not be valid for fractured media involving discrete flow.

However, at LNAPL contaminated sites in fractured bedrock environment, Dippenaar et al. (2005) evaluated both the indirect and direct field approaches and concluded that the direct field approach is more accurate because the assumptions of homogeneity and isotropy that underlie the indirect methods do not hold for most field conditions. Besides, the indirect approach does not account for capillarity. Thus, Dippenaar et al. (2005) proposed a new method termed “the modified Gruszczenski method” to estimate the maximum LNAPL thickness in fractured media. The method is empirical and based on field observations. This study considered the direct field approach suggested by Hughes et al. (1988), and the modified Gruszczenski method described by Dippenaar et al. (2005) to estimate the actual LNAPL thickness at the Colomac mine site.

4.2 Fieldwork

Pertinent field activities in estimating actual LNAPL thickness that corroborate inference drawn in this study include monitoring the depths to LNAPL and water in the MWs, borehole imaging, and rock coring. An interface probe was used to measure the depths of product, water and the apparent bottom of the MWs. Table 4.2 shows the apparent product thicknesses in selected MWs. Most of the MWs had measurable LNAPL since installation. LNAPL persists in MWs in the tank farm area, and around the warehouse and the shoreline of Steeves Lake. LNAPL occurrence is sporadic in some of the MWs shown in Table 4.1. MWs chosen for analysis in this

study are those with free product all year round. Combinations of bailers and pumps were used to recover over 1000 L of free product between 2005 and 2007.

A Well-Vu camera system was used to image the MWs to observe the location of the major fractures and contaminated zones in the subsurface. Imaging results were correlated with the MWs logs and hydraulic tests at the site. Fracture widths were measured where possible from post-image analysis, and zones of marked discoloration were interpreted as product seepage zones. However, the camera system has some important limitations. While easy to deploy, it cannot provide images from oil-smear zones due to reflection of light. The MWs with persistent free product were installed in 2000 using percussion hammer drilling, and formed the basis of analyses in this study. The imaging does not ascertain the interconnectivity or extent of fracturing in the formation, and the observed fractures may be artefacts of MW scarring associated with drilling. Thus, direct correlation of the measured fracture width from the images with the coefficient of permeability is inappropriate.

Multiple seepage zones exist in MWs 12 and 26 north of the tank farm area. Figure 4.9 shows a sample snapshot in one of the MWs. Other selected images of the MWs are given in Appendix E. From the photographic measurement of some of the images, the estimate of average macro fractures is 800 μm , and that of micro fractures are less than 100 μm . Figure 4.10 and Figure 4.11 show the summary of the logged inclinations of the core fractures (SEACOR, 2007). It was not feasible to measure the orientation of the bedrock features in the MWs using the camera because of its uncontrolled rotation when lowered. Bedrock outcrops at the site were used to infer the orientation (i.e., azimuth shown in Figure 4.10) of the fractures at the site. This orientation is the same as dip direction of the fracture planes. Figure 4.10 and Figure 4.11 show that the principal directions of the fractures are northwest, and are mostly sub-vertical and sub-horizontal as discussed in Chapter 2.

In general, the imaging results showed that the fracture intensity at the upper section of the bedrock is high. The MWs drill-logs and the hydraulic tests at the site corroborated such conclusion. Zones with marked discoloration (interpreted as contamination) were observed in the upper section (~ 5 m) of the bedrock. This is in agreement with a previous investigation at the site, which suggested that LNAPL might be trapped in the vadose zone (URS, 2002). However, contrary to that previous investigation, which stated that LNAPL might be limited to the soil-bedrock interface, it appeared that LNAPL had penetrated the shallow interconnected fractured section of the bedrock. Of MWs across the site, only those near the warehouse contained murky water. The murkiness may be due to contamination by oil and grease used in the mechanical workshop at the warehouse.

Between April and June 2007, 15 MWs were installed at the site (using rotary coring) to improve delineation of subsurface geology, contamination extent, and the recovery of free product if found. The drilling also provided an opportunity to obtain core samples from the subsurface. Samples of the recovered rock cores are shown in Figure 4.4. Bedrock was reached at a depth of more than 3 m around the warehouse and south of the site. The rock quality designation (RQD) of the upper 1.5 m of the bedrock was below 50%. Between 1.5 and 5 m, it ranged from 50 to 100%. Below 5 m, it was above 90% for most of the recovered cores (SEACOR, 2007). This agrees with inferences drawn from the hydraulic test results and borehole imaging at the site.

The fracture pattern in the upper section of the bedrock is sub-vertical and horizontal. The inclination of the sub-vertical fractures ranged from 60° to 85° to the horizontal, and that of the sub-horizontal fractures ranged from 0° to 40° to the horizontal. The horizontal fractures are between 0.3 and 1 m apart, and their frequency decreases with depth. At the warehouse, the observed fractures are mainly horizontal with occasional sub-vertical features. Hydrocarbon odor was noticed between 3.3 and 3.6 m

below the surface at the warehouse. At the north side of the site, bedrock is around 4.6 m below the surface, and the overburden consists of blast rock fill. The fracture pattern is similar to that at the south side and the mineralogy of the core samples at depth was calcite quartz (SEACOR, 2007). There is a layer of peat-like material above the bedrock surface with increasing thickness towards the lake. At depth, the bedrock is competent but intercepted with fractures associated with fold remains. Fuel odor was noticed in cores obtained from new MWs near MW 12 and 26 up to 9 m into the bedrock.

4.3 Methodology

Two direct field approaches to determine LNAPL thickness at the site are that of Hughes et al. (1988) and the modified Gruszczenski method as described by Dippenaar et al. (2005). The former involves the probing of MWs to determine depths to static water and LNAPL, and bailing out only the free product (LNAPL) from the MW. The LNAPL and water are then allowed to equilibrate with the formation. During equilibration, a level is reached at which the LNAPL recharge rate decreases at a steady rate until equilibrium. This inflection level is taken as the base of mobile free product layer in the formation. Thus, the actual LNAPL or product thickness is the distance between the inflection point and the initial static level at the top of the LNAPL layer. Determining the inflection point requires plotting the LNAPL level as a function of time after the removal of free product from the MW (Figure 4.8). The challenges of this approach are bailing out only free product from the MW, and monitoring formations with slow LNAPL recharge rates. The physical basis of this test is that if the depth of water table in the formation, which corresponds to the base of the LNAPL layer, can be determined. Then, it is possible to estimate the actual LNAPL thickness in the formation by subtracting the depth to product (DTP) from the depth to water table, assuming the DTP in the monitoring well is the same as that in the formation.

The second direct field approach overcomes the abovementioned difficulties but requires data spanning over a longer period of monitoring. In this method, both oil and water are recovered from the MWs. However, it also requires probing of MWs for water and free product. Thus, for MWs that have undergone periodic bailouts, the logged data for depths to water (DTW) and depths to free product (DTP) are used to estimate the actual product thickness in the MWs. Determining the actual product thickness involves plotting the apparent product thickness against the DTP and DTW. The level corresponding to the intersection of DTP and DTW trends is taken as the static DTW or water level, and the product thickness corresponding to the intersection of the trends is the maximum actual product thickness in the formation (Figure 4.12). The static DTW is the level at which there is no free product suppressing the water (Dippenaar et al., 2005). Formation heterogeneity and temporal water table fluctuation are implicitly factored into the analysis with the determination of the static water level. Thus, the modified Gruszczenski method takes into consideration the historical free product fluctuations, mathematical indiscernible processes (i.e., changing hysteresis, saturation, and capillarity), and historical data. The method does not attempt to determine a single actual product thickness but maximum actual product thickness that can occur in the formation.

Analysis through this direct field approach requires the use of MWs with continuous measurable free product. This is valid only for MWs 12, 26, and 17 as shown in Table 4.2. Other MWs with very thin free product, i.e. MW 30, were analyzed for comparison purposes. The method described by Hughes et al. (1988) was implemented in MW 26 in June 2006 and in MW 12 in December 2006. The amount of LNAPL in the MWs influenced their selection for the test. However, for the modified Gruszczenski method, no special test was carried out because the available historic MWs probe data for DTW and DTP were used for the analysis.

4.4 Results and Discussion

Table 4.3 shows the results of tests conducted in MW 12 and 26 using the method by Hughes et al. (1988). No analysis was performed on the test results because the LNAPL recharge was insignificant during the three- to four-day testing period in both MWs. The reasons for the insignificant recharge may include: (a) slow recharge rate, (b) inactive mechanism mobilizing flow, (c) blockage of migration pathways by ice veins as discussed in Chapter 3, and (d) geology of the site. The slow LNAPL recharge rate may be caused by trapping of the LNAPL in the vadose zone by capillary suction, which is complicated by significant ground ice at the site. LNAPL accumulation in MWs 12 and 26 occurred between 6 and 10 m below the ground surface. Since the overburden soil is only 1.2 m thick in that area, the fracture pattern and orientation will dictate the movement of LNAPL in the fractured upper section of the bedrock. If no pool of LNAPL exists at the depth of accumulation in the MWs, the observed LNAPL may come from a shallower part of the formation as depicted in Figure 4.13. The vertical and sub-vertical fractures intersecting the MW may not be positioned to allow significant recharge of LNAPL in the MW at depth. Reasons for this may include: (1) The intersecting fracture dips up-gradient past the saturated belt of the LNAPL, (2) it is outside the capture zone, (3) the saturated LNAPL layer may be so thin that it requires more time for gravity drainage to occur. If the intersecting fractures are outside the capture zone, the LNAPL may accumulate in other fractures that do not intersect the MW. Remobilization of such LNAPL may require the raising of the water table and thaw of the upper zone.

Some accumulation of LNAPL in the MWs may result from remobilization of LNAPL trapped in the formation resulting from gravity drainage, water table, and thermal fluctuation. Ground warming may enhance LNAPL movement by thawing ice blocking the migration pathway of the mobile LNAPL and/or reducing LNAPL viscosity. Other impacts of ground

warming include increase in volatilization and solubility of LNAPL components, which may reduce the amount of residual free product in the formation. LNAPL recharge and accumulation resulting from ice thawing may be sharp and discontinuous. The same may be true for the freezing process where expanding ice may cause the displacement of isolated blobs of trapped LNAPL in the formation, thereby enhancing their gravity drainage. The magnitude of movement due to freezing induced displacement is dependent on water content and the degree of matrix interconnectivity. Thus, it seems the method described by Hughes et al. (1988) is unsuitable for determining the actual LNAPL thickness in the formation for this site.

Using historical data of depths to product and water for MWs 12, 26, 17, and 30, the modified Gruszczenski method by Dippenaar et al. (2005) was used with results shown in Figure 4.14 to Figure 4.17. Analysis of the data from MWs 12 and 26 suggested that LNAPL accumulation in the MWs occurred between 8 and 10 m below the ground surface. The zone of accumulation does not imply that a pool of LNAPL exists in the formation adjacent to it because the LNAPL did not recover appreciably when bailed out. The estimated maximum actual LNAPL thickness north of the tank farm area around MWs 12 and 26 is 8 cm (Figure 4.14 and Figure 4.15). Comparison of the fracture pattern in this zone with the well log and borehole image does not reveal any special features at that depth. This implies that the accumulated LNAPL may have come from the upper fractured zone in the bedrock. The lack of LNAPL recharge when bailed suggested that temporal fluctuation in the water table played an important role. Raising the water table may cause buoying and remobilization of LNAPL in locked up fractures, which may subsequently drain by gravity when the water table recedes. Thus, raising the water table may recharge vertical and sub-vertical fractures intersecting the MW, thereby enhancing LNAPL accumulation in the MW when the water table recedes. Recent excavation around MW 12 and 26 revealed LNAPL thickness of approximately 3 cm at 8 m below the ground surface (JWA, 2009). This value is below the estimated

maximum actual product thickness and the discrepancy may be attributed to lack of time for LNAPL equalization in the field and cumulative recovery of LNAPL at the site.

The data for MW 30 adjacent to the lake did not present a clear trend as shown in Figure 4.16. The apparent LNAPL thicknesses in MWs adjacent to the lake are lower than the measured apparent LNAPL thicknesses observed in MWs 12 and 26. The data suggest a mixed zone of water and LNAPL within one meter of the ground surface. Thus, migrating LNAPL from the tank farm area and the remobilization of those trapped in the subsurface adjacent to the lake may account for the LNAPL measured at this location. Subsurface characterization also revealed a near vertical feature parallel to the bank of the lake around MW 15, 29, and 30, which may serve as a conduit for LNAPL storage. However, for safety reasons, the area was not excavated.

Analysis of MW 17 data around the warehouse shows that the maximum actual product thickness is zero. Figure 4.17 also showed a clear trend of LNAPL accumulation as the water table recedes. The static water level in the warehouse area is 4.625 m below the ground surface. MW log, bedrock core and borehole imaging suggested that fuel impact is limited to 3 m below the ground surface. However, there is the possibility of LNAPL trapping and storage in shallow vertical and sub-vertical fractures in the area. Water table fluctuation may remobilize trapped mobile free product in this area. The active layer of thermal fluctuation is extended up to 14 m below the water table in this area (Figure 4.18). Thus, freezing displacement and temperature induced capillary drainage associated with cyclic freeze-thaw may play secondary roles in mobilizing free product in that area as discussed in Chapter 3 and Chapter 6.

At this site, the measured apparent free product thicknesses did not come from LNAPL pool above water table in the adjacent formation. The idea of uniform saturated LNAPL thickness is not applicable to all media. Product thickness in the formation is not a single value because it depends on the water table fluctuations, changes in residual saturation, wetting history, and

capillary regime. Thus, the actual product thickness can be construed as equivalent to the thickness of mobile LNAPL in the formation if allowed to accumulate atop the water table. Thus, if the extent of the contaminated area is known, the volume of recoverable hydrocarbon can be estimated.

4.5 Conclusions

In this study, a direct field approach was used to estimate the actual LNAPL thickness in the formation at the abandoned Colomac mine site. Both the modified Gruszczenski method and that described by Hughes et al. (1988) were evaluated. The modified Gruszczenski method provided useful estimates of the actual LNAPL thickness at the tank farm area where most of the contamination occurred. The value obtained was corroborated by excavation at the site around MW 12 and 26. The actual LNAPL thickness varied across the site, but the estimated maximum actual LNAPL thickness north of the tank farm area was 8 cm and the observed actual thickness was 3 cm. This discrepancy is attributable to cumulative LNAPL recovery at the site. The method described by Hughes et al. (1988) was unsuitable for this site because of low LNAPL recharge in the MWs after bailing. The study shows that the depth of LNAPL accumulation in the MW does not always correspond to that of the LNAPL pool in the adjacent formation, especially when dealing with fractured media. Analysis of the data suggests that water table fluctuation plays an important role in mobilizing free product from the formation at the site. Water table elevation plays an additional role of remobilizing the available free product from dead end fractures in the formation. However, engineered fluctuation of the water table to enhance free product recovery without well-controlled boundaries may enhance contaminant migration. Seasonal deep freezing in the fractured bedrock also appears to play a significant role in seasonal LNAPL mobility but the effect is uncertain and requires additional study.

Table 4.1 Drill log for selected monitoring wells (MWs).

Well	BH12	BH15	BH17	BH26	BH30
Date	20/02/00	16/02/00	18/02/00	03/03/00	04/03/00
Elevation (m)	330.479	323.883	328.111	330.949	322.564
Well - OD (mm)	144	144	144	144	144
C - Length (m)	2.3	1.5	4	2.3	1
C - AGL (m)	0.79	0.83	0.88	0.97	0.37
Overburden	0 - 0.5	0 - 0.2	0 - 2.7	0 - 1.2	0.0 - 0.1
Soil type	Gravel fill	Gravel fill	Gravel fill	Gravel fill	S and G fill
Bedrock type	Greywacke	Greywacke	Greywacke	Greywacke	Greywacke
Well depth	20.7	8.83	21.3	21.2	9.3
	F - Depth P -Depth	F - Depth P -Depth	F - Depth P -Depth	F - Depth P -Depth	F - Depth P -Depth
	2.5 11.6 (SO)	4 4	4.8 0.6	2.9 2	3.7 0.4
	3 14.6 (SO)	4.5 4.6 (SO)	6.8 4.5	4.8 4.3	3.8 7.6 (FO)
	4.2 17.5 (FO)	4.6	14 7.6	4.85 9.8	4
	5.4 20.2 (FO)	4.6 to 6 (5)	14.1 10.5 (FO)	8	4.2
	11.2 to 15	6		8.8	5.5
				10.2	5.7
				10.4	6.1 to 6.3
				11.3	6.6
Comment	Drill encountered water at 10.7m Wet cuttings between 10.7 and 12.5			Strata at 9.8m is light, moist, and smells of diesel	

AGL Above ground level G Gravel S Sand
 C Casing FO Faint odor SO Strong odor
 F Fracture P Product

Table 4.2 Apparent LNAPL thickness of selected monitoring wells from 2005 to 2007.

Date	Monitoring wells (MW)								
	MW 8	MW 9	MW 12	MW 14	MW 15	MW 17	MW 19	MW 26	MW 30
Product thickness (cm)									
23/06/05	2	11	4	5	2	51	9	15	3
24/07/05	3	3	7	2	3	26	6	7	2
11/08/05	3	16	6.5	1	14	28	7.5	2	12
12/09/05	6.3	14	7.5		9.4	13.8	2.9	25	6.8
12/12/05		67	501	0.5	9	13.8	3	368	3
15/06/06	2	76.5	21.5	51	6.6	47	28.6	231.9	
06/07/06	2	15	1	9	8	5	21	26	18
06/08/06	2	17	2	8	6.5	4.5	20.5	25	15.5
14/12/06		2	209	13	6	140	6	21	
15/05/07		31.9	22.3	3	4	4	20.5	131	0.1
12/06/07			2.5	2		18	7	120	
13/09/07		2.3	0.3		0.7	0.2		74	

Table 4.3 Data obtained using the method described by Hughes et al. (1988).

MW	DTP (m)	DTW (m)	DTB (m)	PT (m)	Time	Date
26	8.91	11.00	21.80	2.095	9:44 AM	20/06/06
	10.25	10.27	21.40	0.025	10:04 AM	
	9.72	9.77	21.40	0.05	10:34 AM	
	9.55	9.60	21.40	0.055	11:08 AM	
	9.42	9.50	21.40	0.08	1:34 PM	
	9.41	9.48	21.40	0.077	7:35 PM	
	9.40	9.46	21.40	0.065	2:55 PM	21/06/06
	9.40	9.48	21.40	0.075	3:08 PM	22/06/06
MW 12	3.28	3.45	4.85	0.164	2:18 PM	19/06/06
	3.47	3.50	4.89	0.03	2:38 PM	20/06/06
	3.48	3.51	4.90	0.03	3:21 PM	
	3.54	3.56	4.99	0.02	8:15 AM	
	3.59	3.61	4.97	0.015	10:45 AM	21/06/06
	3.71	3.75	5.10	0.045	8:10 PM	
	3.93	3.94	5.24	0.017	3:00 PM	
	4.18	4.20	5.24	0.017	4:00 PM	

DTP - Depth to product

DTW - Depth to water

DTB - Depth to bottom

PT - Product thickness

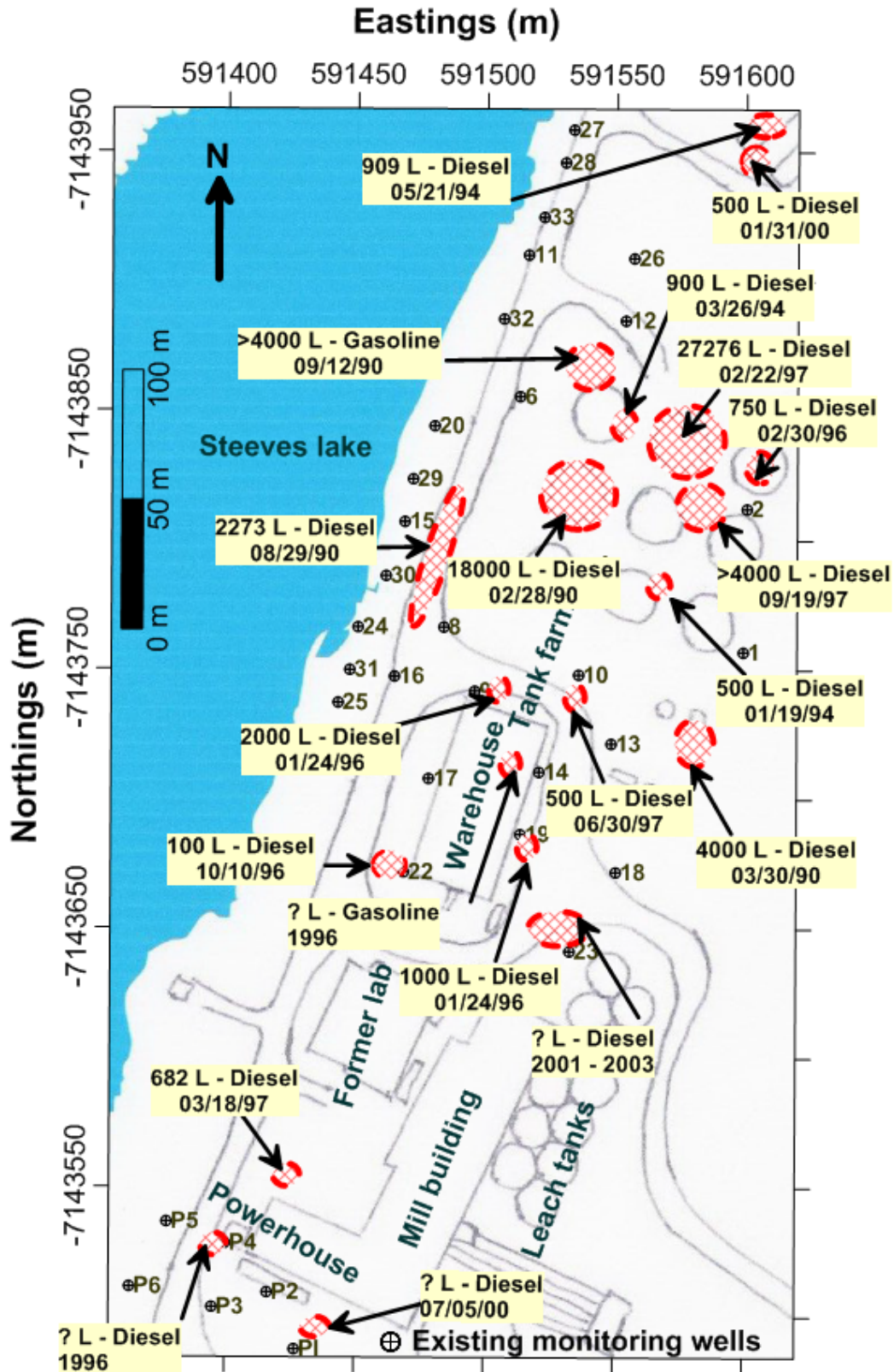


Figure 4.1 Fuel spill history at Colomac mine site. Shown on the map are the quantity spilled (when known), the location, and the date of spillage.

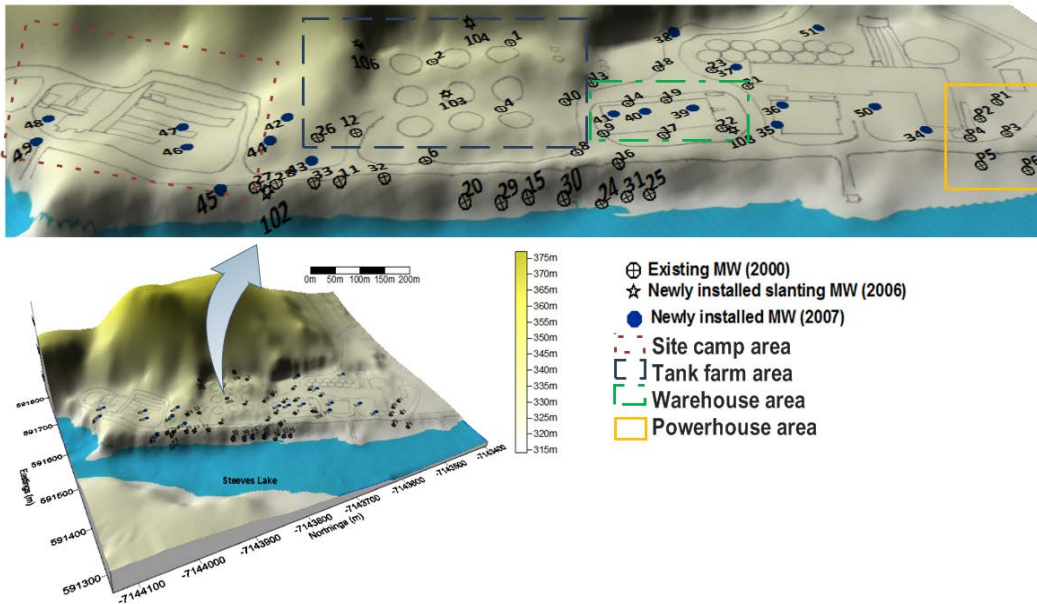


Figure 4.2 Site layout showing the relative location of the installed monitoring wells (MWs).

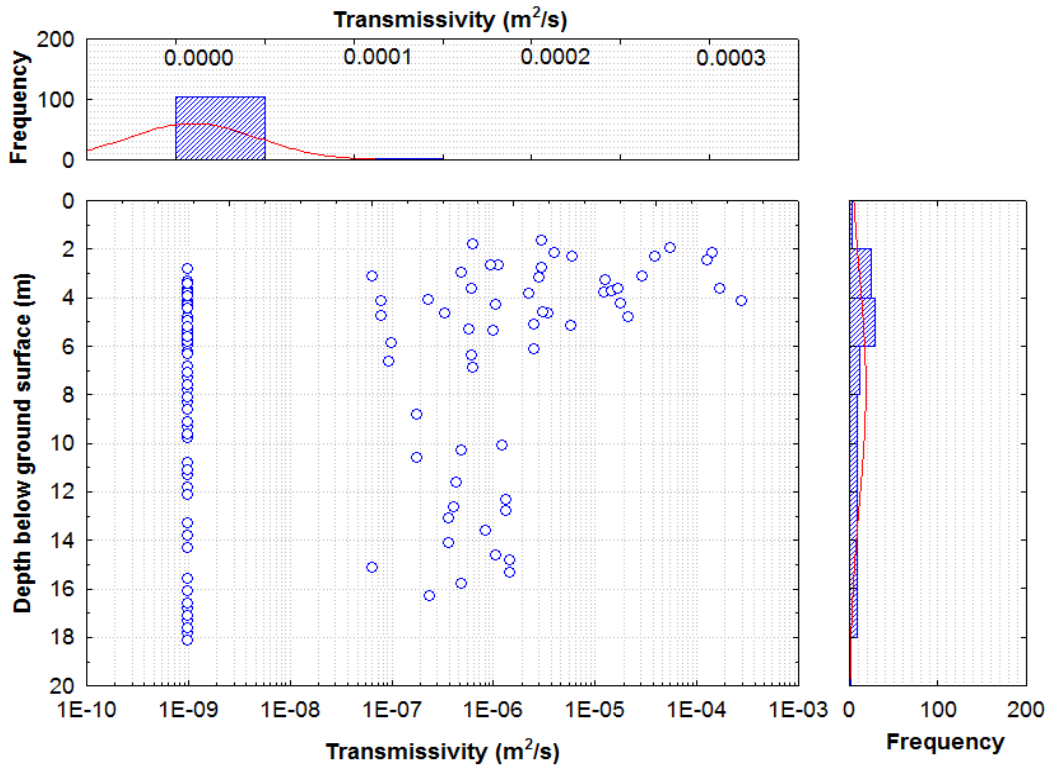


Figure 4.3 Transmissivity distribution at the site showing that the upper sections of the bedrock are more transmissive and that the mean transmissivity may be less than 10^{-9} m^2/s assigned to test sections that were too tight to test due to equipment limitations.

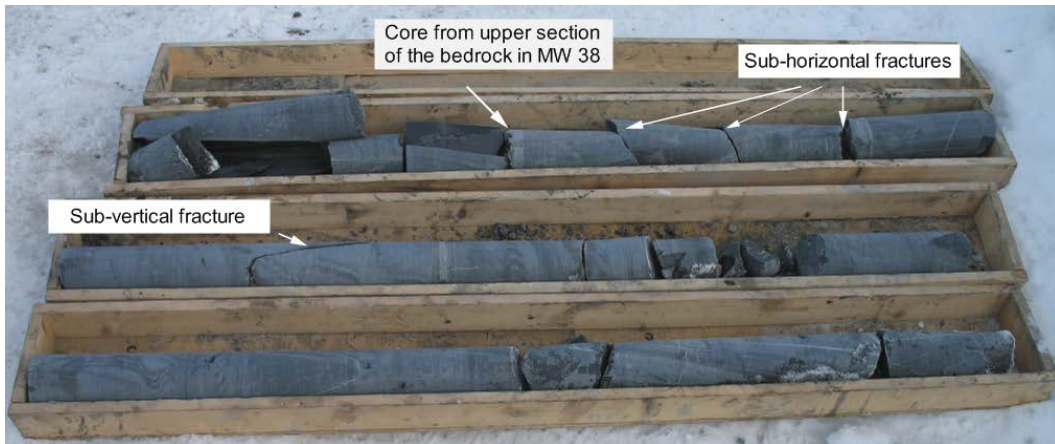


Figure 4.4 Core samples retrieved from one of the newly installed MWs (MW 38) at the site. The cores shown above are from the upper 4 m of the bedrock. The fracture pattern ranged from vertical to horizontal. The upper section of the bedrock is highly fractured with a rock quality designation (RQD) of less than 50% in many cases.

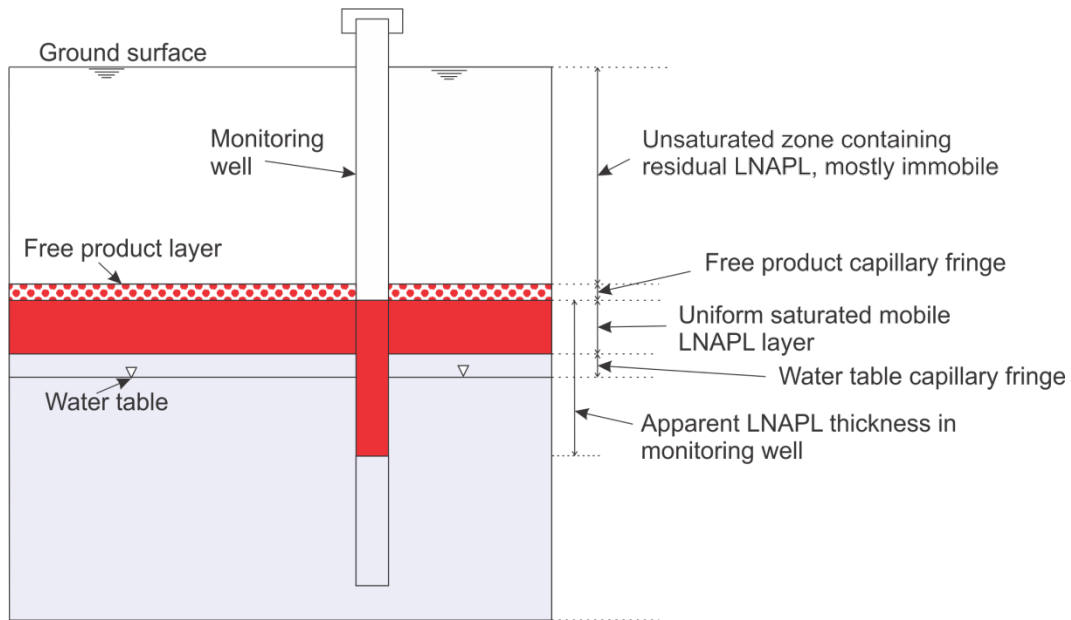


Figure 4.5 Illustration of actual LNAPL thickness in the formation as often construed in the literature (modified after Weiner, 2000).

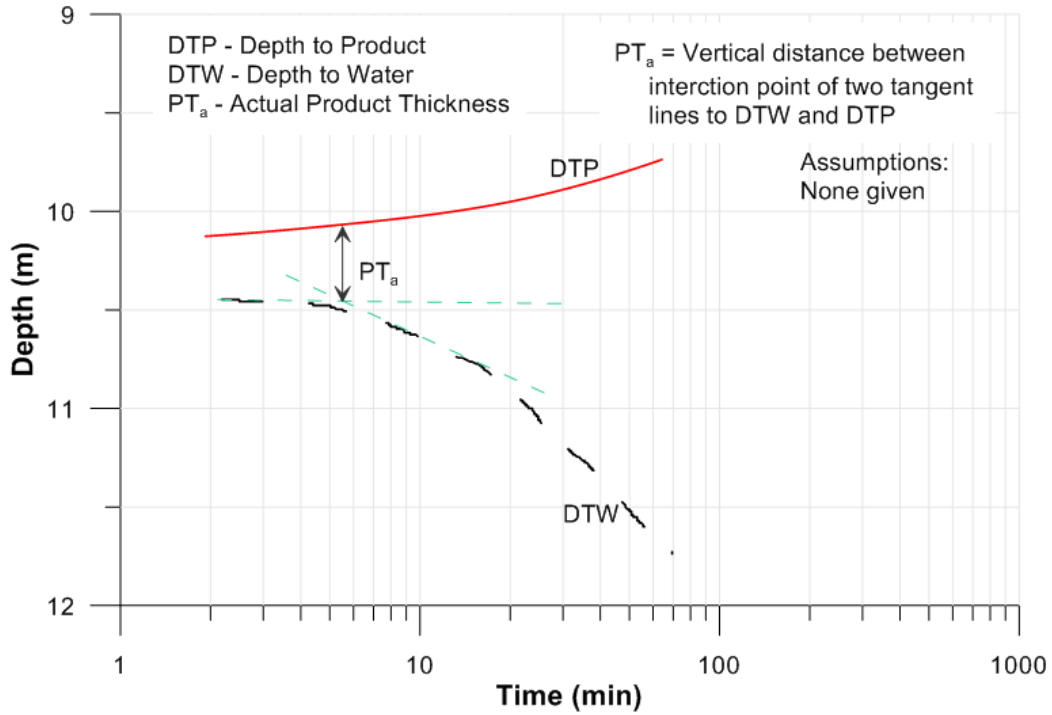


Figure 4.6 Sample of graphical results using Yaniga's method to estimate actual LNAPL thickness in the formation (modified after Hampton et al., 1990).

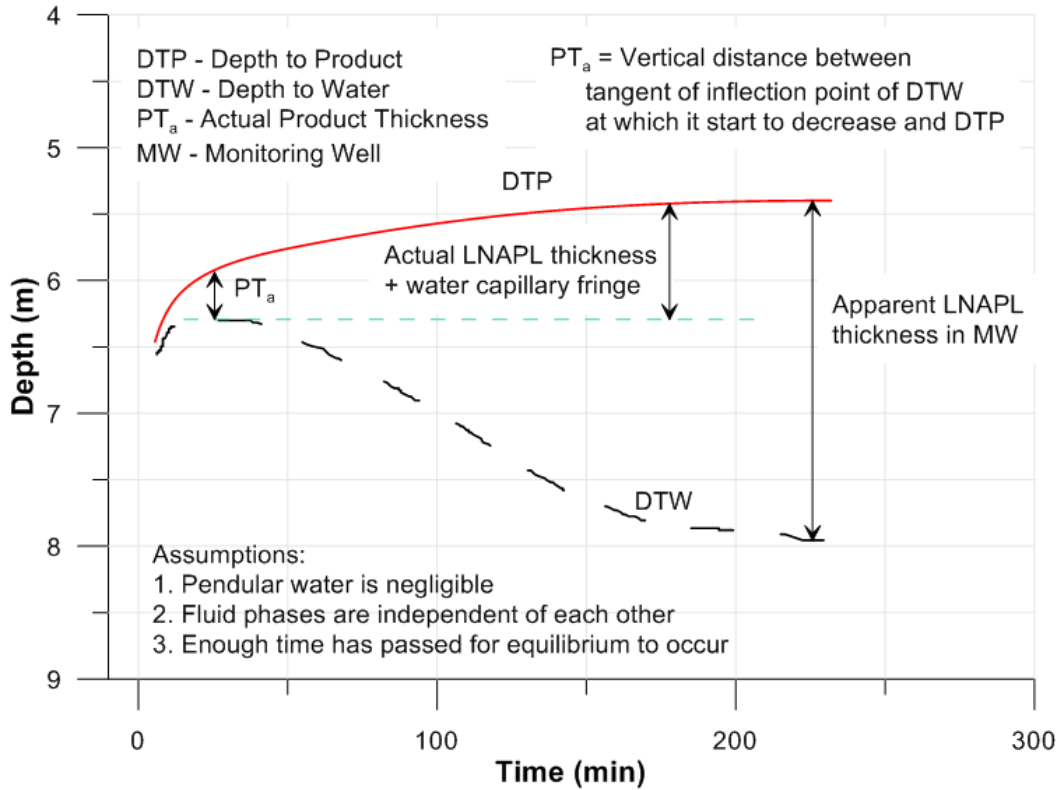


Figure 4.7 Sample of graphical results using Gruszczenski's method to estimate actual LNAPL thickness in the formation (modified after Gruszczenski, 1987).

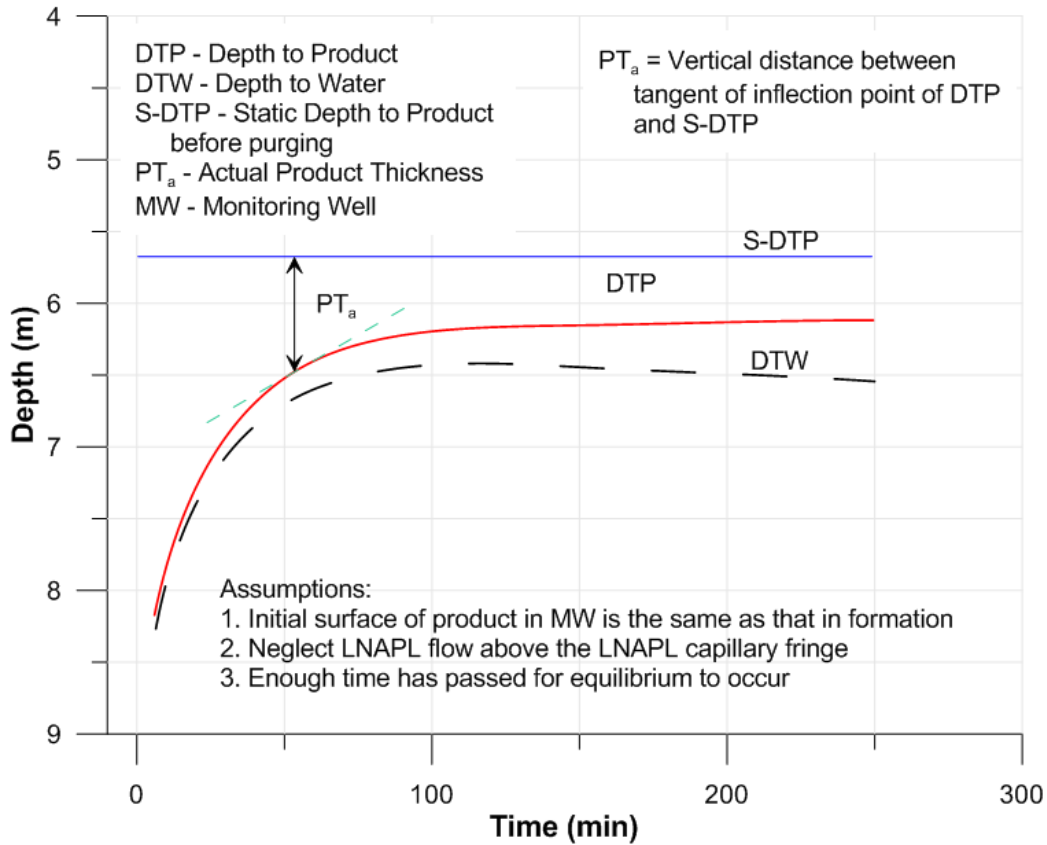


Figure 4.8 Sample of graphical results using Hughes et al. (1988) method to estimate actual LNAPL thickness in the formation (modified after Hughes et al., 1988).

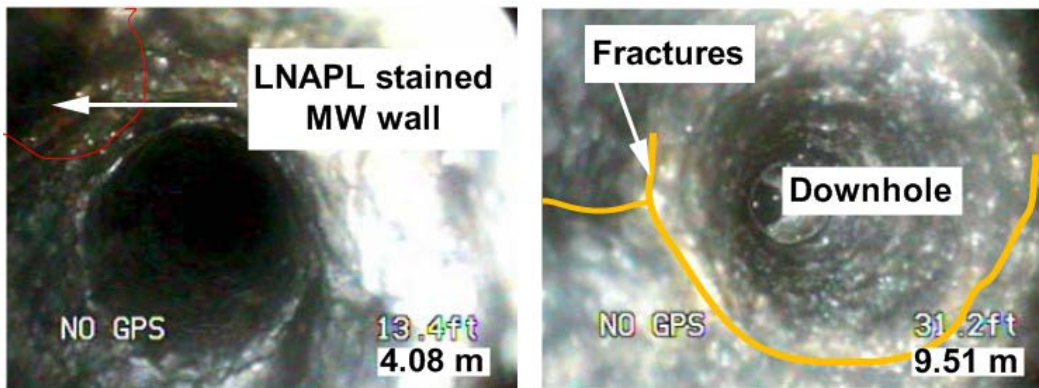


Figure 4.9 Sample of borehole image snapshots from Well-Vu camera. Characteristically stained sections of the MW are rife in the upper section of the bedrock. The image shown above is for MW 26. Accumulated LNAPL in the MW came from the contaminated upper section (~ 7 m) of the bedrock.

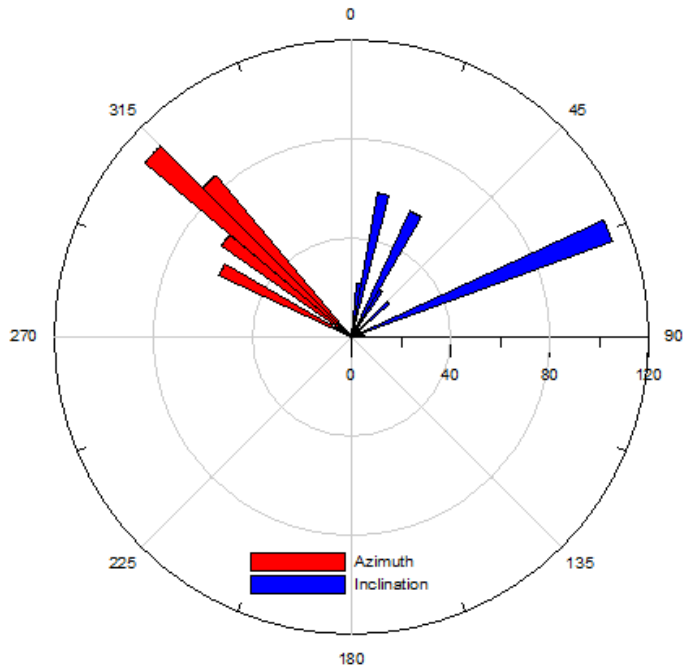


Figure 4.10 Rose diagram summarizing the azimuths and inclinations of fractures from bedrock core samples at the Colomac mine site. The azimuths are inferred from bedrock outcrops.

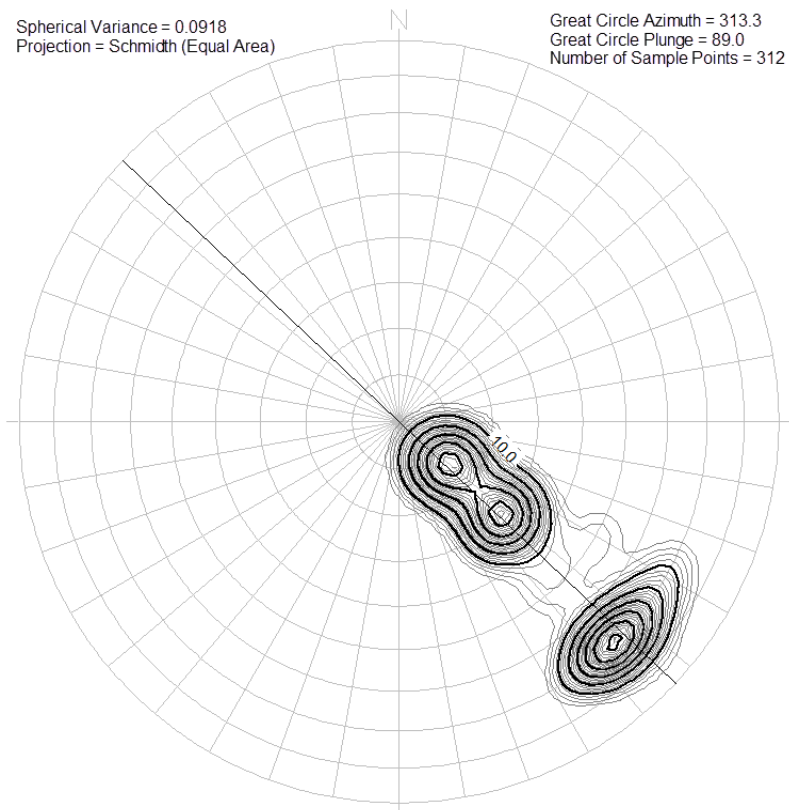


Figure 4.11 Stereonet the bedrock fractures. The data point density contour shows that the fractures are generally sub-vertical and sub-horizontal, and oriented northwest.

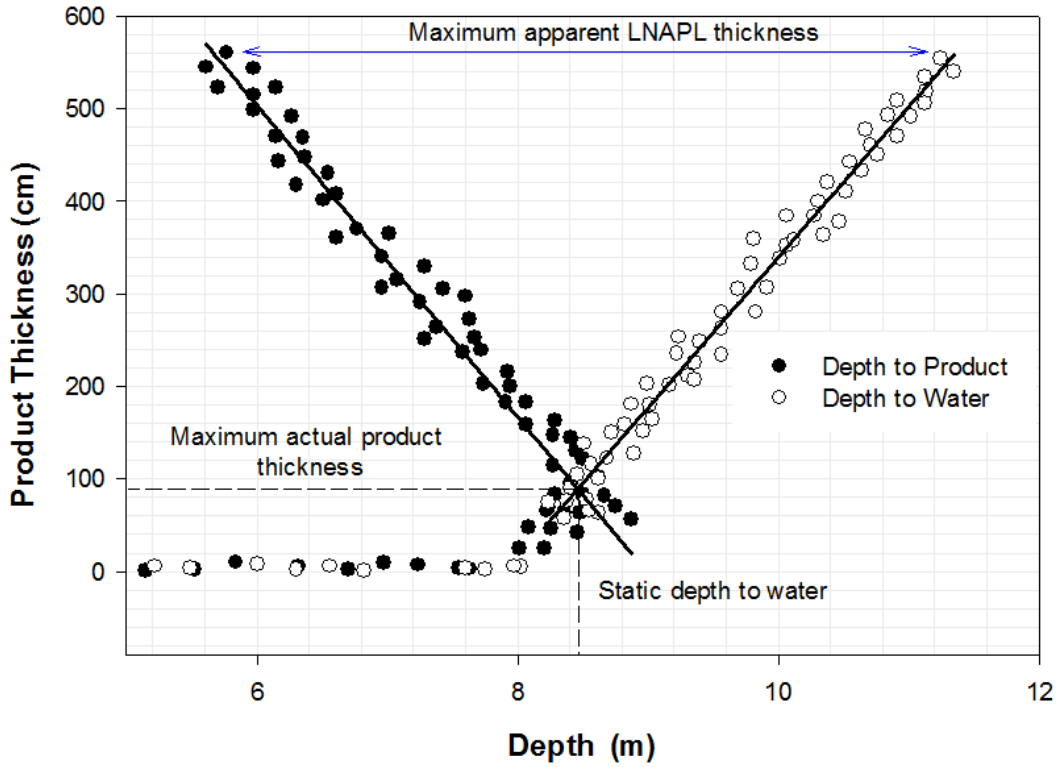


Figure 4.12 Sample of graphical results using modified Gruszczenski method.

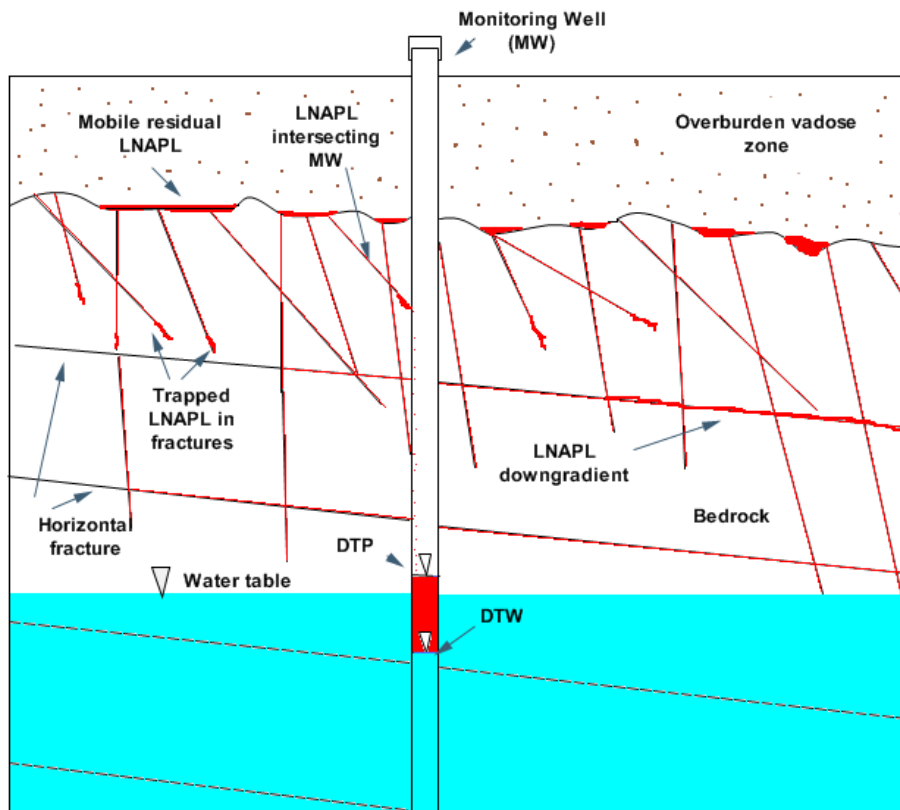


Figure 4.13 Conceptual geological section of subsurface contamination at the Colomac mine site.

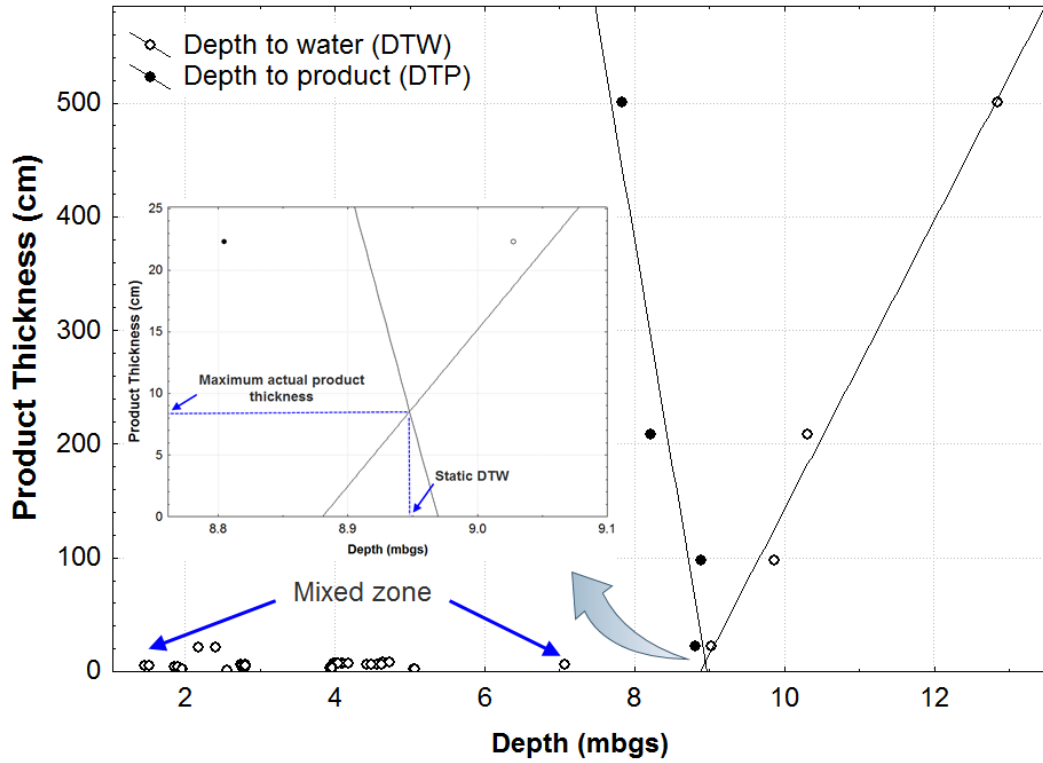


Figure 4.14 Analysis of product thickness estimation in MW 12.

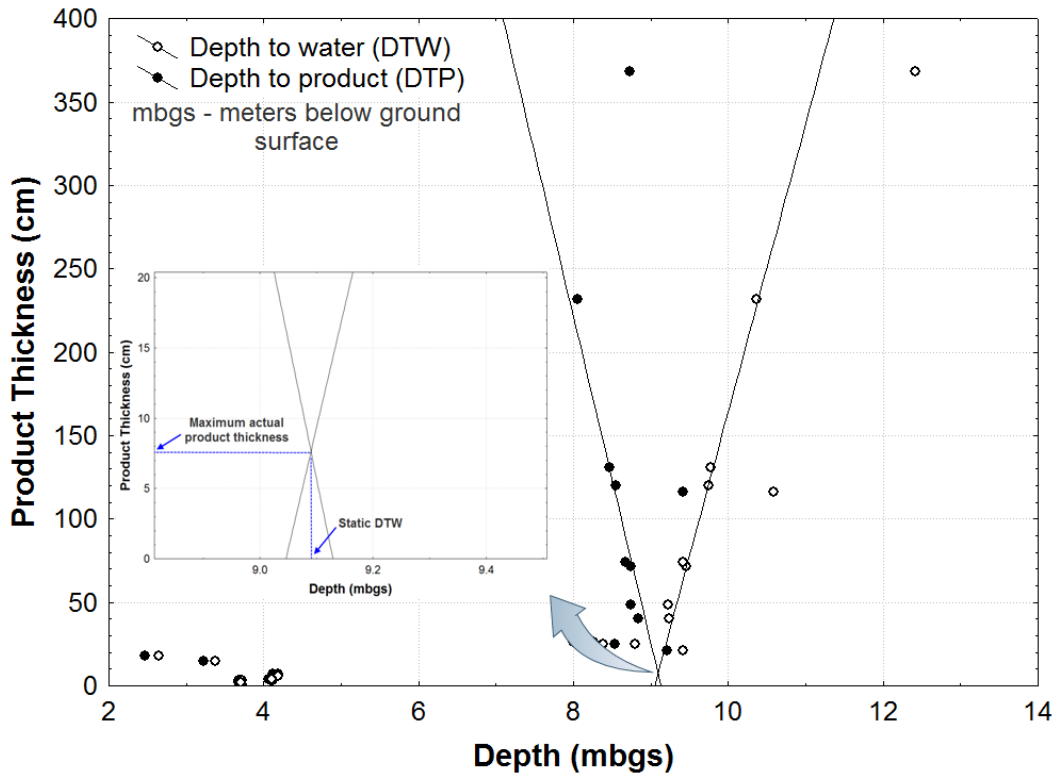


Figure 4.15 Analysis of product thickness estimation in MW 26.

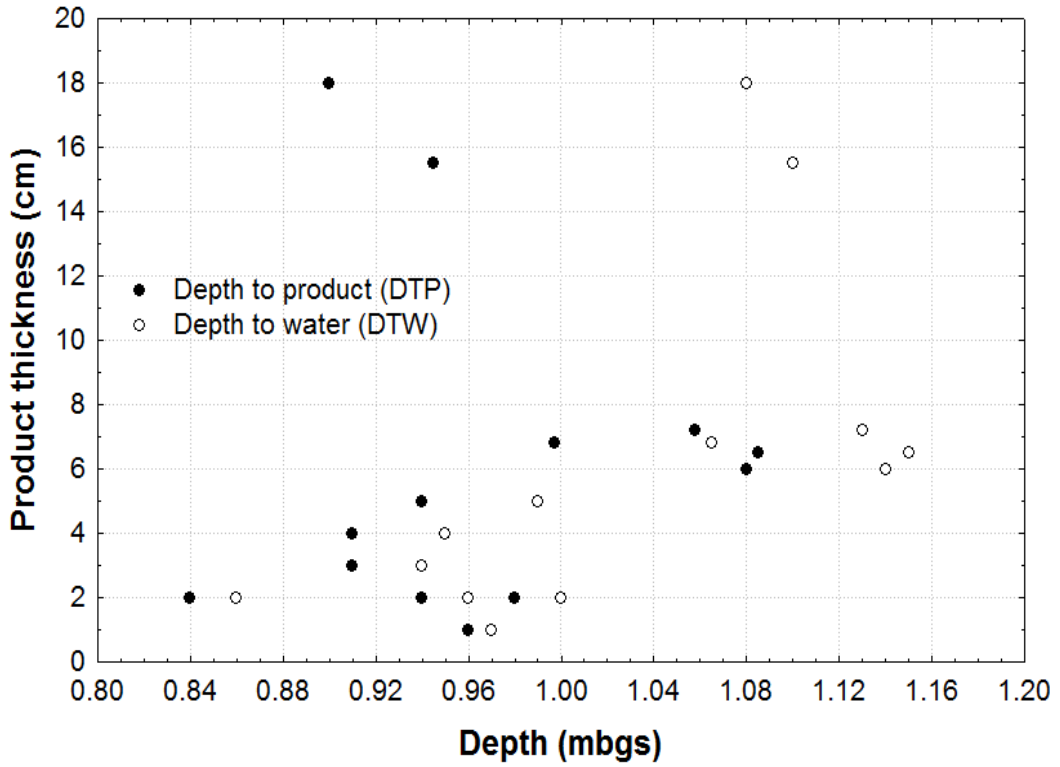


Figure 4.16 Analysis of product thickness estimation in MW 30.

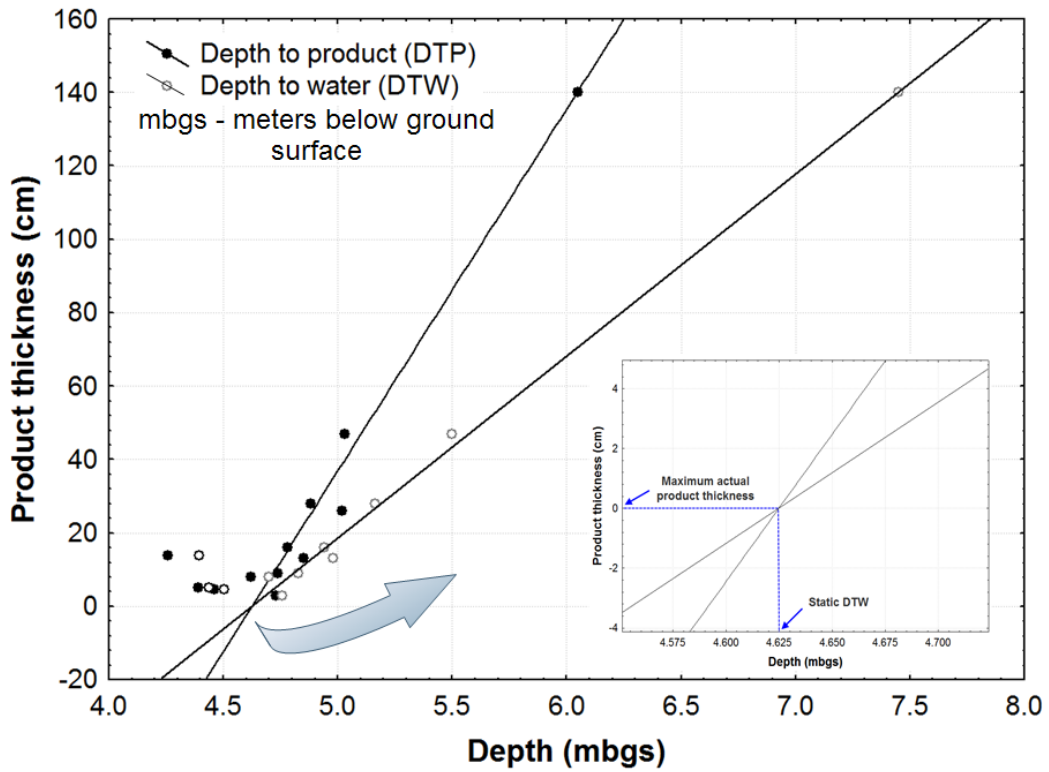


Figure 4.17 Analysis of product thickness estimation in MW 17.

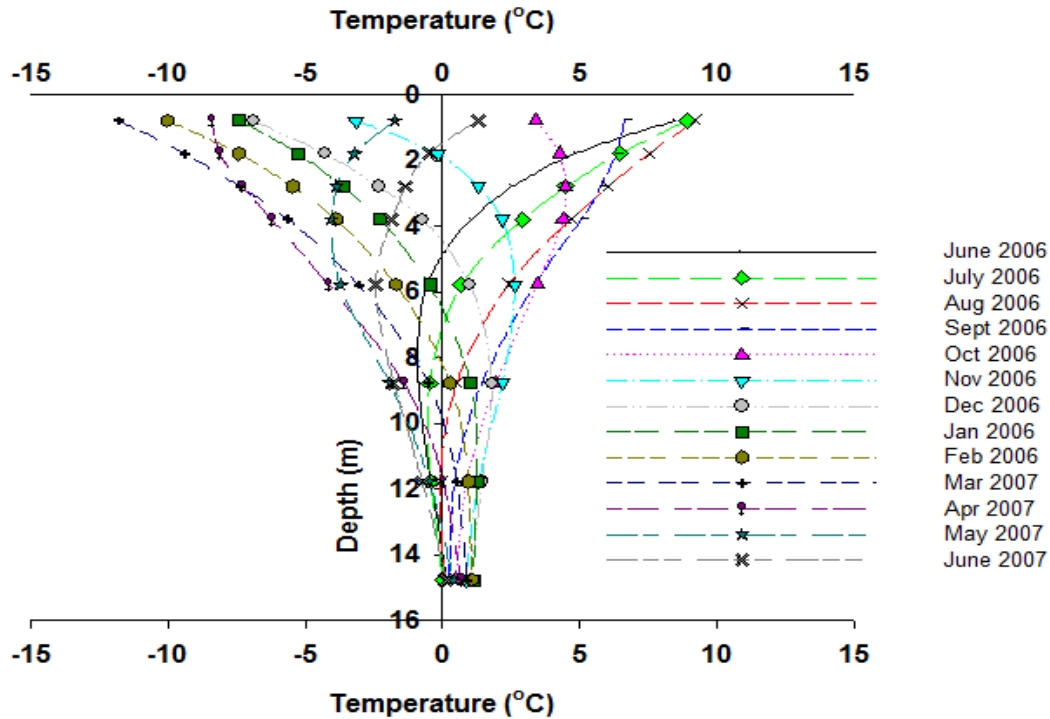


Figure 4.18 Monthly average temperature profile for thermistor probe near MW 9 at the warehouse area.

References

- Aral, M. M., Liao, B., 2002. Effect of groundwater table fluctuations on LNAPL thickness in monitoring wells. *Environmental Geology*, 45:151-161.
- Barnes, D. L., Wolfe, S. M., Filler, D. M., 2004. Equilibrium distribution of petroleum hydrocarbons in freezing ground. United Kingdom. *Polar Record* (214): 245-251.
- Biogenie S.R.D.C. Inc., 2004. Hydrocarbon contamination management. Phase I report—proposed remedial action plan. Report for Tli Cho Logistics, and Indian and Northern Affairs Canada, 47 p. and appendices.
- Catalan, L. J. J., Dullien, F. A. L., 1995. Application of gravity drainage to the recovery of residual LNAPL in homogeneous and lensed sand packs. *Journal of Contaminant Hydrogeology*, 18: 279-306.
- Dippenaar, M.A, Sole, M. D., Van Rooy, J. L., Du Toit, G. J., Reynecke, J. L., 2005. Determining actual LNAPL plume thickness: review and case study in

fractured aquifer. *Bulletin of Engineering Geology and the Environment*, 64: 347–360.

EBA Engineering Consultants Ltd., 2001. Hydrocarbon assessment, Lakefront and waste oil areas, Colomac Mine, NWT. Report to Deton 'Cho Corporation. Yellowknife, NT. 37 p. and appendices.

Gruszczenski, T.S., 1987. Determination of a realistic estimate of the actual formation product thickness using monitor wells: A field bailout test. *Proceedings Conference on Petroleum Hydrocarbons and Organic Chemicals in Ground Water - Prevention, Detection, and Restoration*, National Ground Water Association, Dublin, OH, pp. 235-253.

Hampton, D. R., Wagner, R. B., Heuvelhorst, H. G., 1990, A New Tool to Measure Petroleum Thickness in Shallow Aquifers: In *Proceedings of the National Water Well Association (NWWA) of Groundwater Scientists and Engineers Fourth National Outdoor Action Conference on Aquifer Restoration, Ground Water Monitoring and Geophysical Methods*, pp 127-141.

Hampton, D.R., Miller, P.D.R., 1988, Laboratory Investigations of the Relationship between Actual and Apparent Product Thickness in Sands: In *Proceedings of the National Water Well Association (NWWA) of Ground Water Scientists and Engineers and the American Petroleum Institute Conference on Petroleum Hydrocarbons and Organic Chemicals in Ground Water: Prevention, Detection and Restoration*, 1: 157–181.

Hughes, J. P., Sullivan, C. R., Zinner, R. E., 1988. Two techniques for determining the true hydrocarbon thickness in an unconfined sandy aquifer. In: *Proceedings of the National Water Well Association of Ground Water Scientists and Engineers and the American Petroleum Institute Conference on Petroleum Hydrocarbons and Organic Chemicals in Ground Water: Prevention, Detection and Restoration*, 1: 291–314.

- Huntley, D., 2000, Analytic Determination of Hydrocarbon Transmissivity from Baildown Tests: *Ground Water*, 38(1): 46-52.
- Jacques Whitford AXYS Ltd., 2009. Multi phase extraction system pilot test report. Submitted to Indian and Northern Affairs Canada. Project no. 1027392.02. Yellowknife, 64 p.
- Kemblowski, M.W., Chiang, C.Y., 1990. Hydrocarbon thickness fluctuations in monitoring wells. *Ground Water*, 28(2): 244-252.
- Liao, B., and Aral, M.M., "Interpretation of LNAPL Thickness Measurements under Unsteady Conditions," *Journal of Hydrologic Engineering*, American Society of Civil Engineers, 4(2): 125-134
- Saleem, M., Al-Suwaiyan, M.S., Aiban, S.A., Ishaq, A.M., Al-Malack, M.H., Hussain, M., 2004. Estimation of spilled hydrocarbon volume – the state-of-the-art. *Environmental technology*, 25: 1077-1090.
- SEACOR Environmental Inc., 2007. Environmental investigations of former Colomac mine, Draft report submitted to the Department of Indian Affairs and Northern Development Canada, Yellowknife, 115 p.
- Testa, S.M., Winegardner, D.L., 2000. Restoration of contaminated aquifers. 2nd Ed., Lewis Publishers, CRC Press LLC, Washington.
- URS Norecol Dames and Moore Inc., 2002. Assessment of hydrocarbons within fractured bedrock at the lakefront and waste oil areas and development of a remedial action plan, Colomac Mine, NWT. Report for Public Works & Government Services Canada. Vancouver, BC., 21 p. and appendices.
- Wagner, R.B., Hampton, D.R., Howell, J.A., 1989. A new tool to determine the actual thickness of free product in a shallow aquifer, in NWWA Conference on Hydrocarbons, pp. 45-59.
- Weiner, E. R., 2000. Applications of environmental chemistry: A practical guide for environmental professionals. CRC Press LLC, Florida.
- Yaniga, P.M., 1982. Alternatives in decontamination for hydrocarbon-contaminated aquifers: *Ground Water Monitoring Review*, 2: 40-49.

Yaniga, P.M., Demko, D.J., 1983. Hydrocarbon contamination of carbonate aquifers: Assessment and abatement, in Proc. 3rd National Symposium on Aquifer Restoration: NWW A, pp. 60-65.

5 GROUNDWATER GEOCHEMICAL CHARACTERIZATION AT THE COLOMAC MINE SITE⁴

5.1 Introduction

Restoration of a contaminated site to a site-specific cleanup standard requires a good understanding of the physical hydrogeology, hydrochemical characteristics, and geochemical interaction at the site. These understandings aid in risk assessment, proper selection of remedial technique, and evaluation of its effectiveness. In the Arctic and its environs, the discovery of valuable mineral deposits is increasing mining activities, and contamination arising from these activities can pose a significant challenge. This study attempts to gain insight into the groundwater evolution and geochemical processes at a fuel-contaminated site in a permafrost environment. The choice of the abandoned Colomac mine site was because it provided a rare opportunity to study the fate of petroleum contamination in a fractured bedrock permafrost environment. The main objectives of this study include assessment of the groundwater quality against Canadian Council of Ministers for Environment (CCME) guideline for freshwater habitat, and identification of the main geochemical processes at the site.

5.2 Site description

The Colomac mine site is located in a discontinuous permafrost environment within the Indin Lake Supracrustal Belt (ILSB), approximately 220 km northwest of Yellowknife, Northwest Territories (NWT) (Shelton et al., 2000, Chapter 2). The ILSB contains metavolcanic and metasedimentary rocks subjected to greenschist to amphibolites metamorphism at 2.6 Ga (Morgan, 1990). The site was an open pit gold mine that operated between

⁴ A version of this chapter has been submitted for publication. Iwakun, O., Ulrich, A., Biggar, K.W., and Sego, D., 2010. Geochemical characterization of a fuel contaminated fractured bedrock in a permafrost environment. Submitted to Journal of Environmental Engineering.

1990 and 1997. It became insolvent in 1999 and was closed and abandoned. At present, the contaminants and remediation directorate of Indian and Northern Affairs Canada (INAC) is responsible for its cleanup. The site has between 0 to 4.6 m of overburden soil that is composed primarily of sand and gravel with some peat towards the surrounding lakes, and is underlain by fractured bedrock identified as greywacke. The bedrock is strongly foliated with metamorphosed siliceous and slaty units (Hearn, 1990). At the site, the shallow gold mineralization is sulfide-hosted associated with pyrrhotite, pyrite, arsenopyrite, chalcopyrite, and magnetite (Hearn, 1990). According to Shelton et al. (2000), the mineralization occurred within quartz-carbonate veins within the metavolcanic rocks in close contact with the metasedimentary rocks at the site.

Bedrock outcrops at the site generally appear to be massive and competent, except near occasional site-scale linear features, where they appear weathered and highly fractured. Previous work and an examination of bedrock exposures at the site identified three major fracture sets, one sub-horizontal and two sub-vertical sets (Van Stempvoort et al., 2006; Chapter 3). On-site investigation suggested that the bedrock is competent at depth while the upper section is highly fractured (Chapter 2). While various areas of the mine site are being remediated, this study was carried out in the fuel-contaminated areas. More than twenty-four fuel spills (mainly diesel) were reported at the site between 1990 and 2003 (as shown in Figure 5.1), and various measures have been taken to mitigate fuel migration and to remediate the site. These measures were described in Chapters 2 and 3, and some are summarized in Figure 5.2. On-site efforts to characterize the extent of contamination and groundwater quality necessitated the installation of monitoring wells (MWs) in 2000 and 2005-2007 at the site (Figure 5.2).

5.3 Methodology

Three broad tasks implemented to achieve the stated objectives were depth probe monitoring, groundwater sampling, and installation of dedicated

thermistor boreholes at the site. Eleven thermistor strings with dedicated data-loggers were installed in 2006 to monitor thermal fluctuations of the ground to depths of 15 m (Figure 5.2). Each string had eight sensors spaced at known distances with a thermistor controller (data-loggers) at the top. Wooden frames were used to house the data-loggers one meter above the ground surface, which were operated using battery packs. The sensors with the data-loggers were periodically checked and downloaded, and the batteries replaced at intervals not exceeding six months.

An interface probe was used to measure the depth to the product (i.e., to free product petroleum hydrocarbon), to water, and to the bottom of the well for all sampled MWs before and during sampling when purged. The depth of thaw in the MWs was monitored in 2005 and 2006, wherein ice was inferred when the measured well bottom was less than the known depth of the MW. Several groundwater samples were taken at the site between 2005 and 2007 using a dedicated bailer. Discrete interval sampling using a peristaltic pump and packer assembly was undertaken in late August of 2005 as reported in Chapter 2. When the depth to water was greater than 8 m, a submersible pump was used. Most of the sampled MWs had only a thin film (less than 4 mm) of product or none at all. In MWs with continual free product, the product was removed before sampling. For non-discrete interval sampling, samples were taken at approximately one meter below the water level. The groundwater was sampled for both organic and inorganic constituents. For the non-discrete sampling events, three sample sets were taken, two for inorganic and one for organic constituents. The inorganic samples were subdivided into, namely, ion-samples and dissolved metals samples, and were filtered through 0.45 μm filters in the field. When sampling for dissolved metals, nitric acid (HNO_3) was added to bring the pH of the sample below two after filtration. The samples were then stored in a 200 mL plastic bottles. For ion-sampling, no preservatives were added. Added to samples for the organics, ammonia, nitrate, and nitrite to bring the pH below two was sulfuric acid. All samples were stored below 4°C until

analyzed in the laboratory. In the field, all organics were sampled directly to duplicate 44 mL glass vials without headspace for later direct analysis in the laboratory. Parameters measured *in situ* included pH, temperature, conductivity, and alkalinity. The first three parameters were measured using pH and conductivity probes and the latter with a Hach alkalinity test kit. For detailed sampling in 2005 and 2006, the dissolved oxygen (DO) in selected MWs was measured in the field immediately upon sampling using a CHEMETS DO tester. There were a number of instances of equipment malfunction in the field, especially with the pH and conductivity probes. In some cases, the probes failed to equalize after more than an hour in the harsh northern environmental conditions. Thus, the aforementioned parameters were not measured for all monitoring wells (MWs). Two sampling events were performed in both 2006 and 2007. The MWs were typically sampled in June and September of each year. The June samples represented the groundwater quality after the first snowmelt, and the September samples represented the water quality when the ground was thawed.

In the laboratory, the ions were measured by Ion Chromatography (IC) using a DIONEX ICS-2500 system, with CS12A and AS14A analytical columns for cations and anions respectively; using EPA method 300.1. An Inductively Coupled Plasma Mass Spectrometry (ICPMS) was used to determine dissolved metals, using EPA Method 6020. Analysis for the organics was done using Gas Chromatography with Flame Ionization Detector (GCFID), using EPA method 8015D. The groundwater sample analyses were performed at the Applied Environmental Geochemistry Research Facility at the University of Alberta.

Piper and Stiff diagrams were used for the interpretation of the inorganic constituents at the site. Conclusions inferable from Piper diagrams include the water type, precipitation or solution, mixing, and ion exchange (Hounslow, 1995). Figure 5.3 shows a summary of Piper plots interpretation. For source rock deduction, the bicarbonate to silicate ratio must be considered. Hounslow (1995) presented a table of source-rock deduction

summary of reasoning. This was used in combination with the Piper diagram for the groundwater analyses. In this study, the Stiff diagram is used to complement analyses from Piper diagram. The Stiff diagram reflects ionic composition of the water constituents, which are plotted on parallel axes to form a polygon with cations to the left and anions to the right. The shape of the resulting diagram is useful for source-rock deduction. Hounslow (1995) presents more details on Piper and Stiff diagrams. In this study, Rockware AqQA^(R) was used for internal constituency analyses (i.e., ionic balance). This was combined with Rockware Rockworks^(R) to generate the Piper and Stiff diagrams presented in this paper. A batch geochemical analysis was performed to determine the saturation indices for gypsum, calcite and dolomite for some of the MWs. PHREEQC was used to aid in the interpretation of the groundwater constituents. The updated WATEQ4F thermodynamic database by Ball and Nordstrom (1991) was used for the PHREEQC analyses. PHREEQC was also used to perform inverse modeling of the groundwater to determine its evolution pathway. Solution species for halite, biotite and plagioclase were added to the PHREEQC database used for the simulation.

Bicarbonate and carbonate concentrations were not determined in the laboratory but estimated from the measured total alkalinity in the field using equilibrium relationships based on mass action presented by Manahan (2000). These relationships are used by Rockware AqQA^(R) for computing the fractions of carbonate and bicarbonate in a given solution when the total alkalinity is provided. It is assumed that the main contributors to the alkalinity are the carbonate and bicarbonate species in the water.

The main organic constituents presented in this paper are benzene, toluene, ethyl-benzene, and xylenes (BTEX) with their spatial and time-series concentration. The geochemical analyses presented with respect to the feasibility of natural attenuation at the site are aimed at complementing previous studies discussed in Chapter 2, and Van Stempvoort and Biggar (2008).

5.4 Results and Discussion

Shown in Figure 5.4 are the chemical compositions of the groundwater at the study area for 2006 and 2007. Generally, the water compositions in the monitoring wells (MWs) plotted at the top of the diamond apex and left of it in the Piper plots, have elevated calcium ion (Ca^{2+}), sulfate ion (SO_4^{2-}), and bicarbonate ion (HCO_3^-) concentrations. Thus, in comparison with the Piper-plot interpretation summary (Figure 5.3), the groundwater at the site lay in the region of permanent and temporary hardness, and the source-rock is rich in gypsum. The chloride ion (Cl^-) concentrations of the groundwater were mostly less than 10 mg/L with few outliers, and the ratios of sodium ion (Na^+) to ($Na^+ + Cl^-$) are greater than 0.5 in all samples, implying sodium source other than halite is present. The Stiff diagram in Figure 5.5a shows that the calcium and magnesium concentrations in most of the samples were higher by at least a factor of two than other analytes except HCO_3^- and SO_4^{2-} . Thus, the excess sodium ion is likely not due to ion exchange or natural softening but dissolution of albite (or other plagioclase) in the formation. Except for MW 51 upgradient of the site, the calcium ion (Ca^{2+}) concentrations (in milliequivalent per liter) are greater than the sulfate ion (SO_4^{2-}) concentrations and the ratios of Ca^{2+} to ($Ca^{2+} + SO_4^{2-}$) are greater than 0.5. Thus, sources (i.e., carbonates or silicates) other than gypsum are likely responsible for the excess calcium. The ratios of bicarbonate concentrations (HCO_3^-) to silica concentrations (SiO_2) (in millimol per liter) are mostly greater than unity (Figure 5.5b), which infers that carbonate weathering predominates at the site and accounts for the excess calcium in the groundwater. Albite (plagioclase) weathering can be inferred in instances where the $HCO_3^- < SiO_2$ (Hounslow, 1995). The ratios of magnesium ion (Mg^{2+}) to ($Mg^{2+} + Ca^{2+}$) are less than 0.5, suggesting limestone and dolomite weathering. The calculated total dissolved solids (TDS) for most of the samples are greater than 500 mg/L, giving credence to

carbonate weathering at the site. Furthermore, the positions of the groundwater plots in the Piper diagram suggest that the ongoing geochemical processes are gypsum and calcite dissolution, pyrite oxidation, and albite dissolution. However, due to the difficulty in differentiating between pyrite oxidation from gypsum dissolution, further analysis was performed using PHREEQC as discussed later in this section.

Groundwater samples are further grouped into different sets according to their site location as shown in Figure 5.6. The interpreted contours of autumn groundwater flow is northwest (when the MWs are mostly thawed) as shown in Figure 5.6. The data used to produce the groundwater head contours were corrected for the measured apparent product thickness in the MWs, where applicable. Figure 5.7 and Figure 5.8 show the summary results of the grouped data sets of TDS, sulfate, total alkalinity, and dissolved iron at different locations at the site, subjected to the Kruskal-Wallis statistical test (Montgomery and Runger, 2003). Sample calculations of the analyses are given in Appendix F. The total dissolved solids (TDS) of each MW, calculated as summations of ions and silica in the data-group, and subjected to Kruskal-Wallis tests using STATSOFT STATISTICA®, showed no significant difference in the data sets at 5% significance level (Figure 5.7A). It should be noted that when the calculated probability “p” is greater than the significance level “ α ”, the mean differences are insignificant but when $p < \alpha$, the differences are significant. The same was true for sulfate and alkalinity at the site (Figure 5.7B and Figure 5.8A). However, for dissolved iron, significant differences exist in the grouped data sets (Figure 5.8B). The dissolved iron concentrations in the powerhouse area are significantly more than the other areas, and the differences may be attributed to iron (III) reduction associated with anaerobic degradation of the spilled fuel as discussed later in this section.

The mean sulfate concentration and alkalinity at the upgradient area are approximately 440 mg/L and 250 mg/L of $CaCO_3$, respectively, and the

most elevated at the site. Contrariwise, the sulfate concentrations and alkalinity are lowest at the tank farm and warehouse areas respectively (e.g., 300 mg/L and 160 mg/L of $CaCO_3$). Decreased sulfate is accompanied by elevated dissolved iron at the tank farm area, suggesting sulfate and iron (III) reducing conditions in that area as speculated in Chapter 2. Lower sulfate ion concentrations existed along the bank of Steeves Lake and the warehouse area, but these were not accompanied by increased dissolved iron concentrations. A precipitation reaction between the dissolved iron formed due to iron (III) reduction and the hydrogen sulfide produced due to sulfate reduction may account for the low dissolved-iron concentration (Van Stempvoort and Biggar, 2008). Similarly, the high dissolved-iron concentrations at the powerhouse area are not accompanied by reduced sulfate concentrations. This implies that iron (III) is the dominant electron acceptor in the area. Though the mean sulfate concentration at the powerhouse is lower by approximately 20% than that in the background, it is still high. The mean total alkalinity in the powerhouse area is within statistical variability of the sampled data, but higher by at least 10% than that in the surrounding areas with the exception of the upgradient area. Nevertheless, there are still differences between the hydrochemical features of the different MWs. These differences may be attributed to subtle changes in local geology, fuel contamination, and thermal regime across the site.

Comparisons of groundwater samples from June and September (given in Figure 5.4) showed no dramatic changes in hydrochemical features. In June, the surficial layer of the ground had just thawed, and the groundwater constituents were still expected to bear signatures of the freezing process and snowmelt before significant rainfall and subsequent runoff. Chapter 2 established that groundwater at the site moves from supra-permafrost flow in early spring to intra-permafrost flow in winter. In addition, a pseudo-rise in the water table was observed in some of the MWs due to constriction of the well-bore by ice, as discussed in Chapter 2.

However, major ions and alkalinity in two selected MWs in the tank farm and Steeves Lake areas showed peculiar trends (Figure 5.9). The ground thermal profiles nearest the locations of the MWs are given in Figure 5.10.

In general, site alkalinity tends to increase from June to September, though a few MWs showed decreases or no change, especially at the Steeves Lake and warehouse areas. In MW 4, calcium ions, dissolved iron, and alkalinity followed similar trends (Figure 5.9A). These parameters increased from June to September, while sulfate decreased slightly. Given that the upgradient sulfate concentration was high, the slight decrease in sulfate concentrations, which is lower than the upgradient concentration, is noteworthy. MW 4 was in the fuel-contaminated tank farm area where the overburden had been stripped, and as such, higher geochemical and microbial activities were expected. According to Berner (1971), microbial sulfate reduction can result in the formation of excess bicarbonate, which is corroborated by various studies involving water characterization and biodegradation. Additionally, aerobic respiration and denitrification can also contribute to alkalinity increase. Thus, the decreased sulfate may have been reductions in sulfate and iron (III) associated with microbial degradation of the spilled fuel. Increased concentration of dissolved iron also suggests natural attenuation at the site.

The dissolved oxygen (DO) measured at the site using a CHEMETS colorimeter DO-Tester in 2006 averaged about 1 mg/L, except at the upgradient area, which had measured DO of 4 mg/L, corroborating the 2005 data reported in Chapter 2. This affirms assertions from previous studies that the groundwater is in a reducing condition.

In MW 15 on the shoreline of Steeves Lake, there was little to no change in the dissolved iron concentration over time (Figure 5.9B). The calcium ion and alkalinity had similar trends, and varied with that of the sulfate concentration. In 2006, sulfate concentration decreased from June to September. According to Mawhinney (1979), low temperatures and large thermal gradients due to cryogenic metamorphization (or cryogenic

expulsion) alter groundwater chemistry; however, the variability of the measured sulfate concentrations and other groundwater constituents does not support such a conclusion. Over the same period in 2007, the sulfate concentrations increased, and were accompanied by significant reductions in alkalinity at the site. Pyrite oxidation may have accounted for the increased sulfate concentration, which in turn may have been derived from infiltrated water from near the surface, since pyrite oxidation will only occur in the presence of DO. The groundwater DO in the Steeves Lake area was not measured in 2007. Groundwater speciation using PHREEQC and carbonate equilibria in Rockware AqQA^(R) showed that the water in all the MWs was undersaturated with respect to gypsum, aragonite, dolomite and calcite (Figure 5.11A). Thus, given that the calcium ion concentration was less than the sulfate ion concentration, the increased sulfate was likely due to pyrite oxidation. However, this does not explain the decreased calcium ion concentration in September 2007. Processes known to remove calcium from solution are calcite precipitation and ion exchange reactions. However, since the water thermodynamics do not support calcium loss due to calcite precipitation, cation exchange may be responsible for the decrease in calcium ion concentration. This notion was supported by the increase in sodium ion concentration over the same period.

Moreover, it is unknown to what extent pyrite oxidation contributed to high background sulfate concentration at the site. Analyses from the Piper plot suggested that the water is $Ca-SO_4$ type; however, the inferred dominant processes also suggest pyrite oxidation in addition to gypsum and carbonate dissolution. Pyrite oxidation often takes time in the presence of DO and often leads to decreased pH but increased dissolved-metal concentrations. Acidity contributed by pyrite oxidation can be neutralized by carbonate species in the groundwater leading to pH buffering. Depth concentration profiling at the site (Figure 5.11B) does not explicitly support near surface sulfide leaching and oxidation. Thus, in evaluating the relative

importance of pyrite oxidation to gypsum dissolution, inverse modeling using PHREEQC was performed to evaluate the evolution pathway of the groundwater. The data used for the inverse modeling are summarized in Table 5.1.

The predominant source of fresh water in the Arctic is snowfall (Wrona et al., 2005). However, snowmelt water dominates infiltration in early spring, with a lesser amount of infiltration due to rainfall in late spring. Thus, the assumed freshwater source was a combination of snowfall and rainfall as reflected in the source water concentrations shown in Table 5.1. Figure 5.12 shows the inverse modeling results at 15% uncertainty. The mineral phases considered for each analysis are included in Table 5.1. Analyses were performed with and without dissolution of oxygen from the atmosphere. In inverse modeling using PHREEQC, there is a limit to the number of phases that can be specified for numerical convergence to occur. The number of phases and elements specified must not exceed 32. The choice of phases used for the simulation is based on the mineral phases' saturation indices across the site, summarized in Figure 5.11A.

The redox mole transfers common to all simulated inverse models are dissolved oxygen, iron (III) and sulfide ions. Positive and negative mole transfer infers dissolution and precipitation of the respective mineral phases. Figure 5.12A and B show results of models with the same mineral phases except that for the model output shown in Figure 5.12B, dissolution of atmospheric oxygen is allowed. The net redox mole transfers for both models are the same. Figure 5.12B shows that calcite is precipitated but in comparison with the summarized saturation index in Figure 5.11A, the model is not realistic, though thermodynamically possible. The other model outputs shown in Figure 5.12 have different phase combinations as summarized in Table 5.1. Model output in Figure 5.12D shows high calcite dissolution in response to pyrite oxidation. The model showed that if pyrite oxidation is predominant at the site, oxygen dissolution from the atmosphere

will be relatively high and there is likelihood of melanterite ($FeSO_4 \cdot 7H_2O$) precipitation. However, Figure 5.11A shows that the groundwater is grossly undersaturated with respect to melanterite and there is no observable evidence of melanterite deposition at the site, thus, it is unlikely that pyrite oxidation predominates at the site. Figure 5.12F shows that pyrite oxidation with gypsum dissolution is an important geochemical process at the site, however, the model showed sepiolite ($Mg_2Si_3O_7 \cdot 5OH : 3H_2O$) precipitation, which is at odds with the present geochemical condition at the site because the groundwater is undersaturated with respect to sepiolite (Figure 5.11A). Figure 5.12C and Figure 5.12E show mineral phases in agreement with the present geochemical conditions at the site. Both models showed the relative importance of gypsum dissolution and pyrite oxidation. Though pyrite oxidation is possible, it is not the predominant geochemical process at the site. Both models also showed that gypsum dissolution is the dominant process at the site. Figure 5.12C does not show significant mole transfer with respect to calcite but rather significant transfer with respect to aragonite. In contrast, Figure 5.12E showed both calcite and aragonite dissolution.

The measured BTEX concentrations at the site are grouped into different areas and subjected to Kruskal-Wallis test as shown in Figure 5.13A. The analyses show that significant difference exists in mean BTEX concentrations at the site. The warehouse area had the highest variability in BTEX concentration while the upgradient area had little to no measurable BTEX concentration. The only incident of BTEX measurement at the upgradient area occurred in June 2007 where 0.15 mg/L of m-p xylene was measured in MW 38. Other MWs including MW 104 and MW 51 registered no measurable BTEX compounds when analyzed. Interestingly, the BTEX concentration is relatively low in the tank farm area where most of the original contamination occurred.

Figure 5.13B and Figure 5.14 show trends of BTEX constituents of interest in comparison to CCME (2009) guideline values for the protection of

freshwater aquatic life the. Figure 5.13B shows that the mean benzene concentrations are below CCME limit of 0.37 mg/L at the powerhouse area. The last monitoring, in 2007, also shows the mean benzene concentrations are less than the limit for all areas except at the tank farm area where it remained just above the CCME limit. Considering the variability of the measured concentrations, which may be up to 25% in mean values from Kruskal-Wallis analyses, the CCME limit was not met with respect to the tank farm and Steeves Lake areas.

The temporal variation for the measured ethylbenzene concentrations at the site is shown in Figure 5.14A. Apart from the tank farm area, the mean ethylbenzene concentrations decreased in 2007. However, the measured concentrations were generally above the CCME limit of 0.09 mg/L except at the powerhouse area in 2007. The toluene concentrations at the site were above the CCME limit of 0.005 mg/L with higher concentrations at the warehouse area as shown in Figure 5.14B. The BTEX concentrations at the tank farm area appear relatively constant, unlike other areas where there were significant reductions in 2007. Knowing that pockets of free product petroleum hydrocarbon persists at the site, the relatively constant BTEX concentrations at the tank farm area are understandable. Other geochemical indicators suggesting anaerobic biodegradation is ongoing at the site have been documented. Chapter 2, and Van Stempvoort, and Biggar (2008) discussed the presence of volatile fatty acid (VFA) and enriched isotopes of sulfate (^{34}S) and oxygen (^{18}O) indicative of active biological degradation of PHCs at the site.

The background dissolved iron concentration at the site are above the CCME limit of 0.3 mg/L, thus, iron should not be used as an indicator for the groundwater regulatory compliance at the site. Other inorganic groundwater constituents such as arsenic, lead, and cadmium are generally less than the CCME guideline for freshwater aquatic life at the site except aluminum and nickel (Figure 5.15), although there are instances where concentrations of

arsenic and lead exceeded the CCME limit of 0.005 mg/L and 0.007 mg/L respectively. Such instances are few and discontinuous throughout the monitoring period. Further analyses showed that the background aluminum concentrations are higher than the CCME limit and there is no significant difference in its mean values across the site (Figure 5.16A). However, the background concentrations of nickel are less than 0.1 mg/L and below the CCME limit of 0.15 mg/L. The concentrations at all other areas of the site are significantly higher than upgradient, but not significantly different from one another (Figure 5.16B). The higher nickel concentrations may be due to secondary contamination or mineralization of some sort.

5.5 Conclusions

This study provided insight to the groundwater hydrochemical characteristics at the abandoned Colomac mine site. It showed that the water is predominantly $Ca-SO_4$ type and the active geochemical processes are gypsum dissolution and carbonate weathering. Inverse modeling results showed that while pyrite oxidation may be ongoing, it is of a far smaller magnitude than gypsum dissolution and carbonate weathering at the site. The site shows geochemical indicators of sulfate and iron reduction in support of hydrocarbon biodegradation, which are in agreement with previous studies in Chapter 2 and Van Stempvoort and Biggar (2008).

The organic groundwater quality with respect to BTEX exceeded the CCME limit for freshwater aquatic life. However, most recent data showed a decline in the dissolved BTEX constituents, especially benzene and toluene in support of biodegradation. Due to the persistence of residual phase hydrocarbon at the tank farm area where most of the fuel contamination occurred, the BTEX concentrations were relatively constant over time. The background dissolved iron and aluminum concentrations are above the CCME limit at the site. However, the relatively higher nickel concentrations above the background values require further investigations. Other inorganic

constituents of interests including copper, lead, arsenic, and cadmium are below the CCME limits.

This study underscores the importance of mineralogical composition of the local bedrock on groundwater constituents. The high background sulfate at the site is due to outwashing and dissolution of the surficial minerals. There was no evidence of acid mine drainage at the site and these findings are particularly useful for other active mine sites with similar geology and regional hydrogeology where previous geochemical studies are lacking.

Table 5.1 Summary of parameters used for the inverse modeling.

Dissolved ions/parameters	pH	Si	Ca ²⁺	Ma ²⁺	Na ⁺	K ⁺	S(6)	Cl ⁻	Fe	O(0)	Pe	Alkalinity
Solutions	Default unit is mg/L for ions and dissolved metals. Alkalinity is mg/L of CaCO ₃											
Rainwater/Snow	7.0	0.10	0.05	0.05	0.05	0.05	0.05	0.05	0.00	6.00	12	0.5
MW15	7.1	2.40	167	19.2	19.5	8.30	495	4.10	2.1	1.00	-1	137
Model	Phases											
A	Halite, Gypsum, CO ₂ (g), Pyrite, Albite, Sepiolite, Melanterite, Quartz, Dolomite, Calcite, Biotite, Plagioclase											
B	Halite, Gypsum, CO ₂ (g), Pyrite, Albite, Sepiolite, Melanterite, Quartz, Dolomite, Calcite, Biotite, Plagioclase, O ₂ (g)											
C	Anhydrite, Aragonite, Halite, Gypsum, Biotite, Chalcedony, CO ₂ (g), Pyrite, Plagioclase, Albite, Melanterite, Quartz, Hematite, Dolomite, Goethite, Calcite, Hematite											
D	Halite, Gypsum, CO ₂ (g), Pyrite, Albite, Sepiolite, Melanterite, Quartz, Dolomite, Calcite, Biotite, Plagioclase, Siderite, O ₂ (g)											
E	Halite, Aragonite, Gypsum, Biotite, Chalcedony, CO ₂ (g), Pyrite, Plagioclase, Albite, Melanterite, Quartz, Hematite, Dolomite, Goethite, Calcite, Hematite											
F	Halite, Gypsum, CO ₂ (g), Pyrite, Albite, Sepiolite, Melanterite, Quartz, Dolomite, Goethite, Calcite, Biotite, Plagioclase, Siderite, Fluorite, O ₂ (g)											

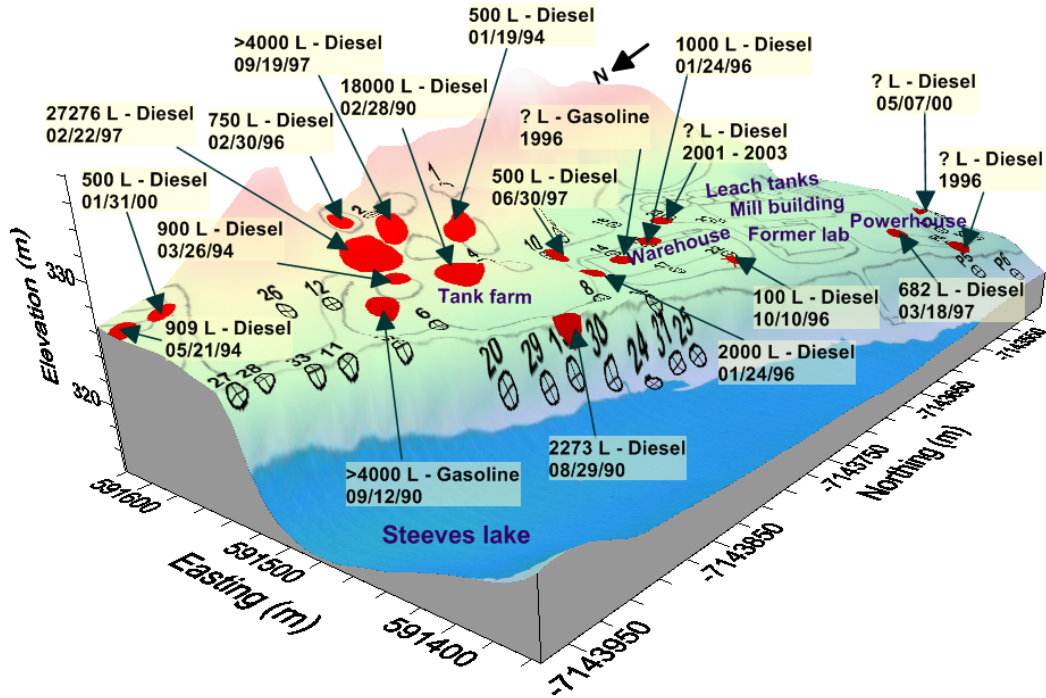


Figure 5.1 Spill history at the abandoned Colomac mine site showing the quantity spilled, relative locations and spill date.

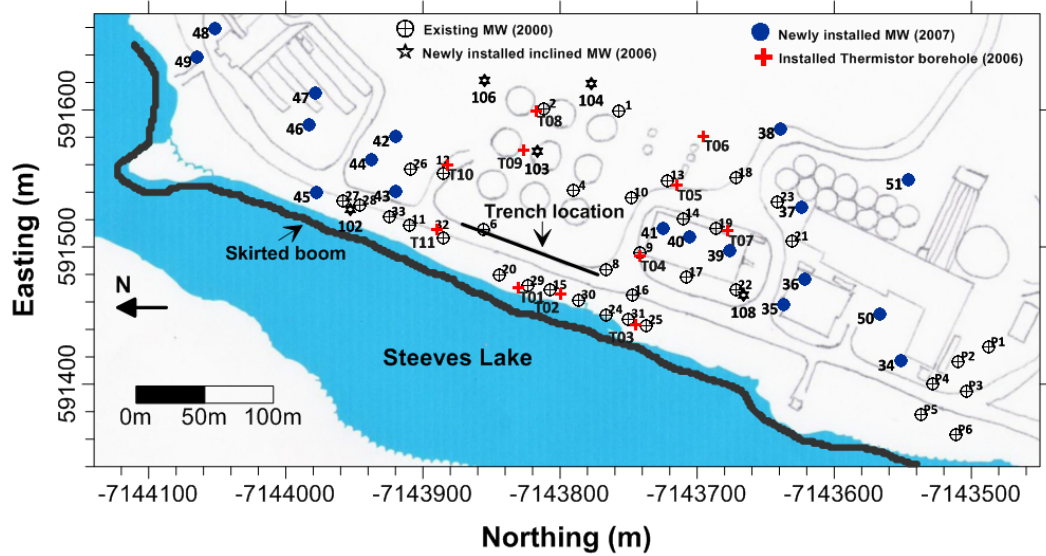


Figure 5.2 Site layout showing the relative locations of the installed monitoring wells (MWs) and thermistor strings with some implemented remedial strategy at the Colomac mine site.

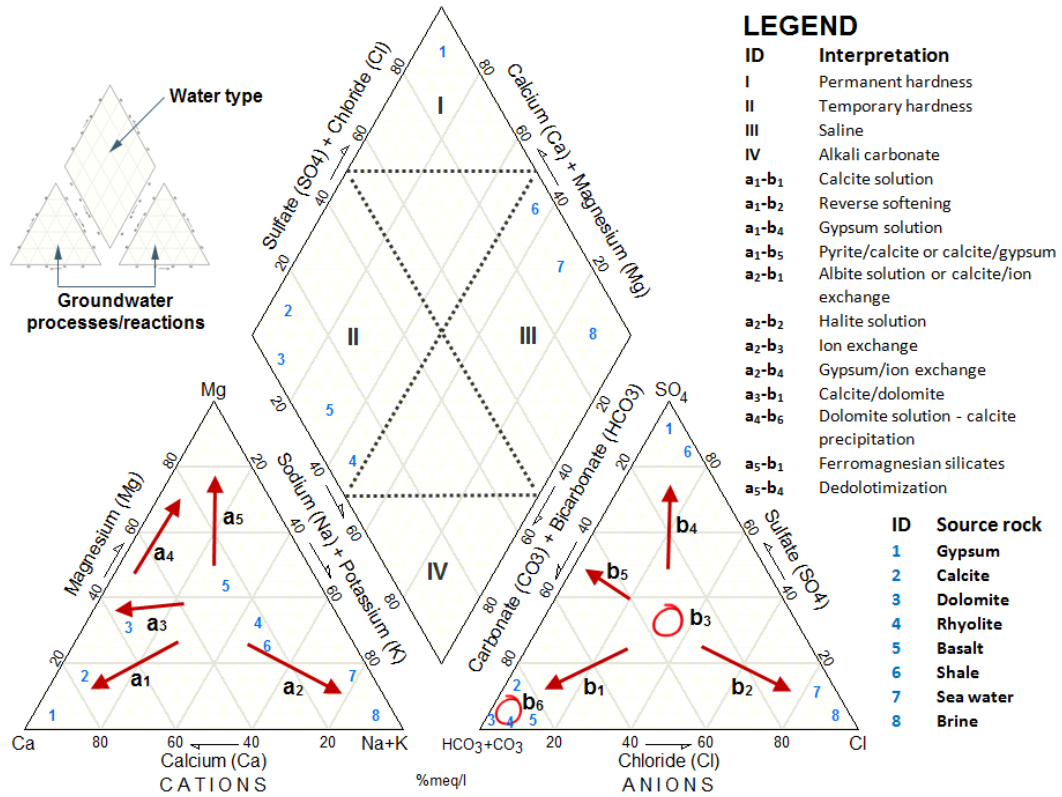


Figure 5.3 Piper plot interpretation summary (modified after Hounslow, 1995).

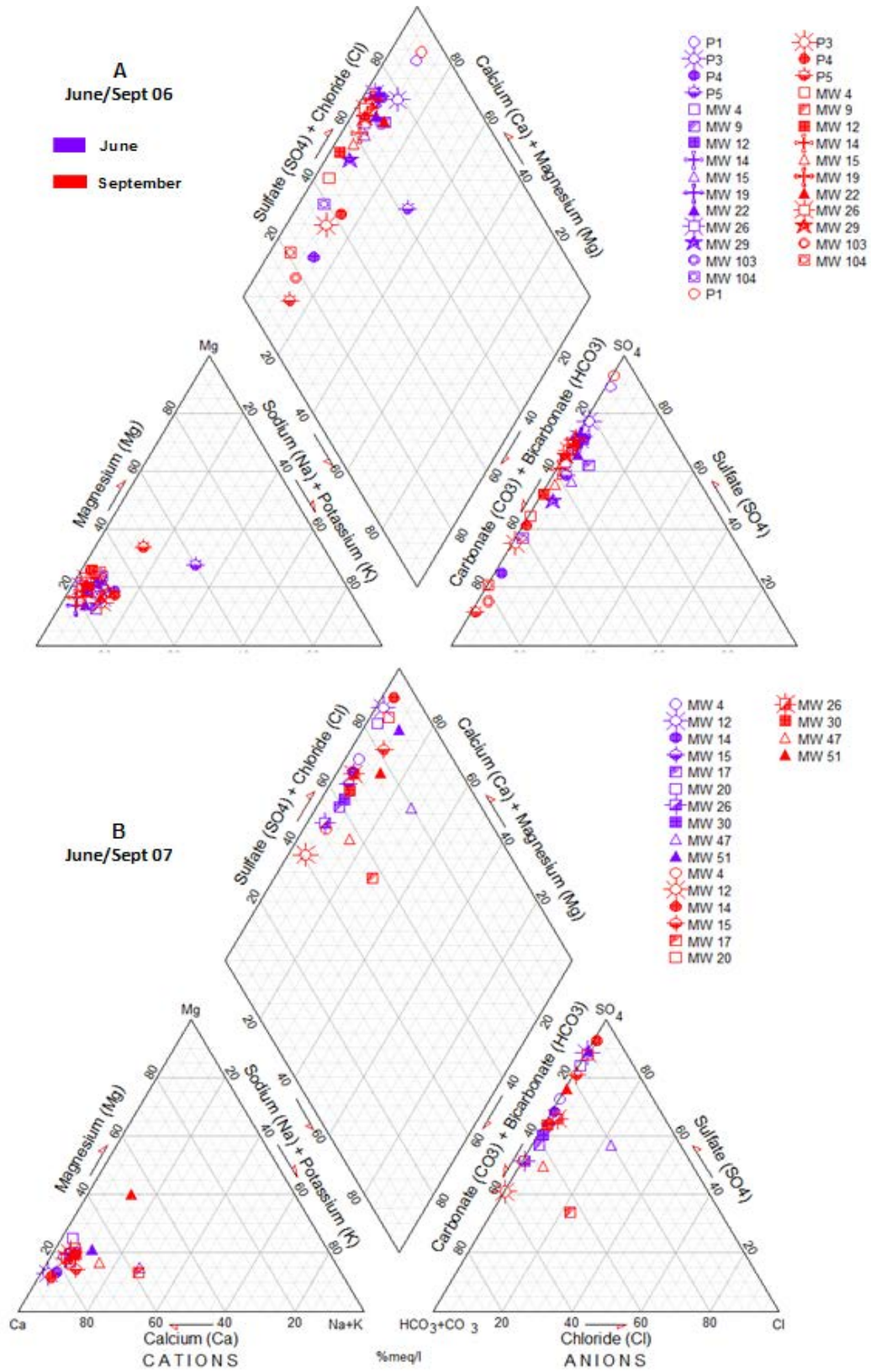


Figure 5.4 Piper plot of major ions in selected MWs at the Colomac mine site.

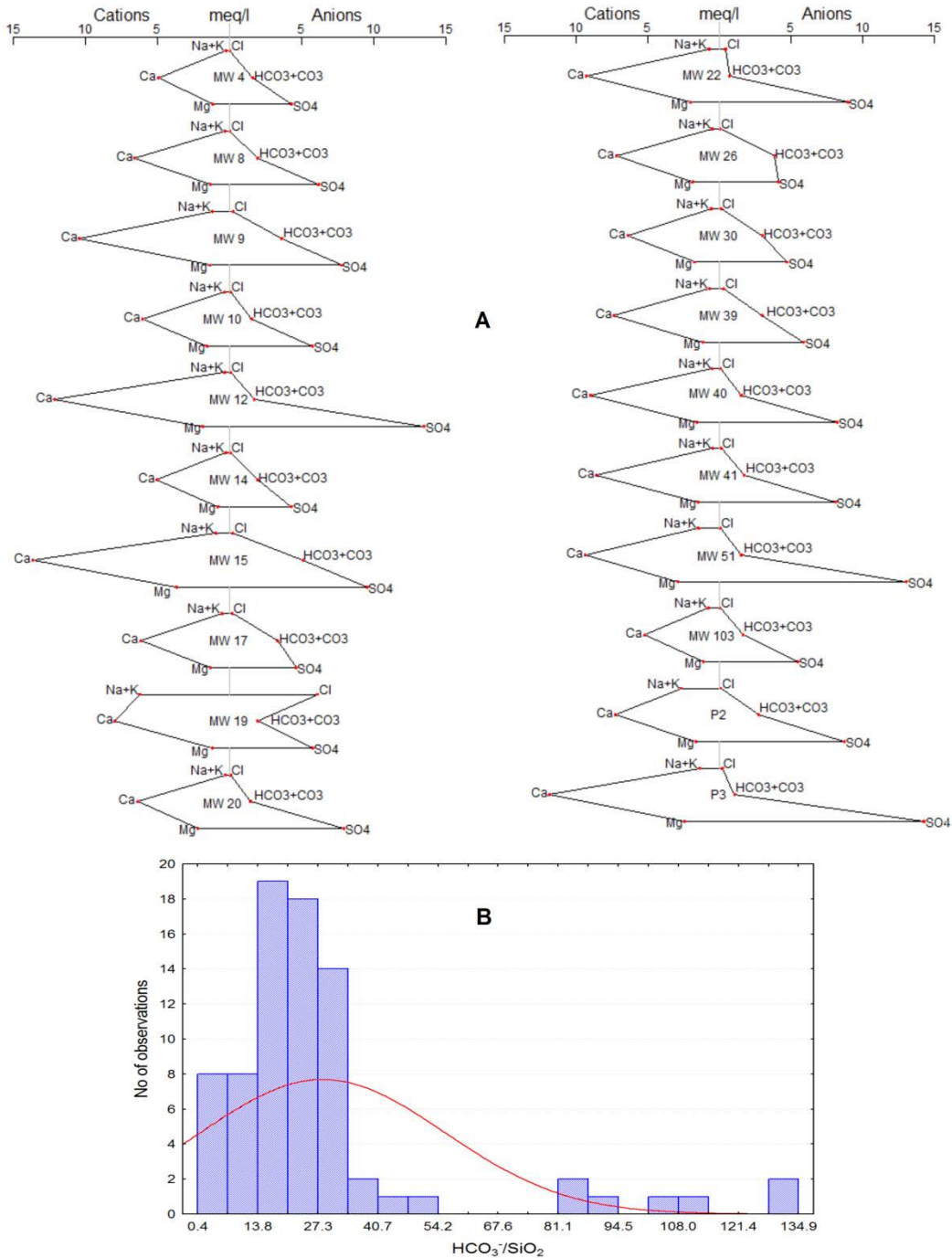


Figure 5.5 The A part shows the Stiff diagram of selected MW samples for June 2007; the polygon shapes are similar for most of the MWs, implying common groundwater source. B shows the ratios of bicarbonate to silica in most monitoring wells at the site.

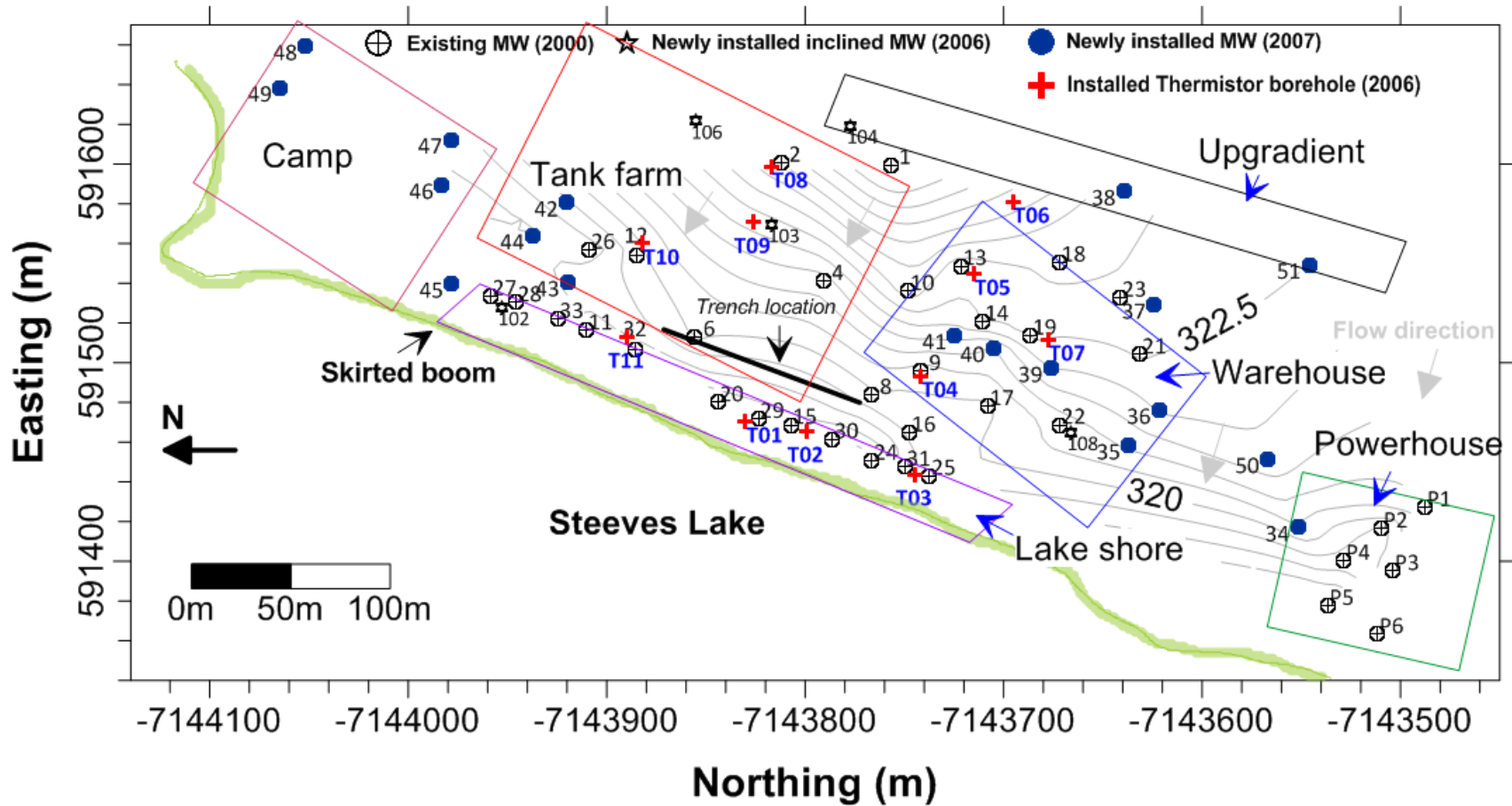


Figure 5.6 Subdivisions of the site based on pre-existing facilities before demolition. The general groundwater flow at the site is northwest.

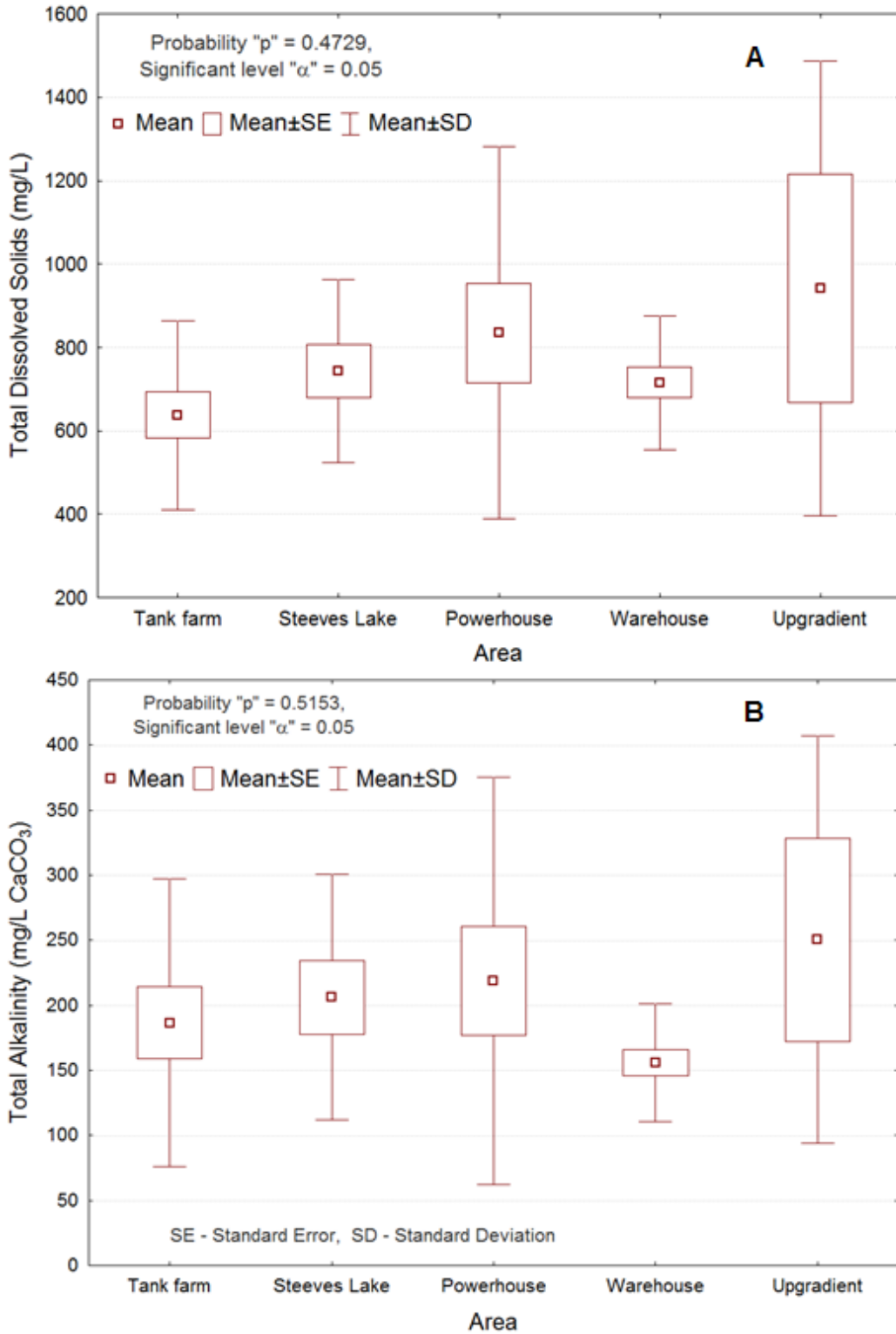


Figure 5.7 Kruskal-Wallis non-parametric test results for (A) Total Dissolved Solids (TDS) and (B) total measured alkalinity at the site.

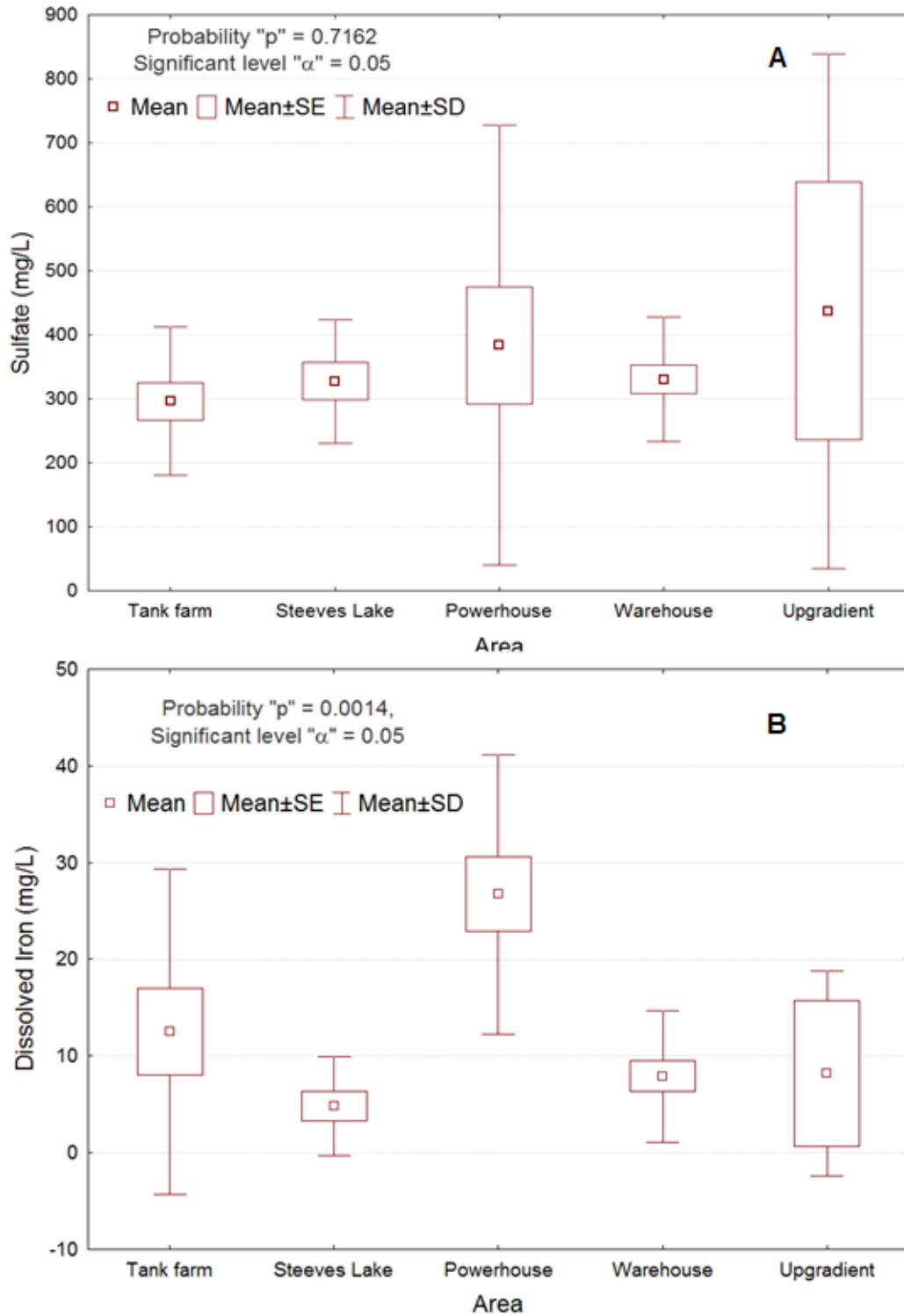


Figure 5.8 Kruskal-Wallis non-parametric test results for (A) sulfate and (B) dissolved iron concentrations at the site.

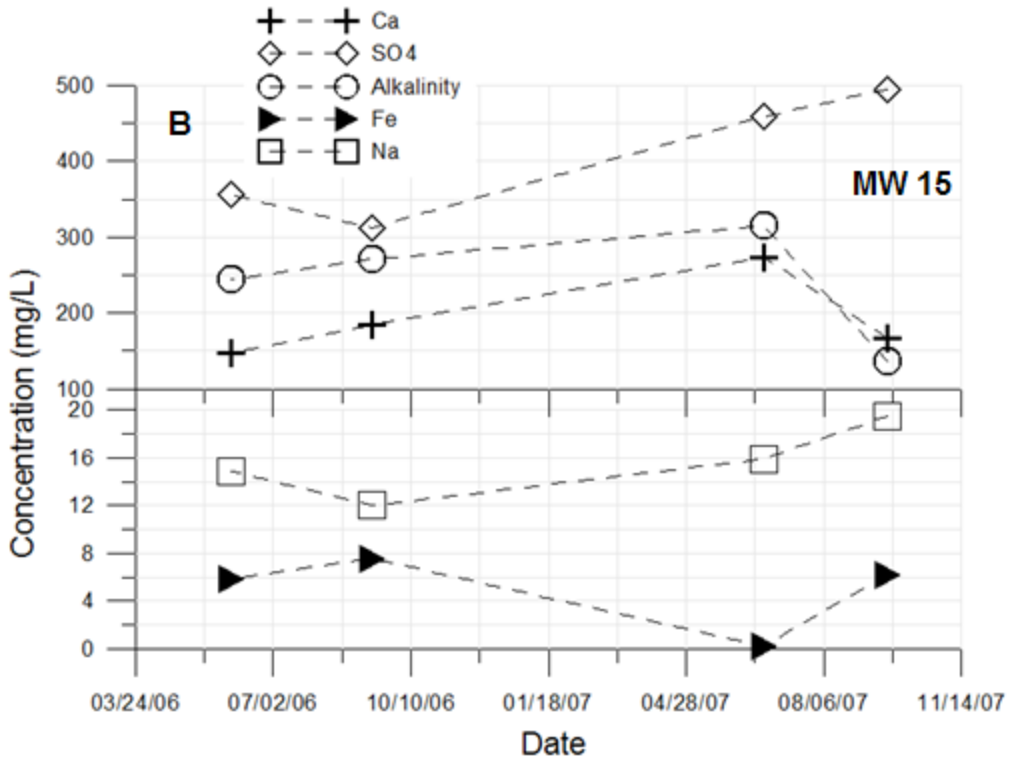
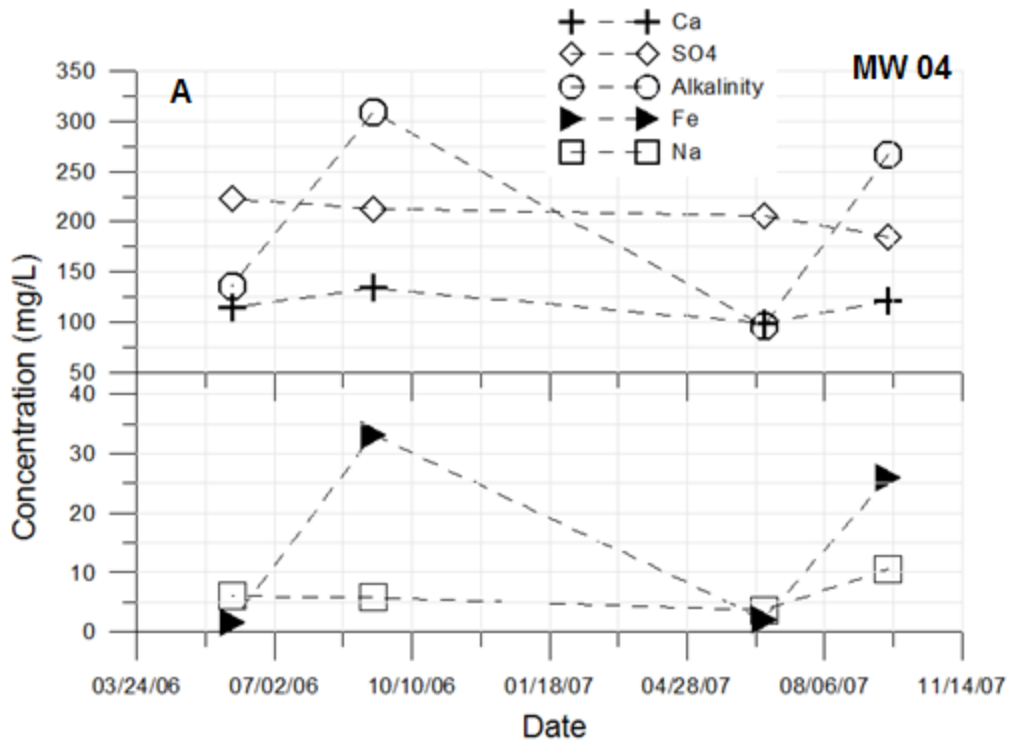


Figure 5.9 Trends of selected ions in MW 4 and MW 15 at the Tank farm and Steeves Lake areas respectively.

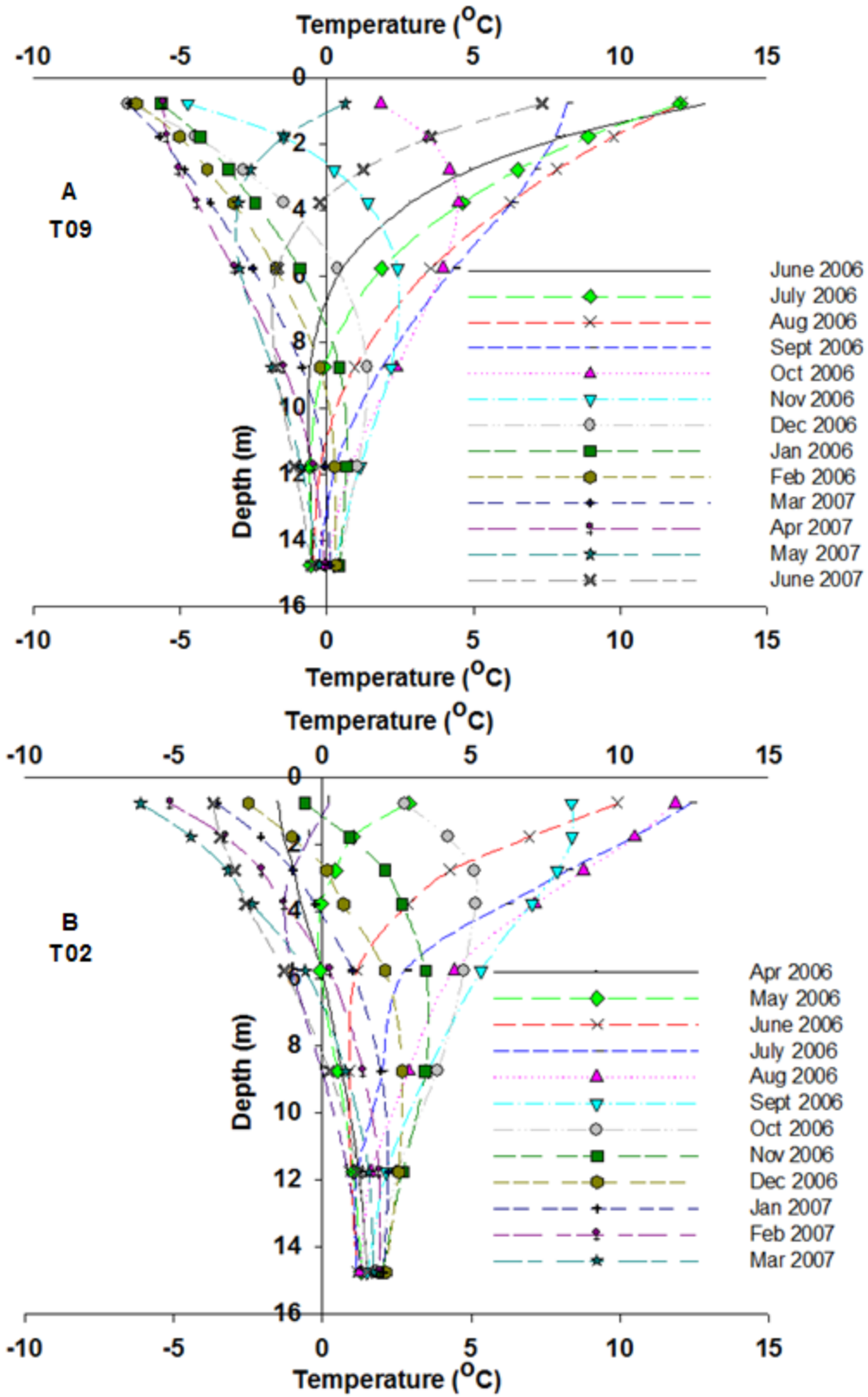


Figure 5.10 The thermal profile from thermistor strings nearest the MWS. T09 is near MW04 and T02 is adjacent to MW 15.

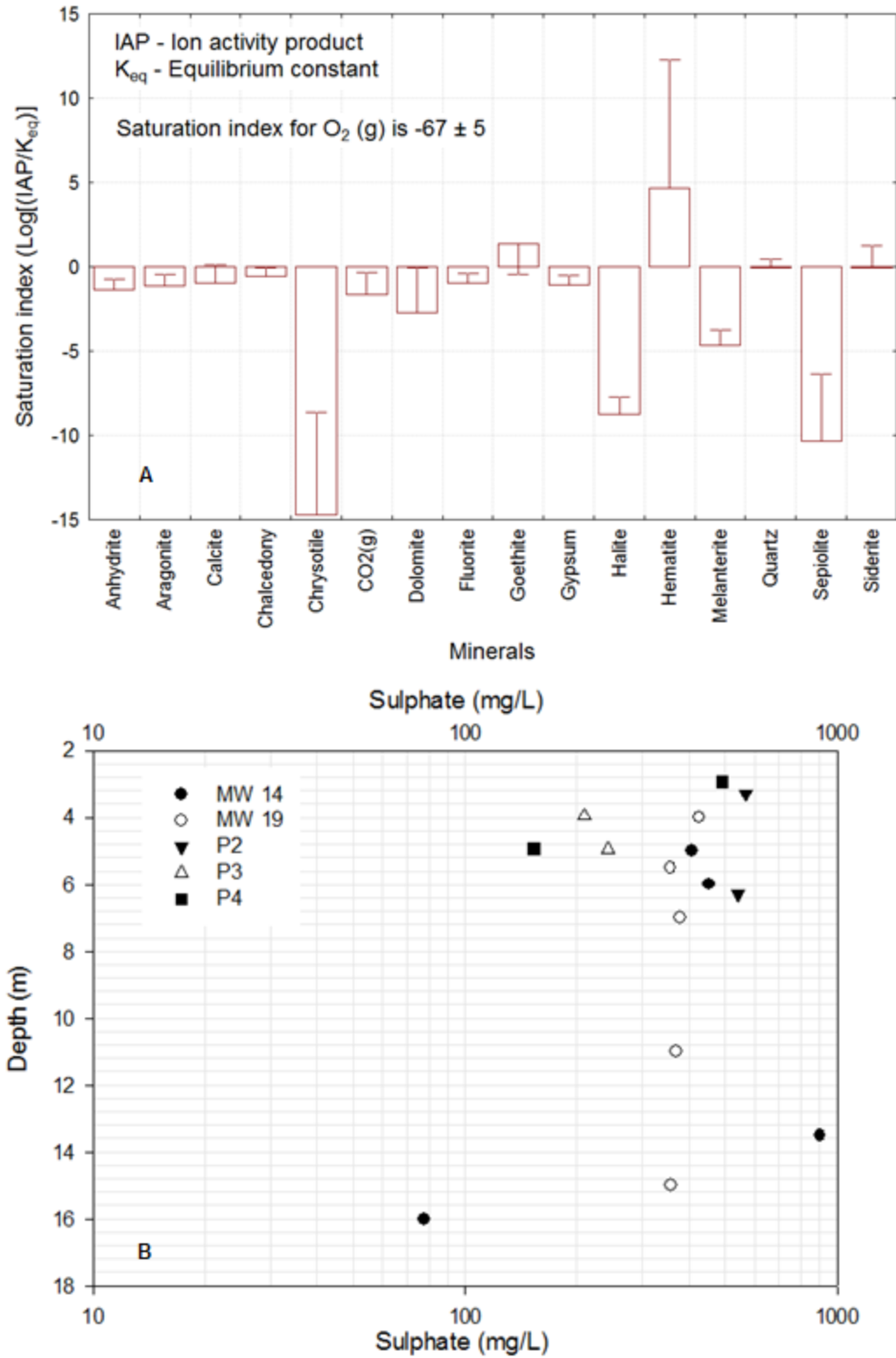


Figure 5.11 Summary of saturation indexes for major mineral phases at the site (A), and the sulfate concentration profile with depth (B).

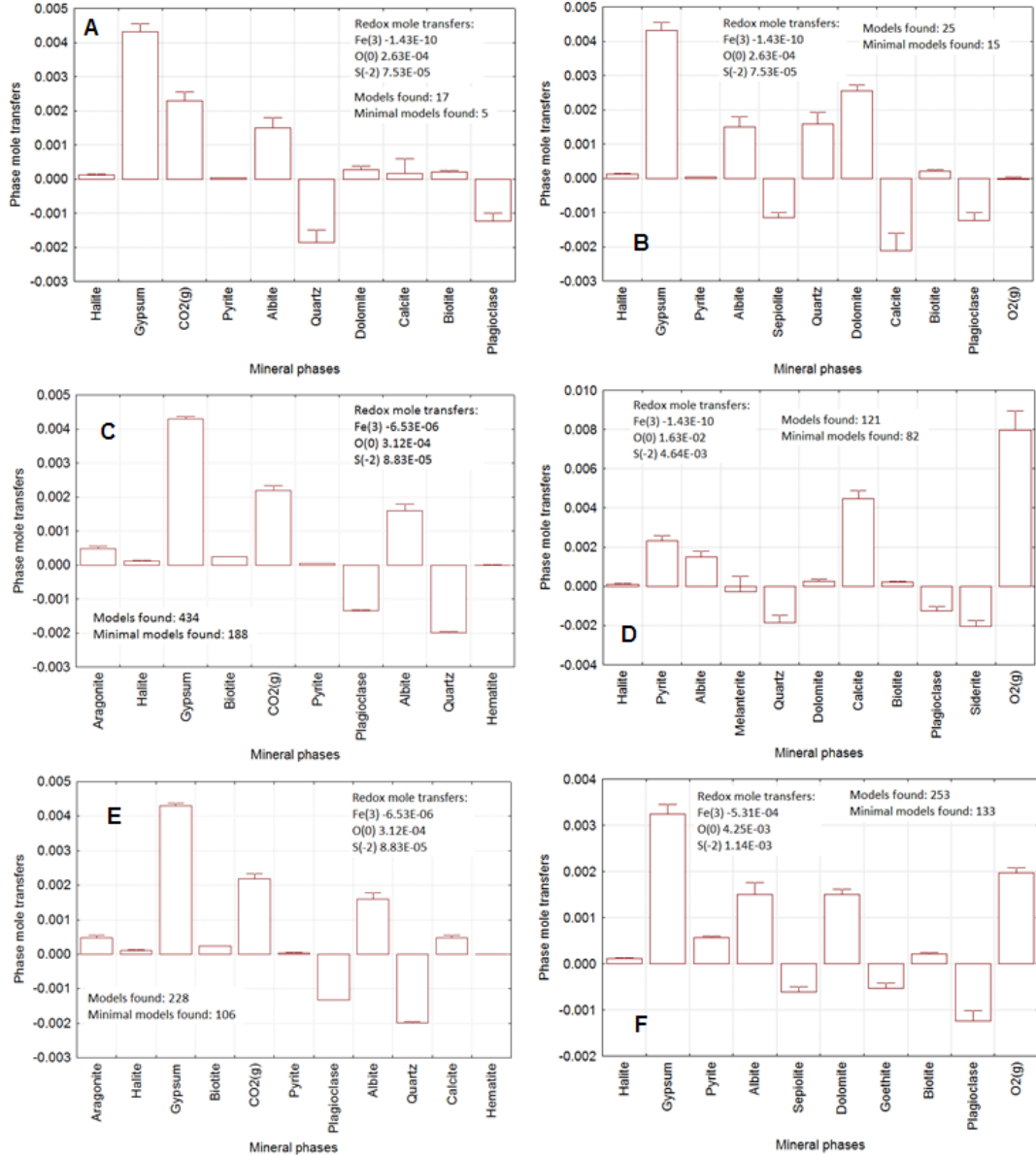


Figure 5.12 Summary of inverse model analyses using PHREEQC. A-C-E are models without dissolvable oxygen phase, while models B-D-F are those with dissolvable oxygen phase. Mineral phases for each model are summarized in Table 5.1.

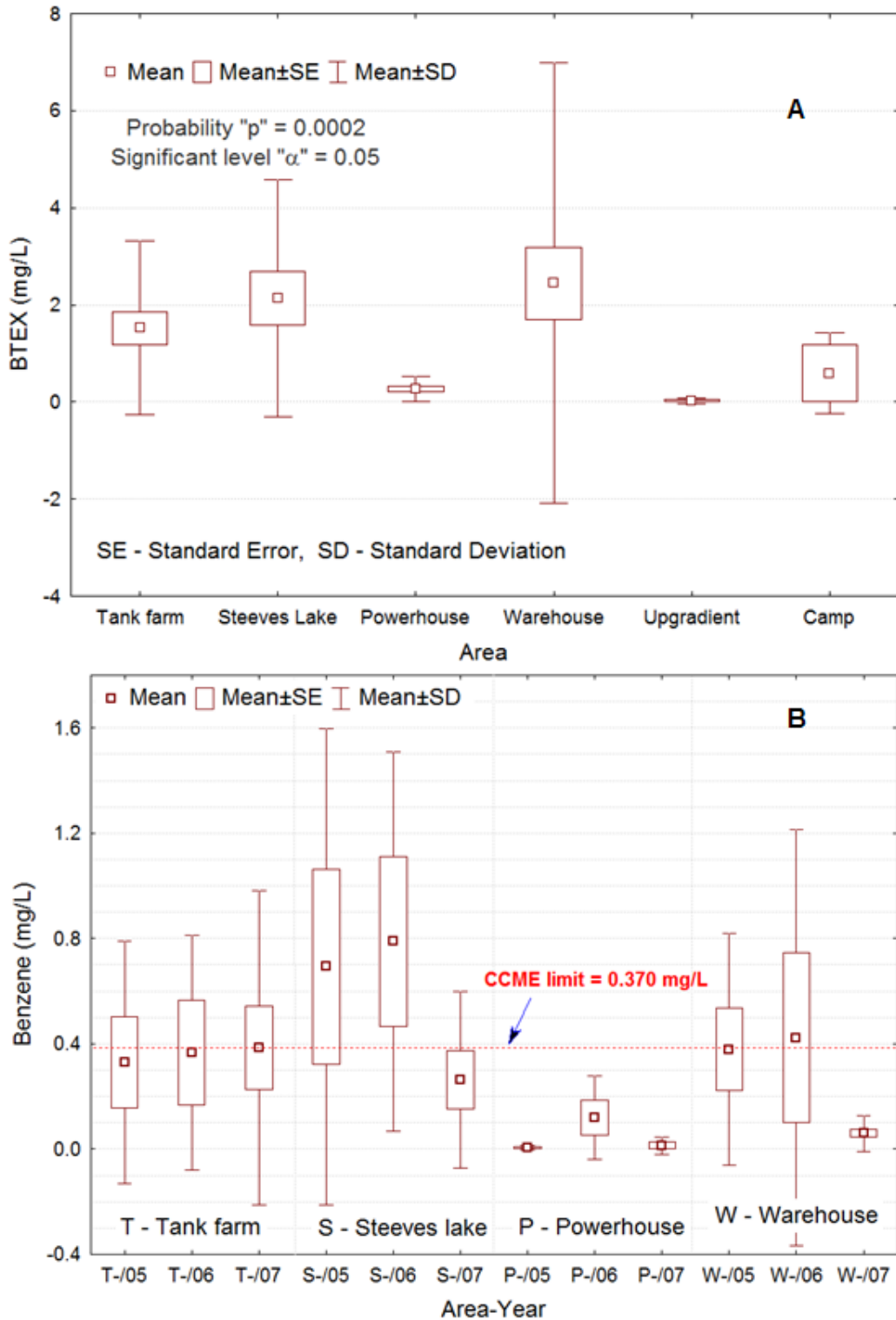


Figure 5.13 Summary of (A) BTEX and (B) benzene concentrations at the site. The benzene concentrations are generally above the CCME limits except the powerhouse area.

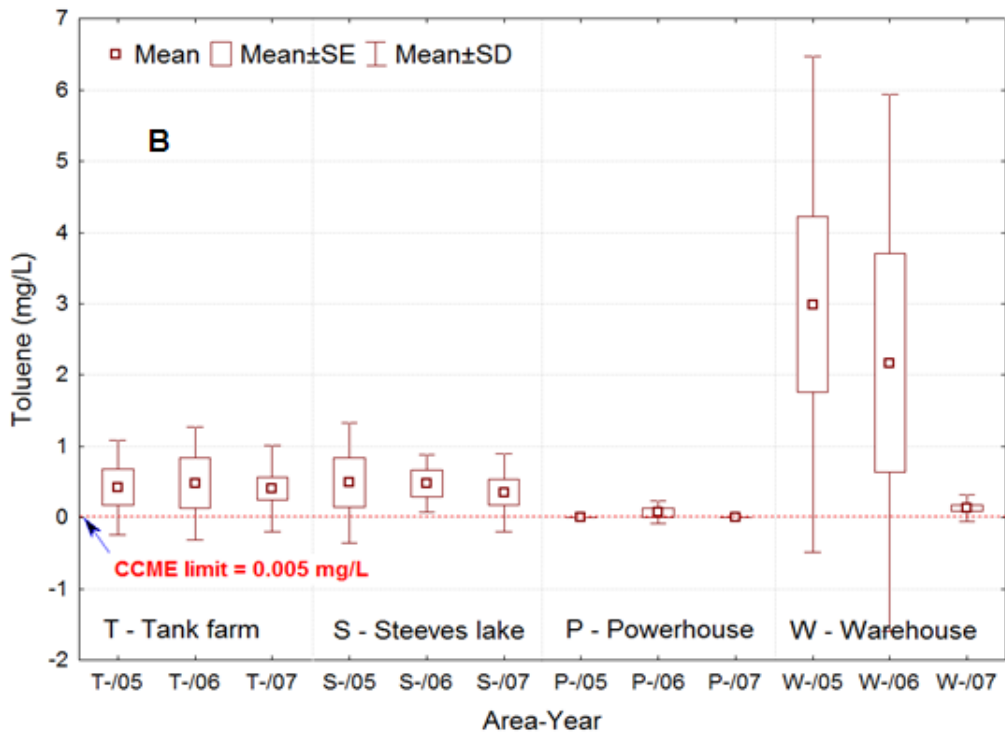
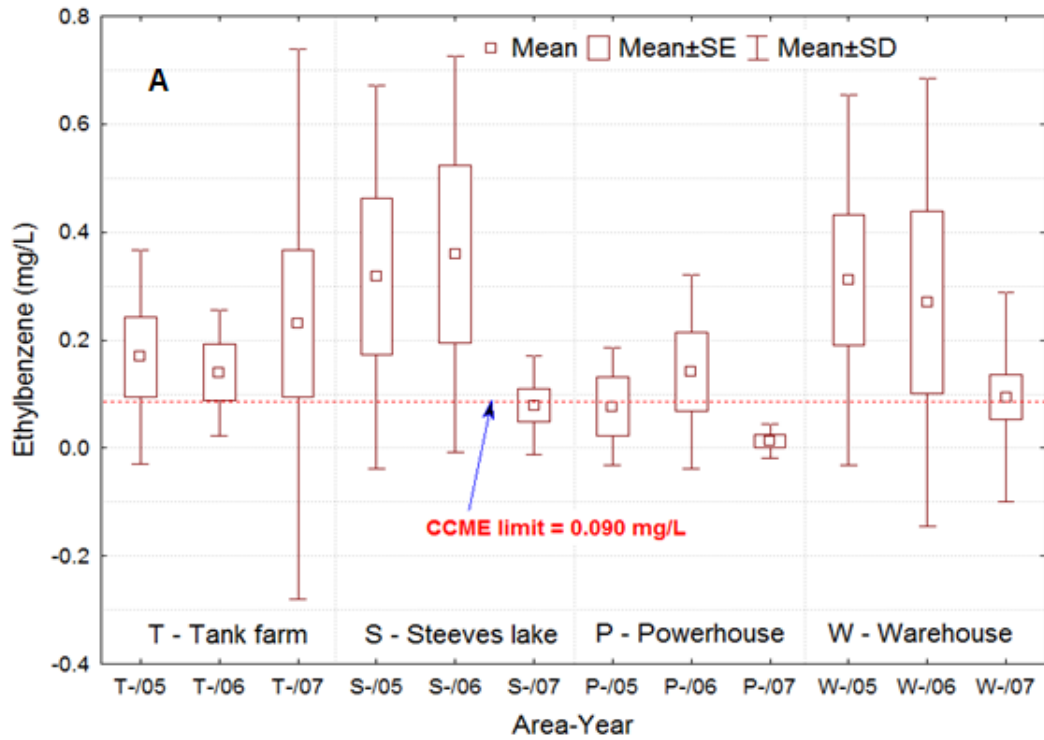


Figure 5.14 Summary of (A) Ethylbenzene and (B) Toluene concentrations at the site.

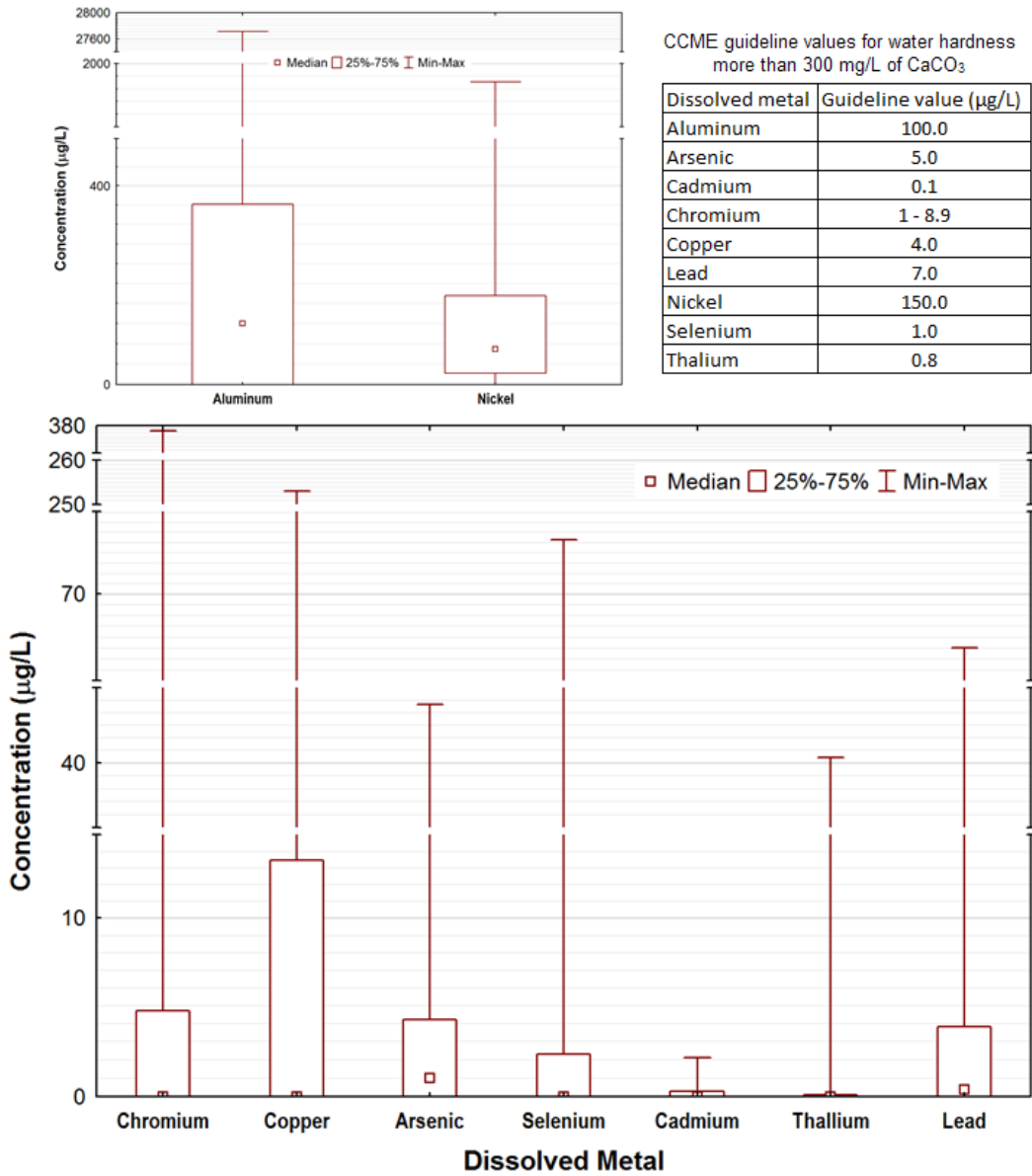


Figure 5.15 Selected dissolved metal concentrations at the site. Apart from aluminum, nickel, and iron, most of the dissolved metals have concentrations that are generally less than CCME guideline values with some few outliers.

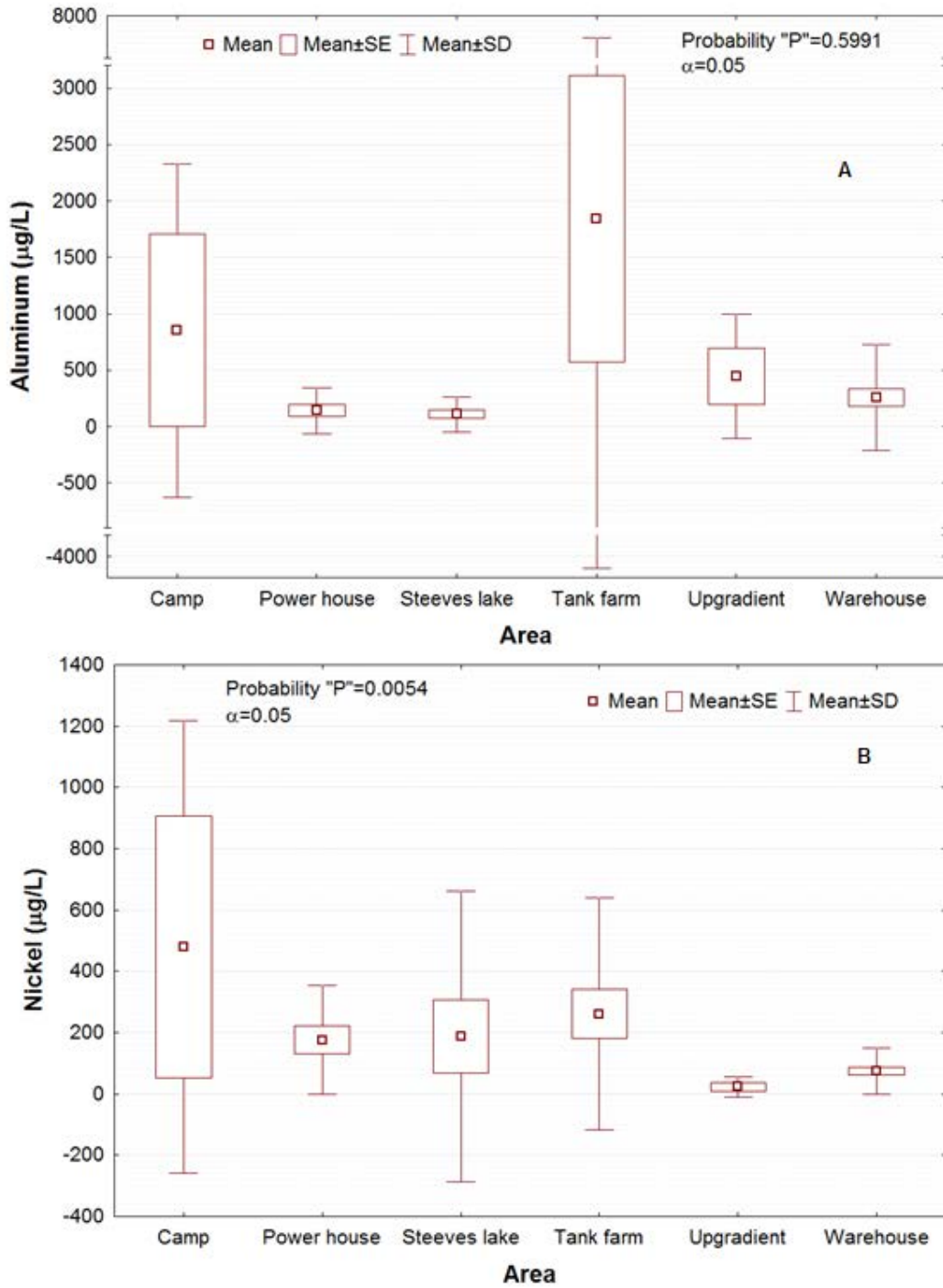


Figure 5.16 Summary of Kruskal-Wallis test results for (A) aluminum, and (B) nickel: The site has high background aluminum concentration and there is no statistical difference in the means of its values. However, nickel has significant concentrations above the background and requires further investigation.

References

- Ball, J.W., Nordstrom, D.K., 1991. WATEQ4F-user's manual with revised thermodynamic data base and test cases for calculating speciation of major, trace, and redox elements in natural waters. US Geological Survey Open-File Report 90-129, 185 pp.
- Berner, R.A., 1971. Principles of Chemical Sedimentology. McGraw-Hill, New York.
- CCME (Canadian Council of Ministers of the Environment), 2007. Canadian water quality guideline for the protection of aquatic life: Summary table. Updated December 2007. In: Canadian environment quality guidelines, 1999, Canadian Council of Ministers of the Environment, Winnipeg.
- Hearn, K., 1990. The Colomac deposit. Geological Survey of Canada Open File Report 2168, pp. 84–89.
- Hounslow, A.W. 1995. Water Quality Data: Analysis and Interpretation, CRC Lewis Publishers, Boca Raton, FL.
- Manahan, S.E., 2000. Environmental Chemistry. 7th Ed. CRC Lewis Publishers, Boca Raton, Florida.
- Mawhinney, 1979. Investigation into the occurrence and development of groundwater in permafrost regime. Unpublished M.Sc. thesis, University of Alberta, Canada.
- Montgomery, D.C., Runger, G.C., 2003. Applied statistics and probability for engineers. 3rd Edition. John Wiley and Sons Inc., New York.
- Morgan, J., 1990. Gold deposits in the Indin Lake Supracrustal Belt. Geological Survey of Canada, Open File Report 2168, pp. 67– 83.
- Shelton, K.L., Costello, C. S., van Hees, E. H., 2000. Contrasting styles of Achaean greenstone gold deposition: Colomac gold mine, Canadian Northwest Territories. Journal of Geochemical Exploration, 69 – 70: 303 – 307.

- Van Stempvoort D., Biggar K.W., Iwakun O., Bickerton G., Voralek J., 2006. Characterization of Fuel Spill Plumes in Fractured Rock at a Permafrost Site: Colomac Mine, NWT. 2005/2006 Program Progress Report, April 2006, National Water Research Institute and University of Alberta.
- Van Stempvoort, D., Biggar, K., 2008. Potential for bioremediation of petroleum hydrocarbons in groundwater under cold climate conditions: A review. *Cold Regions Science and Technology*, 53(1): 16-41.
- Wrona, F. J., Prowse, T. D., Reist, J.D., 2005. Freshwater Ecosystem and Fisheries. In: C. Symon, L. Arris, and B. Heal (Ed.). *Arctic Climate Impact Assessment*, pp 354 - 453, Cambridge University Press.

6 INFLUENCE OF CYCLIC FREEZING ON THE MOBILIZATION OF LNAPL AND SOLUBLE OIL IN A POROUS MEDIA⁵

6.1 Introduction

Understanding the subsurface behavior of spilled fuel in a contaminated site is crucial to its successful remediation. Achieving this often requires detailed site characterization and determination of mechanisms aiding its migration and accumulation in the environment. Most spilled fuels (i.e., gasoline and diesel) are subsets of light nonaqueous phase liquids (LNAPL) because they are less dense than water and mostly immiscible with it. In temperate regions, the behavior of spilled fuel is well documented in the literature. However, in Cold Regions overlapping permafrost environments, subsurface behavior of spilled fuel is an ongoing research area.

The behavior of petroleum hydrocarbon (PHC) contamination in frozen media is important in discerning its behavior in permafrost environments. Permafrost is often viewed as a barrier to contaminant migration in Cold Regions, which has often contributed to improper environmental practices involving spilled fuel (Barnes and Chuvilin, 2009). Studies have shown that ice or completely ice-saturated frozen soil without defects have very low permeability in the order of 10^{-15} cm², and are mostly impervious. This formed the basis for the development and use of frozen core barriers to inhibit contaminant migration. A study by Anderson et al. (1996) on such barrier's resistance to ice erosion by liquid contaminant showed that minimization of ice erosion requires full ice saturation and barrier temperature below the freezing point depression of the contaminant. However, in ice-saturated frozen soil, there is a natural propensity for

⁵ A version of this chapter has been accepted for publication.

Iwakun, O., Biggar, K.W., and Segó, D., 2010. Influence of cyclic freeze-thaw on the mobilization of LNAPL and soluble oil in porous media. *Cold Regions Science and Technology*, doi:10.1016/j.coldregions.2010.06.007, accepted for publication.

microcracks development, especially at temperatures below freezing (Yershov et al., 1988) because frozen ground is a spatially inhomogeneous system (Frolov, 1982).

Laboratory experiments by Biggar and Neufeld (1996) on vertical migration of diesel into columns of saturated silty-sand subjected to freeze-thaw cycles showed no contamination in the permanently frozen soil layer at depth after eight cycles of freeze-thaw. The diesel migration was limited to the saturated soil down to the maximum thaw depth. Thus, they postulated that the contaminant movement into the saturated soil occurred when the soil was frozen due to migration into the fissures induced during freezing. Furthermore, site investigations of fuel migrations into permafrost at two different fuel-contaminated sites in the Canadian Arctic by Biggar et al. (1998), found significant contamination below the permafrost table. They postulated that gravity drainage along fissures induced by thermal contraction or gravity drainage via interconnected air voids accounted for this movement. Thus, permafrost may not be an effective barrier to contaminant propagation.

Laboratory study by Chuvilin et al. (2001) on factors affecting oil migration in frozen ground observed components of oil even in wholly ice-saturated soil, corroborating the work of Biggar et al. (1998). Later work by Chuvilin and Miklyaeva (2003) suggested that capillary transfer via micropores might be responsible for the oil penetration. Chuvilin et al. (2001) showed that surface spreadability of oil increased with increasing ice saturation and oil hardening temperature but decreased from sand to clay to ice as a result of increasing wetting angle on the mineral surfaces respectively. Laboratory experiment by Barnes and Wolf (2008) on the effects of pore-ice on spreadability and penetration of petroleum products in coarse grained soils showed that ice content increased lateral migration of petroleum due to the formation of dead end pores by ice especially in the vadose zone, thereby creating irregular preferential flow paths resulting in deeper contaminant penetration.

The nucleation process that occurs during ice formation is known to cause rejection and concentration of solutes in the unfrozen water (Konrad and Seto, 1991; Tumeo and Davidson, 1993; and Chuvilin et al., 2001). This process is commonly referred to as solute exclusion or rejection in freezing experiments and hydrocarbon exclusion when petroleum products are involved. Barnes and Chuvilin (2009) referred to this process as cryogenic expulsion, and related it to separation of more mobile components from petroleum. In this study, the term “cryogenic expulsion”, is adopted. Different studies have shown that cryogenic expulsion is enhanced at lower freezing rates (Konrad and McCammon, 1990; Konrad and Seto, 1991; Panday and Corapcioglu, 1991), however, the phenomenon has been observed at higher freezing rates (Ershov et al., 1992). In a top-down freezing experiment conducted by Konrad and Seto (1991) on a partially saturated clay sample contaminated with miscible organic solvent (propanol), there was an increase in solvent concentrations in front of advancing freezing front. Other studies conducted in the laboratory corroborated such observation (Chuvilin et al., 2001; Tumeo and Davidson, 1993; Panday and Corapcioglu, 1991). According to Wilson and Mackay (1987), freezing can cause oil to weather, which may lead to increased density and viscosity, thereby enhancing downward pull potential but decreased fluid’s mobility. In addition to the concept of cryogenic expulsion, Barnes et al. (2004) proposed the mechanism of physical displacement of mobile LNAPL from pore spaces as water expands.

At the commencement of freezing in the winter period, the water table is often low due to decreased water infiltration. Fluctuations of the water table have been shown to enhance LNAPL entrapment and remobilization in the formation (Lenhard et al., 1993; Catalan and Dullien, 1995; and Dobson et al., 2007), and numerical models were developed by Aral and Lao (2002) to mimic this behavior. Dobson et al. (2007) further showed that water table fluctuation enhances biodegradation and dissolution of LNAPL components, and increases its migration down-gradient. Ryan and

Dhir (1993) performed laboratory column tests using glass bead packs of various sizes to investigate the effect of particle diameter on LNAPL entrapment due to a slowly rising water table. The results showed enhanced LNAPL entrapment for pre-wetted particles but insignificant effect for particle sizes less than 710 μm with an average residual saturation of 11%. Larger particles significantly reduced residual saturation.

At the Colomac mine site, Chapter 3 showed increase in LNAPL accumulation in some of the MWs in early winter, which corresponds to decreased groundwater elevation and vice-versa in early spring when the water table was elevated. This observed inverse correlation between the water table and accumulated LNAPL in monitoring wells is well established in the literature (i.e., Kemblowski and Chiang, 1990; Weiner, 2000; Hardisty et al., 2003). Besides, there was no significant recharge of LNAPL in the MWs following a product recovery test in the winter (Chapter 3), inferring the mechanisms enhancing LNAPL accumulation at the site are not continuous. Further investigations at the site showed that LNAPL contamination is generally limited to the upper seven meters of the subsurface, which consists of 0 – 4.6 m of overburden soil underlain by fractured bedrock (Chapter 2). From the site characterization efforts at the site, Chapter 3 suggested that freezing-induced displacement associated with cyclic freeze-thaw and water table fluctuations are mechanisms controlling LNAPL migration and accumulation in MWs at the site. Thus, this study was designed to complement the previous studies presented in Chapter 3 and Chapter 4, and evaluate the hypothesis that freezing induced displacement may play a secondary role in mobilizing contaminant at the site.

Consequent to discussions above, a freezing cell made of two parallel glass plates representing a fracture was constructed to evaluate the influence of freezing-induced displacement and freeze-thaw cycles on LNAPL mobility, and the effect of freezing on soluble oil in the formation. The method used in this study was a modification of those used by various authors to investigate

pore-scale behavior of contaminant in freezing porous media (Niven and Singh, 2008; Barnes and Wolfe, 2008; and Arenson and Segó, 2006).

6.2 Methodology

Equipment and materials used for this experimental study include process control equipment (RTD regulator; range $\pm 199.9^{\circ}\text{C}$, MODEL 4201APC2-T, omega), two glycol baths (LAUDA BRINKMANN, ecoline RE 120), a digital camera (Canon SLR 1000D), two computers, and freezing cell. Others are Agilent data acquisition unit, diesel, soluble oil, fluorescein, two fluorescent light tube-units, an air bag heater, a water bath, insulated enclosures, RTD probes, copper freezing plates, and weights.

6.2.1 Freezing cell

The freezing cell is constructed from Perspex glass as shown in Figure 6.1. It consists of sealed parallel glass plates interspaced at 1 mm (1000 μm) to mimic a fracture. The initial intent was to roughen the internal surfaces of the glasses but this would have impaired visibility to view the behavior, so glass beads were placed within the fracture instead. The objective of placing beads within the freezing cell is to enable entrapment of LNAPL within the water column.

The emplacement of the beads was done by first setting the required fracture width at both ends of the parallel glass plates and sealing the sides with silicone-laminated glass and the base with a porous filter. The beads were cleaned with hydrofluoric acid before placement into the created aperture. It should be noted that the beads were not of uniform size and shapes. Thus, during placement, some beads were stuck and had to be pushed down using thin wire gauze. Non-uniformity of the bead's geometry led to slight overlapping of some beads within the cell. Porous filter-glass was used between the RTD ports and the beaded filled-annulus of the cell to enable direct contact between the RTD and fluid within the cell.

The dimensions of the freezing cell are shown in Figure 6.1. Five RTD probes were fitted to one of the edges of the cell to monitor the thermal profile during the test. A control valve with pressure relief cork was fitted to the base of the cell. The control valve was used to moderate water filling while the pressure relief cork was used to prevent cracking of the apparatus due to volume change of ice. The tube connecting the control valve to the cell was made of expandable rubber to accommodate for displaced water during top-down freezing.

The top of the cell was uncovered, but had an emplaced aluminum mesh with 0.5 mm openings to prevent the beads from falling and to enhance heat dissipation. The apparatus was checked for leaks prior to testing and the RTD probes were calibrated before attachment to the cell using silicone glue.

The cell was insulated as shown in Figure 6.1 prior to the testing. The insulation consisted of foam with a glass window. The glass window provided the needed opening for photographing during testing. The base of the assembly was then placed inside a water bath in an environmental chamber (Figure 6.2), which was made up of a deep freezer with external temperature control equipment.

6.2.2 Setup

Three steps taken in setting up the experimental system were: cell-filling, cell-placement, and testing. Shown in Figure 6.2 is the layout of the experimental system. Fluorescein was added to the water used for the experiment because it provides an excellent way to discern frozen from unfrozen water during the experiment (Arenson and Segó, 2006). The elevation of the camera and bath units within the chamber were aligned before the start of the experiment.

6.2.3 Cell-infilling

Infilling of the cell was carried out from the bottom up at 0.5 mL/min via gravity displacement. An external reservoir consisting of a graduated

cylinder containing a fluorescein-water mixture with a fitted control valve was connected to the bottom control valve of the freezing cell via rubber tubing. Both valves were opened to achieve the desired flow rate. The cell was tilted during initial infilling with the pressure relief cork removed to allow the escape of air and prevent the formation of air-bubbles within the cell. When all the air at the base of the cell was displaced, the pressure relief cork was inserted, the cell was straightened up and filled until the upper open chamber was a quarter full.

To create a mixture of diesel and water, diesel was introduced at the open-end of the cell atop the fluorescein-water with the control valves of both the cell and the reservoir kept open. The water level in the reservoir was then lowered to allow downward flow of the diesel into the cell. This is akin to fluctuation of the water table in the field. Additional water was introduced via the top in conjunction with lowering the water level in the reservoir until LNAPL entrapment occurred. The valves were then closed and the system was allowed to equilibrate. The equilibration often involved some vertical movement of un-trapped LNAPL to the top of the cell within the first 15 minutes of the cell-infilling. In this study, the filled-cell was allowed to sit for more than one hour after placement in the environmental chamber before testing.

In tests involving soluble oils (i.e., Mobilcut-102, and BAND-ADE® sawing fluid), the soluble oils were mixed with the fluorescein-water mixture in the external reservoir, and used in filling the cell as discussed previously by gravity displacement. The properties of the soluble oils and diesel used for the experiment are given in Table 6.1.

6.2.4 Cell-placement

After filling the cell with the fluid(s) of interest, the RTD probes at the side of the freezing cell were reattached to the Agilent data acquisition unit, which was connected to the computer. The freezing-cell assembly was then placed inside the environmental chamber with its base sitting in the water

bath as shown in Figure 6.2. The freezing plate was attached to the top of the cell and in contact with the open section of the cell. The freezing plate was firmly secured to the stand inside the environmental chamber. The fluorescent lights were turned on and arranged at the top and bottom of the windowed area of the camera chamber to achieve optimum picture quality. The camera was turned on and weights ranging from 10 to 20 kg were placed atop the environmental chamber for proper sealing (Figure 6.2a).

6.2.5 Testing

After placement of the freezing cell and closure of the environmental chamber, the two glycol baths were turned on to maintain the temperatures at the top and bottom of the cell. One glycol bath controlled the temperature of the lower water bath while the other controlled the temperature of the freezing plate. The data loggers for both the camera and the RTD Agilent data acquisition unit were then turned on.

For the tests described in this paper, the temperature of the glycol bath controlling the lower water bath was set to +10°C and that of the freezing plate was set to -10°C. For the control experiment, the temperatures were varied to study heat propagation through the test cell. The temperature inside the environmental chamber was set to -2.5°C using the external temperature control unit. However, another RTD probe placed inside the environmental chamber showed that the temperature varied slightly (-3 ±1°C).

6.2.6 Test series

Three series of tests were involved in the evaluation of the study objectives. The first series was the control phase, which was aimed at assessing the system performance. In this series, only the fluorescein-water mixture was used for the test, and freezing was top-down. The freezing rate and the rate of frost penetration under different thermal gradients were

measured, and used to benchmark later tests. The cooling (or freezing) rates were calculated using:

$$\frac{dT}{dt} = \frac{dT}{dx} \times \frac{dx}{dt} \quad \left\{ \begin{array}{l} \frac{dT}{dx} \rightarrow \text{Thermal gradient at freezing front} \\ \frac{dx}{dt} \rightarrow \text{Rate of frost penetration} \end{array} \right. \quad 6.1$$

The second series was aimed at evaluating the influence of freeze-thaw on LNAPL and soluble oil movement. This series involved the use of diesel fuel and soluble oil. It should be noted that the diesel fuel used for this test was not colored because coloring caused it to adhere to the glass beads. The last series of the test involved evaluating the influence of freezing from the second test series on the development of micro-fissures. In this series, the step temperature at the top was varied from -10°C to +1°C, while the base and ambient temperatures were kept constant. The maximum temperature to the top surface during thaw was limited to +2°C because sudden thermal changes in the temperature caused moisture deposition on the surface of the freezing cell, leading to blurred photographic images.

6.3 Results and Discussion

Shown in Figure 6.3 is the thermal propagation for the control experiment. The rate of frost penetration was initially rapid until a steady state was reached after about 19 hours (Figure 6.4a). The average cooling rate of the system at steady state thermal gradient was 1.4°C/day and the frost front continued to move downward at a decreasing rate. Though the experimental cooling and frost penetration rate were more than an order of magnitude greater than that observed in the field (Figure 6.4b), they were within range of values reported in the literature (i.e., Konrad and Seto, 1991). Figure 6.3a shows that freezing caused the fluorescein-water to change color from green to grey. During the first freezing test (control experiment), rearrangement of the glass beads occurred within the cell as the freezing front propagated downward. This behavior was expected because freezing was known to enhance consolidation in porous media. Subsequent freezing

tests had no glass beads rearrangement during freezing because optimum compaction of the beads was achieved during the first freezing (control experiment). One of the four pins in RTD 103 attached to the side of the cell was accidentally cut and replaced before placement in the environmental chamber. Thus, readings from RTD 103 had more noise than other RTDs and was excluded from thermal profiles of subsequent tests.

The results for the second test series involving diesel fuel are summarized in Figure 6.5 and Figure 6.6. There was delayed frost penetration into the cell due to lower thermal conductivity of the diesel fuel compared to water. The cooling rate was $0.7^{\circ}\text{C}/\text{day}$ less than that of the control experiment during the first test series to establish steady state thermal gradient (Figure 6.5). At the onset of freezing, LNAPL rearrangement occurred within the cell, causing upward displacement of the LNAPL (Figure 6.6). The freezing displacement occurred during phase change due to suction generated as illustrated in Figure 6.7. As freezing progressed, no downward movement of the mobile LNAPL was observed. Instead, freezing caused upward remobilization of the trapped but mobile LNAPL (Figure 6.6 and Figure 6.7). Along the cell, there were instances where the expanding ice caused rearrangement of isolated blobs of LNAPL. The displacement resulting from this rearrangement was small. The reason for this may be that the forces generated by the expanding ice were not mobilized before freezing-induced suction and buoyant forces on the LNAPL blobs at the onset of freezing were established. Using the general equation at the freezing front developed from the Clausius-Clapeyron equation (eqn. 6.2), negative pressure or suction is generated at the freezing front. Combination of this with buoyancy of the LNAPL blob and capillary action favors upward movement of the LNAPL as freezing is initiated.

$$\begin{aligned}
P_w &= \frac{L}{V_w} \ln \frac{T^*}{T_o} + \frac{V_i}{V_w} P_i \quad (\text{from } dG_{ice} = dG_{water} \text{ at freezing front}) \\
\rightarrow \Delta P &= \left(P_w - \frac{V_i}{V_w} P_i \right) = \frac{L}{V_w} \ln \frac{T^*}{T_o} = \frac{L(T^* - T_o)}{V_w T_o} \Big|_{T^* \rightarrow T_o} \quad 6.2 \\
\therefore \Delta P &= \frac{L\Delta T}{V_w T}
\end{aligned}$$

Where, P, G, V, L, and T in equation 5 stand for pressure, Gibbs' free energy, specific volume, latent heat, and temperature. Subscript w and i indicate water and ice respectively. T* stands for temperature at which both water and ice co-exists (i.e., T* < 0°C), and T_o stands for reference freezing temperature of pure water (= 0°C or 273 K).

In bottom-up freezing tests by Niven and Singh (2008), they postulated that freezing-induced ice pressure on LNAPL ganglia could account for its upward mobilization and ganglia rupture. This freezing-induced pressure was estimated to be in the order of 1 MPa if fully mobilized, and is dependent on the LNAPL saturation. However, no downward LNAPL mobilization was observed in the top-down freezing tests in this study. The observed LNAPL displacement that took place after cyclic freezing in this study was upward, and opposite to the direction of freezing. Due to difficulty in quantifying lateral mobility in these tests, the observed cumulative upward LNAPL displacement was used to quantify upward mobility shown in Figure 6.6.

The initial position of the entrapped LNAPL was used as the baseline as shown in Figure 6.6b. The results showed that LNAPL mobilization and displacement took place at the onset of freezing and during thawing. Figure 6.7 illustrates the displacement that took place at the onset of freezing. The freezing induced displacement occurred during the phase change before the freezing front became visible in the photographic window. During freezing, the LNAPL within the cell remained unfrozen as the surrounding water changed phase. The expansion of the water surrounding the LNAPL during freezing may have induced pressure on the LNAPL. Thus, on thawing, the

pressure relief coupled with the LNAPL's buoyant nature enhanced its upward mobility. There was little displacement after the second thaw (2-T) and third freezing (3-F) cycles because insufficient time was allowed for pressure dissipation and ice melting within the cell (Figure 6.6a). Moreover, this test showed that freezing induced displacement is a viable mechanism for LNAPL movement. This is the first time the phenomenon described above is observed, and underscores the importance of cyclic freeze-thaw on the mobilization of LNAPL.

It is well established in the literature that decreasing temperature causes an increase in surface tension and capillarity in a porous media (Grant and Bachmann, 2002). To evaluate whether the observed displacement is due to increased capillarity due to decreasing temperature or suction induced at the commencement of phase change in the water (during freezing), a simple test was performed in the laboratory involving the use of a 1 mm diameter capillary tube with water. In this test, the capillary tube was set into a water filled glass beaker and placed inside the environmental chamber, which was cooled to -2°C from initial room temperature of +19°C. The results showed an increase in the capillarity height of 4 mm as the temperature decreased from +19°C to -2°C. Thus, for the dimensions of the freezing cell used in this study, the change in capillarity due to decreasing temperature was relatively small compared with the freezing-induced suction.

The observed upward mobility of the LNAPL at the commencement of the freezing process implies that LNAPL accumulation may occur at the onset of freezing in the formation during the winter period atop the water table, which may ultimately drain and accumulate in monitoring wells intersecting the formation. The accumulation of LNAPL in the monitoring wells may be enhanced by decreased groundwater elevation in the winter period as discussed in Chapter 3 and Chapter 4. Upon removal of the accumulated LNAPL in the monitoring wells, there may be little to no recharge from the formation because the driving mechanisms are discontinuous. However, as

winter ends, and spring brings warmer temperature, the accumulable LNAPL in the monitoring well may not be of the same magnitude as that observed during the winter period. Reasons for these may be one or combinations of the following:

- Elevation of the water table in early spring as winter ends due to infiltration of snowmelt and precipitation may cause trapping of released LNAPL below the water table.
- The released LNAPL due to thawing may be pushed back into the formation by the rising water table, and entrapped in localized fissures that may be hydraulically disconnected from the main interconnected fracture network in fractured media.
- Increase in water elevation may enhance downgradient migration of the released LNAPL, thereby reducing the accumulable LNAPL in the monitoring well.

Thus, mobilization of the LNAPL in the formation may result from freezing induced displacement coupled with decreased groundwater elevation due to little to no water precipitation and infiltration in the winter period.

The results of using the Mobilcut-102 soluble oil are summarized in Figure 6.8 and Figure 6.9. Mixing was done at 12.5% volume ratio (oil to water) to emphasize visual contrast during analysis because the color of the oil is akin to the color of the fluorescein-water when frozen. The results showed progressive expulsion of the soluble oil forward of the freezing front as shown in Figure 6.8, and in agreement with previous studies i.e., Konrad and Seto (1991), Chuvilin et al. (2001a and 2001b). The thickness of the excluded oil increased from 0 to 15 mm as freezing progressed downward in the cell. After eight hours, micro-fissures development was observed around the freezing front and the exclusion occurred as fingering as shown in Figure 6.8a. The cooling rate at steady state varied from 1.7 to 0.6°C/day as shown in Figure 6.9, and below the value of $4 \pm 1^\circ\text{C}/\text{day}$ reported by Konrad and Seto

(1991) for the optimum occurrence of cryogenic expulsion. Mixing of the soluble oil at 2% volume ratio produced similar results with a thin film of excluded oil below the freezing front (Appendix G). In addition to the Mobilcut-102 soluble oil, a slightly denser soluble oil named “BAND-ADE® Sawing Fluid” was used with a specific gravity of 1.02 (Table 6.1). The results were similar to that described above as shown in Appendix G.

The observed micro fissures may be due to thermal contraction of the formed ice as the temperature decreased. However, experimental microstructure study of freezing oil polluted sediments (silts) by White and Coutard (1999) and White and Williams (1999) in the laboratory, showed that small concentrations of petroleum (below 200 ppm) caused a decrease in interparticle spacing. The decreased interparticle spacing caused fissuring leading to increased hydraulic conductivity. Contrastingly, at high content of petroleum, soil particle aggregation promoted consolidation, resulting in decreased hydraulic conductivity. Investigation into the influence of petroleum on segregated ice formation in fine grain soils by Grechishev et al. (2001a and 2001b) showed that hardening temperature of petroleum hydrocarbon affected ice segregation and frost heave. The studies found that hardening temperature above zero reduced both ice segregation and frost heave, while that below zero produced the opposite. Thus, since the hardening temperature (i.e., pour point) of soluble oil used in this study was below zero, the observed micro fissures may also be due to ice segregation in the freezing cell. It should also be noted that most fuel-contaminants of interests (i.e., diesel, gasoline, etc.) have hardening temperature below zero, thereby increasing the likelihood of ice segregation in the contaminated media.

To evaluate the possibility of fissure development in the absence of oil, a new freezing cell was setup and subjected to prolonged continuous freezing. After four days, there were visible micro-fissures in the freezing cell (Figure 6.10). This agrees with the statement of Yershov et al. (1988) that there is a natural tendency for micro-fissures development in frozen media

and reinforces conclusions from previous studies (i.e., Biggar et al., 1998; and Chuvilin and Miklyaeva, 2003) that the developed micro-fissures are a potential pathway for contaminant propagation in frozen media.

The processes discussed above were physical processes, thus, reversible. Another reversible physical process is the regelation phenomenon in ice, which involves pressure melting at the interface and refreezing with pressure relief. According to Miller et al. (1975), continuous mobile liquid phase will allow transport from regelation of pore ice. In an unfrozen porous and fractured media, the pressure balance on the LNAPL can be written as follows (Hardisty et al., 1998):

$$h_L \rho_L g = h_{L-W} \rho_w g + \left(\frac{2\sigma \cos \phi}{b} \right) \quad 6.3$$

Where h_L and h_{L-W} are the height of the LNAPL above and below the water table respectively. The LNAPL density is ρ_L , b is the aperture width and ϕ is the contact angle. According to Hardisty et al. (1998), a one meter head of LNAPL will penetrate a fracture as small as 10 μm . However, when dealing with ice in frozen media, the relevant equation may be derived by combining equation 6.2 and 6.3 as:

$$\begin{aligned} h_L \rho_L g &= h_{L-W} \rho_w g + \left(\frac{2\sigma \cos \phi}{b} \right) + \Delta P_{ice} \\ &= h_{L-W} \rho_w g + \left(\frac{2\sigma \cos \phi}{b} \right) + \frac{L\Delta T}{T\Delta V_w} \end{aligned} \quad 6.4$$

Where ΔV_w is the specific volume change and ΔP_{ice} is the pressure required to melt ice from Clausius Clapeyron equation. The ΔP_{ice} term is often large in the range of 13 MPa per temperature change ($^{\circ}\text{C}$) below freezing. Thus for regelation to be a significant mechanism in LNAPL transport below freezing, the pressure head on the ice would have to be large.

Thus, cyclic freeze-thaw may enhance vertical migration of a contaminant due to capillary transfer and gravity drainage through interconnected micro-fissures induced in ice and porous media by freezing. Additionally, cyclic freeze thaw may cause upward mobility of entrapped LNAPL below the water table, and subsequently enhance lateral migration of LNAPL after thaw from these LNAPL saturated networks of macropores or fissures in the formation. Furthermore, according to Barnes and Chuvilin (2009), cyclic freeze-thaw may influence the distribution of disconnected LNAPL blobs and increase its downward migration.

6.4 Conclusions

The findings in this study showed that freezing-induced displacement is a viable mechanism contributing to LNAPL migration and accumulation in freezing and thawing media. Upward LNAPL mobility was observed at the commencement of freezing and during thawing. The suction induced at the onset of freezing was attributed to the upward mobility of the LNAPL for the top-down freezing experiment. During thawing, pressure relief coupled with the buoyant nature of the LNAPL enhanced upward remobilization. Test results using soluble oil showed progressive exclusion forward of freezing front and corroborated previous studies by Konrad and Seto (1991).

In petroleum contaminated sites in the permafrost environment where free product hydrocarbon persists, remedial activities involving LNAPL recovery are often performed in the summer seasons when freezing-induced displacement is inactive. The findings above suggest that to optimize recovery of LNAPL, more emphasis should be placed on recovery efforts at the commencement of winter period when this mechanism coupled with lowered groundwater elevation are active.

Furthermore, development of micro-fissures was observed in the ice formed within the freezing cell under prolonged freezing and at the freezing front region when soluble oil was used. This reinforces previous assertions by Biggar et al. (1998) and Chuvilin and Miklyaeva (2003) that the micro-

fissures developed in freezing media are potential pathways for LNAPL propagation in frozen media.

Table 6.1 Characteristics of the fuel and soluble oil used for the experiment.

Parameter	Diesel	Mobilcut-102	BAND-ADE® Sawing fluid
Solubility in water (20°C)	Insoluble (< 40 mg/L)	100%	100%
Specific gravity (25°C)	0.8171	0.89	1.02
Appearance	Colorless	Translucent amber	Translucent amber
Pour point (°C) or hardening temperature	-30	-6	-6
Dynamic viscosity (cp)	4 @ 0°C 2 @ 15°C	30 @ 40°C	9.5 @ 25°C
Surface tension (mN/m)	27.7 @ 0°C 23.8 @ 25°C		

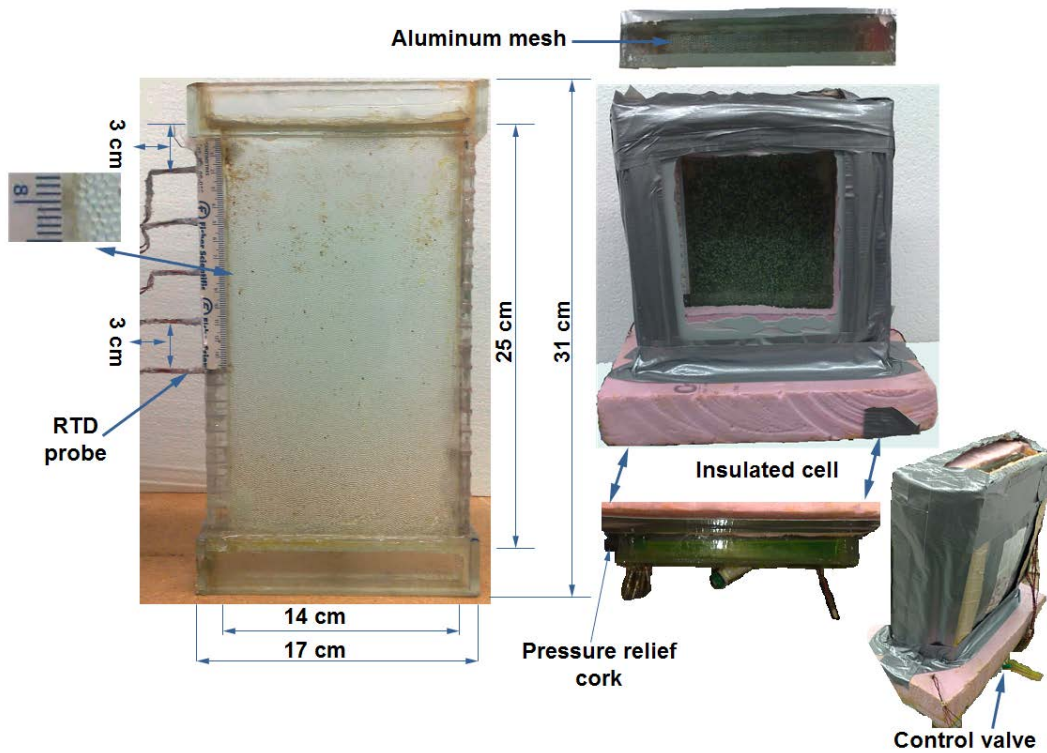


Figure 6.1 Fabricated freezing cell used for the experiment.

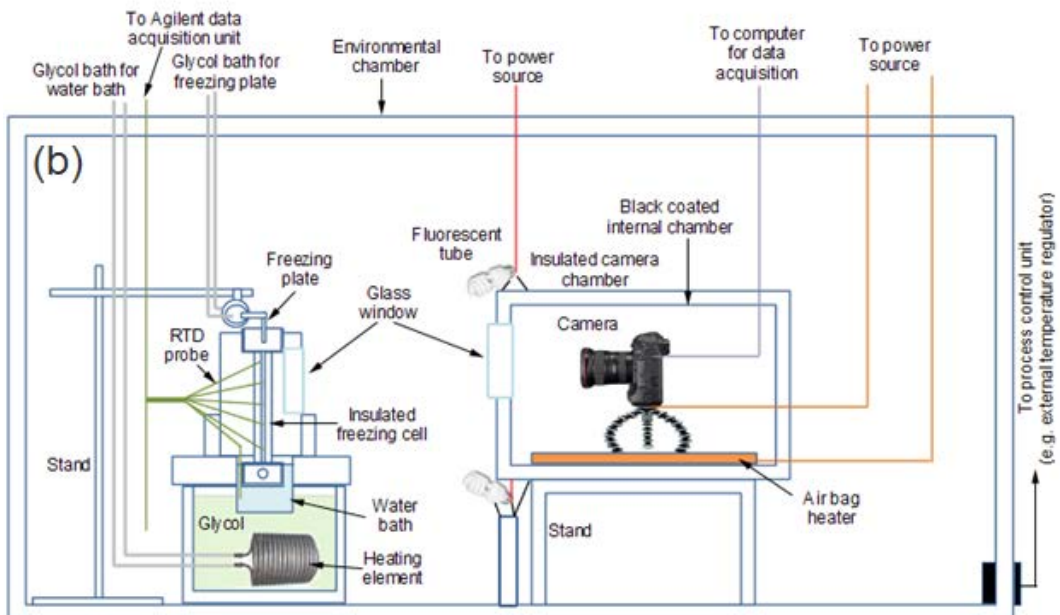
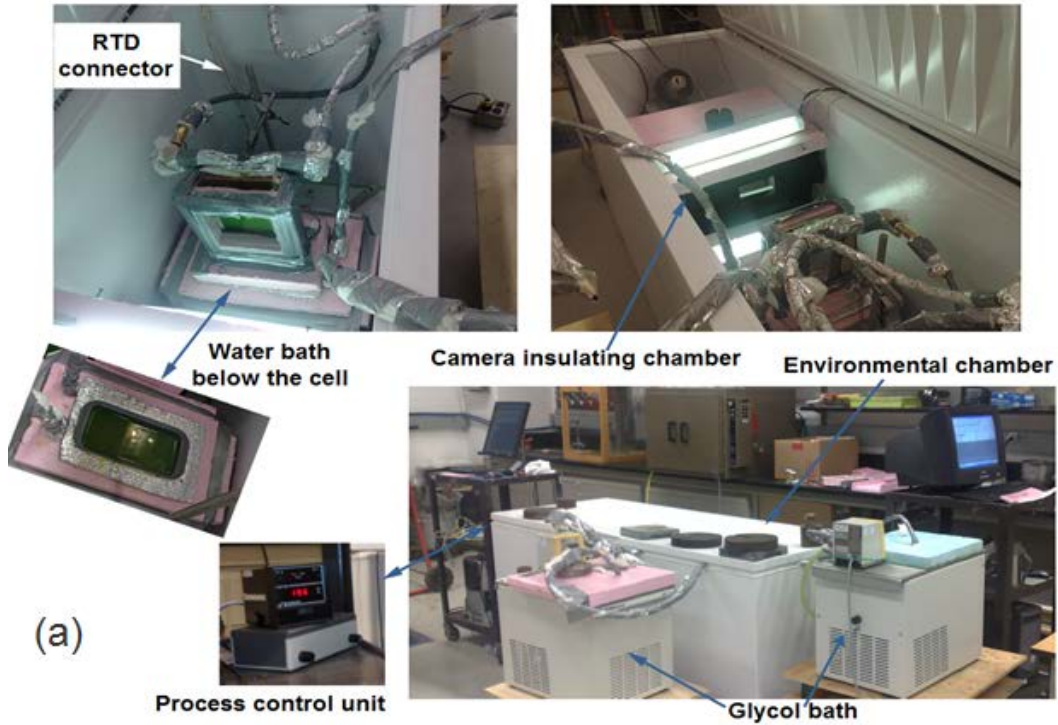
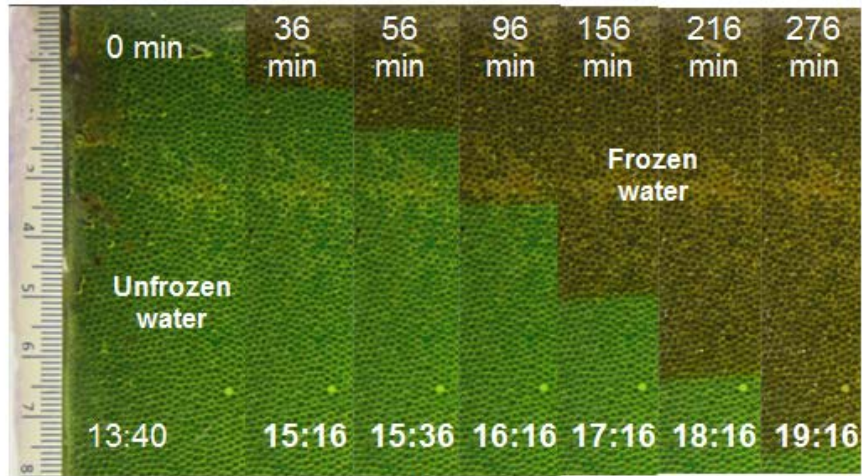


Figure 6.2 Setup of the laboratory system showing (a) freezing cell placement in the environmental chamber, and (b) schematic layout of the setup.



(a) Freezing cell sectional profile

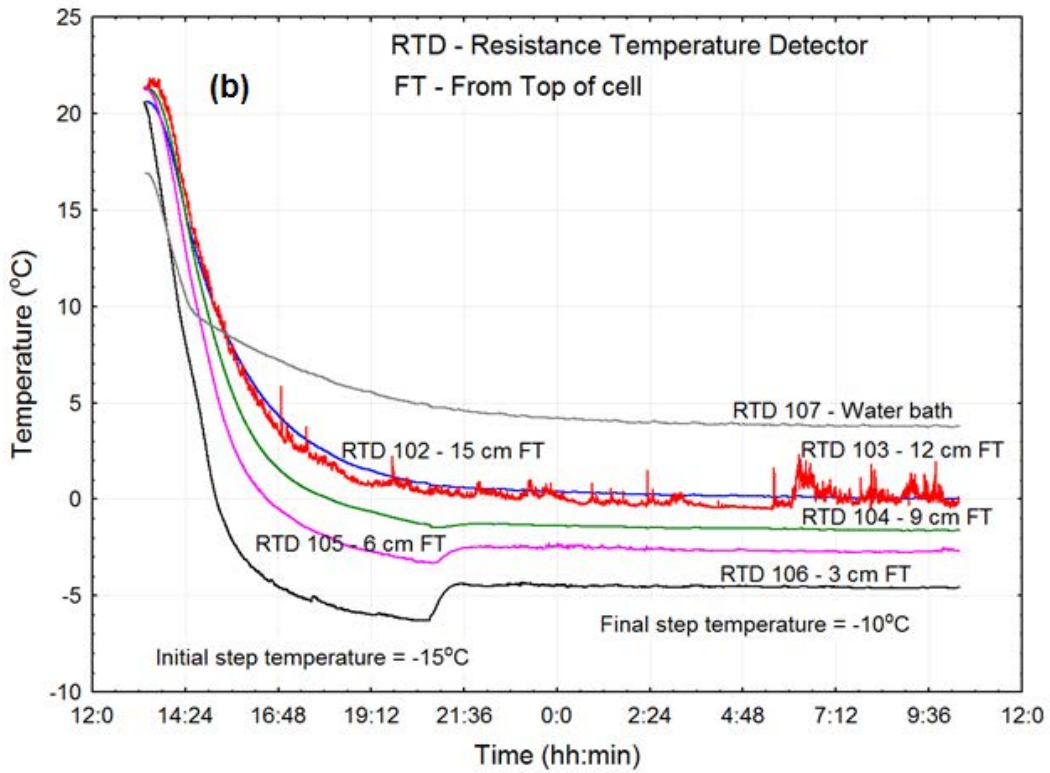


Figure 6.3 Thermal propagation for the control experiment, (a) Snapshots of freezing progression in the cell; (b) temperature profile.

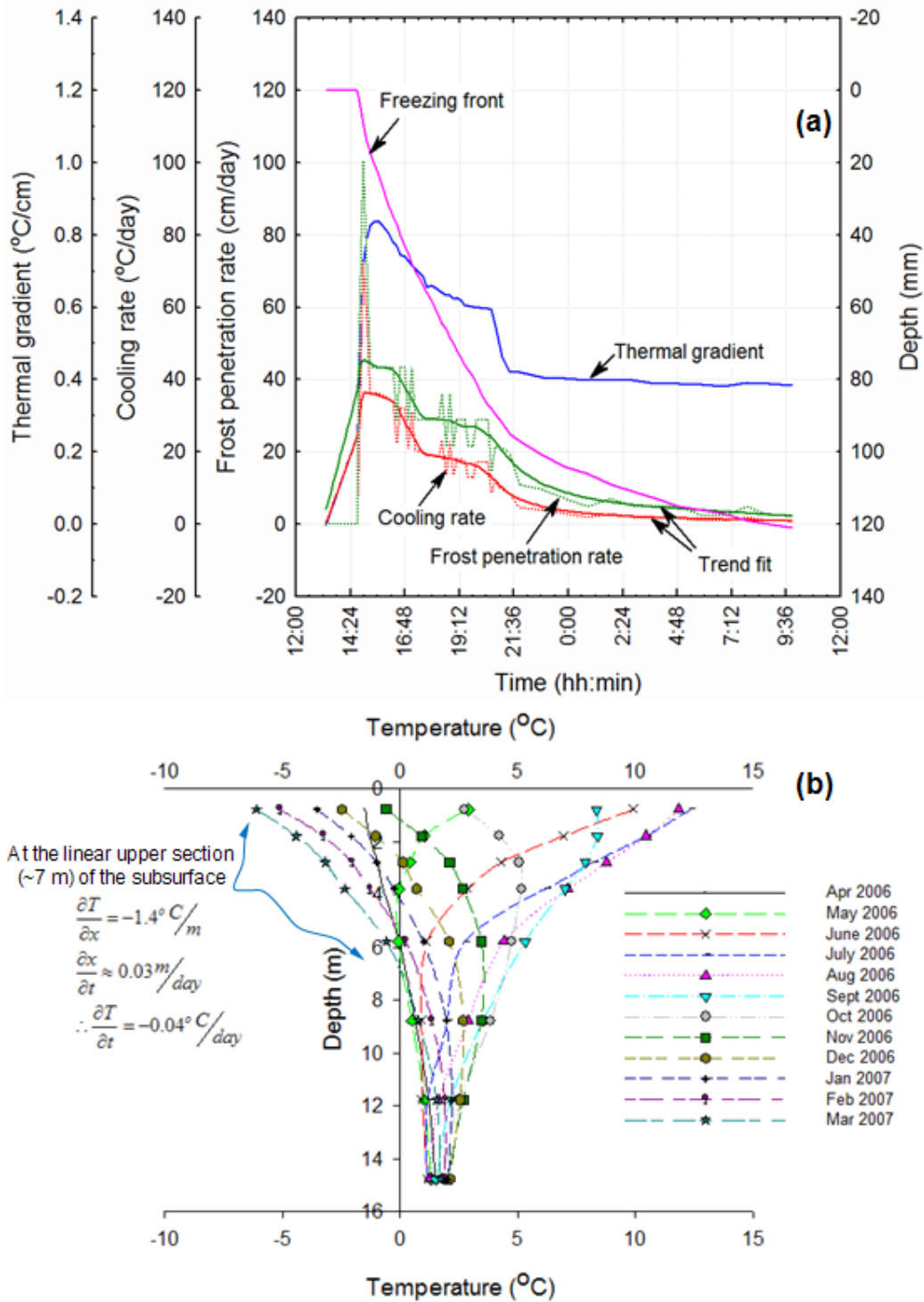


Figure 6.4 Comparison of laboratory and field thermal profile: (a) Frost penetration profile for the control experiment, and (b) sample of temperature profile in MW 15 at the Colomac mine site.

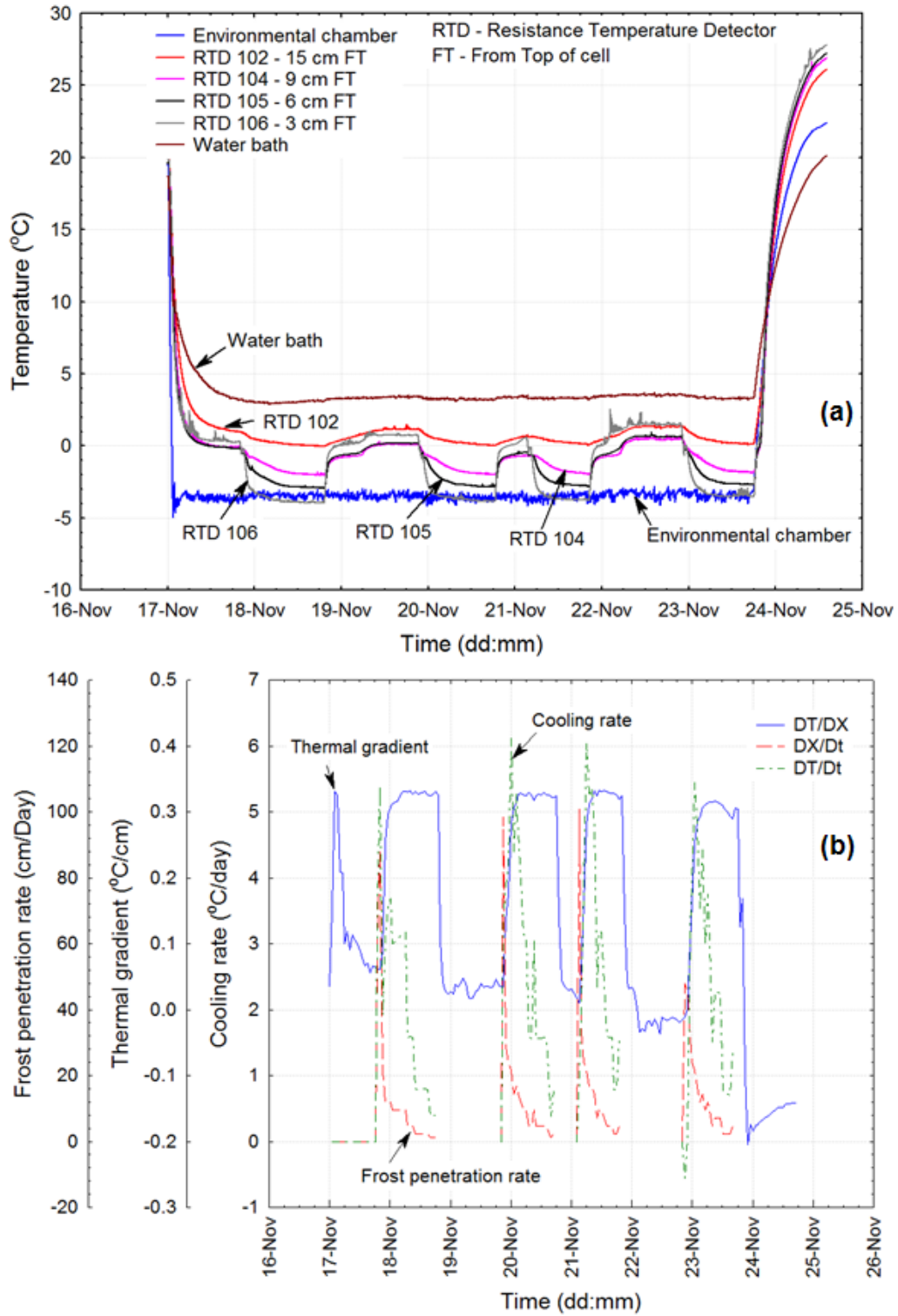
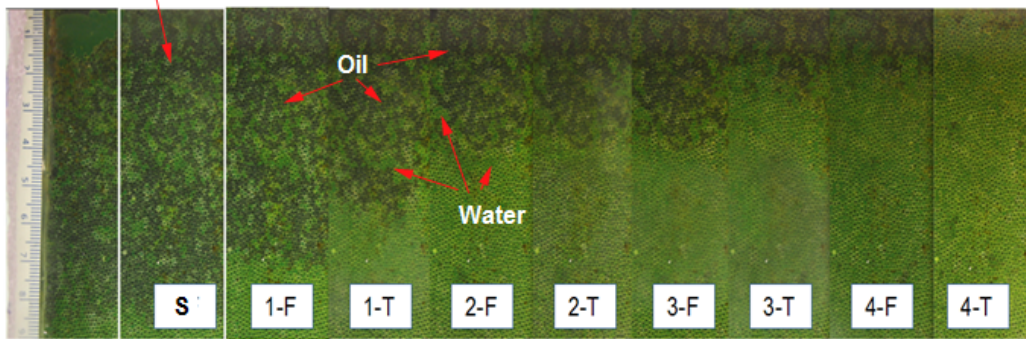


Figure 6.5 Freezing-test results using diesel subjected to freeze-thaw cycles. (a) Temperature profile; (b) profile for thermal propagation rates.

(a) Repeated photographic section



Note: Images with suffix "F" are those taken after cooling but before the freezing of water has progressed beyond 3 mm into the cell, and images with suffix "T" are those taken after complete thaw.

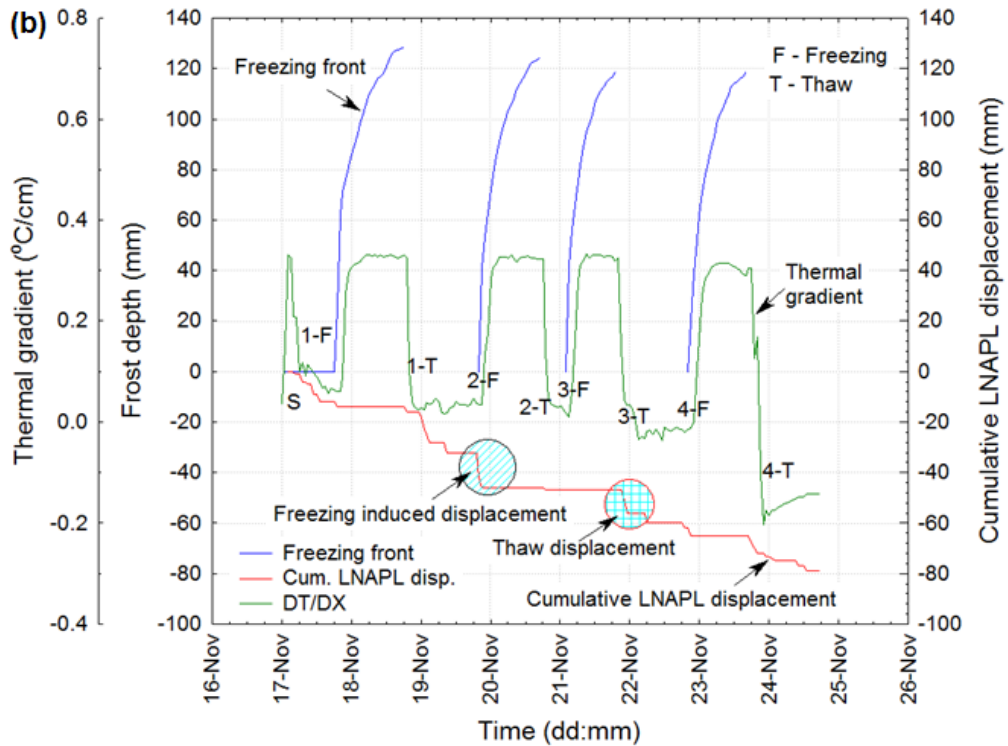


Figure 6.6 Frost penetration profile for freezing test with diesel (Figure 5): (a) Snapshots of upward displacement of diesel at the start of freezing and after thawing; (b) Plots of cumulative LNAPL displacement and frost penetration for each freeze-thaw cycle.

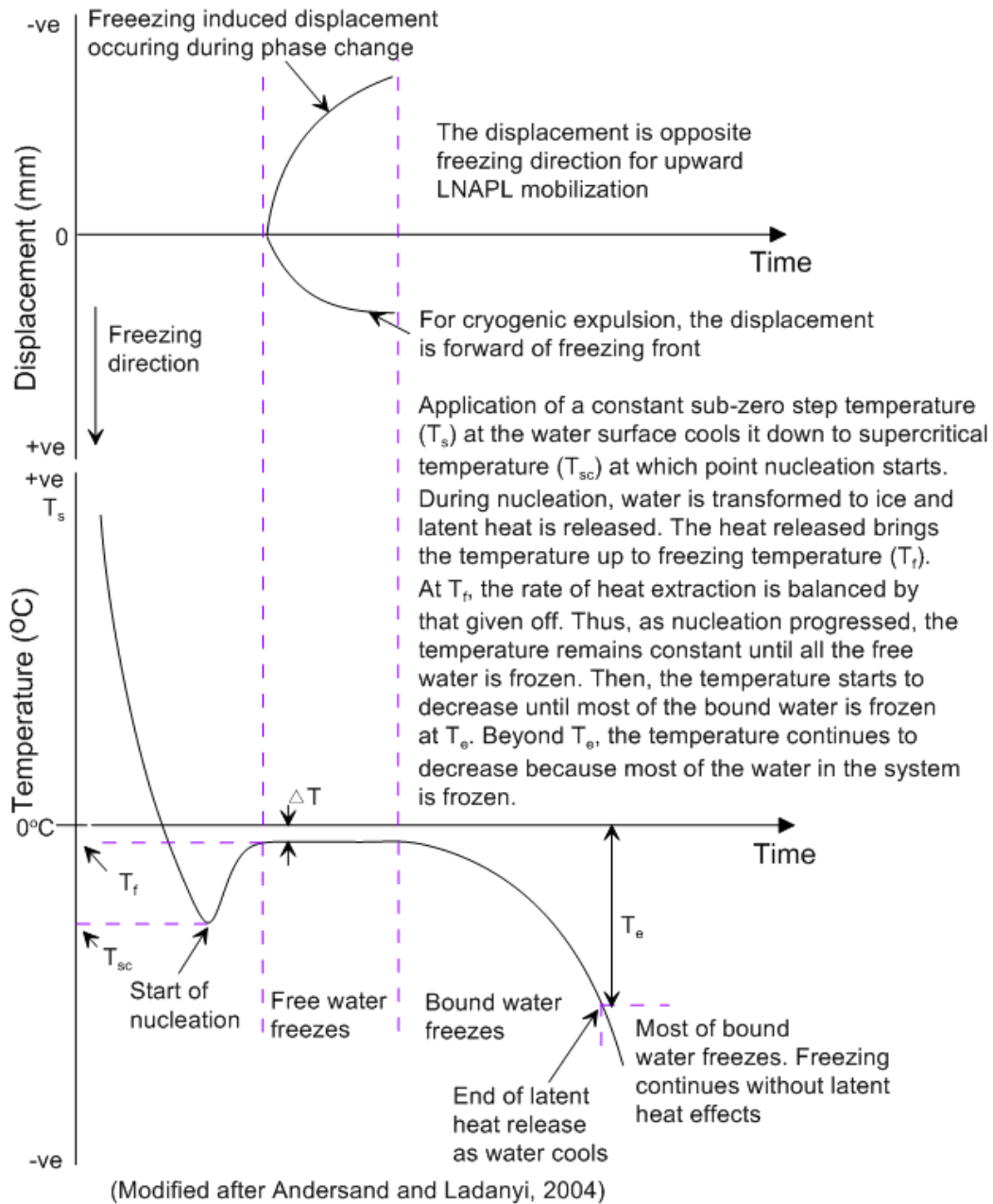


Figure 6.7 Illustration of freezing induced displacement that takes place during water nucleation process as ice is formed. For LNAPL-water system, suction induced during the phase change of water causes upward mobilization of entrapped LNAPL below the water table. For dissolved organics, the nucleation process causes forward exclusion of the organics from freezing water ahead of freezing front.

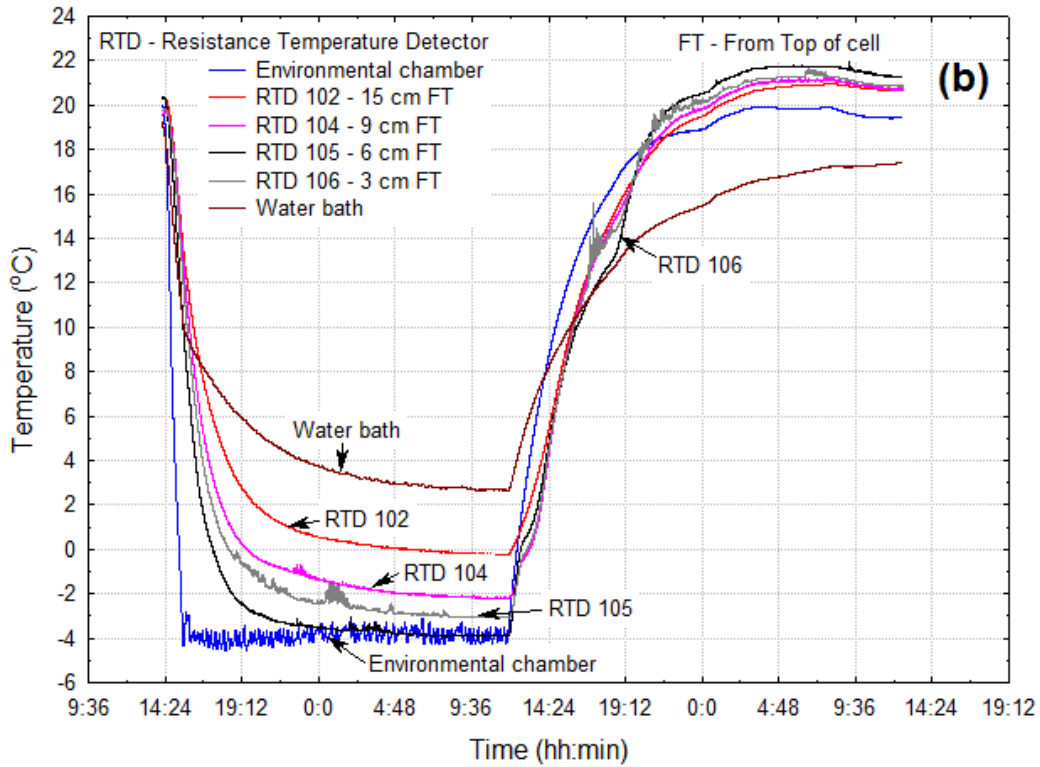
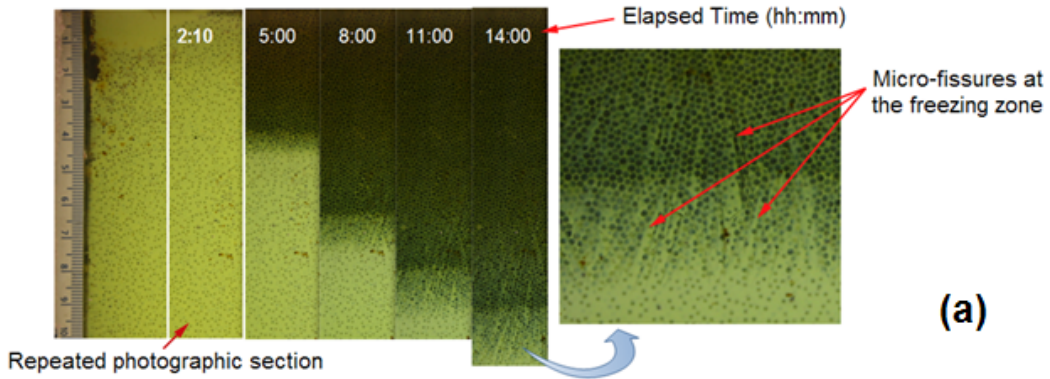


Figure 6.8 Profile of thermal propagation for freezing test using Mobilcut-102 soluble oil: (a) Snapshots of the observed progressive cryogenic expulsion; (b) temperature profile for the test.

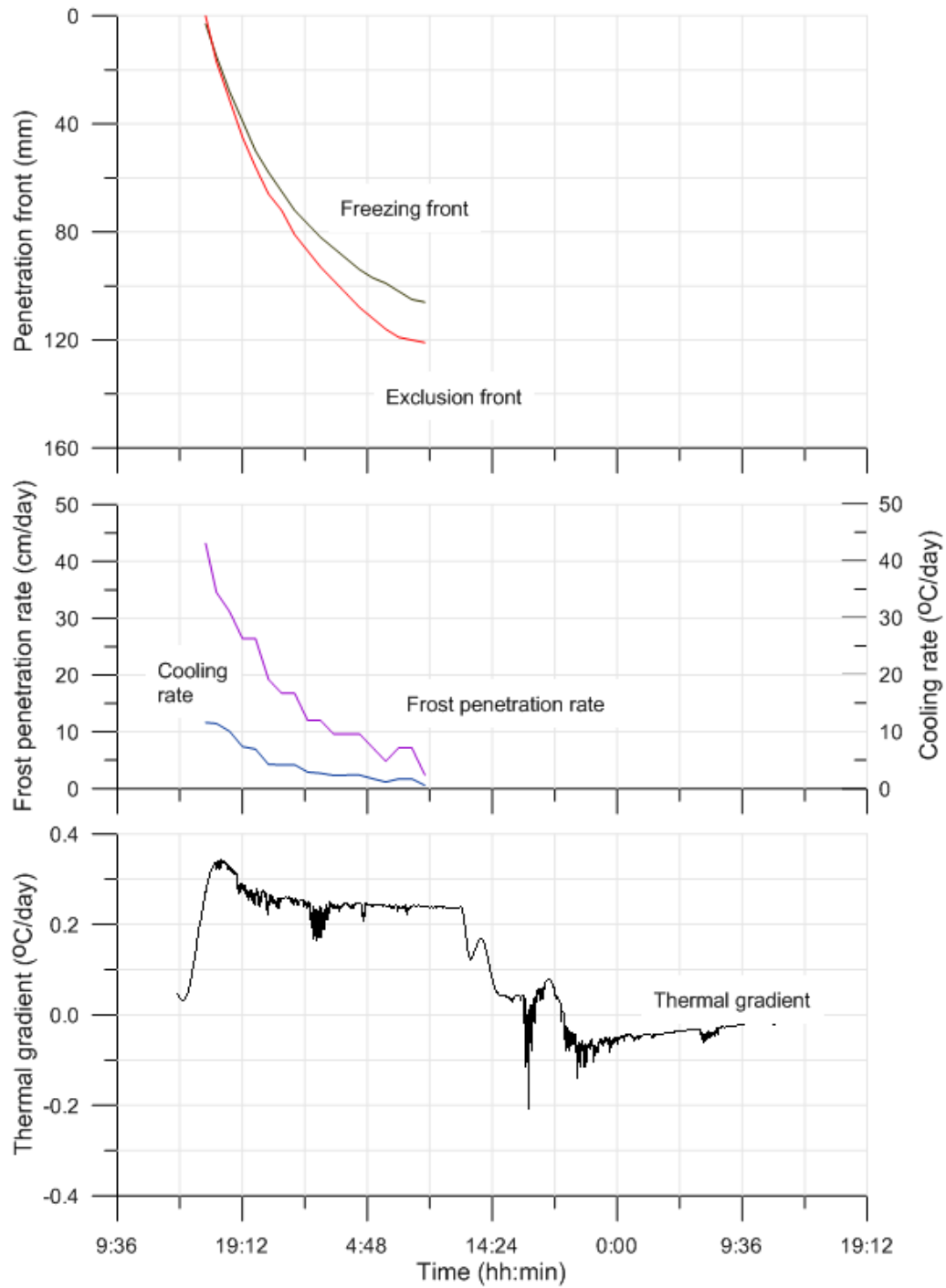


Figure 6.9 Condensed plot of freezing test using Mobilcut-102 soluble oil, showing the freezing and exclusion fronts, thermal propagation rates and the thermal gradient.

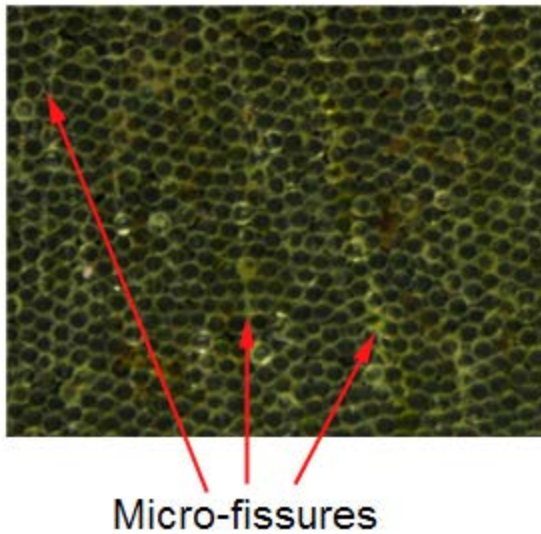


Figure 6.10 Snapshots of the observed micro-fissures in freezing test from a freezing cell under prolonged freezing with fluorescein-water only.

References

- Andersand, O.B., Ladanyi, B., 2004. Frozen Ground Engineering. 2nd Edition, John Wiley and Sons, Inc., New Jersey.
- Andersand, O.B., Wiggert, D.C., Davies, S.H., 1996. Frozen soil subsurface barriers: formation and ice erosion. *Journal of Contaminant Hydrology*, 23: 133-147.
- Aral, M.M., Liao, B., 2002. Effect of groundwater table fluctuations on LNAPL thickness in monitoring wells. *Environmental Geology* 45: 151-161.
- Arenson, L.U., Segó, D.C., 2006. The effect of salinity on the freezing of coarse grained sands. *Canadian Geotechnical Journal*, 43: 325-337.
- Barnes, D. L., Chuvlin, E., 2009. Migration of petroleum in permafrost-affected regions. *Permafrost soils*, R. Margesin (Ed). *Soil biology*, 16: 263–278. Springer, Germany.
- Barnes, D.L., Wolfe, S.M., 2008. Influence of ice on the infiltration of petroleum into frozen coarse grain soil. *Petroleum Science Technology*, 26: 856–867.

- Barnes, D.L., Wolfe, S.M., Filler, D.M., 2004. Equilibrium distribution of petroleum hydrocarbons in freezing ground. *Polar Record*, 40: 245–251.
- Biggar, K. W., Haidar, S., Nahir, M., Jarrett, P.M., 1998. Site investigations of fuel spill migration into permafrost. *Journal of Cold Regions Engineering*, 12: 84–104.
- Biggar, K.W., Neufeld, J.C.R., 1996. Vertical migration of diesel into silty sand subject to cyclic freeze-thaw. In: Carlson, R. (editor). *Proceedings of the Eighth International Conference on Cold Regions Engineering*. Fairbanks: American Society of Civil Engineers: pp 116–127.
- Catalan, L. J. J., Dullien, F.A.L., 1995. Application of gravity drainage to the recovery of residual LNAPL in homogeneous and lensed sand packs. *Journal of contaminant Hydrogeology*, 18: 279-306.
- Chuvilin, E.M., Miklyaeva, E. S., 2003. Investigation of the influence of salinity and cryogenic structure in the dispersion of oil and oil products in frozen soils. *Cold Regions Science and Technology*, 37: 89-95.
- Chuvilin, E.M., Naletova, N.S., Miklyaeva, E.C., Kozlova, E.V., Instanes, A., 2001. Factors affecting spreadability and transportation of oil in regions of frozen ground. *Polar Record*, 37: 229–238.
- Dobson, R., Scroth, M.H., Zeyer, J., 2007. Effect of water table fluctuation on dissolution of a multi-component light nonaqueous phase liquid. *Journal of Contaminant Hydrogeology* 94: 235-248.
- Ershov, E. D., Lebedenko, Yu, P. Chuvilin, E.M., Naumova, N.S., 1992. Mass transfer in freezing saline soils. *First International Conference Oil Pedology*, Pushchino, Russia, pp: 115-122
- Frolov, A.D., 1982. Physical model of frozen rocks. *wIzvestiia vysshikh uchebnykh zavedeniix Geologii i irazvedka*, 11: 134–141, Nov. Žin Russian.
- Grant, S.A., Bachmann, J., 2002. Effect of temperature on capillary pressure. In: *Environmental Mechanics, Water, Mass and Energy Transfer in the Biosphere* (Raats, P.A.C., D.E. Smiles, and A.W. Warrick, Eds.)

- Geophysical Monograph Series, v. 129. Washington, DC: American Geophysical Union, 199-212. (ERDC/CRREL MP-02-5905)
- Grechischev, S.G., Instanes, A., Sheshin, J.B., Pavlov, A.V., Grechishcheva, O.V., 2001a. Laboratory investigation of the freezing point of oil-polluted soils. *Cold Regions Science and Technology*, 32: 83–189
- Grechischev, S.G., Instanes, A., Sheshin, J.B., Pavlov, A.V., Grechishcheva, O.V., 2001b. Laboratory studies of the oil-contaminated fine-grained soils freezing and their negative temperature fabric model. *Cryosphere Earth*, N2:48–53.
- Hardisty, P. E., Wheater, H. S., Johnston, P. M., Bracken, R. A., 1998. Behavior of Light Immiscible Liquid Contaminants in Fractured Aquifers. *Geotechnique*, 48(6): 747–760.
- Hardisty, P.E., Wheater, H.S., Birks, D., Dottridge, J., 2003. Characterisation of LNAPL in Fractured Rock. *Q.J. Eng. Geol & Hydrgeol*. 36: 343-354.
- Kemblowski, M.W., Chiang, C.Y., 1990. Hydrocarbon thickness fluctuations in monitoring wells. *Ground Water*, 28(2): 244-252.
- Konrad, J.M., McCammon, A.W., 1990. Solute partitioning in freezing soils. *Canadian Geotechnical Journal*, 27(6): 726-736.
- Konrad, J.M., Seto, J. T. C., 1991. Freezing of a clayey silt contaminated with an organic solvent. *Journal of Contaminant Hydrology*, 8(3–4): 335–356.
- Lenhard, R.J., Johnson, T.G., Parker, J.C., 1993. Experimental observations of nonaqueous-phase liquid subsurface movement. *Journal of Contaminant Hydrology*, 12: 79-101.
- Miller, R.D., Loch, J.P.G., Breseler, E., 1975. Transport of water and heat in a frozen permeameter. *Soil Science Society of America Journal*, 39(6): 1029-1036.
- Niven, R.K., Singh, K., 2008. Mobilization and rupture of LNAPL ganglia during freeze-thaw: Two dimensional cell experiments. *Environmental Science and Technology*, 42(15):5467-5472.
- Panday, S., Corapcioglu, M.Y., 1991. Solute rejection in freezing soils, *Water Resources Research*, 27(1): 99-108.

- Ryan, R., Dhir, V.K., 1993. The Effect of Soil Particle Size on Hydrocarbon Entrapment Near a Dynamic Water Table. *Journal of Soil Contamination*, 2(1): 59-90, 1993.
- Ryan, R.G., Dhir, V.K., 1996. The effect of interfacial tension on hydrocarbon entrapment and mobilization near a dynamic water table. *Journal of Soil Contamination*, 5(1): 9-34.
- Tumeo, M.A., Davidson, B., 1993. Hydrocarbon exclusion from ground water during freezing. *Journal of Environmental Engineering-ASCE*, 119(4): 715-724.
- Weiner, E.R., 2000. *Applications of environmental chemistry: A practical guide for environmental professionals*. CRC Press LLC, Florida.
- White, T.L., Coutard, J.P., 1999. Modification of silt microstructure by hydrocarbon contamination in freezing ground. *Polar Record*, 35:34-41.
- White, T.L., Williams, P.J., 1999. The influence of soil microstructure on hydraulic properties of hydrocarbon-contaminated freezing ground. *Polar Record*, 35: 25-32.
- Wilson, D.G., Mackay, D., 1987. The behavior of oil in freezing situations. Unpublished report of Environmental Protection Directorate, River Road Environmental Technology, Ottawa. 78p.
- Yershov, E.D., Lebedenko, Yu.P., Chuvilin, E.M., Yazynin, O.M., 1988. Microstructure of frozen soils. In: Yershov, E.D. (Ed.), *Moscow State University, Moscow*, p. 186. In Russian.

7 SUMMARY CONCLUSIONS AND RECOMMENDATIONS

7.1 Summary Conclusions

In this dissertation, different related field and laboratory studies were presented towards understanding the subsurface behavior of spilled fuel in a permafrost environment. The field study was implemented at the abandoned Colomac mine site, in the Northwest Territories (NWT), where extensive fuel contamination consisting mostly of diesel fuel occurred. Minor spills at the site included gasoline and some lubricating oil, but this research focused mainly on the fuel spills, which are light nonaqueous phase liquid (LNAPL) hydrocarbon. The site is underlain by fractured bedrock identified as greywacke, and has between zero and five meters of overburden soil consisting of sand, gravel, rock-fills, and peat at the shoreline of the adjacent lake (known as Steeves Lake). Fuel contamination is sporadic across the site but major spills occurred at the fuel storage area referred to as the tank farm.

Improved understanding of the subsurface behavior of spilled fuel at the site was gained and the key mechanisms influencing its migration and accumulation were inferred as water table fluctuations and freezing-induced displacements. Site characterization efforts showed that the bedrock fracturing is most intense at its upper section and the fuel contamination is generally limited to the upper seven meters of the underlying bedrock at the site. Thus, in contradiction to previous free product hydrocarbon assessment by URS (2002) that the contamination is mostly along the soil-bedrock interface, the fuel contamination had penetrated the densely fractured upper section of the bedrock. The measured apparent LNAPL thicknesses in the installed monitoring wells (MWs) varied across the site from 0.02 m to 5 m but were most persistent in the tank farm area. Though fuel seepage was observed in the shoreline of adjacent Steeves Lake, most of the free product contamination was localized adjacent to the original contamination release areas.

Further tests at the site showed that efficient recovery of free product or LNAPL alone by the use of a skimmer pump may not be feasible due to very slow recharge of the LNAPL after purging because the mechanism influencing its migration is not continuous over time. Most of the reported fuel spills at the site occurred in the winter period, which corresponds to a decreased water table across the site. At the tank farm area, the water table in the winter period was as low as 13 m below the surface, thus, significant penetration and lateral downward spreading of the spilled fuel into the bedrock might have occurred. This also explains in part why the installed frozen core interceptor trench was ineffective in curbing migration of the spilled fuel towards the adjacent lake. The trench was just 5 m deep, thus, not deep enough to intercept the free product. Additionally, the permafrost at the site is very discontinuous, and the active layer of thermal fluctuation extended more than 15 m in most locations at the site. Thus, placement of the trench in the active zone is not the most ideal.

The findings from site characterization implied that water table fluctuations influence mobility of LNAPL at the site. Greater LNAPL accumulation in the MWs near the spill areas corresponded to lowered water table, and vice versa for elevated water table at the site. This study suggests that decreasing water table enhanced gravity drainage of mobile LNAPL in the subsurface, thereby, leading to greater LNAPL accumulation in the MWs. Other studies in the literature support this behavior (Hardisty et al., 2004; Kemblowski and Chiang, 1999). Besides, in the spring when infiltration of snowmelt and rain occurs, this study suggests that the drained LNAPL may be transported farther downgradient along major fractures, which explains why LNAPL seepage always occurs at the shoreline of Steeves Lake in response to high precipitation event when the water table is elevated. More so, the rising water table may result in entrapment of LNAPL below it, and caused LNAPL ensnarement in less interconnected fractures beneath the subsurface. Study by Hardisty et al. (2004; and 2003) support this behavior.

A direct field approach using the modified Gruszczenski method was used to estimate the maximum actual product thickness in the formation. The results indicated that the maximum LNAPL thickness in the formation was 8 cm, north of the tank farm area, which compared to a 3 cm thick LNAPL layer atop the water in a later excavation at the area. Due to the observed fuel behavior at the site, the actual product thickness was redefined as the equivalent thickness of mobile LNAPL if allowed to accumulate atop the water table.

Groundwater geochemical analyses at the site indicated gypsum dissolution and carbonate weathering as the dominant geochemical processes at the site. Prevailing cold temperature coupled with rich sulfide bearing rocks may have enhanced dissolution of gypsum and that of carbon-dioxide (CO₂), leading to higher carbonate formation and weathering. The analyses also showed that the water was Ca-SO₄ type and there were geochemical indicators of anaerobic biodegradation involving sulfate and iron reduction in support of intrinsic biodegradation of dissolved fuel components. However, due to the persistence of free product at the site, natural attenuation cannot be relied on as the sole remedial option at the site.

The measured groundwater organic concentrations of benzene, toluene, and ethylbenzene were above the Canadian Council of Minister of the Environment (CCME) guideline for the protection of freshwater aquatic life in some MWs at the site. Other inorganic concentrations of interests were less than the CCME guideline values with few outliers except iron, aluminum and nickel. The background concentrations of iron and aluminum were above the CCME guideline values, thus, unsuitable as regulatory compliance criteria. However, the nickel concentrations were above both the background and CCME guideline values.

A laboratory study was used to evaluate the viability of freezing-induced displacements of LNAPL as proposed from the field studies as a significant mechanism contributing to LNAPL accumulation at the site. The

results showed that freezing-induced displacement is a viable mechanism, which may contribute to LNAPL migration and accumulation in a Cold Regions experiencing alternate freezing and thawing. Remobilization of entrapped diesel fuel was upward during freezing and thawing. The suction generated during phase change and pressure relief during thawing were attributed to the upward remobilization during freezing and thawing respectively. Progressive exclusion forward of freezing front was observed when solubilized oil was used; thereby corroborating the findings of Konrad and Seto (1991). Micro-fissures were observed in the ice formed within the freezing cell under prolonged freezing and within the freezing zone when solubilized oils were used. The observed development of micro-fissures strengthens previous assertions by Biggar et al. (1998) and Chuvilin and Miklyaeva (2003) that in frozen media, the micro-fissures are potential pathway for LNAPL migration.

7.1.1 Contributions

This research work is original and is the first well-documented body of work on the behavior of spilled fuel in a permafrost fractured bedrock environment. Because of the characterization efforts, the most impacted areas of the site were identified and mechanisms contributing to LNAPL migration at the site were inferred. These findings have led to the implementation of other remedial approaches as discussed in Appendix H, which resulted in the recovery of over 8000 liters of LNAPL at the site. The inferred mechanisms contributing to LNAPL migration at the site are freezing-induced displacement in addition to water table fluctuations. This study showed that these mechanisms are discontinuous in time. Thus, planning of remedial systems involving free product recovery at the start of winter period has the potential of optimizing LNAPL recovery in permafrost environment.

When dealing with fractured media, this work showed that the measured apparent LNAPL thicknesses in the monitoring wells might come

from zones other than adjacent depth atop the groundwater in the formation, and from non-pooled sources. This challenges the conventional thinking and interpretation of the meaning of actual LNAPL thickness, which was often construed as a uniform LNAPL layer in the adjacent formation.

This research work showed that intrinsic biodegradation is ongoing at the Colomac mine site. The geochemical characterization provided the baseline studies that other nearby mine sites can reference during and after closure.

Furthermore, this work reinforces the concept of cryogenic expulsion ahead of freezing front involving dissolved hydrocarbon and showed that prolonged freezing will lead to the formation of micro-fissures, which may serve as a conduit for contaminant transport in permafrost environments.

7.1.2 Project limitations

The laboratory work presented in this study did not consider lateral movements or displacements, which might have occurred in a three-dimensional heterogeneous system. Additionally, there was no mandate to implement a pilot scale study of a remedial system at the site, which might have provided additional insight into what works and what does not when dealing with such contamination scenarios. However, a pilot study conducted by Jacques Whitford AXYS Ltd. (2009) based on findings from this study are discussed in Appendix H.

7.2 Recommendations

7.2.1 Remediation

Improved understanding of the site showed that any combination of remedial systems involving water table fluctuation, manipulation of formation temperature, use of surfactants, hydraulic gradient control, pumping and sump monitoring, and volatile organic capture and treatment might be applicable at the site. Though more aggressive methods involving

excavation of the impacted bedrock including the use of multiphase single-well extraction system have been adopted and implemented at the site. Of the reported over 50,000 liters of spilled fuel at the site, over 8,000 liters of LNAPL were recovered with the use of these methods. Furthermore, the proposed enhanced LNAPL recovery system for the site by Iwakun and Biggar (2008) is outlined below:

7.2.1.1 Enhanced LNAPL recovery at the site

To increase displacement of LNAPL from the formation, formation flushing in combination with heating and containment are one option to treat the site. Steps in this approach are:

- Proper delineation of the contaminated area.
- Division of the contaminated area into treatment zones taking into consideration its topography, ease of access, existing monitoring wells, and nearness to the receptor (i.e. Steeves Lake).
- Installation of thermal siphon or other ground freezing systems to isolate each treatment zone. The frozen barrier created should extend up to at least 5 meters below the water table. Other structures involving hydraulic containment could also be used.
- Installation of ground heating systems or steam to achieve the following:
 - Breakdown any frozen LNAPL ganglia in the ground
 - Decrease the capillary pressure i.e. suction in the ground
 - Decrease the LNAPL viscosity and interfacial tension
 - Increase LNAPL mobility in the formation
- Create an artificial gradient by decreasing the water table at the sump well.
- Flush the treatment zone with surfactants to decrease the LNAPL-water interfacial tension and mobilize the trapped LNAPL in the formation towards the sump.

- Extract mobile LNAPL with the flushing solution from the sump well to LNAPL separator, and reuse the flushed fluid. There may be a requirement for VOC extraction to limit air pollution due to LNAPL volatilization from heating the ground.

The groundwater in adjacent MWs within and outside the treatment zone will have to be monitored. Before full-scale remediation, it would be prudent to conduct a pilot study at the site.

7.2.1.2 Engineering considerations

Engineering consideration for such a remedial system will include the following:

- Logistics in the movement of equipment and material to the site
- Capacity, number and cost of thermal siphon systems required at the site
- Monitoring the integrity of the artificial frozen wall or structure to prevent enhanced migration of the contaminant to uncontaminated zones
- Ensure hydraulic interconnectivity at the treatment zone to the sump
- Curtailing air pollution due to ground heating
- Labor, power requirements and cost

7.2.2 Natural attenuation

The complexity of the fracture pattern at the Colomac mine site may preclude cost-effective deployment of any active remedial systems at the site. It will be reasonable to assume that significant petroleum hydrocarbons (PHCs) in interstices of the bedrock in both free and adsorbed phases may persist irrespective of any elaborate remedial systems deployed at the site. The time-dependent desorption and release of these hydrocarbons may remain significant sources of contamination at the site. According to McNaughton (2002), despite the observed hydrocarbon seepage along the shoreline of Steeves Lake, the concentrations of dissolved hydrocarbons in the lake are below the CCME guideline values for the protection of freshwater aquatic life. Thus, given that natural attenuation is amenable at

the site, which may require hundreds of years for significant biodegradation of the spilled fuel to take place, the question is; are the regulatory authorities in charge willing to accept the reality that PHCs may persist at the site irrespective of any deployed remedial systems? Accepting this reality will be cost-saving but set a regulatory precedent, which other potential polluters might abuse when fuel-contamination is involved. According to McNaughton (2002), this will be tantamount to sending the wrong message that potential polluters can act without penalty. However, putting a regulatory clause that due diligence be exercised before resulting to natural attenuation may be worthwhile. This approach may also require periodic sampling of the soil, groundwater, and surface water, to ascertain reduction of PHCs load at the site.

7.2.3 Further assessments

The groundwater analyses at the Colomac mine site showed that the nickel concentrations exceeded the CCME guideline values for the protection of freshwater aquatic lives and background concentrations. Thus, further investigations are required to determine the underlying factors. In areas where the background concentrations of the constituents of interests are above the CCME guideline values, they are unsuitable as remediation compliance criteria. In essence, site based approach is recommended when conducting assessment for remediation. Additionally, there should be periodic monitoring of the groundwater constituents at the site to evaluate effectiveness of natural attenuation at the site.

7.2.4 Future directions

The objectives for this study were met. The extents of contamination were determined in Chapters 2, 3, and 4. Identification of factors and mechanisms contributing to LNAPL migration and accumulation were presented in Chapters 3, and 4. The active geochemical processes were determined in Chapter 5. Conceptual models of the site were presented in

Chapters 2, 3, and 4. Besides, a proposed remedial strategy was presented in this Chapter. Chapters 2 and 3 showed that natural attenuation is amenable at the site. Chapters 3, 4 and 6 succinctly showed that water table fluctuations and cyclic-freeze thaw influence LNAPL migration and accumulation at the site. Future research should focus on pilot scale studies of novel remedial approaches involving fuel contamination in the Canadian Arctic. The freezing cell developed in this study could be improved to evaluate regelation phenomenon and conditions that favor forward physical displacement of LNAPL blobs ahead of freezing front due to expanding ice as stipulated by Barnes et al. (2004).

References

- Biggar, K. W., Haidar, S., Nahir, M., Jarrett, P. M., 1998. Site investigations of fuel spill migration into permafrost. *Journal of Cold Regions Engineering*, 12:84–104.
- Chuvilin, E.M., Mikiyaeva, E.S., 2003. Investigation of the influence of salinity and cryogenic structure in the dispersion of oil and oil products in frozen soils. *Cold Regions Science and Technology* (37): 89-95.
- Hardisty, P.E., Roher, J., Dottridge, J., 2004. LNAPL Behavior in Fractured Rock: Implications for Characterization and Remediation, U.S. EPA/NGWA Fractured Rock Conference: State of the Science and Measuring Success in Remediation, Portland Maine, pp 129-134.
- Hardisty, P.E., Wheeler, H.S., Birks, D., Dottridge, J., 2003. Characterisation of LNAPL in Fractured Rock, *Quarterly Journal, Engineering Geology and Hydrogeology*, 36: 343-354.
- Iwakun, O., Biggar, K., 2008. Characterization of fuel spill plumes in fractured bedrock at a permafrost site: Colomac mine, NWT. Progress report submitted to Indian and Northern Affairs Canada (INAC).
- Jacques Whitford AXYS Ltd., 2009. Multi phase extraction system pilot test report. Submitted to Indian and Northern Affairs Canada. Project no. 1027392.02. Yellowknife. 64 p.

- Kemblowski, M.W., Chiang, C.Y., 1990. Hydrocarbon thickness fluctuations in monitoring wells. *Ground Water*, 28(2): 244-252.
- Konrad, J.M., Seto, J. T. C., 1991. Freezing of a clayey silt contaminated with an organic solvent. *Journal of Contaminant Hydrology*, 8 (3-4): 335-356.
- McNaughton, D. C., 2002. Colomac mine hydrocarbon cleanup Investigation options. A report submitted to Public Works and Government Services Canada. 7 pp.
- URS Norecol Dames and Moore Inc., 2002. Assessment of hydrocarbons within fractured bedrock at the lakefront and waste oil areas and development of a remedial action plan, Colomac Mine, NWT. Report for Public Works & Government Services Canada. Vancouver, BC. 21 pp. and appendices.

**APPENDIX A: PACKER TEST PROCEDURE AND SAMPLE
DATA**

1. Overview

This test was used to determine the hydraulic conductivity and fracture width of the fractured bedrock at Colomac mine. The principle used for this particular site was based on constant head test. The test was done by isolating zone of interest by means of inflated packers; the isolated well-water was then allowed to equilibrate in pressure to obtain initial head by means of a calibrated transducer attached to the packers. Then, water was injected into the well under pressure to bring about a two to three millivolts change in the transducer reading, and the head in the well was allowed to come into equilibrium with the injected water. The time and volume change of the injected water at constant head was measured and used to calculate the permeability, transmissivity, and the average fracture width in that zone. Equations used for the fracture width and hydraulic conductivity calculations are given below:

$$Z_T = C_{TE} - D_{BCT} \quad (A.1)$$

$$Z_B = Z_T - Z_L \quad (A.2)$$

$$Q = \frac{L_F}{T_F} * F_{VL} \quad (A.3)$$

$$H_D = \Delta V_R * C_{LV} \quad (A.4)$$

$$T = \frac{Q}{2\pi H_D} * \text{Log}_e \left(\frac{R}{r} \right) \quad (A.5)$$

$$K = \frac{T}{Z_L} \quad (A.6)$$

$$2b = 10^6 \left(\frac{T * 12\eta}{\rho g} \right)^{1/3} \quad (A.7)$$

Where,

ZT = Top of zone (m)

CTE = Casing top elevation (m)

DBCT = Depth below casing top (m)

ZB = Bottom of zone (m)

ZL = Length of zone (m) i.e. distance between isolated capture zone of the packer

Q = Flow rate (m³/s)

LF = Length of flow in the tank (cm)

TF = Time between the measured length of flow (s)

FVL = Flow volume per length of tank (m³/cm)

HD = Head difference in the test zone (m)

ΔVR = Difference in transducer Volts reading (V)

CLV = Calibrated pressure head per voltmeter reading of the transducer (m/V)

T = Transmissivity of the zone (m²/s)

R = Radius of influence of the well (m)

"r" = Radius of well (m)

K = Permeability of the test zone (m/s)

2b = Fracture thickness (μm)

η = Viscosity of water (Ns/m²)

2.0 System Set-Up

The system set-up consists of the packer assembly, reservoir/tank assembly, winch/pulley system and the analogue electronic system as shown in Figure A.1.

2. System Assembly

2.1 Packer assembly

The packer assembly is shown in Figure A.2. It has three openings for water, air, and transducer at the upper end excluding the winch line anchor. The water and transducer openings are connected to the shaft, which is essentially a pipe rod with a PVC sheath. The air opening was connected to the annulus of the inflatable gland and the shaft. Two packers were connected together as shown in Figure A.2 leaving an un-inflatable zone between them. The length of the un-inflatable zone was called the zone

length and the union connecting the two shafts of the packers was perforated at this zone. The annulus of the two packers at this zone was connected together by a small diameter pipe as shown in the Figure A.2. During water injection/flushing, it flows through the pipe rod to the formation at the uninflatable zone with perforated openings. The length of test zone is limited by the zone length of the packer.

2.2 Reservoir Assembly

The reservoir assembly for the Packer test used for the calculations of the flow rate and control the amount of injected water is shown in Figure A.3. It consists of three calibrated tanks of different diameters of 10, 6, and 1.25 inches respectively. The approximate height of each reservoir was about 1.4m and the general layout is shown in Figure A.3. Each reservoir has an air line and a water line except Tank 1 with an extra air vent and water feed line. Each line is fitted with a valve to control inflow and outflow. A two-way valve is fitted to the air line, one connecting it to the compressor and the other to vent the air in the tank.

2.3 Electronic System

The electronic system consists of a power source, multi-meters, and a chart-sheet data logger. The multi-meters and the chart-sheet data logger are coupled with the transducer from the packer. The multi-meter records the voltage response of the pressure head in the well, and the chart-sheet logger plots the analogue signal received. Before testing, the data logger system is calibrated to determine the calibrated pressure head per voltmeter reading of the transducer (CLV). This is done by dipping the transducer over a meter head of water and measuring the voltmeter difference in the logger. The value obtained is used to calculate the CLV of the system.

2.4 Winch/Pulley System

This consists of a hand-craft winch and a pulley, clamped to the well casing. The winch line of the packer is attached to the winch via the pulley to

ease lifting and lowering of the packer into the well. During lowering and lifting of the packer, the air, water and transducer lines have to be guided to prevent kinking of any of the lines in the well.

3. Test Set-Up

The set-up procedures before the beginning of test operation are:

1. Move the analogue electronic data logger system near the well to be tested
2. Move the tent covering the electronic system near the test well and put the data logger system in it
3. Clamp the winch/pulley system to the well stick up pipe
4. Move the packer assembly to the test well and connect it to the winch
5. Move the air compressor, water storage tank and the reservoir assembly to a suitable location near the well
6. Measure the depth to water (DTW) and depth to bottom (DTB) of the well
7. Calculate the number of zones needed to characterize the well
8. Calculate the depth of the un-inflatable zone below the top casing
9. Couple the electronic system together with the transducer and lower the packer into the well
10. Connect the data logger system to the power source and give it about five minutes to warm up
11. Start the test operation

3.1 Test Operation

The major stages involved in the test operation are filling of tanks, system flushing, packer inflation, water injection, and deflation of packers. Logging of data is incorporated in the stages involved

A. *Filling of tanks*

The procedures involved in the filling of tanks are outline below:

Vent the air in the tanks by turning the two-way valve to the vent line to depressurize the tank

1. Open the ball valve at the base of the tanks with the main injection valve closed (note: the tanks are interconnected at the base and can be isolated from each other :- Figure A.3)
2. Open the water feed line valve at the base of the largest reservoir (Tank 1)
3. Pump water from an external water source (i.e. water storage tank) to the feed line
4. Monitor the water rise in the tanks
5. Close the water feed line valve when the tanks are full
6. Close the vent valves and the ball valves for each tank
7. Choose the tank intended for the test
8. Connect the air line of the tank to the air compressor line and proceed to the next stage

Note: it is possible to fill one tank from the other or the two smaller tanks from the largest tank (Tank 1). To do this, the tanks to be filled are vented and the ball valves opened with the main injection valve closed. The air line of the filling tank is then connected to the air compressor line (note: the compressor has adjustable knob to control the pressure of the compressed air released). The compressed air is used to force water from the tank to the ones to be filled. When the other tanks are filled, the air line of the filling tank and the vent valves of the filled tanks are closed.

B. System flushing

This is the flushing of water through the water line of the packer assembly to remove any occluded air in the water line. This is done when the packer is deflated at the start of each test. The procedures involved are:

1. Pressurizing the tank to be used for the compression to about 10psi (usually Tank 1)

2. Slowly opening the ball valve of the tank and that of the main injection valve only
3. Allow five liters equivalent height drop in the tank (usually 10cm for Tank 1)
4. Close the main injection valve and the ball valve of the tank
5. Close the air line of the tank and proceed to the next stage
6. Note: Flushing is required at the start of each test in a well during initial set-up. As the test progresses down the well, it may be skipped when there is no perceived air traps in the water line.

C. Packer inflation

This is done to isolate zones of interest to be tested. The procedures involved at this stage are given below:

1. Lower the packer assembly to the zone of interest (i.e. for tests conducted, the entire zones below casing volume is of interest, thus, the zones are divided into 0.5m interval starting below the bottom of casing down the well)
2. Connect the packer air line to the air compressor and inflate to about 75 to 100psi
3. Monitor the pressure signature on the chart-sheet recorder of the data logger of the transducer (this will aid in choosing the type of tank to be used for the water injection)
4. Allow the pressure in the formation to equilibrate at this zone, which is indicated by constant pressure signature of the data logger
5. Record the value of the constant pressure value (in millivolts as initial head "VR₀")
6. Choose the tank to be used for water injection based on the pressure signature and move to the next stage

⁶ This may actually be kPa

Note: Choosing tank for water injection based on pressure signature is usually based on experience as test proceeds. If the formation is not fractured or the fracture is very small (i.e. tight formation), there will be a large difference in the pressure signature from its initial value and it will take a long time to come into equilibrium. For highly fractured formation/zone, the pressure signature difference will be small. Thus, in essence, the tightness of the zone is proportional to the pressure signature difference.

D. Water injection

This is done to determine the flow rate in the formation and final head used in the computation of the permeability and the fracture width. The procedures involved are:

1. Connect the air line of the chosen tank to the air compressor line
2. Slowly open the ball valve of the tank and the main injection valve
3. Increase the compressor pressure to about 5psi or low/high enough to bring about two to three change in millivolts readings of the transducer in the data logger
4. Monitor the pressure signature
5. Allow the injected water to come into equilibrium in the formation, which is indicated by constant pressure signature (i.e. transducer readings in millivolts)
6. Record this value and by means of stop watch, record the time taken for about 10cm drop in the calibrated tank with the corresponding millivolts values in the transducer
7. Average the transducer readings within the time interval and record as the final head in millivolts " VR_f " and determine the difference in transducer volts readings " ΔVR " (Note: this may be done during computation for fracture width and hydraulic conductivity after the tests)
8. Repeat steps "c" to "g" one to two more times for duplicity of results

9. Stop injecting by closing the main injection valve and the ball valve of the tank
10. Close the air line, decrease the pressure in the tank by venting off the compressed air in it and move to the next stage

Note: During water injection for a tight zone, any slight bump in pressure will register a very large difference in volts readings (pressure signature) and the flow rate into the formation will be quasi static.

E. Deflation of packer

This is necessary after each test in a zone to move the packer up and down the well. The procedures involved are simple as given below:

1. Close the packer air line with the air compression line (using the two way valve)
2. Connect the packer air line to the vent line (using the two way valve) to deflate the packer
3. Check the torque in the winch line to know when the packer is free to move within the well
4. Move the packer by 0.5m up/down the well to the zone of interest using the winch line and pulley system
5. Repeat the test operation from stage 1 through five till the zones of interest are completed
6. Move the packer out of the well, shut down the data logger and repeat the test set-up procedure for another well of interest.

Note: When the packer is totally deflated, hydrostatic pressure may compress the gland of the packer laterally to the walls of the formation, making it difficult to remove the packer from the well. To overcome this, the packer is not totally deflated (i.e. about 20psi is left within the gland to overcome the hydrostatic pressure) or during packer assembly, water may be poured into its annulus to increase its structural rigidity. A setup of the system at the site is shown in Figure A.4.

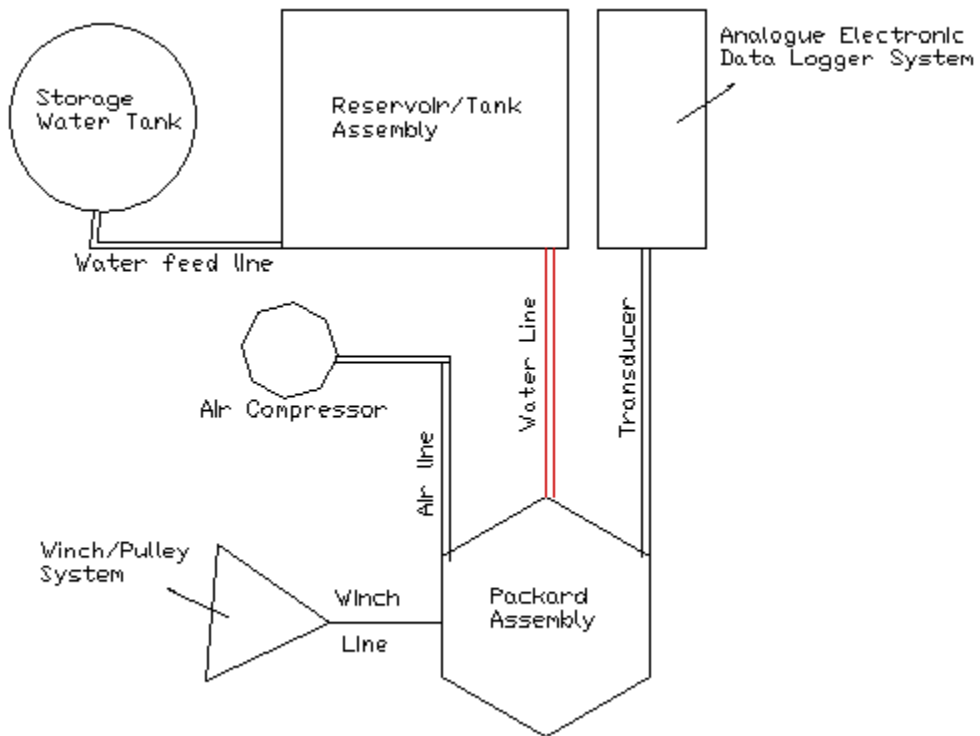


Figure A.1 System flow chart

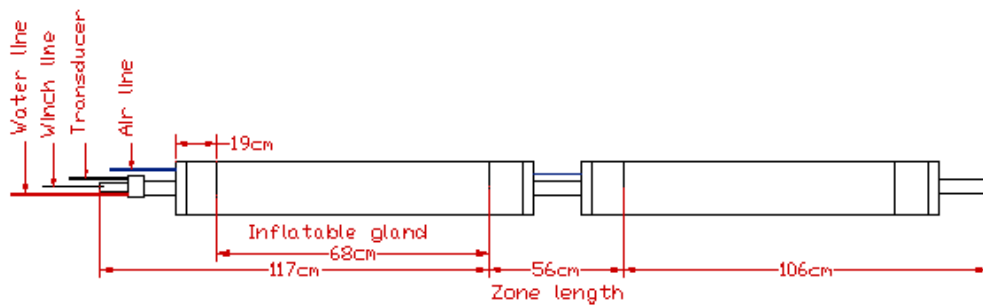


Figure A.2 Packer assembly layouts

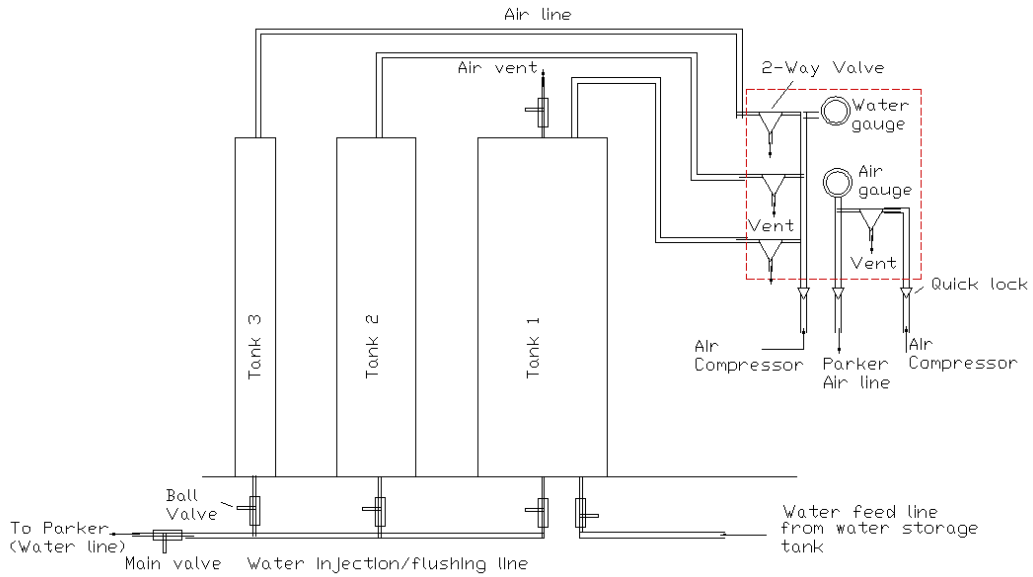


Figure A.3 Layout of the reservoir assembly

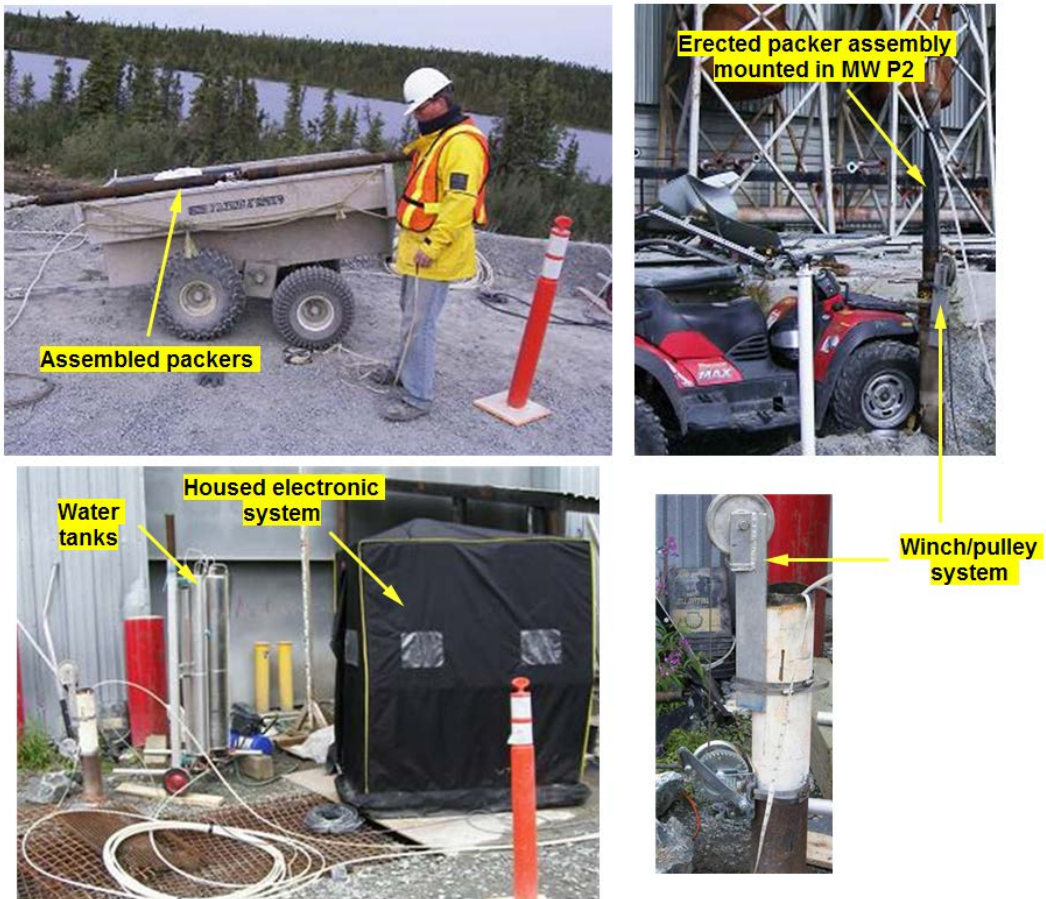


Figure A.4 Packer test setup on site (modified after Van Stempvoort et al., 2005).

Table A.1 Sample of measured hydraulic test data

Well ID	D (m)	ZT (m)	ZB (m)	T(m ² /s)	K (m/s)	2b (μm)
P2	6.29	315.419	318.402	5.88E-06	1.05E-05	222
	5.79	315.919	315.359	3.43E-06	6.12E-06	183
	5.29	316.419	315.859	1.00E-09	1.79E-09	<50
	4.79	316.919	316.359	1.00E-09	1.79E-09	<50
	4.29	317.419	316.859	6.50E-08	1.16E-07	49
	3.79	317.919	317.359	1.13E-06	2.03E-06	128
	3.29	318.419	317.859	4.04E-06	7.22E-06	195
	2.79	318.919	318.359	3.00E-06	5.36E-06	176
P1	6.83	318.422	317.862	1.00E-09	1.79E-09	<50
	6.33	318.922	318.362	1.00E-09	1.79E-09	<50
	5.83	319.422	318.862	1.00E-09	1.79E-09	<50
	5.33	319.922	319.362	1.00E-09	1.79E-09	<50
	4.83	320.422	319.862	1.00E-09	1.79E-09	<50
	4.33	320.922	320.362	1.00E-09	1.79E-09	<50
	3.83	321.422	320.862	1.00E-09	1.79E-09	<50
	3.33	321.922	321.362	6.06E-06	1.08E-05	223
2.83	322.422	321.862	6.26E-07	1.12E-06	105	
P3	5.45	319.802	319.242	1.00E-09	1.79E-09	<50
	4.95	320.302	319.742	1.22E-05	2.17E-05	283
	4.45	320.802	320.242	1.27E-05	2.26E-05	286
	3.95	321.302	320.742	2.99E-06	5.33E-06	177
3.45	321.802	321.242	3.93E-05	7.01E-05	418	
P4	5.43	316.907	316.347	3.39E-07	4.20E-07	76
	4.93	317.407	316.847	2.79E-04	4.99E-04	804
	4.43	317.907	317.347	1.70E-04	3.04E-04	681
	3.93	318.407	317.847	2.81E-06	5.03E-06	173
	3.43	318.907	318.347	9.32E-07	1.66E-06	120
	2.93	319.407	318.847	1.43E-04	2.56E-04	643
P6	7.25	318.002	317.442	1.00E-09	1.79E-09	<50
	6.75	318.502	317.942	1.00E-09	1.79E-09	<50
	6.25	319.002	318.442	1.00E-09	1.79E-09	<50
	5.75	319.502	318.942	1.00E-09	1.79E-09	<50
	5.25	320.002	319.442	1.00E-09	1.79E-09	<50
	4.75	320.502	319.942	1.00E-09	1.79E-09	<50
	4.25	321.002	320.442	4.88E-07	8.56E-07	97
	3.75	321.502	320.942	1.26E-04	2.25E-04	616
3.25	322.002	321.442	5.46E-05	9.75E-05	466	
P5	4.70	320.552	319.982	1.45E-05	2.54E-05	299
	5.20	320.052	319.482	1.78E-05	3.13E-05	321
	5.70	319.552	318.982	7.88E-08	1.38E-07	53
	6.20	319.052	318.482	1.00E-09	1.16E-09	<50
	6.70	318.552	317.982	1.00E-09	1.16E-09	<50
	7.20	318.052	317.482	1.00E-09	1.16E-09	<50

Table A.1 Sample of measured hydraulic test data (contd)

Well ID	D (m)	ZT (m)	ZB (m)	T(m ² /s)	K (m/s)	2b (μm)
MW22	6.00	318.391	317.821	1.01E-06	1.77E-06	123
	6.50	317.891	317.321	1.01E-07	1.77E-07	57
	7.00	317.391	316.821	6.19E-07	1.09E-06	105
	7.50	316.891	316.321	6.32E-07	1.11E-06	106
MW14	5.00	320.252	319.682	2.22E-06	3.90E-06	160
	5.50	319.752	319.182	1.05E-06	1.85E-06	125
	6.00	319.252	318.682	2.14E-05	3.76E-05	341
	6.50	318.752	318.182	5.82E-07	1.02E-06	103
	7.00	318.252	317.682	1.00E-09	1.16E-09	<50
	7.50	317.752	317.182	1.00E-09	1.16E-09	<50
	8.00	317.252	316.682	1.00E-09	1.16E-09	<50
	8.50	316.752	316.182	1.00E-09	1.16E-09	<50
	9.00	316.252	315.682	1.00E-09	1.16E-09	<50
	9.50	315.752	315.182	1.00E-09	1.16E-09	<50
	10.00	315.252	314.682	1.76E-07	3.08E-07	69
	10.50	314.752	314.182	1.00E-09	1.16E-09	<50
	11.00	314.252	313.682	1.00E-09	1.16E-09	<50
	11.50	313.752	313.182	4.85E-07	8.51E-07	97
	12.00	313.252	312.682	1.00E-09	1.16E-09	<50
	12.50	312.752	312.182	1.00E-09	1.16E-09	<50
	13.00	312.252	311.682	1.00E-09	1.16E-09	<50
	13.50	311.752	311.182	1.34E-06	2.35E-06	135
	14.00	311.252	310.682	1.33E-06	2.33E-06	135
	14.50	310.752	310.182	1.00E-09	1.16E-09	<50
15.00	310.252	309.682	1.00E-09	1.16E-09	<50	
15.50	309.752	309.182	1.00E-09	1.16E-09	<50	
16.00	309.252	308.682	1.46E-06	2.57E-06	140	
16.50	308.752	308.182	1.46E-06	2.57E-06	140	
17.00	308.252	307.682	4.88E-07	8.56E-07	97	
17.50	307.752	307.182	2.39E-07	4.20E-07	76	
18.00	307.252	306.682	1.00E-09	1.16E-09	<50	
18.50	306.752	306.182	1.00E-09	1.16E-09	<50	
19.00	306.252	305.682	1.00E-09	1.16E-09	<50	

Table A.1 Sample of measured hydraulic test data (contd)

Well ID	D (m)	ZT (m)	ZB (m)	T(m ² /s)	K (m/s)	2b (μm)
MW19	4.00	321.252	320.682	2.88E-05	5.06E-05	374
	4.50	320.752	320.182	6.09E-07	1.07E-06	104
	5.00	320.252	319.682	2.29E-07	4.01E-07	75
	5.50	319.752	319.182	3.08E-06	5.40E-06	179
	6.00	319.252	318.682	2.50E-06	4.39E-06	167
	6.50	318.752	318.182	1.00E-09	1.16E-09	<50
	7.00	318.252	317.682	2.53E-06	4.43E-06	167
	7.50	317.752	317.182	9.49E-08	1.66E-07	56
	8.00	317.252	316.682	1.00E-09	1.16E-09	<50
	8.50	316.752	316.182	1.00E-09	1.16E-09	<50
	9.00	316.252	315.682	1.00E-09	1.16E-09	<50
	9.50	315.752	315.182	1.00E-09	1.16E-09	<50
	10.00	315.252	314.682	1.00E-09	1.16E-09	<50
	10.50	314.752	314.182	1.00E-09	1.16E-09	<50
	11.00	314.252	313.682	1.23E-06	2.15E-06	132
	11.50	313.752	313.182	1.78E-07	3.12E-07	69
	12.00	313.252	312.682	1.00E-09	1.16E-09	<50
	12.50	312.752	312.182	4.29E-07	7.53E-07	92
	13.00	312.252	311.682	1.00E-09	1.16E-09	<50
	13.50	311.752	311.182	4.15E-07	7.28E-07	92
14.00	311.252	310.682	3.70E-07	6.49E-07	88	
14.50	310.752	310.182	8.47E-07	1.49E-06	116	
15.00	310.252	309.682	3.70E-07	6.49E-07	88	
15.50	309.752	309.182	1.06E-06	1.86E-06	125	
16.00	309.252	308.682	6.50E-08	1.16E-07	49	
16.50	308.752	308.182	1.00E-09	1.16E-09	<50	
17.00	308.252	307.682	1.00E-09	1.16E-09	<50	
17.50	307.752	307.182	1.00E-09	1.16E-09	<50	
18.00	307.252	306.682	1.00E-09	1.16E-09	<50	
18.50	306.752	306.182	1.00E-09	1.16E-09	<50	
19.00	306.252	305.682	1.00E-09	1.16E-09	<50	
MW8	4.70	319.589	319.019	1.70E-05	2.99E-05	315
	5.20	319.089	318.519	7.88E-08	1.38E-07	53

Symbol

- D Depth below top of casing
- ZT Zone top elevation
- ZB Zone bottom elevation
- T Transmissivity of zone
- K Hydraulic conductivity
- 2b Fracture width

- Sample Zones using Packer assembly
- Inferred K at depth

References

- Van Stempvoort, D., Biggar, K., Iwakun, O., Bickerton, G., Voralek, J., 2005. Characterization of fuel spill plumes in fractured rock at a permafrost site: Colomac mine site, NWT. Interim report submitted to Indian and Northern Affairs Canada (INAC), Canada.

**APPENDIX B: ELEVATION DATA AND SAMPLE CALCULATION
FOR WATER TABLE CORRECTION**

Groundwater elevation correction

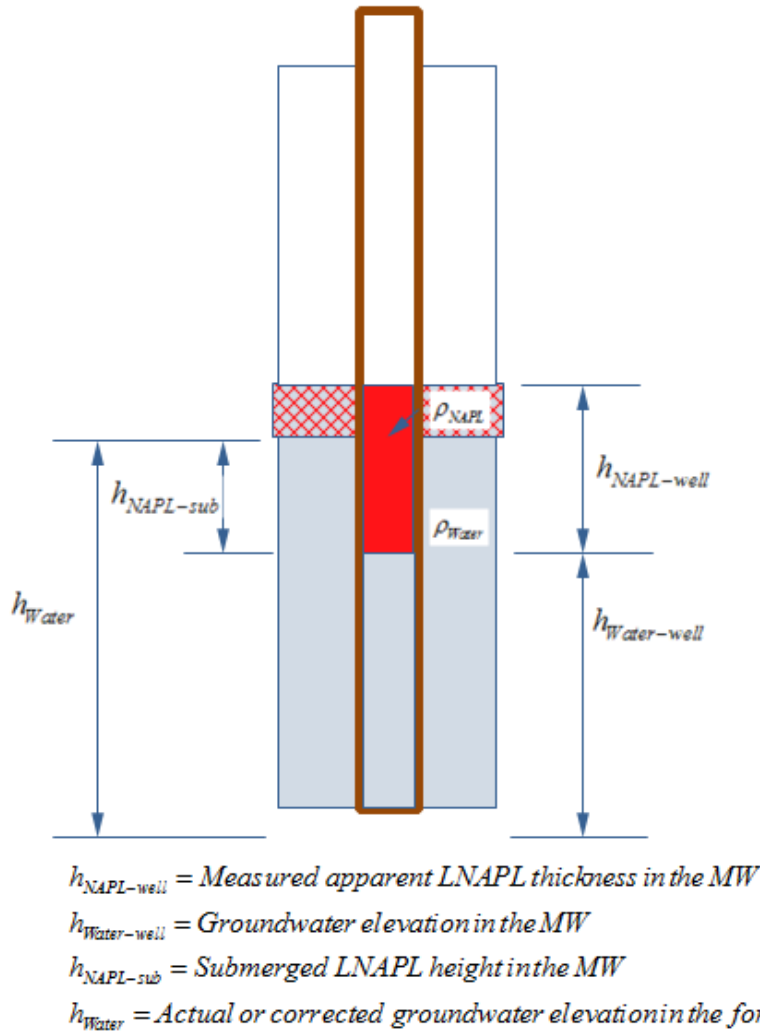


Figure B.1 Idealized sketch of LNAPL in the monitoring well (MW).

From the basic principle of floatation that states that a floating object displaces its weight on the liquid in which it floats, the balance of forces within the MW is:

$$\rho_{NAPL} g h_{NAPL-well} A_{well} = \rho_{Water} g h_{NAPL-sub} A_{well}$$

$$\Rightarrow h_{NAPL-sub} = \frac{\rho_{NAPL} h_{NAPL-well}}{\rho_{Water}} \quad (B.1)$$

From Figure B.1 above, the actual water elevation in the formation is given by:

$$h_{Water} = h_{Water-well} + h_{NAPL-sub} \quad (B.2)$$

Sample calculation:

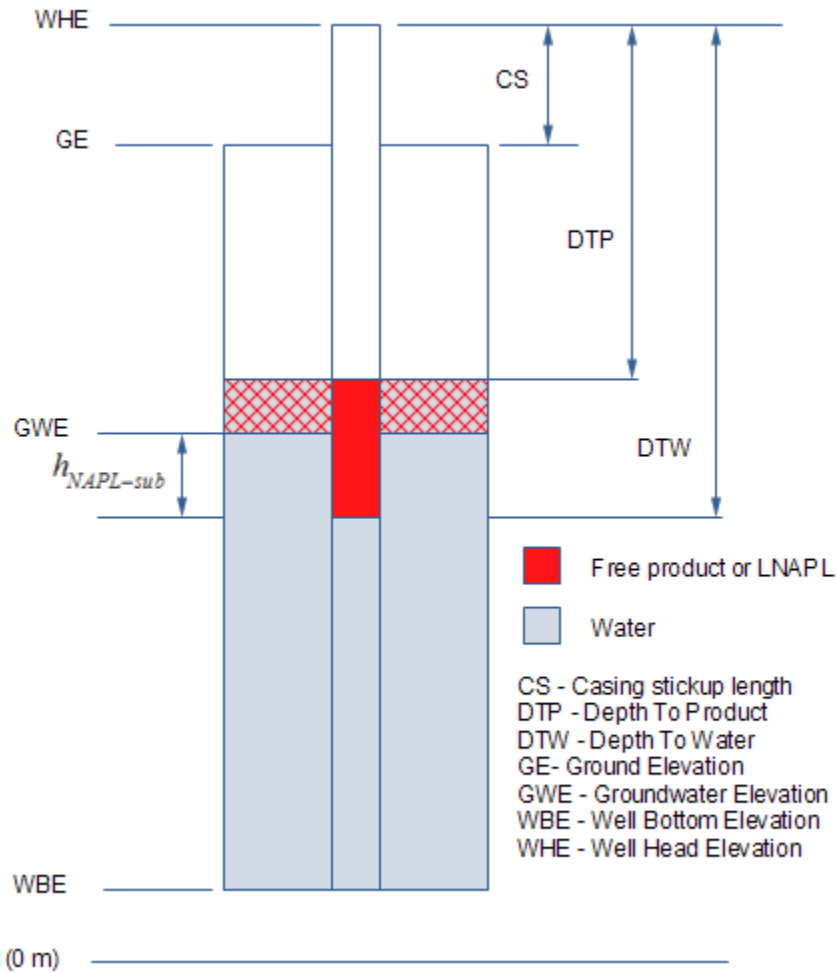


Figure B.2 Idealized monitoring well (MW) configuration at the site.

At the site, $h_{Water-well}$ has to be determined based on the measured depth to water (DTW) in the MW. Thus, Figure B.1 is redrawn in Figure B.2 to reflect site conditions. Rewritten equations for the site conditions are given below:

$$h_{NAPL-sub} = \frac{\rho_{NAPL} h_{NAPL-well}}{\rho_{Water}} = \frac{\rho_{NAPL} (DTW - DTP)}{\rho_{Water}} \quad (B.3)$$

$$GWE = h_{Water} = WHE - DTW + h_{NAPL-sub} \quad (B.4)$$

Using the measurement from MW 12 in August 17, 2005, given in Tables B.1 to B.4, the calculated GWE is given below:

$$h_{NAPL-sub} = \frac{\rho_{NAPL} h_{NAPL-well}}{\rho_{Water}} = \frac{0.88(5.38 - 5.31)}{1} = 0.0616 m \quad (B.5)$$

$$\begin{aligned} GWE = h_{Water} &= WHE - DTW + h_{NAPL-sub} \\ &= 327.5 - 5.38 + 0.0616 \approx 322.2 m \end{aligned} \quad (B.6)$$

A summary of the calculated GWE for selected dates are given in Table B.6. Some of the included data were provided by Environment Canada, Indian and Northern Affairs Canada (INAC), and the year 2000 data were obtained from EBA (2001) report for the site. The spatial location of the MWs and elevation contour of the site before the removal of overburden at the tank farm area are shown in Figures B.3 and B.4.

Table B.1 Monitoring wells elevation data

X (m)	Y (m)	Well #	CS (m)	Depth (m)	WHE (m)	GE (m)	BE (m)	WBE (m)
-7143756.9	591599.4	1	1.38	27.5	331.2	329.8	327.3	302.3
-7143812.2	591600.6	2	0.00	27.5	329.5	329.5	327.6	302.0
-7143790.6	591540.9	4	0.61	27.4	326.8	326.2	324.8	298.8
-7143855.4	591512.8	6	0.88	18.3	325.9	325.0	324.5	306.7
-7143766.4	591483.7	8	1.07	17.6	325.2	324.2	322.7	306.6
-7143741.7	591495.7	9	0.91	21.3	325.3	324.4	323.4	303.1
-7143748.0	591535.8	10	0.62	20.7	326.0	325.4	323.3	304.7
-7143910.1	591516.0	11	0.83	21.3	325.8	325.0	321.4	303.7
-7143884.8	591553.6	12	0.75	20.7	327.5	326.8	326.3	306.1
-7143721.4	591548.5	13	0.82	16.8	326.4	325.6	323.0	308.8
-7143710.4	591520.6	14	1.19	21.0	325.6	324.4	322.4	303.4
-7143807.1	591468.5	15	0.87	8.8	321.0	320.1	319.9	311.3
-7143747.4	591464.7	16	1.10	17.4	324.9	323.8	320.8	306.4
-7143707.9	591478.0	17	0.90	21.3	325.3	324.4	321.7	303.1
-7143671.8	591550.4	18	0.07	21.0	324.7	324.6	323.1	303.6
-7143686.4	591513.5	19	0.88	20.7	325.4	324.5	323.0	303.8
-7143844.0	591479.9	20	0.88	8.8	321.2	320.3	319.3	311.5
-7143631.0	591504.0	21	0.87	20.9	325.7	324.9	323.4	304.0
-7143671.8	591468.5	22	0.63	21.4	325.1	324.5	322.2	303.0
-7143641.2	591532.7	23	0.46	21.4	325.2	324.7	323.7	303.3
-7143766.4	591450.5	24	1.13	9.4	319.1	318.0	316.1	308.6
-7143737.2	591442.9	25	1.13	8.7	319.7	318.5	316.8	309.8
-7143908.8	591556.7	26	0.88	21.2	328.2	327.3	326.1	306.1
-7143958.4	591533.3	27	0.77	20.6	325.7	324.9	320.8	304.3
-7143945.8	591530.1	28	0.59	26.8	325.6	325.0	320.4	298.2
-7143823.6	591471.6	29	0.41	9.2	320.1	319.7	319.1	310.5
-7143786.2	591461.3	30	0.44	9.3	319.2	318.8	317.8	309.5
-7143749.9	591447.4	31	0.58	9.3	319.2	318.7	316.6	309.4
-7143885.4	591506.5	32	0.00	0.0	325.6	325.6	323.9	325.6

CS - Casing Stick-up length
WHE - Well Head Elevation
GE - Ground Elevation
BE - Bedrock Elevation
WBE - Well Bottom Elevation

Note: All the monitoring wells (MWs) are open wells with casing extended up to 1 m into the bedrock. The diameters of the MWs are 144 mm with the exception of the slanting wells with approximately 80 mm outside diameter.

Table B.1 Monitoring wells elevation data (contd)

X (m)	Y (m)	Well #	CS (m)	Depth (m)	WHE (m)	GE (m)	BE (m)	WBE (m)
-7143924.7	591521.9	33	0.15	18.7	325.2	325.1	321.4	306.4
-7143551.7	591417.0	34	0.87	12.2	323.4	322.6	321.0	310.4
-7143636.7	591458.1	35	0.81	22.6	324.8	324.0	322.4	301.4
-7143621.5	591476.1	36	1.16	22.0	325.3	324.1	322.4	302.1
-7143624.0	591528.9	37	1.30	22.0	325.8	324.5	323.9	302.5
-7143639.2	591586.1	38	1.24	22.0	325.9	324.6	323.6	302.6
-7143676.2	591497.0	39	0.15	22.0	324.6	324.4	323.5	302.4
-7143705.3	591507.1	40	0.58	22.0	325.0	324.4	323.7	302.4
-7143724.5	591513.5	41	0.19	22.0	324.7	324.5	323.8	302.5
-7143920.1	591580.4	42	1.08	25.0	330.1	329.0	328.5	304.0
-7143919.5	591540.3	43	1.00	19.4	326.5	325.5	323.9	306.1
-7143937.2	591563.7	44	1.08	21.0	329.6	328.5	327.0	307.5
-7143977.9	591539.6	45	0.73	25.6	325.6	324.9	320.5	299.3
-7143983.0	591589.3	46	0.87	26.8	326.4	325.5	323.0	298.7
-7143978.6	591612.1	47	0.73	26.8	326.5	325.7	322.7	298.9
-7144051.6	591659.1	48	1.09	26.8	326.7	325.6	322.2	298.8
-7144064.5	591638.2	49	1.10	26.8	326.2	325.1	319.9	298.3
-7143566.8	591451.2	50	1.19	14.9	324.6	323.4	321.1	308.5
-7143545.9	591549.2	51	1.17	14.9	326.2	325.1	321.7	310.2
-7143487.5	591426.5	P1	1.02	11.8	322.9	321.9	320.1	310.1
-7143509.0	591415.7	P2	1.15	10.8	322.6	321.4	320.3	310.6
-7143503.3	591394.0	P3	1.17	11.0	322.4	321.2	319.2	310.2
-7143528.0	591399.0	P4	0.78	10.3	322.3	321.5	320.0	311.2
-7143536.2	591376.9	P5	0.97	5.4	320.7	319.7	318.5	314.3
-7143510.3	591362.3	P6	1.30	5.8	320.2	318.9	316.8	313.1
-7143952.6	591527.6	102	Slanting well			324.2		
-7143816.5	591569.4	103	Slanting well			Located in excavated area		
-7143777.0	591619.3	104	Slanting well			333.8		
-7143855.3	591621.6	106	Slanting well			Located in excavated area		
-7143666.0	591464.7	108	Slanting well			324.2		

CS - Casing Stick-up length
WHE - Well Head Elevation
GE - Ground Elevation
BE - Bedrock Elevation
WBE - Well Bottom Elevation

Note: All the monitoring wells (MWs) are open wells with casing extended up to 1 m into the bedrock. The diameters of the MWs are 144 mm with the exception of the slanting wells with approximately 80 mm outside diameter.

Table B.2 Measured depth to free product in the monitoring wells across the site. (All measurements are in meters).

Well #	7/23/00	6/17/05	6/23/05	7/7/05	7/8/05	7/9/05	7/15/05	7/16/05	7/21/05	7/22/05	7/23/05	8/4/05	8/11/05	8/17/05	8/28/05	9/12/05	12/12/05	6/15/06	7/6/06	8/6/06	12/14/06	5/15/07	6/12/07	7/6/07	9/13/07	
1																										
2																										
3	3.27																									
4	3.44													3.58						3.60		8.87		9.04		
5	4.69																			5.90						
6	3.10													3.84	3.94	3.76				4.17					5.78	
7	2.03																									
8	3.29	3.17	3.47	3.52	3.52	3.50	3.53	3.52	3.61	3.62	3.60	3.52	3.68	3.70	3.78	3.70			3.48	3.78						
9	2.41	2.07	2.15	2.71	2.67		2.71	2.67	2.91	2.87	2.89	2.91	4.03	4.03	4.45	2.53	5.80	6.69	2.53	4.45	6.91	7.28		7.40	5.08	
10	2.90				2.68										2.29	1.80			2.79							
11	6.10																		0.00		7.77	7.92	8.66	7.95	7.10	
12	4.63	2.21	2.60	3.49	3.50	3.50	3.51	3.50	4.76	4.72	4.75	4.68	5.17	5.31	5.39	4.86	7.88	8.58	3.30	5.80	8.96	9.55	2.69	9.64	7.74	
13																			3.03							
14	2.66	2.07	2.40	2.57	2.45	2.44	2.48	2.45	2.75	2.77	2.73	2.66	2.88	2.90	2.83		5.85	7.08	2.39	2.53	6.87	6.47	2.26	6.98		
15			3.06	3.21	3.20	3.19	3.23	3.20	3.21	3.20	3.21	3.19	3.23	3.23	3.25	3.10	2.66	3.33	3.09	3.15	3.27	2.69		3.37	2.77	
16	7.16													5.58	4.57	3.93	4.45	5.46	0.00						5.34	
17	4.45	7.77	7.73	7.72	7.85	7.85	7.81	7.85	5.58	5.54	5.47	5.52	5.43	5.44	5.36	4.94	4.12	4.94	5.16	5.24	6.87	6.81	5.31	6.89	5.40	
18														1.41												
19	2.28	1.70	1.89	2.12	2.14	2.14	2.16	2.14	2.24	2.22	2.25	2.22	2.42	2.47	2.52	2.11	5.98	6.83	2.02	2.17	6.02	3.27	1.90	7.12		
20	3.45																								3.14	
21														2.95	2.99	2.98	2.65				2.77	5.27	5.55		3.19	
22	3.37															3.34	5.16	5.66				4.45	2.96	7.04	4.42	
23		1.28	1.68						2.05	2.03	1.98	2.05	2.07	2.07	2.10	1.90							3.96	3.07	3.98	2.36
24		1.27																								
25																										
26	6.41	3.35	4.11	4.57	4.57	4.58	4.59	4.57	5.00	5.01	4.98	4.95	4.57	9.63	9.72	9.43	8.75	9.62	8.89	9.02	10.09	9.35	9.43	10.31	9.58	
27			21.41						21.40	21.45	21.52	21.68	21.39		21.43	21.39	20.66	21.38	21.37	21.00	21.35	21.35	21.35		21.42	
28	19.38	4.87	4.84		4.86	4.88	4.89	4.86					4.86	4.86	4.85	4.85	4.29	4.86	4.86	4.86	4.87					
29	2.52		3.20											3.36	3.36	3.40	3.24	3.09	3.50							
30		1.39	1.35	1.38	1.38	1.35	1.42	1.38	1.38	1.40	1.28	1.38	1.49	1.50	1.53	1.44	1.11	1.56	1.34	1.39		1.21		1.52		
31																										
32	3.38																									
33																				3.42						
P1																										
P2																										
P3																										
P4													2.51			2.52										
P5														2.87	2.90		2.34	3.17								
P6													2.86													

Well #	12/14/06	5/15/07	6/12/07	7/6/07	9/13/07
34		4.27		1.11	2.94
35		8.23	8.18	6.03	3.69
36		5.57	4.06	1.92	3.22
37		0.98	1.03		2.92
38		1.08	1.27		2.75
39		1.27	1.54		2.58
40		3.8	3.4		4.12
41		1.03	1.31		3
42		4.76			
43		8.74	8.69		8.08
44		11	10.9		11.2
45		6.43			4.31
46		8.57	8.56		8.1
47		6.45	6.9		7.87
48		3.54	3.53		3.54
49		3.21			3.32
50		1.83			2.74
51		7.85			3.74
102					
103			2.14		6.54
104			4.27		7.45
106					2.02
108					

Omitted values were either not measured or have no LNAPL at the time of measurement

Table B.3 Measured depth to water in the monitoring wells across the site.
(All measurements are in meters).

Well #	7/23/00	6/7/05	6/23/05	7/7/05	7/8/05	7/9/05	7/15/05	7/16/05	7/21/05	7/22/05	7/23/05	8/4/05	8/11/05	8/17/05	8/28/05	9/12/05	12/12/05	6/15/06	7/6/06	8/6/06	12/14/06	5/15/07	6/12/07	7/8/07	9/13/07	
1	3.63			3.19	3.19	3.22	3.22	3.19	3.21	3.17	3.21	3.15	3.38	3.47	3.60		5.08			3.31			1.60	1.32	4.71	
2	4.84	2.55	2.69	2.43	2.43	2.45	2.45	2.43	2.93	2.91	2.95	2.86	2.87	3.14	5.13					1.35					5.50	
3	4.00																									
4	3.63	0.91	0.99	1.55	1.55	1.55	1.57	1.55	2.25	2.20	2.27	2.23	3.31	3.58	3.49	2.78		2.10		3.63		8.97	1.79		5.61	
5	4.92																			6.02		1.82				
6	3.82			2.96					3.29	3.26	3.29	3.16	3.71	3.85	3.95	3.78	5.29	2.88	3.58	4.18	7.52	7.70	2.84		5.82	
7	2.04																									
8	3.29	3.18	3.49	3.55	3.55	3.55	3.56	3.55	3.64	3.64	3.63	3.53	3.71	3.74	3.79	3.76		3.18	3.50	3.80	6.87	6.83	2.51		5.30	
9	2.92	2.13	2.26	2.78	2.73		2.74	2.73	2.94	2.91	2.92	2.93	4.19	4.20	4.59	2.67	7.36	3.12	2.68	4.62	6.93	7.60	6.96		5.11	
10	3.02	0.46	1.77	1.92	1.94	2.73	1.96	1.94	2.07	2.04	2.05	2.02	2.16	2.21	2.30	1.83			2.80	2.90			2.75		2.75	
11	21.46																				7.96	8.92			7.16	
12	6.52	2.26	2.64	3.55	3.55	3.54	3.55	3.55	4.83	4.79	7.81	4.71	5.23	5.38	5.47	4.93	13.59	3.15	3.31	5.82	11.05	9.77	2.72		7.74	
13	3.20			3.27	3.05	3.03		3.05	3.14	3.14	3.15	3.14	3.29	3.31	3.34	3.05			3.04	3.14	7.38	1.16	1.75		3.76	
14	2.69	2.09	2.45	2.60	2.51	2.49	2.52	2.51	2.77	2.80	2.75	2.68	2.89	2.90	2.83	2.45	7.08	2.88	2.48	2.61	7.00	6.50	2.28	7.01	3.03	
15	2.90	3.06	3.08	3.27	3.25	3.22	3.25	3.25	3.24	3.23	3.24	3.21	3.37	3.34	3.35	3.20	3.42	3.21	3.17	3.22	3.33	2.73	3.20		2.78	
16														5.59	4.57	3.93	5.48			4.50		7.36			5.35	
17	7.41								5.84	5.67	5.56	5.55	5.71	5.60	5.44	5.08	5.08		5.21	5.28	8.27	6.85	5.49	7.95	5.40	
18	2.26	0.88	1.10	1.27	1.31	1.31	1.33	1.31	1.32	1.32	1.30	1.29	1.37	1.38	1.41	1.28		1.24							1.52	
19	2.37	1.78	1.98	2.18	2.19	2.17	2.18	2.19	2.30	2.29	2.31	2.25	2.50	2.54	2.55	2.14	6.86	2.26	2.23	2.38	6.08	3.48	1.97	7.20	2.78	
20	3.46	1.16	1.37	1.42	1.42	1.42	1.44	1.42	1.45	1.45	1.43	1.41	3.18	3.42	4.23	3.30	2.14		2.44	2.19		2.75	1.50		3.14	
21	2.94								2.99	2.95	3.01	2.91	2.97	3.21	3.00	2.70				2.80		5.60			3.20	
22	3.58	2.92	3.03	3.06	3.07	3.10	3.09	3.07	4.45	4.42	4.45	4.39	3.46	3.53	3.57	3.34	5.67		3.15	3.49	6.18	4.53	3.00	7.43	4.43	
23	2.10	1.29	1.76						2.09	2.06	2.02	2.09	2.11	2.12	2.11	1.94					2.03				2.36	
24	1.01	1.34	1.46	1.59	1.59	1.61	1.59	1.59	1.59	1.55	1.55	1.55	1.92	2.12	1.44	1.23			1.19	1.23		1.41	1.36		1.36	
25																									2.14	
26	9.21	3.53	4.26	4.60	4.59	4.61	4.60	4.59	5.07	5.07	5.01	4.99	4.59	10.34	10.13	9.68	13.30	11.26	9.15	9.27	10.30	10.66	10.63	11.47	10.30	
27				21.40	21.39	21.41	21.41	21.39																		
28				4.87					4.89	4.86	4.86	4.87											4.87			
29	2.64	3.21	3.23	3.30	3.30	3.31	3.33	3.30	3.31	3.30	3.21	3.29	3.40	3.40	3.41	3.28	3.54	3.21	3.21	3.28		3.54				
30	1.44	0.42	1.38	1.43	1.40	1.39	1.44	1.40	1.40	1.41	1.30	1.40	1.74	1.57	1.59	1.51			1.38	1.52	1.54	1.21	1.47		1.40	
31																							1.81			
32	4.36																									
33													3.19		3.44	3.44	3.44			3.46		5.08			4.66	
P1	1.77		1.52	1.53	1.40	1.40	1.41	1.40	1.58	1.54	1.53	1.54	1.63	1.69	1.77	1.57	2.60	1.54		1.63		4.68			2.00	
P2	2.90		1.92	1.88	1.81	1.81	1.79	1.81	2.31	2.28	2.24	2.29	2.68		2.95	2.83	3.99	2.16		2.89		5.11	2.37		3.30	
P3	2.06	3.49	1.40	2.21	2.32	2.32	2.33	2.32	1.94	1.94	1.92	1.91	1.98	2.03	2.09	2.00	3.61	3.38		2.07		4.95	3.85		2.62	
P4	2.72		4.96	2.45	2.58	2.61	2.60	2.58	2.43	2.41	2.41	2.37	2.51		2.66	2.52	4.17	3.15		2.55		5.06			3.04	
P5	2.57			2.54	2.53	2.55	2.54	2.53	2.27	2.26	2.22	2.22	2.87	2.87	2.91	2.69	3.17	2.63				3.62			2.98	
P6	1.80		1.65	1.70	1.71	1.71	1.73	1.71	1.77	1.75	1.75	1.69	1.87													

Well #	12/14/06	5/15/07	6/12/07	7/8/07	9/13/07
34		4.27		1.11	2.94
35		8.23	8.18	6.03	3.69
36		5.57	4.06	1.92	3.22
37		0.98	1.03		2.92
38		1.08	1.27		2.75
39		1.27	1.54		2.58
40		3.8	3.4		4.12
41		1.03	1.31		3
42		4.76			
43		8.74	8.69		8.08
44		11	10.9		11.2
45		6.43			4.31
46		8.57	8.56		8.1
47		6.45	6.9		7.87
48		3.54	3.53		3.54
49		3.21			3.32
50		1.83			2.74
51		7.85			3.74
102					
103			2.14		6.54
104			4.27		7.45
106					2.02
108					

Omitted values were either not measured or have no water at the time of measurement

Table B.4 Measured depth to monitoring wells bottom across the site. (All measurements are in meters).

Well #	712300	6/17/05	6/23/05	7/7/05	7/8/05	7/9/05	7/15/05	7/16/05	7/21/05	7/22/05	7/23/05	8/4/05	8/11/05	8/17/05	8/28/05	9/12/05	12/12/05	6/15/06	7/6/06	8/8/06	12/14/06	5/15/07	6/12/07	7/6/07	9/13/07	
1	3.63	5.92	2.56	5.13	5.14	5.17	5.13	5.14	5.18	5.17	5.20	5.13	7.45	8.08	9.06		11.11			10.00			10.62		12.71	
2	4.84	3.33	3.42	5.34	5.34	5.35	5.33	5.34	6.39	6.40	6.39	6.34	5.34	5.34	7.27					7.52		1.60	2.96	1.58	12.10	
3	4.00																									
4	3.63	3.78	4.13	4.78	4.78	4.78	4.76	4.78	6.10	6.08	6.11	6.01	7.71	8.21	8.92	9.60		5.55		11.41		8.97	4.70	9.08	15.66	
5	4.92																			7.23						
6	3.82	0.29	0.27	3.80	0.29	0.29	0.29	0.29	4.80	4.82	4.82	4.68	6.20	6.47	6.64	6.88	8.22	3.30	6.92	8.37	13.80	7.70	4.42	7.71	11.36	
7	2.04																									
8	3.29	3.06	3.90	3.89	3.89	3.92	3.91	3.89	4.44	4.44	4.45	4.39	5.65	6.25	6.55	7.08		3.87	6.36	8.36	13.03	6.83	4.83		11.76	
9	2.92	1.55	2.67	3.78	4.04		4.05	4.04	4.96	4.99	4.94	4.84	7.21	8.12	9.01	10.31	20.64	3.54	8.65	21.16	22.12		7.59	7.56	14.86	
10	3.02	2.32	2.56	2.98	3.16	4.70	3.18	3.16	4.41	4.45	4.39	4.38	5.99	6.36	6.86	7.74			6.50	8.10			3.03		3.03	
11	21.46	5.99	6.03	5.98	5.87	5.89	0.00	5.87	5.98	5.71	2.99	5.96	5.98	6.16	6.13	6.00		5.69	6.42	6.40	9.70	8.92	9.38	8.91	9.00	
12	6.52	2.86	3.66	4.76	4.75	4.74	4.76	4.75	6.00	6.01	8.02	5.93	8.13	8.94	9.81	10.82	19.44	3.84	8.52	11.06	20.27	9.77	3.53	10.62	20.82	
13	3.20	2.66	2.44	2.80	2.97	2.98	2.98	2.97	4.24	5.96	4.23	4.10	5.56	5.94	6.53	7.11		2.91	6.96	7.90	11.20		3.10	6.98	9.74	
14	2.69	6.64	19.49	20.41					17.55	3.80	14.53	15.44	20.13	20.15	20.37	20.17	20.10	21.17	21.99	21.28	22.40	6.50	22.20	21.33	22.05	
15	2.90	5.31	5.94	8.35	8.30	8.23	8.31	8.30	8.32	8.34	8.35	8.16	8.32	8.36	8.82	8.33	8.30	8.33	8.88	8.95	9.35		4.53	3.38	9.21	
16	-	4.73	4.74	4.74	4.74	4.72	4.77	4.74	4.75	4.78	4.62	4.62	4.70	4.80	4.79	5.16	7.43		4.76	5.25		7.36	7.39	7.37	8.76	
17	7.41	7.37	7.42	7.10	7.52	7.51	7.42	7.52	8.04	8.07	7.83	7.92	20.71		16.00	20.68	20.68	5.03	21.10	21.45	19.00		7.67	18.24	18.80	
18	2.26	2.14	2.65	2.87	4.34	4.34	4.37	4.34	4.97	4.95	4.78	4.95	6.22	6.28	6.78	7.34		2.30							9.16	
19	2.37	20.19	20.79		20.97	21.03	21.08	20.97				20.57	20.65	20.11	20.65	20.65	20.51	1.68	22.29	21.38	22.17		22.20	21.38	22.40	
20	3.46	2.33	2.57	2.59	2.60	2.62	2.62	2.60	2.62	2.64	2.59	2.56	7.31	7.43	7.40	7.32	7.30		7.91	7.97		2.75	2.45		9.14	
21	2.94	2.72	2.80	2.84	2.83	2.67	2.83	2.83	2.66	2.83	2.75	2.77	2.82	2.86	2.84	2.90		2.38		3.60			5.60	5.72	5.97	
22	3.58	8.45	9.02	10.95	11.28	11.31	11.33	11.28					21.00	20.92	18.90	21.00	20.98	1.02	22.24	21.45	22.20		22.60	21.47	22.30	
23	2.10	1.40	1.40	1.22	1.19	1.23	1.22	1.19	3.13	3.16	3.12	3.01	4.15	4.46	4.87	5.09		1.27		5.49	5.76	4.09	3.17	4.07	6.68	
24	1.01	0.67	0.94	1.05	1.05	1.08	1.05	1.05	1.05	1.07	1.10	0.97	1.29	1.28	1.44	7.29			7.95	8.21		1.41	2.06	1.43	2.06	
25	-	1.25	1.30	1.29	1.31	1.34	1.34	1.34	1.31	1.32	1.34	1.32	1.24	1.29	1.33	1.31	1.28		1.37	2.12	2.30		2.14	2.12	2.30	
26	9.21	9.06	7.21	6.68	6.58	6.60	6.60	6.58	7.59	7.61	7.55	7.51	6.58	11.86	21.09	20.63	20.61	21.44	21.64	21.46	22.13		21.06	21.47	22.00	
27	-	20.21											20.78	19.49	21.27	20.68	20.74		22.13	2.14	22.00		22.05		22.22	
28	-	4.34	4.40	4.39	4.36	4.36	4.36	4.36	4.39	4.38	4.38	4.39	4.40	4.48	4.41	4.37		4.36	4.90	4.89	4.87	4.87	4.86	10.81	4.82	
29	2.64	3.79	4.42	8.97	8.97	9.00	9.02	8.97	9.00	8.97	8.90	9.26	8.94	9.12	9.08	8.95	8.93	8.97	9.49	9.33		3.54	3.58	3.51	3.58	
30	1.44	4.73	5.94	8.53	8.53	8.56	8.56	8.53	8.57	8.60	8.52	8.61	8.49	8.63	8.69	8.52		8.50	8.63	8.90			4.97	1.58	9.26	
31	-	1.22	1.20	1.19	1.19	1.20	1.22	1.19	1.22	1.24	1.19	1.16	0.58	4.24	1.23	1.21		1.24		1.80		1.81	1.85		1.83	
32	4.36																									1.59
33	-	2.78	2.79	2.73	2.77	2.78	2.77	2.77	2.68	2.90	2.88	2.78	3.08	3.27	3.40	3.40	3.40	3.31	3.47	3.72		5.08	5.10		5.23	
P1	1.77	3.09	3.33	5.31	5.57	5.56	5.59	5.57	6.95	6.96	6.98	6.91	9.35	9.16	14.85	14.56	14.54	3.74		15.43		4.68	4.67		15.43	
P2	2.90	3.54	1.85	5.70	5.99	5.81	6.01	5.99	6.23	2.32	2.30	6.51	8.24		9.33	11.15	14.15	5.01		15.12		5.11	5.09	5.11	15.60	
P3	2.06	3.68	0.39	3.08	3.02	3.04	3.03	3.02	4.03	4.03	3.99	3.99	5.77	6.04	6.62	7.60	12.81	2.73		8.66		4.95	5.06	4.95	14.12	
P4	2.72	4.48	4.48	3.35	3.69	3.69	3.69	3.69	4.41	4.43	4.33	4.37	6.12		6.60	7.45	9.62	2.77		8.21		5.06	5.06	5.09	10.02	
P5	2.57	2.60	2.57	2.75	2.96	2.98	2.96	2.96	2.41	2.42	2.35	2.38	7.76	8.08	7.93	7.92	7.92	2.57		8.73		3.62	3.61		9.00	
P6	1.80	8.29	7.36	7.38	7.33	7.33	7.33	7.33	7.31	7.28	7.26	7.27	7.50													

Well #	12/14/06	5/15/07	6/12/07	7/6/07	9/13/07
34			4.31	3.13	9
35			8.84		11
36			6.25		11.6
37			2.4		7.14
38			3.47		9.35
39			22		22.8
40			24.1	24.1	24.9
41			23.2	3.15	22.4
42		4.76	6.79		7.97
43		8.74	9		21.3
44			23.2		23.7
45		6.43	4.43		4.44
46		8.57	8.65		10.6
47			10.6		11.1
48		3.54	3.53		4.16
49		3.21	3.2		4.67
50					9.8
51					16.2
102			6.47		6.47
103			6.79		14
104			5.9		20.1
106			1.48		10
108			2.01		2.01

Omitted values were not measured. Some of the monitoring wells (MWs) had measurable LNAPL but no water.

Table B.5 Measured apparent free product thickness in the monitoring wells at the site. (All measurements are in centimeters).

Well#	7/23/00	6/17/05	6/23/05	7/7/05	7/8/05	7/9/05	7/15/05	7/18/05	7/21/05	7/22/05	7/23/05	8/4/05	8/11/05	8/17/05	8/28/05	9/12/05	12/12/05	6/15/06	7/6/06	8/6/06	12/14/06	5/15/07	6/12/07	7/6/07	9/13/07	
1														0.0												
2														0.0												
3	73.0																									
4	19.0													0.1				16.0		3.0		9.8		4.0		
5	23.0																			12.0						
6	72.0													1.8	1.1	2.2				0.5					4.0	
7	1.0																									
8	0.0		2.0	3.0	3.0	5.0	3.0	3.0	3.0	2.0	3.0	1.0	3.0	3.2	1.5	6.3		2.0	2.0	2.0						
9	51.0	6.0	11.0	7.0	6.0		3.0	6.0	3.0	4.0	3.0	2.0	16.0	16.5	13.7	14.0	67.0	76.5	15.0	17.0	2.0	31.9		16.0	2.3	
10	12.0					5.0									0.3	3.0				1.0						
11	1536.0																				19.0	100.1	72.0	96.0	5.5	
12	189.0	5.0	4.0	6.0	5.0	4.0	4.0	5.0	7.0	7.0	6.0	3.0	6.4	6.5	8.2	7.5	501.0	215	1.0	2.0	209.0	22.3	2.5	98.0	0.3	
13																				1.0						
14	3.0	2.0	5.0	3.0	6.0	5.0	4.0	6.0	2.0	3.0	2.0	2.0	10	0.1	0.1		0.5	51.0	9.0	8.0	13.0	3.0	2.0	3.0		
15			2.0	6.0	5.0	3.0	2.0	5.0	3.0	3.0	3.0	2.0	14.0	11.5	9.6	9.4	9.0	6.6	8.0	6.5	6.0	4.0		1.0	0.7	
16														0.5	0.1	0.5	1.5								0.5	
17	296.0	42.0	51.0	20.0	49.0	48.0	43.0	49.0	26.0	13.0	9.0	3.0	28.0	16.0	8.0	13.8	13.8	47.0	5.0	4.5	140.0	4.0	18.0	105.5	0.2	
18															0.2				0.2							
19	9.0	8.0	9.0	6.0	5.0	3.0	2.0	5.0	6.0	7.0	6.0	3.0	7.5	6.6	2.7	2.9	3.0	28.6	21.0	20.5	6.0	20.5	7.0	8.0		
20	1.0																							0.0	0.5	
21														2.2	22.2	2.7	5.2			3.5		32.7	17.0		1.3	
22	21.0																0.2	0.5				8.7	4.0	39.0	1.0	
23		1.0	8.0						4.0	3.0	4.0	4.0	4.5	5.0	0.9	3.7						12.4	10.0	9.0	0.2	
24		7.0																								
25																										
26	280.0	18.0	15.0	3.0	2.0	3.0	1.0	2.0	7.0	6.0	3.0	4.0	48.5	71.2	40.5	25.0	368.0	231.9	26.0	25.0	21.0	131.0	120.0	116.5	74.0	
27													11.0		56.5	1.0	8.0				65.0	67.7	70.0		80.0	
28		4.0	13.0		7.0	5.0	4.0	7.0					11.0	18.6	12.7	9.0	8.0	5.9			0.5					
29	12.0		3.0										4.0	4.0	0.8	4.5	4.0									
30		3.0	3.0	5.0	2.0	4.0	2.0	2.0	2.0	1.0	2.0	2.0	8.0	7.2	6.5	6.8	3.0		18.0	15.5		0.1		6.0		
31																										
32	98.0																									
33																										
P1																										
P2																				0.2						
P3																				0.1						
P4													0.5			0.1				0.2						
P5													0.5		0.6		0.2	0.1								
P6																										

Well#	12/14/06	5/15/07	6/12/07	7/6/07	9/13/07
34					
35					
36					
37					
38					
39		0.5			
40			0.8		
41					
42					
43					127.0
44		11.1	10.0		11.0
45					
46					
47					
48					
49					
50					
51					
102				307.5	
103					
104					
106					
108					

Omitted values either had no LNAPL accumulation or not measured.

Table B.6 Corrected groundwater elevation in selected monitoring wells. (All measurements are in meters).

Well #	X	Y	6/17/05	6/23/05	7/9/05	7/16/05	8/4/05	8/17/05	9/12/05	12/12/05	6/15/06	7/6/06	8/6/06	12/14/06	6/12/07	7/6/07	9/13/07
1	-7143756.9	591599.4			328.0	328.0	328.0	327.7		326.1	331.2	331.2	327.9	331.2	331.2	331.2	326.5
2	-7143812.2	591600.6	327.0	326.8	327.1	327.1	326.6	326.4			329.5	329.5	328.2	329.5	328.2	329.5	324.0
4	-7143790.6	591540.9	325.9	325.9	325.3	325.3	324.6	323.3	324.1		324.9	326.8	323.2	326.8	325.1	326.9	321.2
6	-7143855.4	591512.8															320.1
8	-7143766.4	591483.7	322.0	321.7	321.7	321.7	321.7	321.5	321.5		322.1	321.7	321.4	318.3	322.7		319.9
9	-7143741.7	591495.7	323.2	323.1		322.6	322.4	321.2	322.7	318.5	322.9	322.7	320.8	318.4	318.3	325.4	320.2
10	-7143748.0	591535.8	325.6	324.3	323.4	324.1	324.0		324.2		326.0	323.3	323.1	326.0	323.3		323.3
11	-7143910.1	591516.0									325.8	325.8	325.8	318.0	326.4	326.6	318.7
12	-7143884.8	591553.6	325.3	324.9	324.0	324.0	322.9	322.2	322.7	318.4	324.6	324.2	321.7	318.3	324.9	328.4	319.8
13	-7143721.4	591548.5			323.4	323.4	323.3				326.4	323.4	323.3	319.0	324.7		322.6
14	-7143710.4	591520.6	323.5	323.2	323.1	323.1	322.9	322.7		318.5	323.2	323.2	323.0	318.7	323.3	318.6	322.6
15	-7143807.1	591468.5	317.9	317.9	317.8	317.8	317.8	317.8	317.9	317.7	317.9	317.8	317.7	317.8	321.0	321.0	318.2
16	-7143747.4	591464.7						319.4	321.0	319.5	324.9	324.9	320.5	324.9	324.9		319.6
17	-7143707.9	591478.0					319.8	319.8	320.3	320.3	325.7	320.1	320.1	318.3	320.0	318.3	319.9
18	-7143671.8	591550.4	323.8	323.6	323.4	323.4	323.4				323.4	324.7	324.7	324.7	324.7		323.2
19	-7143686.4	591513.5	323.7	323.5	323.3	323.3	323.2	322.9	323.3	318.6	323.4	323.4	323.2	319.4	323.5	318.3	322.6
20	-7143844.0	591479.9	320.1	319.9	319.8	319.8	319.8				321.2	318.8	319.0	321.2	319.7		318.1
21	-7143631.0	591504.0					322.8	322.7	323.1		325.7	325.7	323.0	325.7	325.9		322.6
22	-7143671.8	591468.5	322.2	322.1	322.0	322.0	320.7		321.7	319.4	325.1	321.9	321.6	318.9	322.1	318.0	320.7
23	-7143641.2	591532.7	323.9	323.5			323.1	323.1	323.3		325.2	325.2	323.2	325.2	325.3		
24	-7143766.4	591450.5	317.8	317.6	317.5	317.5	317.5				319.1	317.9	317.9	319.1	317.7		317.7
25	-7143737.2	591442.9									319.7	319.7	319.7	319.7	319.7		319.7
26	-7143908.8	591556.7	324.9	324.1	323.6	323.7	323.3	318.5	318.8	318.2	319.0	319.3	319.2	318.1	318.6	317.8	318.6
27	-7143958.4	591533.3									325.7	325.7	325.7	326.3	326.3		
28	-7143945.8	591530.1					320.7				325.6	325.6	325.6	325.6	325.6		
29	-7143823.6	591471.6	316.9	316.9	316.8	316.8	316.8	316.8	316.9	316.6	316.9	316.9	316.9	320.1	320.1		
30	-7143786.2	591461.3	318.8	317.9	317.9	317.9	317.9	317.7	317.8		317.9	317.9	317.8	319.2	317.8	319.3	317.8
31	-7143749.9	591447.4									319.2	319.2	319.2	319.2	319.2		
32	-7143885.4	591506.5									325.6	325.6	325.6	325.6	325.6		
33	-7143924.7	591521.9									325.2	325.2	321.8	325.2	325.2		
P1	-7143487.5	591426.5		321.4	321.5	321.5	321.4				321.4	322.9	321.3	322.9	322.9		320.9
P2	-7143509.0	591415.7		320.6	320.8	320.8	320.3				320.4	322.6	319.7	322.6	320.2		319.3
P3	-7143503.3	591394.0	318.9	321.0	320.1	320.1	320.5				319.0	322.4	320.3	322.4	318.5		319.8
P4	-7143528.0	591399.0		317.3	319.7	319.7	319.9		319.8		319.1	322.3	319.7	322.3	322.3		319.2
P5	-7143536.2	591376.9			318.1	318.1	318.4	317.8		317.5	318.0	320.7	317.8	320.7	320.7		317.7
34	-7143551.7	591417.0													323		320
35	-7143636.7	591458.1													317		321
36	-7143621.5	591476.1													321		322
37	-7143624.0	591528.9													325		323
38	-7143639.2	591586.1													325		323
39	-7143676.2	591497.0													323		322
40	-7143705.3	591507.1													322		321
41	-7143724.5	591513.5													323		322
42	-7143920.1	591580.4													330		
43	-7143919.5	591540.3													318		320
44	-7143937.2	591563.7													319		318
45	-7143977.9	591539.6													326		321
46	-7143983.0	591589.3													318		
47	-7143978.6	591612.1													320		
48	-7144051.6	591659.1													323		323
49	-7144064.5	591638.2													326		323
50	-7143566.8	591451.2													325		322
51	-7143545.9	591549.2													326		323

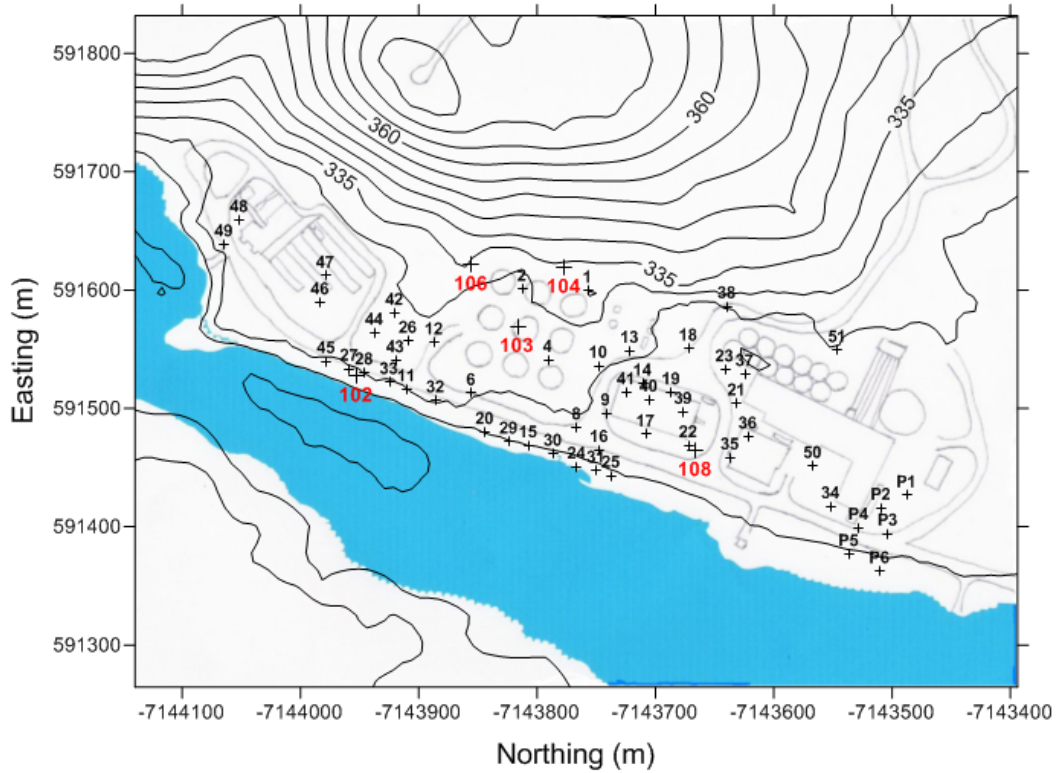


Figure B.3 Spatial location of the installed monitoring wells (MWs) at the site.

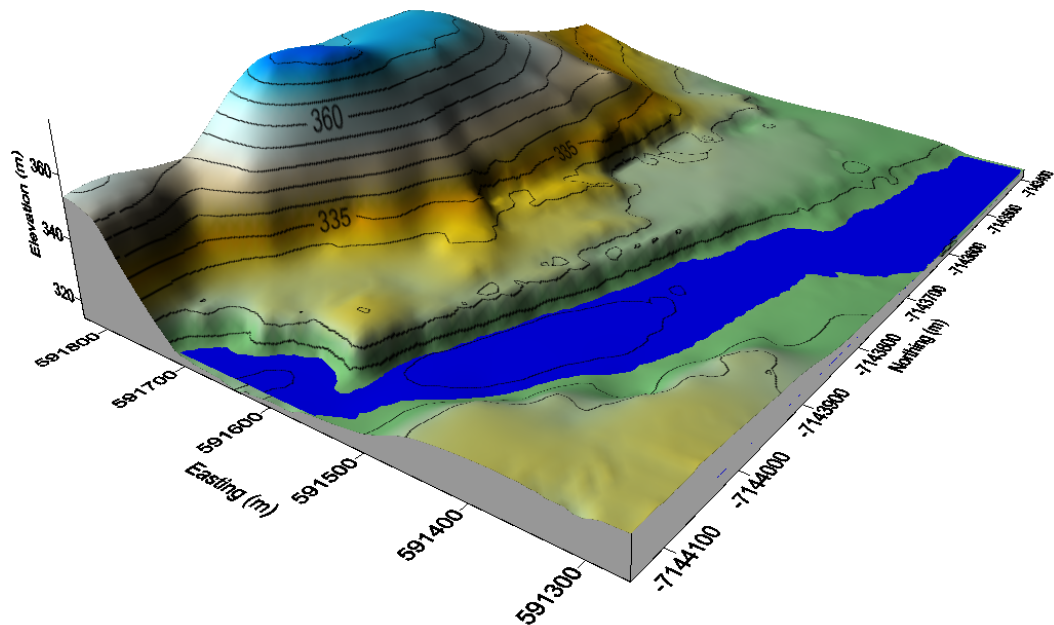


Figure B.4 Elevation contour of the site before the removal of overburden.

References

EBA Engineering Consultants Ltd., 2001. Hydrocarbon assessment, Lakefront and waste oil areas, Colomac Mine, NWT. Report to Deton 'Cho Corporation. Yellowknife, NT. 37 p. and appendices.

**APPENDIX C: UPDATED THERMISTOR PROFILE ACROSS THE
SITE**

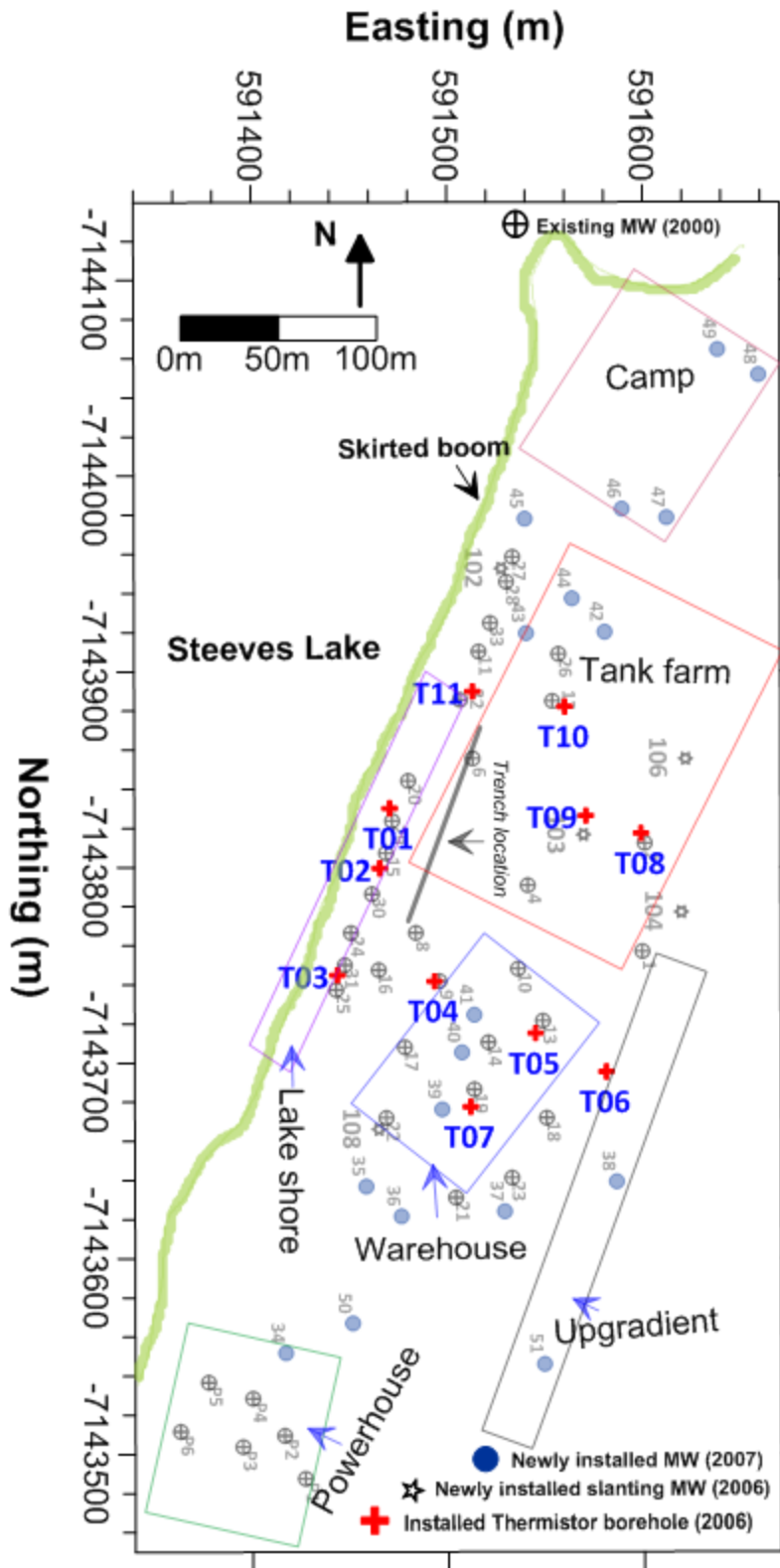


Figure C.1 Spatial locations of the installed thermistor boreholes. T06 malfunctioned and was decommissioned.

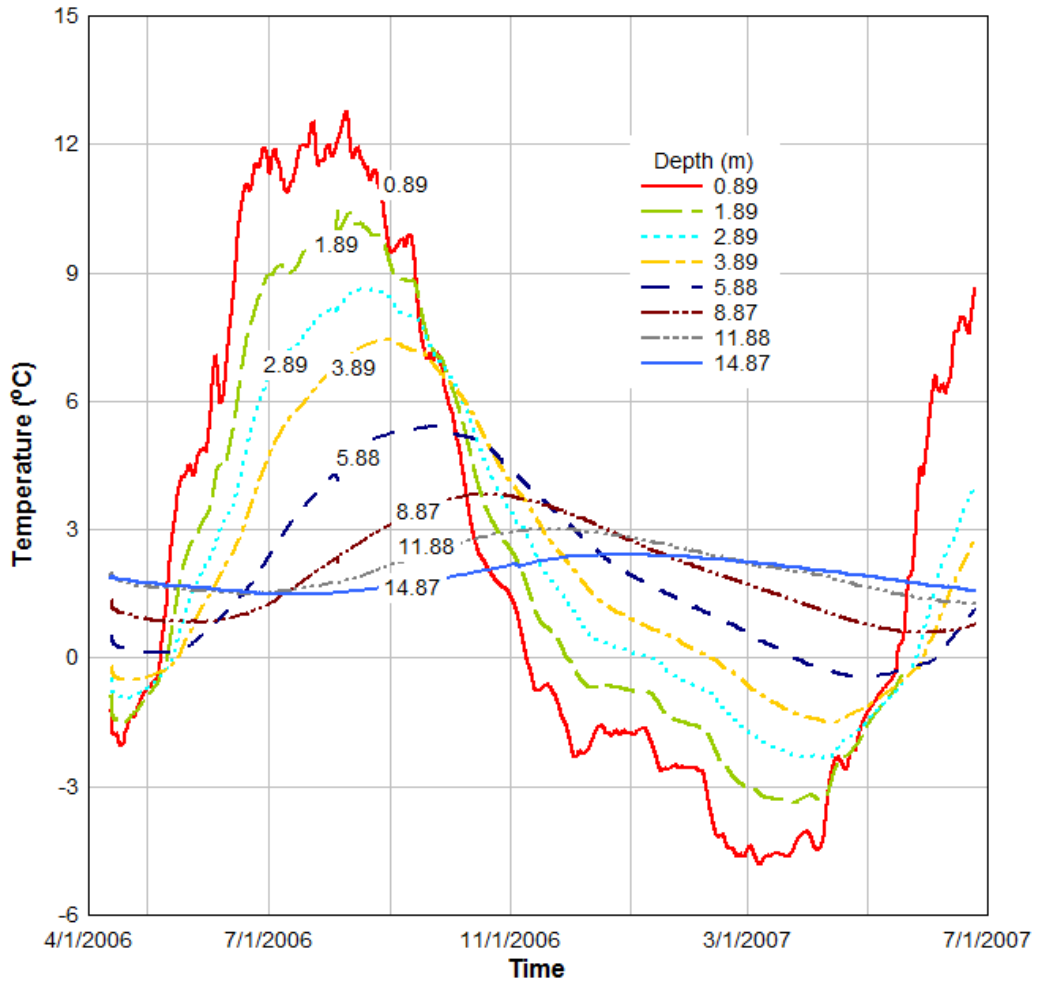


Figure C.2 Temperature profile for T01 near MW 29.

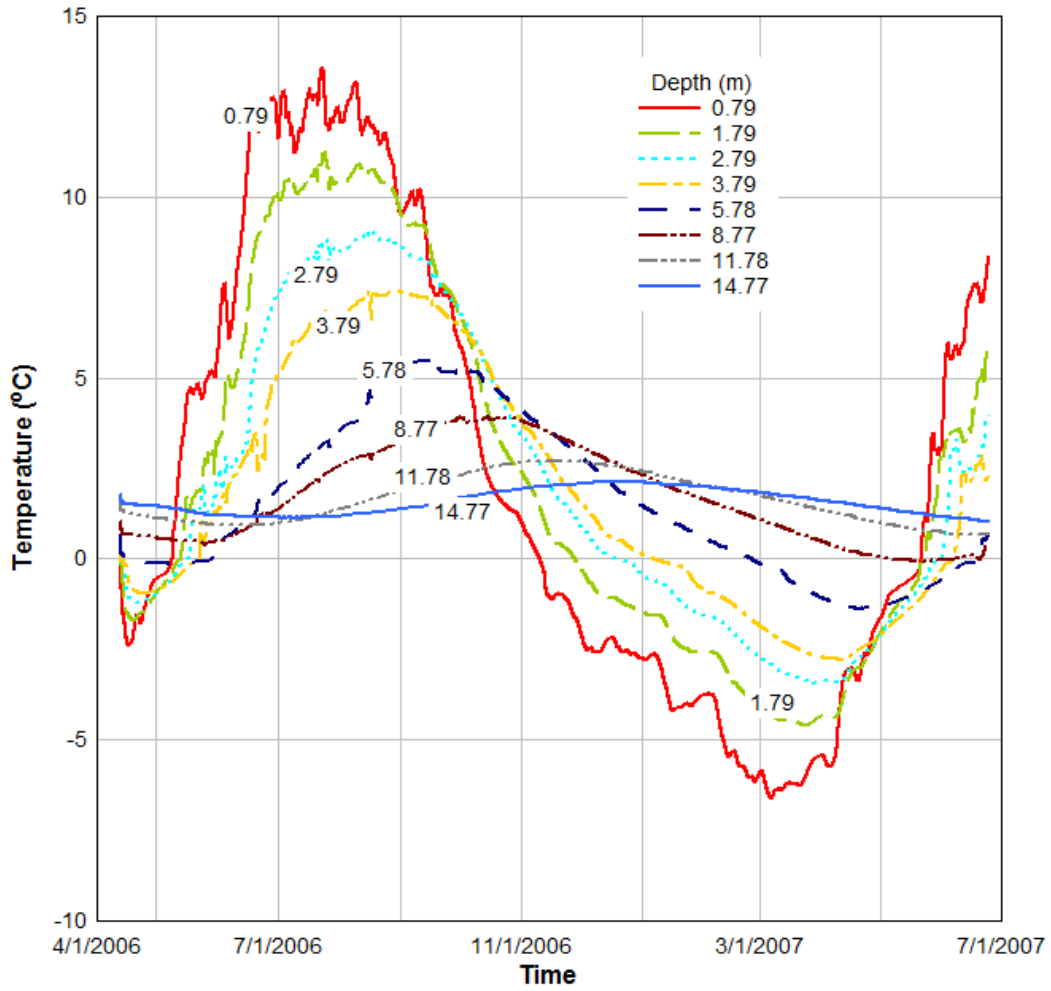


Figure C.3 Temperature profile for T02 near MW 15.

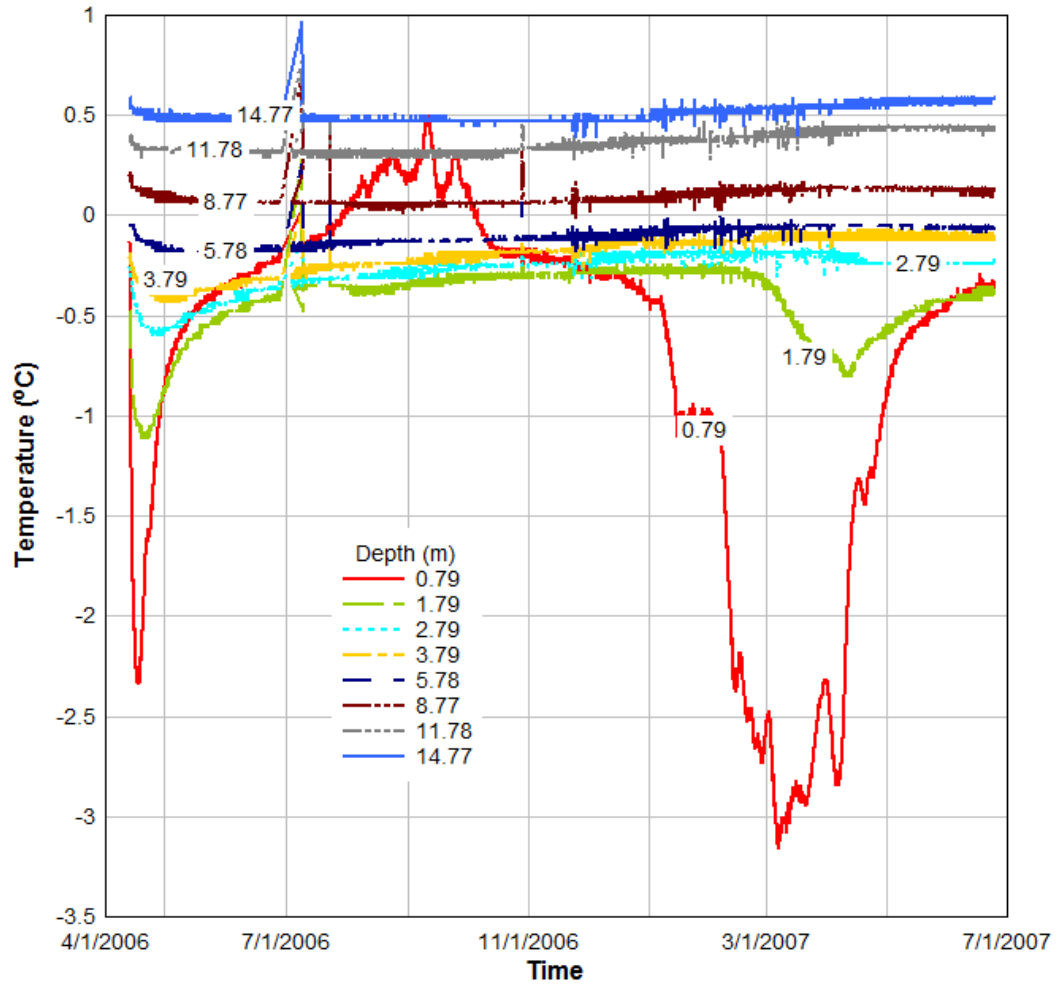


Figure C.4 Temperature profile for T03 near MW 31.

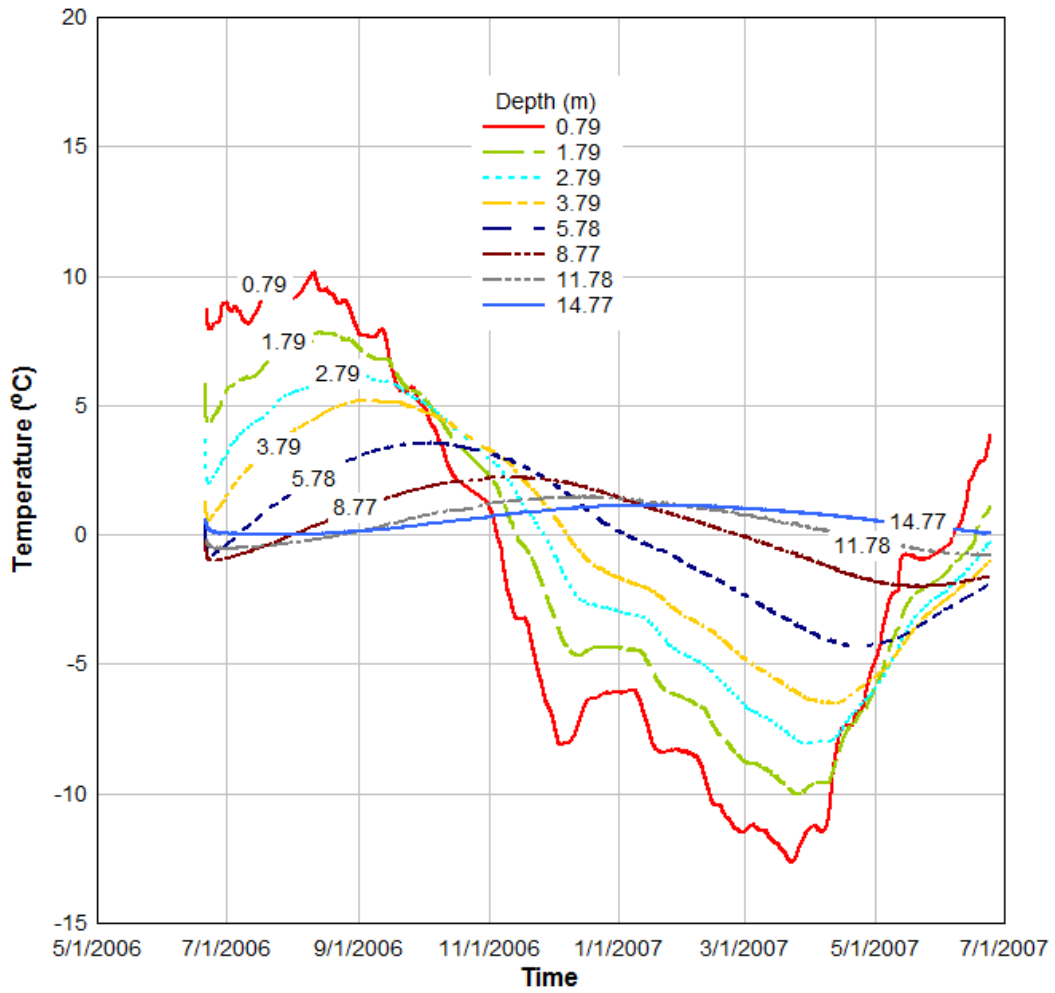


Figure C.5 Temperature profile for T04 near MW 09.

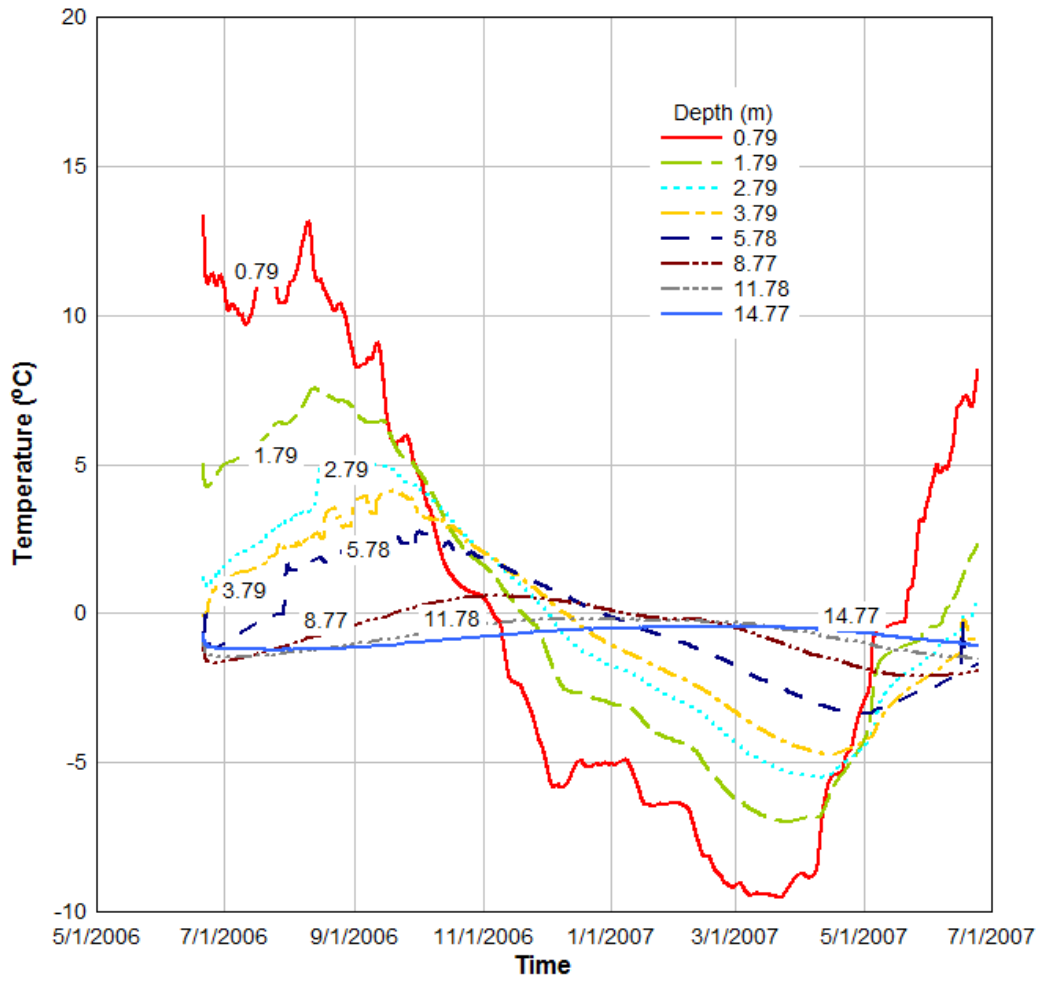


Figure C.6 Temperature profile for T05 near MW 13.

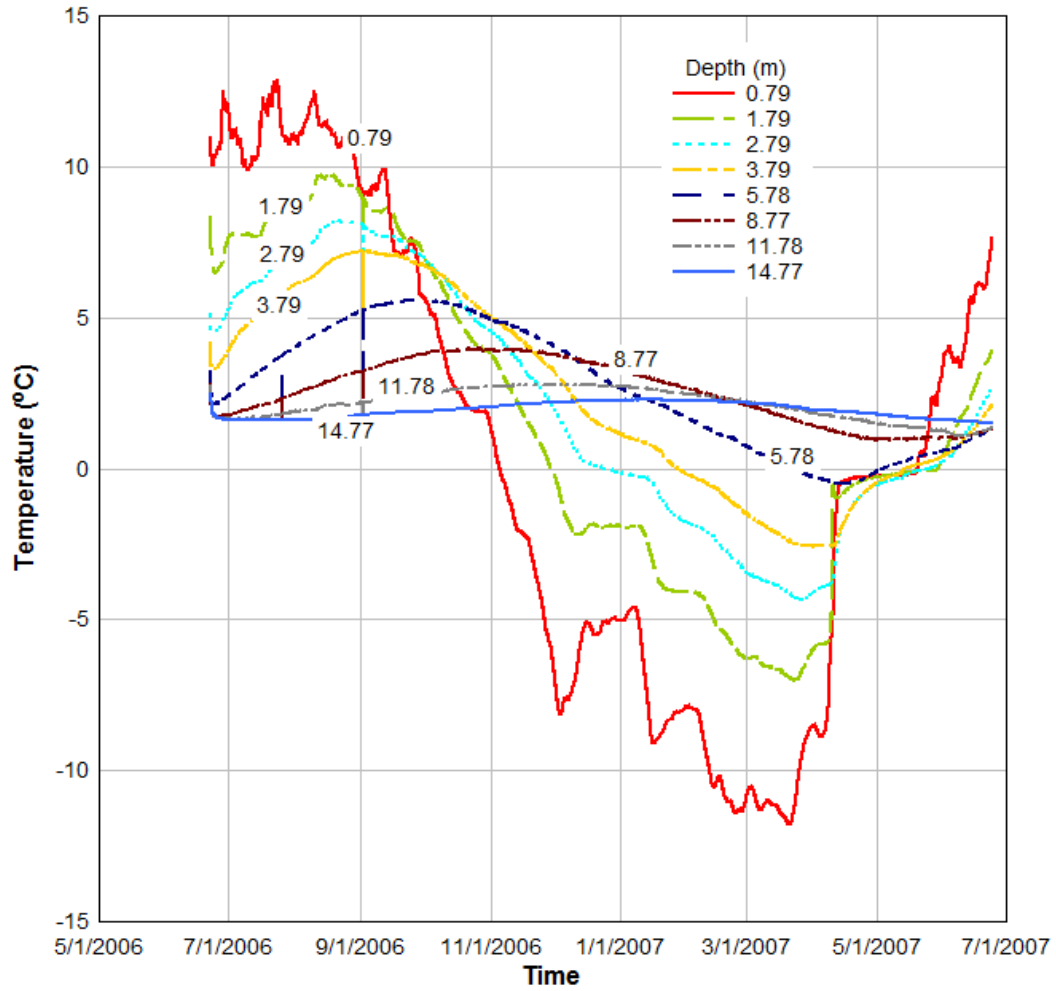


Figure C.7 Temperature profile for T07 near MW 19.

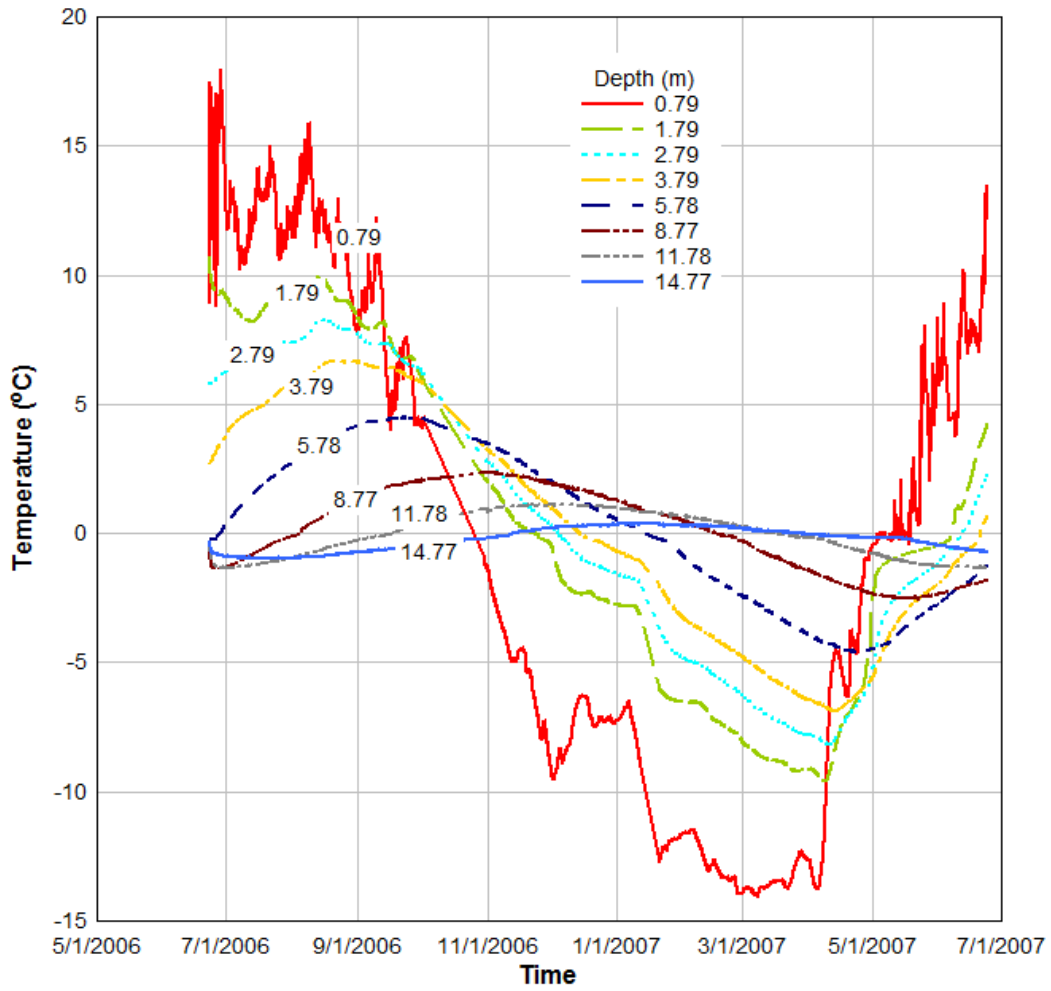


Figure C.8 Temperature profile for T08 near MW 02.

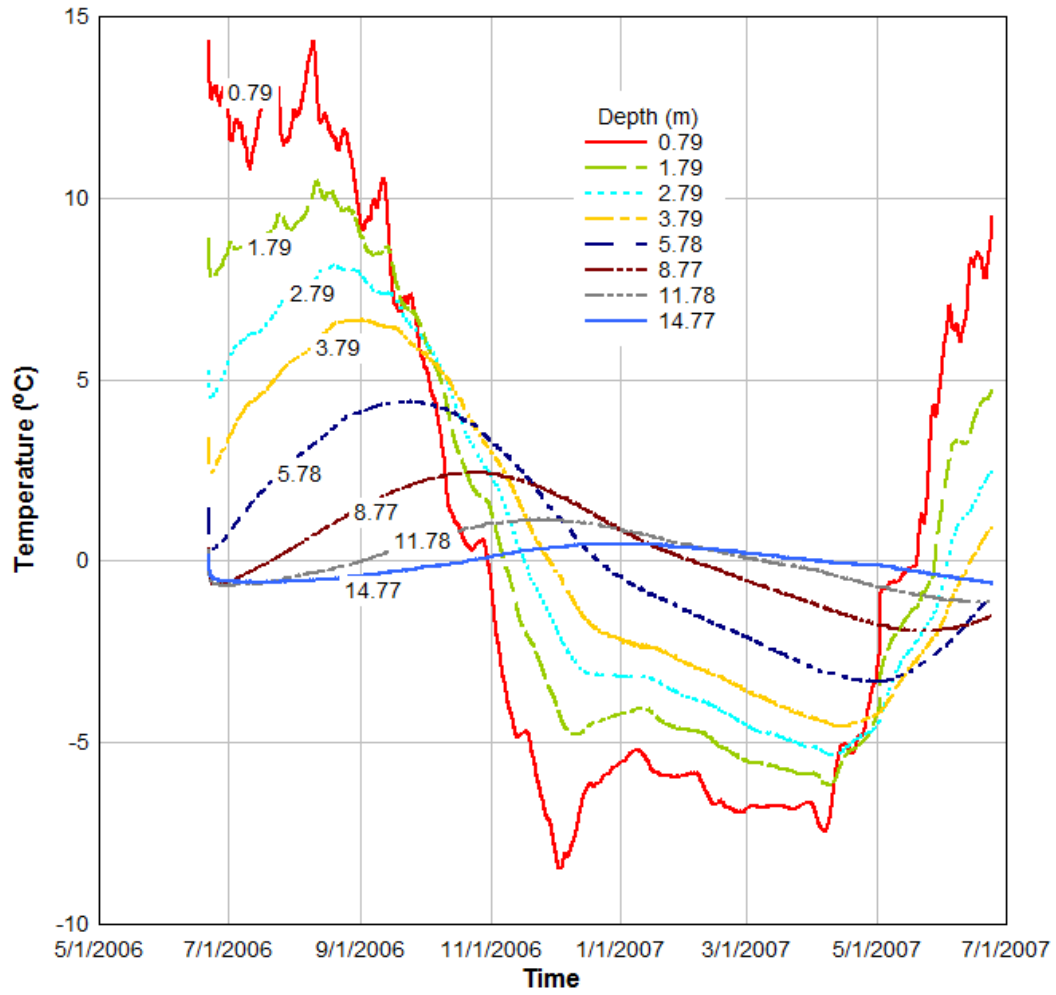


Figure C.9 Temperature profile for T09 near MW 103.

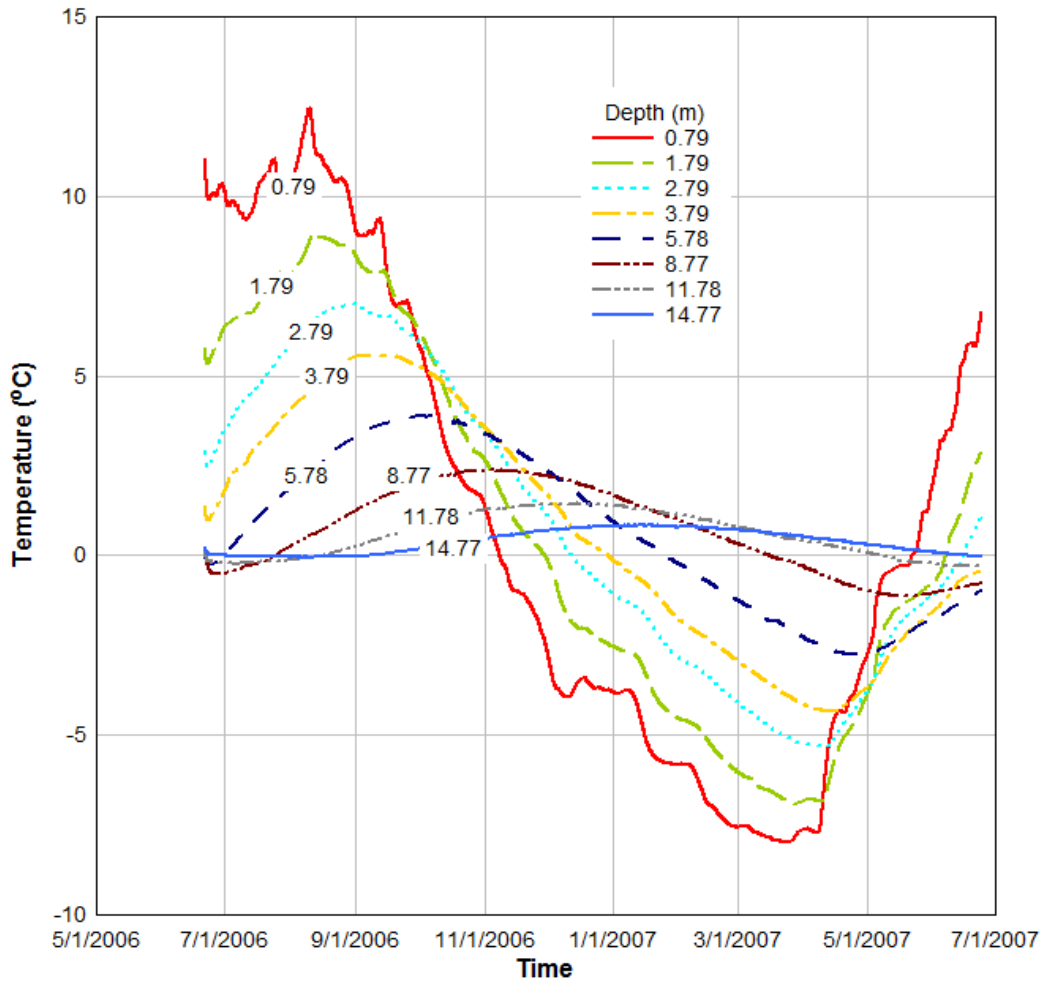


Figure C.10 Temperature profile for T10 near MW 12.

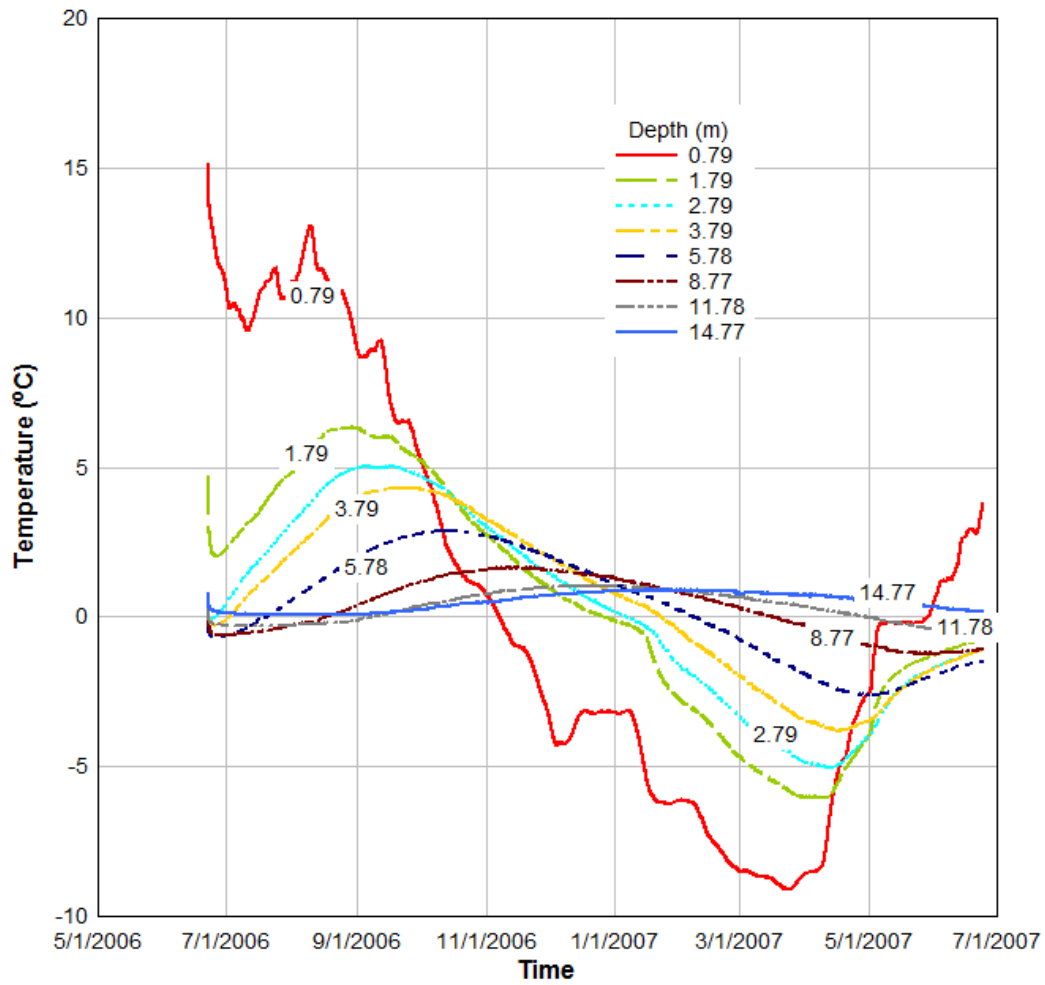


Figure C.11 Temperature profile for T11 near MW 32.

APPENDIX D: MEASURED GROUNDWATER CONSTITUENTS

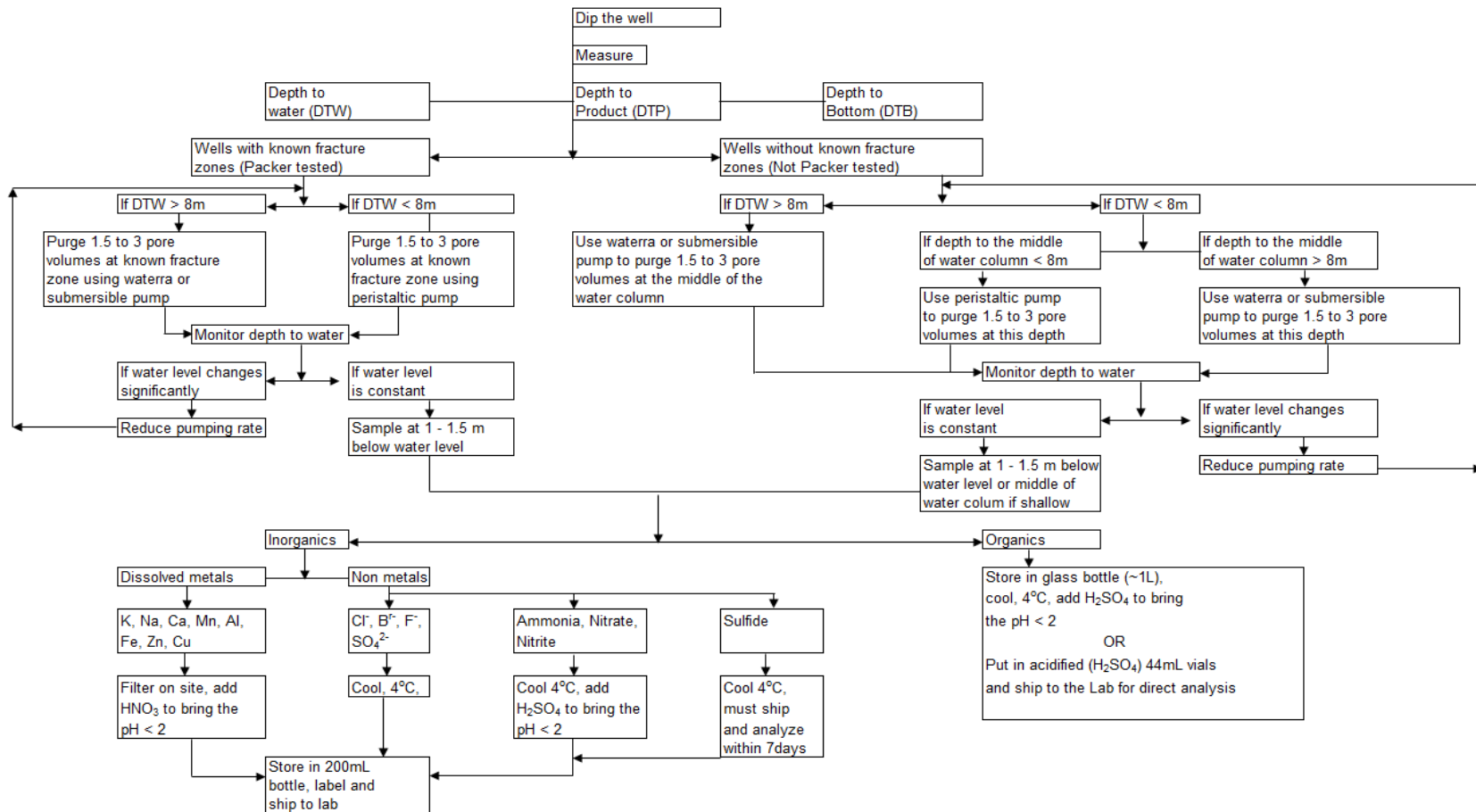


Figure D.1 Sampling procedure at the Colomac mine site.

Table D.2 Summary of parameters of BTEX compounds (Pitchel, 2007)

Compound	Unit	Benzene	Toluene	Ethylbenzene	Orthoxylene	Metaxylene	Paraxylene
Molecular Formula		C ₆ H ₆	C ₇ H ₈	C ₈ H ₁₀	C ₈ H ₁₀	C ₈ H ₁₀	C ₉ H ₁₂
Molecular Weight	(g/mol)	78.11	92.14	106.17	106.17	106	120
Specific Gravity @25°C		0.878	0.867	0.867	0.88	0.867	0.86
Solubility @25°C	(mg/L)	1780 ± 45	515 ± 17	161	1.75 ± 8	146 ± 1.6	156 ± 1.6
Viscosity	(cP)	0.652	0.59	0.669	0.81	0.62	0.648
Boiling Point	(°C)	80	111	136.2	142	138.9	138
Vapor Pressure	(mm of mercury)	76@20°C	22@20°C	4.53@25°C	10@25.9°C	10@28.3°C	10@27.3°C
Flash point	(°C)	-11	4	18	27	27	27

Table D.3 Compositions of oil of interest in the environment (Fingas, 2001)

Group	Compound Class	(%) Gasoline	Diesel	Light Crude	Heavy Crude	IFO	Bunker C
Saturates		50 to 60	65 to 95	55 to 90	25 to 80	25 to 35	20 to 30
	alkanes	45 to 55	35 to 45				
	cyclo-alkanes	5	30 to 50				
	waxes		0 to 1	0 to 20	0 to 10	2 to 10	5 to 15
Olefins		5 to 10	0 to 10				
Aromatics		25 to 40	5 to 25	10 to 35	15 to 40	40 to 60	30 to 50
	BTEX	15 to 25	0.5 to 2.0	0.1 to 2.5	0.01 to 2.0	0.05 to 1.0	0.00 to 1.0
	PAHs		0 to 5	10 to 35	15 to 40	40 to 60	30 to 50
Polar Compounds			0 to 2	1 to 15	5 to 40	15 to 25	10 to 30
	resins		0 to 2	0 to 10	2 to 25	10 to 15	10 to 20
	asphaltenes			0 to 10	0 to 20	5 to 10	5 to 20
Metals				30 to 250	100 to 500	100 to 1000	100 to 2000
Sulphur		0.02	0.1 to 0.5	0 to 2	0 to 5	0.5 to 2.0	2 to 4

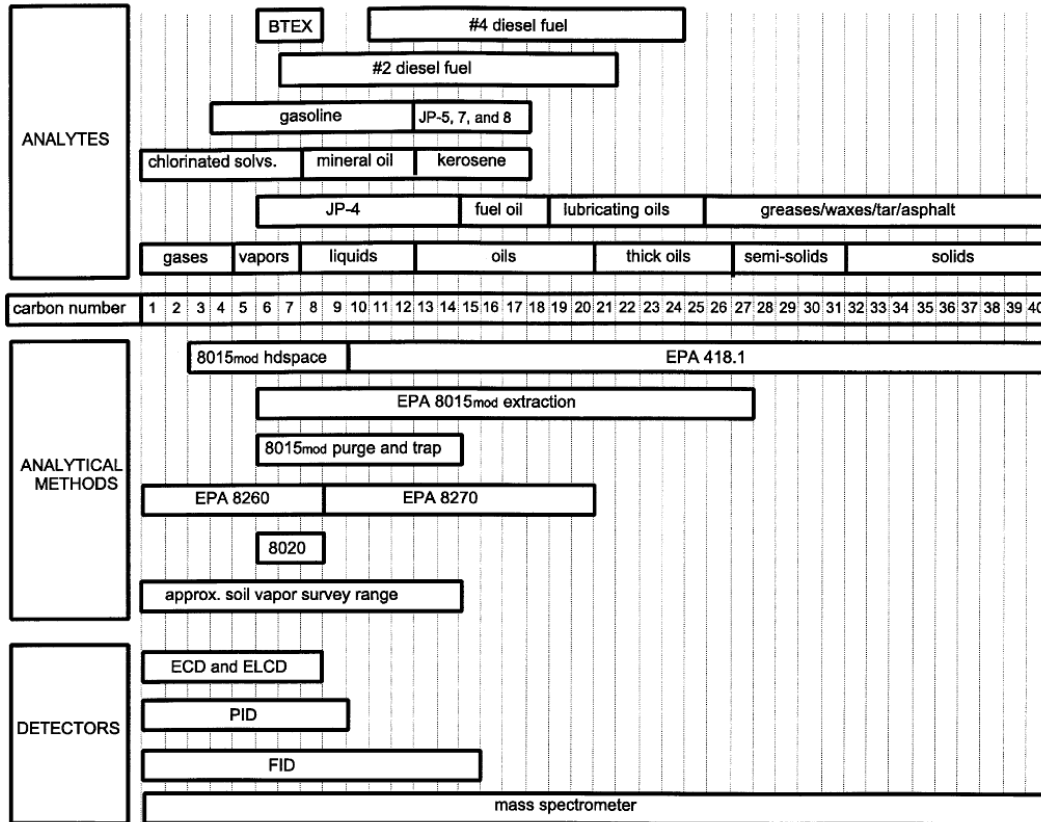


Figure D.2 Hydrocarbon analytes, carbon composition, and analytical methods (Werner, 2000).

2005 Results

Table D.4 Recovered diesel fuel composition at the Colomac mine (Van Stempvoort et al., 2006)

Maxxam ID		K53251	K53252	K53253		
Sampling Date		12/12/05	12/12/05	12/12/05		
COC Number		na	na	na		
	Units	9	12	17	RDL	QC Batch
F1 PHC and BTEX						
Benzene	ug/g	ND	ND	ND	100	913007
Toluene	ug/g	6200	630	2400	100	913007
Ethylbenzene	ug/g	2200	940	3000	100	913007
o-Xylene	ug/g	5400	1300	6300	100	913007
p+m-Xylene	ug/g	14000	4400	19000	200	913007
Total Xylenes	ug/g	19000	5700	25000	200	913007
F1 (C6-C10)	ug/g	200000	220000	300000	50000	913007
F1 (C6-C10) - BTEX	ug/g	180000	210000	270000	50000	913007
F2-F4 PHC						
F2 (C10-C16 Hydrocarbons)	ug/g	640000	640000	550000	10000	912972
F3 (C16-C34 Hydrocarbons)	ug/g	240000	170000	190000	10000	912972
F4 (C34-C50 Hydrocarbons)	ug/g	ND	ND	ND	10000	912972
Reached Baseline at C50	ug/g	YES	YES	YES		912972
Surrogate Recovery (%)						
1,4-Difluorobenzene	%	99	100	98		913007
4-Bromofluorobenzene	%	105	106	105		913007
D10-Ethylbenzene	%	97	122	111		913007
D4-1,2-Dichloroethane	%	99	101	101		913007
o-Terphenyl	%	129	123	123		912972

ND = Not detected

RDL = Reportable Detection Limit

QC Batch = Quality Control Batch

Table D.5 Measured groundwater organic compounds in August, 2005.

Well ID	Benzene	Toluene	Ethyl benzene	M&P-Xylene	O-Xylene	BTEX	F1 (CCME)
Concentration (mg/L)							
P2	0.005	0.006	0.040	0.057	0.019	0.127	0.700
P3	0.001	0.002	0.007	0.012	0.009	0.031	0.440
P4	0.003	0.006	0.021	0.059	0.169	0.258	1.110
P5	0.015	0.002	0.238	0.125	0.122	0.503	1.800
1	0.001	0.010	0.002	0.007	0.006	0.026	0.060
2	0.003	0.001	0.006	0.016	0.023	0.050	0.300
4	0.018	0.042	0.067	0.103	0.139	0.370	1.170
6	0.012	0.023	0.003	0.049	0.113	0.201	0.720
8	0.477	1.579	0.318	0.885	0.763	4.022	7.080
9	1.052	5.782	0.891	1.784	1.446	10.955	17.740
10	0.068	0.614	0.095	0.513	0.578	1.868	3.440
12	0.583	0.161	0.291	1.032	0.988	3.054	7.030
13	0.539	6.865	0.648	0.315	0.238	8.666	25.060
14	0.168	0.323	0.066	0.528	0.440	1.524	3.020
15	2.216	0.374	0.738	0.760	0.130	4.218	6.430
17	1.004	8.559	1.025	3.332	2.436	16.355	20.640
18	0.001	0.000	0.000	0.001	0.010	0.013	0.060
19	0.056	1.233	0.235	0.946	0.711	3.180	6.160
20	0.001	0.015	0.002	0.007	0.006	0.030	0.030
21	0.072	0.424	0.122	0.315	0.428	1.361	2.420
22	0.015	0.135	0.167	0.542	0.575	1.434	3.470
23	0.048	0.294	0.129	0.136	0.328	0.935	1.780
24	0.197	0.101	0.019	0.059	0.029	0.405	0.490
26	1.209	1.181	0.493	0.687	0.659	4.229	13.980
29	1.387	0.058	0.429	0.344	0.000	2.219	3.130
30	0.289	2.189	0.707	1.512	0.387	5.084	14.570
33	0.067	0.209	0.006	0.017	0.032	0.331	0.300

Table D.6 Measured major ions in July, 2005.

Well ID	Fluoride	Chloride	NO2- as N	Bromide	NO3- as N	Phosphate	Sulfate
	Concentration (mg/L)						
P2	0.0	3.5	0.0	0.0	0.0	0.0	259.2
P3	0.0	4.0	0.0	0.0	0.0	0.0	511.8
P6	0.1	12.0	0.0	0.1	0.0	0.0	181.8
2	0.2	2.5	0.0	0.0	0.1	0.0	205.3
4	0.1	3.2	0.0	0.0	0.0	0.0	274.6
10	0.2	3.1	0.0	0.0	0.0	0.0	237.5
14	0.1	3.0	0.0	0.0	0.0	0.0	143.0
15	0.1	11.2	1.0	0.0	0.9	0.0	372.3
18	0.3	2.8	0.0	0.0	0.0	0.0	418.8
20	0.0	2.8	0.0	0.0	0.1	0.0	129.1
22	0.1	4.9	0.0	0.0	0.0	0.0	211.9
24	0.2	8.9	0.0	0.0	0.0	0.0	408.8
Well ID	Lithium	Sodium	NH4+ as N	Potassium	Magnesium	Calcium	
P2	0.0	24.9	1.7	9.6	20.7	115.4	
P3	0.0	27.6	3.4	12.7	26.7	191.1	
P6	0.0	47.8	1.8	11.1	43.8	63.1	
2	0.0	3.5	0.2	3.2	12.5	100.7	
4	0.0	3.9	0.4	4.5	22.3	146.4	
10	0.0	6.0	0.8	4.2	16.3	92.6	
14	0.0	5.3	0.1	6.5	12.6	121.2	
15	0.0	14.4	5.7	6.2	34.7	170.0	
18	0.0	5.0	0.3	4.7	22.4	185.8	
20	0.0	3.3	0.1	2.0	12.5	48.9	
22	0.0	7.6	0.5	5.0	13.5	108.7	
24	0.0	20.9	0.8	13.4	54.5	228.1	

Table D.7 Measured major ions in August, 2005.

Well ID	Fluoride	Chloride	NO₂⁻ as N	Bromide	NO₃⁻ as N	Phosphate	Sulfate
Concentrations (mg/L)							
P2	0.076	3.853	0.000	0.000	0.025	0.000	197.657
P3	0.068	4.758	0.000	0.000	0.019	0.000	545.060
P6	0.045	12.697	0.000	0.066	0.024	0.000	175.157
1	0.103	2.590	0.058	0.000	0.030	0.000	479.909
2	0.156	2.405	0.000	0.000	0.057	0.000	178.015
4	0.088	4.225	0.000	0.000	0.092	0.000	233.020
10	0.200	3.419	0.000	0.000	0.037	0.000	294.689
14	0.152	3.680	0.000	0.000	0.014	0.000	250.213
15	0.079	13.596	1.302	0.000	0.148	0.000	448.790
18	0.245	3.101	0.000	0.000	0.025	0.000	458.014
20	0.022	2.610	0.000	0.000	0.036	0.000	136.827
22	0.108	4.835	0.000	0.000	0.000	0.000	234.412
24	0.039	2.748	0.000	0.000	0.019	0.000	44.185
30	0.054	6.703	0.000	0.000	0.073	0.000	213.362
Well ID	Lithium	Sodium	NH₄⁺ as N	Potassium	Magnesium	Calcium	
P2	0.005	25.227	2.064	11.467	15.931	118.243	
P3	0.004	26.611	3.338	11.752	24.975	203.619	
P6	0.007	46.661	1.718	10.344	38.821	53.871	
1	0.013	7.539	0.216	9.490	49.044	169.161	
2	0.002	3.021	0.281	2.870	9.427	89.174	
4	0.004	4.444	0.545	4.603	18.073	144.223	
10	0.009	5.385	0.552	3.905	19.330	110.922	
14	0.014	5.929	0.409	6.760	15.000	151.324	
15	0.004	14.803	2.837	4.889	27.887	153.879	
18	0.006	5.324	0.366	4.952	20.047	195.670	
20	0.001	3.366	0.115	2.090	10.752	52.239	
22	0.008	8.219	0.792	5.177	11.988	114.025	
24	0.002	3.590	0.165	2.107	6.449	50.245	
30	0.008	10.484	2.925	5.334	26.365	136.606	

Table D.8 Measured major ions in September, 2005.

Well ID	Fluoride	Chloride	NO2- as N	Bromide	NO3- as N	Phosphate	Sulfate
Concentrations (mg/L)							
P2	0.22	3.86	0.00	0.00	0.00	0.00	160.01
P3	0.06	4.54	0.00	0.00	0.00	0.00	389.33
P6	0.1	12.3	0.0	0.0	0.0	0.0	173.5
1	0.1	2.3	0.0	0.0	0.0	0.0	405.9
4	0.07	4.34	0.00	0.00	0.45	0.00	230.50
10	0.16	3.39	0.00	0.00	0.00	0.00	318.91
14	0.16	3.52	0.00	0.00	0.26	0.00	257.64
15	0.07	7.71	0.72	0.00	1.04	0.00	316.48
18	0.23	3.01	0.00	0.00	0.01	0.00	380.10
20	0.04	2.84	0.00	0.00	0.04	0.00	137.52
22	0.15	4.09	0.00	0.00	0.02	0.00	210.99
24	0.04	2.01	0.00	0.00	0.01	0.00	42.25
30	0.05	5.21	0.05	0.00	0.04	0.00	220.52
Well ID	Lithium	Sodium	NH4+ as N	Potassium	Magnesium	Calcium	
P2	0.01	22.46	1.74	10.16	15.39	107.05	
P3	0.00	19.05	2.25	8.96	20.01	153.21	
P6	0.01	45.7	1.5	10.7	41.4	55.9	
1	0.01	6.4	0.1	8.3	44.2	145.6	
4	0.00	4.49	0.32	4.96	19.30	145.31	
10	0.01	5.32	0.14	3.80	23.95	124.01	
14	0.02	6.22	0.26	7.44	17.68	158.93	
15	0.01	11.82	6.55	6.52	32.27	170.92	
18	0.01	5.06	0.32	4.90	19.34	160.14	
20	0.00	3.20	0.12	2.08	11.73	54.45	
22	0.01	8.75	0.67	5.72	12.70	110.86	
24	0.00	3.26	0.15	2.05	6.73	50.56	
30	0.01	10.34	2.59	5.30	28.45	138.83	

Table D.9 Summary of measured geochemical parameters in August, 2005 (Van Stempvoort, 2006).

Well ID	Date	Temperature (°C)	pH	DO (mg/L)	ORP (mV)
2	23-Aug-05	7.90	7.54	8.23	-20.20
4	24-Aug-05	9.41	6.49	0.43	-84.70
6	23-Aug-05	5.41	6.89	0.24	-78.60
8	23-Aug-05	4.91	6.63	0.58	-75.60
10	23-Aug-05	5.33	7.56	0.16	-136.40
13	24-Aug-05	6.33	7.38	0.24	-133.00
18	23-Aug-05	7.02	8.24	0.34	-180.40
20	24-Aug-05	6.00	6.44	2.00	-57.10
29	23-Aug-05	5.43	5.85	0.47	-60.40

Table D.10 Measured groundwater compounds with depth for selected monitoring wells (MWs) in August, 2005.

Well ID		P2-1	P2-2	P3-1	P3-2	P4-1	P4-2	14-1	14-2	14-3	14-4
Depth	(m)	3.29	6.29	3.95	4.95	2.93	4.93	5.00	6.00	13.50	16.00
S04		569.20	543.20	209.50	242.60	492.30	153.50	407.90	452.30	899.10	77.60
Fe		1.47	52.42	40.74	40.58	6.12	4.02	6.31	4.68	4.25	5.27
Mn		5.02	8.43	10.67	11.34	2.65	3.80	1.41	1.42	1.37	1.51
Ca		143.80	246.50	267.60	276.50	82.21	145.80	234.30	248.10	256.10	261.70
Mg		20.03	40.59	29.32	29.67	8.89	12.69	23.39	24.79	25.51	28.61
Na		52.99	49.94	41.89	43.31	10.61	16.81	7.89	9.52	9.94	23.71
F1		0.25	0.7		0.44	0.72	1.11	3.02	3.39	1.3	2.56
Benzene		0.001	0.005	0.001	0.001	0.005	0.003	0.168	0.105	0.526	0.184
toluene		0.007	0.006	0.003	0.002	0.010	0.006	0.323	0.544	0.231	0.528
ethyl benzene		0.009	0.040	0.006	0.007	0.018	0.021	0.066	0.051	0.022	0.033
m,p-xylene		0.013	0.057	0.011	0.012	0.049	0.059	0.528	0.586	0.201	0.334
o-xylene		0.017	0.019	0.008	0.009	0.110	0.169	0.440	0.523	0.187	0.310
Well ID		19-1	19-2	19-3	19-4	19-5	22-1	22-2			
Depth		4	5.5	7	11	15	6	7			
S04		426.60	356.70	377.60	370.20	357.30	577.50	262.20			
Fe		3.09	1.82	3.90	3.31	3.09	1.39	2.06			
Mn		1.26	1.09	1.18	1.17	1.13	2.15	2.03			
Ca		226.70	202.80	210.40	215.30	206.80	117.90	125.30			
Mg		21.44	18.83	19.41	19.76	19.14	14.53	14.28			
Na		1.92	<1.0	<1.0	1.98	7.86	22.69	22.82			
F		6.52	6.16	4.38	4.03	4.15	0.65	3.47			
Benzene		0.033	0.056	0.043	0.046	0.031	0.033	0.015			
toluene		0.848	1.233	0.898	1.264	0.821	0.019	0.135			
ethyl benzene		0.238	0.235	0.183	0.231	0.169	0.019	0.167			
m,p-xylene		1.283	0.946	0.619	0.739	0.571	0.067	0.542			
o-xylene		0.941	0.711	0.500	0.602	0.459	0.093	0.575			

Table D.11 Measured volatile fatty acid in selected MWs (Van Stempvoort, 2006)

Well ID	Volatile Fatty Acid (mg/L)
1	0.0
2	0.6
4	0.0
6	0.3
8	0.9
9	0.0
10	1.2
12	3.8
13	2.7
14	0.4
15	0.0
17	0.0
18	0.7
19	0.4
20	0.9
22	0.6
24	0.5
26	0.0
29	0.0
30	0.4
33	0.0

Table D.12 Measured dissolved metals in 2005.

Well ID	Be	Na	Mg	Al	K	Ca	V	Cr	Iron	Mn	Ni	Co	Cu	Zn	Ga	As	Se	Rb	Sr	Ag	Cd	Cs	Ba	Tl	Pb	U	
	ug/L	ug/L	ug/L	ug/L	ug/L	ug/L	ug/L	ug/L	ug/L	ug/L	ug/L	ug/L	ug/L	ug/L	ug/L	ug/L	ug/L	ug/L	ug/L	ug/L	ug/L	ug/L	ug/L	ug/L	ug/L	ug/L	
July, 2005																											
P2	0	21816	15081	110	8773	84745	0	0	6337	5357	175	163	31	27	0	0	4	2	282	0	0	0	21	0	16	0	
P3	0	23754	18590	94	10783	152810	0	0	52300	10755	228	281	39	51	0	0	5	2	370	0	0	0	39	0	14	6	
P6	0	39396	30489	84	9742	30766	0	0	2550	2297	5	1	50	16	0	0	0	2	120	0	0	0	10	0	16	0	
2	0	3149	8676	572	3774	79850	0	0	3716	845	67	5	161	35	0	1	2	1	143	0	0	0	54	0	28	1	
4	0	3952	17855	606	5108	102380	0	0	2207	7507	296	136	86	24	0	4	2	4	236	0	0	0	51	0	23	2	
10	0	5740	12634	498	3921	65230	0	0	2053	914	83	28	62	30	0	1	3	3	153	0	0	0	28	0	20	0	
14	0	5622	13357	556	6379	111898	0	0	15720	1073	114	39	74	29	0	9	4	3	177	0	0	0	36	0	22	2	
15	0	11956	27466	472	6002	123942	0	0	5282	8578	135	15	59	38	0	11	0	9	241	0	0	0	28	0	18	20	
18	0	3027	12426	7	3650	73938	0	0	6286	592	10	3	28	23	0	1	0	2	117	0	0	0	16	0	3	0	
20	0	2750	11551	31	2952	74916	0	0	3716	455	20	3	30	30	0	0	0	2	125	0	0	0	17	0	3	1	
22	0	4882	8148	55	4462	67773	0	0	10815	1288	33	23	17	26	0	1	1	2	104	0	0	0	16	0	2	1	
24	0	5321	13925	11	4903	64433	0	0	6552	2907	17	2	5	10	0	0	3	1	191	0	1	0	14	0	0	0	
August, 2005																											
P2	0	24921	15021	139	10058	89182	0	0	12302	5061	231	212	22	9	0	0	0	2	312	0	0	0	22	0	1	1	
P3	0	27041	22823	148	11322	181015	0	0	52976	11480	292	388	22	21	0	0	0	1	377	0	1	0	22	0	1	8	
P6	0	43641	34624	146	9057	51294	0	0	12294	2802	5	3	21	9	0	0	0	1	184	0	1	0	10	0	1	0	
1	0	6550	46035	135	9732	120486	0	0	9453	931	124	40	36	37	0	0	4	6	199	0	1	0	17	0	0	8	
2	0	2397	8933	125	3031	67460	0	0	2785	699	28	4	16	12	0	0	2	2	143	0	1	0	16	0	0	1	
4	0	3177	15472	255	4191	99100	0	0	9477	12704	281	148	29	26	0	0	0	3	237	0	1	0	56	0	2	3	
10	0	4664	15779	131	4133	73745	0	0	3343	1203	74	44	34	13	0	0	0	2	156	0	1	0	22	0	2	0	
14	0	5205	17075	120	6539	135687	0	0	15539	1161	105	45	15	34	0	2	0	3	212	0	1	0	22	0	2	3	
15	0	11112	23814	138	4566	105508	0	0	4366	11337	170	27	10	26	0	0	0	4	173	0	1	0	12	0	0	1	
18	1	3748	15313	124	4690	104015	0	0	9374	838	18	3	13	11	0	0	0	2	194	0	1	0	20	0	1	1	
20	0	2523	9988	134	2202	35316	0	0	29	394	17	2	7	17	0	0	0	0	67	0	1	0	11	0	0	0	
22	0	7036	10941	132	5166	78198	0	0	12736	1570	38	20	19	22	0	0	0	3	140	0	1	0	18	0	2	1	
24	0	2409	5280	109	2018	32065	0	0	2145	2775	24	4	4	17	0	0	0	1	97	0	1	0	8	0	0	0	
30	0	7225	16880	120	4526	68969	0	0	917	2359	3	1	5	29	0	7	0	2	195	0	1	0	15	0	0	11	

Table D.12 Measured dissolved metals in 2005, contd.

Well ID	Be	Na	Mg	Al	K	Ca	V	Cr	Iron	Mn	Ni	Co	Cu	Zn	Ga	As	Se	Rb	Sr	Ag	Cd	Cs	Ba	Tl	Pb	U
	ug/L	ug/L	ug/L	ug/L	ug/L	ug/L	ug/L	ug/L	ug/L	ug/L	ug/L	ug/L	ug/L	ug/L	ug/L	ug/L	ug/L	ug/L	ug/L	ug/L	ug/L	ug/L	ug/L	ug/L	ug/L	ug/L
	September, 2005																									
P2	0	25331	14714	146	10848	103229	0	2	6989	4563	173	163	7	42	0	1	0	3	282	0	0	0	31	0	0	2
P3	1	19500	17684	182	8631	130321	0	0	23987	8751	183	267	3	351	0	1	0	3	277	0	0	0	25	0	0	6
P6	0	51065	41438	165	10623	66575	0	0	14337	3126	7	3	5	0	0	0	0	3	184	0	0	0	15	0	0	0
1	0	6068	42405	163	3027	132048	0	0	10313	972	39	35	4	0	0	0	0	7	180	0	0	0	22	0	0	7
4	0	4815	17266	180	5226	129517	0	3	14691	19394	275	165	8	1	0	4	4	5	269	0	0	0	65	0	0	5
10	1	5424	22386	139	4420	113301	0	0	3856	2087	101	69	1	0	0	0	0	3	168	0	0	0	29	0	0	0
14	0	6383	2127	231	7703	177187	0	0	17861	1635	103	44	17	0	0	6	3	5	233	0	0	0	28	0	0	3
15	0	52629	27972	241	6552	147560	0	0	4150	4923	50	7	13	0	0	6	0	8	266	0	0	0	12	0	0	27
18	0	14753	19844	132	5939	160436	0	0	6910	1051	14	2	8	0	0	0	0	2	221	0	0	0	22	0	0	1
20	0	2972	10695	157	1838	47052	0	0	259	431	29	2	4	0	0	0	0	2	72	0	0	0	17	0	0	0
22	0	8396	11390	155	6108	95451	0	0	10811	1706	64	32	7	0	0	0	0	3	139	0	0	0	21	0	0	2
24	1	3226	5822	127	1829	41727	0	0	1156	2963	92	4	10	0	0	0	0	1	98	0	0	0	12	0	0	0
30	0	11207	27858	167	6155	127006	0	0	366	2626	5	1	8	0	0	36	2	4	300	0	0	0	30	0	0	13

2006 Results

Table D.13 Measured geochemical parameters in selected (MWs) in 2006.

Well ID	Alk	PH	T (°C)	Well ID	Alk-U	Alk	PH	T (°C)	DO (mg/L)	EC (mS)
	June-06				September-06					
P1	127.2	6.93	25.7	P1	99	99	7.18	10.9	1	
P2	136	8.49	21.1	P2		0	6.8	7.6	1	1.82
P3	144	8.36	10.6	P3	334	334	7.48	9.2	2	1.82
P4	229.6	7.69	8.9	P4	332	332	7.46	12.5	2	1.96
P5	113.6	7.66	12.5	P5	642	642	7.22	13.2	1	2.44
4	136	7.65	13.9	4	309	309	7.23	8.7	1	1.91
6	98.8	8.03	8.5	9	216	216	7.35	7.4	1	2.04
8	124.4	7.9	8.2	12	395	395	7.12	6.4	1	2.55
9	122.4	8.78	7.1	13	203	203	7.46	14.6	1	2.43
12	96	8.93	17.9	14	234	234	7.13	10.4	1	2.13
14	138.4	9.17	13.2	15	271	271	7.36	11.1	1	2.31
15	244	8.74	13.4	17	150		7.86	6.1		0.757
18	35.6	7.79	10.4	19	195	195	7.65	6.5	1	2.41
19	150.4	8.4	10.2	22	177	177	7.62	13.8	1	1.9
22	142.4	7.62	18.1	26	162	162	7.29	6.5	2	1.443
26	108.4	8.72	10.4	29	210	210	7.19	10.6	3	1.96
29	272.4	7.85	9.8	30		0	7.16	9.3	1	1.8
30	252.8	7.87	14.6	103	78	78	8.18	9.2		0.458
103	136	8.18	8.1	104	429	429	8.95	10.5	4	0.94
104	171.6	8.95	10.5	106	117		7.75	8	1	1.875
				108	169	169	7.43	11.6	1	2.6

Alk - Alkalinity in mg/L of Ca CO₃

DO - Dissolved Oxygen

T - Temperature

EC - Electrical Conductivity

Table D.14 Measured organic compounds in June, 2006.

Well ID	Benzene	Toluene	Ethyl benzene	M&P Xylene	O Xylene	Xylene	BTEX
Concentration (mg/L)							
29	1.330	0.614	0.796	1.510	0.704	2.218	4.961
30	1.751	1.063	0.711	2.150	3.830	5.980	9.506
P1	0.071	0.065	0.065	0.127	0.061	0.188	0.388

Table D.15 Measured major ions in June, 2006.

Well ID	Fluoride	Chloride	NO ₂ - as N	Bromide	NO ₃ - as N	Phosphate	Sulfate
Concentrations (mg/L)							
P1	0.102	10.922	0.130	0.000	0.335	0.000	906.999
P2	0.103	4.294	0.000	0.000	0.000	0.000	219.731
P3	0.028	5.328	0.000	0.000	0.076	0.000	489.692
P4	0.132	4.306	0.000	0.000	0.000	0.000	72.222
P5	0.094	7.911	0.000	0.000	0.091	0.000	162.495
4	0.155	3.634	0.061	0.000	0.000	0.000	222.753
6	0.113	3.740	0.094	0.000	0.093	0.000	377.489
8	0.103	4.505	0.000	0.000	0.116	0.000	431.280
9	0.150	25.268	0.179	0.000	0.000	0.000	248.576
12	0.047	6.560	0.087	0.000	0.424	0.000	247.600
14	0.203	5.790	0.000	0.000	0.000	0.000	348.914
15	0.107	29.705	0.874	0.000	0.587	0.000	355.833
18	0.225	4.159	0.000	0.000	0.000	0.000	50.168
19	0.333	5.977	0.000	0.000	0.000	0.000	392.093
22	0.293	11.233	0.000	0.000	0.110	0.000	279.782
26	0.053	4.013	0.126	0.000	0.362	0.000	271.073
29	0.169	18.347	0.000	0.000	0.240	0.000	273.948
30	0.126	13.954	0.000	0.000	0.854	0.000	268.966
103	0.206	7.384	0.000	0.000	0.000	0.000	282.826
104	0.101	4.151	0.000	0.000	0.315	0.000	99.988
Well ID	Lithium	Sodium	NH ₄ ⁺ as N	Potassium	Magnesium	Calcium	
P1	0.010	43.200	3.195	13.261	49.093	350.500	
P2	0.009	20.789	0.904	9.435	19.721	115.722	
P3	0.008	24.817	2.220	13.557	27.172	197.019	
P4	0.006	15.974	0.278	11.009	16.456	98.514	
P5	0.012	52.189	0.000	4.343	24.849	59.372	
4	0.009	6.044	0.114	4.818	17.398	114.775	
6	0.009	7.764	0.081	5.655	17.209	132.589	
8	0.011	7.118	0.053	5.587	19.078	140.408	
9	0.020	13.727	0.661	6.189	10.732	106.559	
12	0.005	7.502	0.069	2.962	18.740	119.902	
14	0.009	7.309	0.131	6.014	17.210	168.144	
15	0.006	14.907	2.360	4.375	30.035	146.437	
18	0.002	1.635	0.171	0.655	1.652	22.786	
19	0.007	6.931	0.104	5.461	16.103	155.782	
22	0.011	9.161	0.389	5.440	12.618	116.330	
26	0.004	3.713	0.079	1.507	17.118	106.099	
29	0.008	14.344	0.876	4.394	25.888	147.677	
30	0.009	9.577	1.251	4.339	24.323	112.467	
103	0.023	14.702	0.222	8.034	20.099	119.522	
104	0.008	4.622	0.067	5.675	13.776	65.571	

Table D.16 Measured dissolved metals in June, 2006.

Well ID	Be	B	Na	Mg	Al	Si	P	K	Ca	V	Cr	Fe	Ni	Mn	Co
Concentrations (µg/L)															
P1	0	0	31347	36925	0	531	1086	9314	248659	0	0	19246	157	4682	42
P2	0	0	19807	18050	0	2504	751	8831	100495	0	0	21723	416	7388	434
P3	0	0	20291	20062	0	2362	988	10673	143272	0	0	50329	193	10503	227
P4	0	44	16200	16877	0	5391	1116	11633	92998	0	8	22215	68	3347	55
P5	0	174	48439	23887	0	8578	1793	4418	52118	0	11	1726	40	2106	14
4	0	40	4343	13402	0	3204	248	3193	77931	4	0	1625	181	7314	87
6	0	30	7401	19286	0	2899	869	6555	125790	7	7	317	168	2617	79
8	0	0	6311	22220	0	2130	1135	5907	130644	4	0	208	153	1685	62
9	0	0	16009	12882	0	1994	567	6808	106467	3	0	333	119	1618	31
12	0	0	5493	17617	0	3396	1088	2831	99262	1	0	1194	207	6101	62
14	0	0	7495	20639	0	2500	1041	6969	183951	1	0	3916	101	861	42
15	0	0	18082	37084	0	5653	1047	4897	166751	0	0	5812	66	4501	11
18	0	0	818	1794	0	0	376	782	20617	0	0	1526	12	218	1
19	0	0	6894	18940	26	1995	534	6226	163310	0	0	2719	101	693	40
22	0	0	11366	16178	0	2710	778	5610	135320	0	0	8241	96	1651	48
26	0	0	3367	21291	0	4175	895	1280	117596	0	0	313	180	906	4
29	0	0	18655	34361	0	6545	379	5516	195084	0	0	7987	41	4583	7
30	0	0	15163	41249	0	5991	487	6692	175073	0	0	1644	4	2127	1
103	0	0	14538	20365	0	5239	386	7295	107049	0	0	1966	138	4074	52
104	0	0	3149	13264	0	2959	514	4598	53734	0	0	0	10	30	0
Well ID	Cu	Zn	Ga	As	Se	Rb	Ba	Ag	Mo	Cd	Cs	Sr	Tl	Pb	U
Concentrations (µg/L)															
P1	0	0	0	0	0	1	53	0	4	1	0	399	2	0	1
P2	0	0	0	1	0	1	26	0	1	0	0	280	2	0	1
P3	0	0	0	0	0	2	31	0	0	1	0	321	1	0	3
P4	0	83	0	0	0	3	29	0	2	0	0	241	1	0	3
P5	0	0	0	1	5	1	30	0	0	1	0	176	1	0	1
4	9	0	0	5	13	3	41	0	2	0	0	165	2	4	1
6	11	0	0	4	4	4	26	0	2	1	0	201	3	2	2
8	6	49	0	3	22	3	23	0	2	0	0	198	2	1	2
9	21	8	0	2	10	4	22	0	3	0	0	158	2	13	3
12	4	0	0	2	12	1	23	0	1	0	0	173	2	5	1
14	3	0	0	6	13	2	22	0	3	0	0	230	2	3	3
15	1	0	0	38	0	4	25	0	1	0	0	288	2	0	6
18	0	0	0	0	2	1	12	0	2	0	0	46	2	0	0
19	8	0	0	2	8	2	22	0	2	0	0	236	2	2	3
22	2	0	0	5	0	4	27	0	4	0	0	175	2	1	2
26	0	0	0	0	6	1	9	0	0	1	0	182	2	0	0
29	3	0	0	64	0	2	35	0	2	0	0	344	2	0	13
30	2	0	0	57	0	3	28	0	1	0	0	410	2	1	5
103	6	0	0	2	0	6	27	0	4	0	0	235	2	1	2
104	8	0	0	0	0	3	7	0	2	0	0	120	2	0	3

Table D.17 Measured organic compounds in September, 2006.

Well ID	Benzene	Toluene	Ethyl benzene	M&P Xylene	O Xylene	BTEX	F1 (CCME)
	Concentrations (mg/L)						
P1	0.043	0.041	0.046	0.092	0.046	0.268	0.012
P2	0.000	0.000	0.000	0.096	0.049	0.144	0.090
P3	0.000	0.000	0.062	0.227	0.104	0.393	0.665
P4	0.045	0.000	0.000	0.123	0.223	0.390	0.356
P5	0.240	0.000	0.351	0.410	0.000	1.001	1.593
4	0.050	0.043	0.078	0.218	0.107	0.496	0.678
9	0.130	0.412	0.067	0.685	0.366	1.660	1.943
12	0.724	0.395	0.158	1.150	0.420	2.847	3.678
13	0.272	2.077	0.326	1.925	0.813	5.411	5.584
14	0.047	0.071	0.000	0.483	0.185	0.785	0.981
15	0.520	0.124	0.160	0.399	0.122	1.324	1.398
17	2.025	9.706	1.085	5.669	2.227	20.712	22.427
19	0.069	0.441	0.096	0.756	0.304	1.666	2.263
22	0.000	0.042	0.046	0.092	0.045	0.226	0.016
26	0.967	1.863	0.336	1.977	1.120	6.262	6.972
29	0.060	0.053	0.000	0.108	0.079	0.300	0.129
30	0.285	0.541	0.129	0.890	0.415	2.260	2.409
103	0.045	0.048	0.058	0.138	0.101	0.000	0.365
104	0.000	0.000	0.000	0.000	0.000	0.048	0.000
106	0.046	0.054	0.069	0.110	0.117	0.396	0.138
108	0.000	0.000	0.000	0.000	0.000	0.000	0.026

Table D.18 Measured major ions in September, 2006.

Well ID	Bromide	Chloride	Fluoride	NO2	NO3	Sulphate
	Concentration (mg/L)					
P1	0.087	4.929	0.092	0.043	0.122	1187.217
P2	0.084	4.590	0.098	0.099	0.081	248.738
P3	0.108	3.122	0.070	0.046	0.078	164.422
P4	0.062	3.999	0.101	0.147	0.568	212.377
P5	0.111	5.590	0.146	0.070	0.087	71.221
4	0.000	1.779	0.181	0.141	0.054	212.903
9	0.000	3.417	0.161	0.055	0.037	411.594
12	0.000	2.540	0.055	0.065	0.096	357.963
13	0.000	1.977	0.105	0.371	0.797	603.008
14	0.000	3.071	0.215	0.033	0.317	304.932
15	0.144	9.829	0.074	2.968	28.344	312.053
17	0.000	6.692	0.097	0.095	9.982	38.624
19	0.000	1.467	0.265	0.060	0.161	440.372
22	0.000	3.668	0.161	0.071	0.540	385.954
26	0.000	0.915	0.076	0.879	0.224	288.627
29	0.000	2.607	0.044	0.261	1.746	332.202
30	0.000	3.829	0.060	2.482	7.362	322.449
103	0.000	2.029	0.052	0.070	0.095	13.723
104	0.000	1.166	0.088	0.032	0.104	107.996
106	0.000	4.139	0.229	0.047	0.050	366.010
108	0.000	7.314	0.158	1.098	4.967	397.663
Well ID	Lithium	Sodium	NH4+ as N	Potassium	Magnesium	Calcium
P1	0.032	59.172	10.673	17.663	80.581	458.408
P2	0.013	46.074	2.829	12.672	34.269	149.702
P3	0.011	17.414	1.193	10.927	16.015	132.960
P4	0.009	22.878	0.969	9.636	18.700	121.313
P5	0.011	38.136		5.946	53.069	134.352
4	0.029	5.762	0.513	5.488	24.199	134.103
9	0.061	11.522	1.285	8.799	32.751	212.001
12	0.018	7.944	0.333	6.735	53.069	237.920
13	0.024	8.986	1.073	7.542	56.731	231.233
14	0.025	9.721	0.231	8.626	24.747	187.380
15	0.011	12.009	12.438	6.669	39.591	184.866
17	0.006	23.213	0.607	3.074	7.083	38.156
19	0.013	6.266	0.451	6.819	26.712	211.262
22	0.016	19.516	1.232	9.148	21.197	150.639
26	0.004	3.949	0.455	1.621	22.178	116.278
29	0.007	7.553	0.312	2.816	23.351	141.274
30	0.006	8.340	2.372	4.281	20.019	104.604
103	0.019	2.840	0.285	2.001	3.265	20.630
104	0.010	3.494	0.142	3.059	12.062	53.970
106	0.008	7.199	0.196	7.486	19.326	139.024
108	0.017	37.760	1.760	12.120	28.397	198.469

Table D.19 Measured dissolved metals in September, 2006.

Well ID	Be	B	Na	Mg	Al	Si	P	K	Ca	V	Cr	Fe	Ni	Mn	Co
Concentrations (µg/L)															
P1	0	268	43903	51992	0	2990	855	13477	354676	0	0	26368	138	8910	64
P2	0	265	39639	24652	0	6930	330	12174	125713	0	0	4612	252	6387	157
P3	0	293	16107	11887	0	10387	1060	11822	124908	0	0	36701	143	5419	166
P4	0	464	29545	20874	0	10222	523	14914	160377	0	0	36340	52	6583	62
P5	0	476	34037	39759	0	15034	355	6079	119279	2	0	51602	88	15300	56
4	0	152	5175	18809	0	8134	815	6949	139294	0	0	33181	270	20491	180
9	0	155	8139	23419	9	4719	484	8428	179244	0	0	18444	94	2832	37
12	0	92	5197	34374	150	15588	899	6581	186643	0	0	46429	130	20095	119
13	0	144	8316	47686	0	3594	1140	8748	247773	0	0	8558	226	1178	55
14	0	193	6858	17186	13	4106	724	7883	151422	0	0	14126	34	2017	27
15	0	268	11444	30457	73	7994	1345	7570	167800	0	0	7591	56	8035	7
17	0	249	22827	5878	272	4160	1459	4152	33919	0	0	759	21	94	1
19	0	155	5464	22233	21	3825	731	7869	204120	0	9	16750	158	1860	96
22	0	238	22936	20332	0	3959	489	11745	169936	0	0	1896	102	2273	37
26	0	105	3522	18753	0	4027	312	2220	111136	0	0	1444	151	2249	7
29	0	186	7686	22384	99	6576	320	4549	154422	0	0	1339	137	4816	25
30	0	183	9832	21099	0	3122	478	6551	129544	0	0	6043	41	7258	36
103	0	249	2337	2860	39	2306	1325	2706	20003	0	0	1088	32	404	6
104	0	207	4001	13242	40	2760	540	4970	64188	0	0	667	12	330	1
106	0	159	7810	19807	18	2011	720	10128	159069	0	0	6460	13	904	2
108	0	375	38442	23597	0	3800	725	12854	189397	0	0	1079	134	2221	25
Well ID	Cu	Zn	Ga	As	Se	Rb	Sr	Ag	Mo	Cd	Cs	Ba	Tl	Pb	U
P1	9	45	0	0	0	3	543	1	8	0	0	14	1	1	2
P2	6	0	0	0	0	2	293	0	5	0	0	28	1	2	4
P3	8	0	0	13	0	3	285	0	3	0	0	40	0	1	5
P4	10	11	0	15	2	4	369	0	4	0	0	48	0	1	6
P5	25	0	0	4	3	3	226	0	6	0	0	85	0	1	11
4	17	0	0	8	6	5	292	0	4	0	0	77	0	2	8
9	107	0	0	2	0	4	262	0	2	0	0	30	0	1	3
12	106	37	1	20	0	3	325	0	2	0	0	132	0	1	16
13	104	4	0	0	7	4	304	0	0	1	0	15	0	1	13
14	96	16	0	4	0	5	219	0	1	0	0	25	0	2	3
15	100	86	0	31	0	7	352	0	2	1	0	36	0	1	9
17	131	220	0	0	0	1	52	0	1	1	0	18	0	3	1
19	113	10	0	6	0	4	273	0	2	1	0	25	0	1	5
22	96	33	0	1	0	7	274	0	3	0	0	44	0	1	4
26	142	0	0	0	0	1	173	0	0	1	0	13	0	2	1
29	200	371	0	2	0	2	238	0	0	1	0	39	0	2	2
30	165	169	0	14	0	7	232	0	2	0	0	31	0	1	4
103	161	61	0	1	0	2	45	0	1	0	0	12	0	2	0
104	247	322	0	2	0	1	120	0	2	1	0	11	0	1	3
106	157	322	0	1	0	2	351	0	6	0	0	20	0	1	1
108	172	30	0	0	0	2	300	0	3	1	0	48	0	1	4

2007 Results

Table D.20 Measured geochemical parameters in 2007.

Well ID	T (°C)	EC (µS)	Alk	PH	MWID	T (°C)	EC (µS)	Alk	PH	Well ID	T (°C)	EC (µS)	Alk	PH
Jun-07					Sep-07									
2	6.5	116	100	7.05	1	1.6	1306		8.04	41	10.8	1986		5.50
4	7.6	149	96	7.06	2	2.0	1214		7.71	43	1.7	1635		5.70
6	4.0	912		7.35	4	2.9	1622	266	6.69	44	2.9	1913		6.58
8	5.7	1285	98	8.29	6	2.1	1861		7.25	46	2.6	928		6.34
9	5.1	1845	197	7.37	8	1.9	2470		7.21	47	3.2	771	227	6.87
10	13.9	1383	78	8.32	9	2.4	2500		6.59	50	6.0	1613	38	5.94
12	3.4	49	122	6.73	11	10.0	1833		5.39	51	3.4	4290	324	7.28
13	5.1	659	142	9.27	12	2.9	2360	433	7.30	103	3.7	1830		5.73
14	7.8		100	7.82	13	2.0	2840		5.65	104	2.0	1421	166	7.17
15	6.0	41	315	6.98	14	5.4	2470	195	5.56	106	3.3	2620		7.70
17	4.2	1446	175	7.65	15	5.4	2290	137	7.09	P1	4.1	2490	21	6.71
19	5.3	1668	100	7.75	16	1.3	2180		6.42	P2	4.4	2230		7.24
20	4.8	1232	77	7.73	17	3.2	970	129	6.36	P3	5.0	2330		6.80
22	8.4	2380	58	6.52	18	5.0	1930	201	6.55	P4	4.5	1892	207	5.64
26	4.1	4	255	6.83	19	5.2	2190		5.90	P5	4.5	2430	362	5.07
30	9.9	29	170	7.23	20	3.7	1073	22	8.25					
35	4.3	2420	313	7.09	21	6.1	2720		7.00					
36	10.6	30200	89	4.80	22	7.8	1646		5.86					
37	5.3	609	65	8.20	23	4.6	2310		6.61					
38	6.7	164	47	8.34	26	2.4	1316	148	7.11					
39	11.0	11	165	7.29	29	5.3	2150	269	5.92					
40	10.0	1048	141	6.42	30	6.0	2440	298	6.61					
41	7.9	1067	127	6.66	33	2.3	857		5.62					
47	5.9	11	173	6.20	34	3.9	2750		8.21					
50	9.0	748	141	7.58	35	3.6	2230	182	6.20					
51	5.7	2570	78	7.98	36	5.1	2380		6.07					
103	5.1	683	88	7.46	37	2.9	2990		6.86					
104	4.6	90	115	8.54	38	3.9	998		7.07					
P2	8.5	1978	158	7.16	39	10.7	1980		6.27					
P3	13.4	2760	157	6.05	40	12.3	2360		5.71					

EC - Electrical Conductivity
T - Temperature
Alk - Total Alkalinity in mg/L
of CaCO₃

Table D.21 Measured organic compounds in June, 2007.

Well ID	Benzene	Toluene	Ethyl benzene	M&P-Xylene	O-Xylene	BTEX
Concentration (mg/L)						
2	0.000	0.000	0.000	0.000	0.000	0.000
4	0.000	0.000	0.000	0.154	0.000	0.154
6	0.081	0.075	0.000	0.187	0.117	0.460
8	0.082	0.116	0.094	0.311	0.177	0.780
9	0.212	0.508	0.110	0.353	0.174	1.358
10	0.083	0.106	0.000	0.219	0.200	0.608
12	0.092	0.086	0.084	0.176	0.087	0.525
13	0.084	0.147	0.086	0.204	0.098	0.619
14	0.085	0.143	0.085	0.228	0.107	0.648
15	1.065	0.126	0.190	0.407	0.151	1.939
17	0.212	0.646	0.115	0.361	0.174	1.508
19	0.080	0.103	0.085	0.199	0.096	0.563
20	0.000	0.000	0.000	0.000	0.000	0.000
22	0.000	0.075	0.000	0.155	0.082	0.312
26	1.526	1.179	0.400	1.834	1.019	5.959
30	0.271	0.095	0.091	0.187	0.084	0.729
35	0.000	0.000	0.000	0.000	0.000	0.000
36	0.000	0.000	0.000	0.000	0.000	0.000
37	0.000	0.000	0.000	0.000	0.000	0.000
38	0.000	0.000	0.000	0.154	0.000	0.154
39	0.000	0.000	0.000	0.000	0.000	0.000
40	0.000	0.000	0.000	0.000	0.000	0.000
41	0.000	0.000	0.000	0.000	0.000	0.000
42	0.000	0.000	0.000	0.000	0.000	0.000
50	0.080	0.000	0.000	0.000	0.109	0.189
51	0.000	0.000	0.000	0.000	0.000	0.000
104	0.000	0.000	0.000	0.000	0.000	0.000
106	0.000	0.000	0.000	0.000	0.000	0.000
P2	0.000	0.000	0.084	0.164	0.113	0.360
P3	0.000	0.000	0.000	0.000	0.000	0.000

Table D.22 Measured major ions in June, 2007.

Well ID	Calcium	Potassium	Lithium	Magnesium	Sodium	NH4+ as N	Sulphate	Chloride
Concentration (mg/L)								
2	84.225	4.197	0.002	7.443	3.663	0.110		
4	99.338	3.888	0.004	14.366	3.728	0.000	206.103	0.442
6	71.079	3.468	0.002	9.403	3.490	0.000		
8	131.989	5.036	0.003	16.303	4.679	0.000	296.520	0.773
9	208.901	12.433	0.029	16.779	19.963	0.000	371.684	8.741
10	121.331	5.356	0.005	19.249	5.241	0.000	276.083	1.753
12	243.755	3.617	0.001	22.638	5.759	0.000	647.518	1.488
13	42.813	4.841	0.006	3.560	2.386	0.426		
14	101.454	3.843	0.004	10.009	4.118	0.000	204.988	1.896
15	273.577	10.561	0.007	44.794	15.909	22.445	458.607	7.714
17	123.700	4.746	0.007	16.328	9.584	0.493	221.606	6.411
19	159.612	8.858	0.005	14.828	137.710	0.000	276.895	216.648
20	128.022	2.910	0.003	26.903	5.222	0.647	380.739	1.488
22	186.562	7.042	0.008	24.677	12.737	0.530	429.878	15.393
26	144.188	1.287	0.003	22.666	10.847	0.000	197.540	1.788
30	128.188	5.297	0.004	21.454	10.535	9.037	227.445	4.196
35	57.178	30.032	0.019	17.914	134.657	20.732		
36	812.943	120.619	0.000	69.349	4203.392	0.000	360.489	7917.600
37	11.384	7.560	0.003	7.029	35.155	6.073		
38	11.648	1.101	0.001	1.210	7.784	0.773		
39	147.856	6.534	0.004	14.145	12.350	0.000	281.940	10.239
40	180.061	4.921	0.009	19.164	8.733	0.000	394.022	2.685
41	172.367	6.102	0.012	18.404	7.364	0.000	389.226	3.855
47	101.588	8.373	0.002	16.017	51.411	16.821	194.615	58.506
50	12.808	14.272	0.006	9.084	26.887	14.007		
51	187.848	14.956	0.007	35.308	25.410	10.531	626.686	1.685
103	104.647	3.291	0.003	13.501	16.161	1.153	263.055	1.127
104	55.607	0.918	0.003	9.404	5.038	0.000		
P2	145.943	11.965	0.006	20.094	53.979	2.392	419.149	3.671
P3	238.037	14.146	0.011	29.731	23.484	2.765	685.954	6.548

Table D.23 Measured dissolved metals in June, 2007.

Well ID	Li	Be	B	Na	Mg	Al	Si	P	K	Ca	Sc	v	Cr	Fe	Mn	Ni	Co
2	0.000	0.001	0.000	13.851	7.661	2.405	0.000	0.000	5.763	75.461	0.000	0.000	0.020	0.536	0.787	0.044	0.005
4	0.000	0.000	0.000	3.726	13.346	0.436	3.696	0.000	5.216	96.314	0.000	0.000	0.000	2.169	8.944	0.277	0.135
6	0.000	0.001	0.000	13.452	13.550	0.307	1.593	0.000	4.457	95.934	0.000	0.000	0.003	0.000	2.890	0.188	0.068
8	0.000	0.000	0.000	4.316	16.095	0.291	1.460	0.000	5.694	129.045	0.000	0.000	0.000	0.000	1.560	0.135	0.049
9	0.000	0.000	0.202	23.340	20.509	0.514	5.618	0.000	15.744	243.122	0.000	0.000	0.001	0.000	3.726	0.253	0.070
10	0.000	0.001	0.000	3.969	18.422	0.437	1.508	0.000	5.622	108.768	0.000	0.000	0.000	0.000	0.701	0.107	0.026
12	0.000	0.000	0.000	5.296	21.387	0.327	2.012	0.000	3.935	222.808	0.000	0.000	0.000	5.892	1.051	0.126	0.020
13	0.000	0.000	0.055	5.313	3.936	0.448	0.542	1.595	6.246	43.886	0.000	0.000	0.010	1.859	0.173	0.000	0.001
14	0.000	0.000	0.000	5.576	15.092	0.572	1.793	0.000	5.547	133.589	0.000	0.000	0.000	0.000	1.425	0.110	0.056
15	0.000	0.000	0.000	18.412	54.445	0.381	5.243	0.000	11.912	310.682	0.000	0.000	0.000	0.251	9.150	0.050	0.009
17	0.000	0.000	0.000	7.979	16.177	0.305	3.142	0.000	4.967	121.260	0.000	0.000	0.000	0.844	3.335	0.028	0.010
19	0.000	0.001	0.000	7.210	15.720	0.392	2.155	0.000	7.306	164.520	0.000	0.000	0.000	0.892	0.824	0.088	0.041
20	0.000	0.000	0.000	5.298	29.396	0.322	0.371	0.000	4.195	135.006	0.000	0.000	0.002	17.545	1.924	0.122	0.013
22	0.000	0.000	0.000	12.406	31.499	0.313	3.903	0.000	9.305	229.706	0.000	0.000	0.000	13.870	3.592	0.198	0.107
26	0.000	0.000	0.000	8.600	27.958	0.311	7.488	0.000	3.090	183.932	0.000	0.000	0.000	0.000	5.877	0.301	0.016
30	0.000	0.000	0.000	11.431	32.738	0.343	3.705	0.000	8.186	175.108	0.000	0.000	0.006	2.882	4.449	0.014	0.003
34	0.000	0.001	0.014	257.803	22.712	0.362	11.187	0.915	35.574	74.114	0.000	0.009	0.379	0.000	0.099	0.024	0.003
36	0.000	0.000	0.079	4341.270	97.462	0.605	3.504	0.000	110.188	958.646	0.000	0.014	0.132	2.253	3.040	0.365	0.049
37	0.000	0.001	0.000	37.092	9.017	0.310	0.377	0.000	10.632	11.784	0.000	0.000	0.050	0.000	0.037	0.020	0.001
38	0.000	0.000	0.000	7.559	2.228	0.391	0.000	0.000	2.781	12.816	0.000	0.000	0.012	0.000	0.029	0.000	0.000
39	0.000	0.000	0.000	12.805	19.321	0.428	3.938	0.000	8.656	173.373	0.000	0.000	0.008	3.181	2.016	0.056	0.041
40	0.000	0.000	0.000	7.053	25.806	0.471	4.809	0.000	7.859	201.970	0.000	0.000	0.005	8.064	2.317	0.073	0.043
41	0.000	0.000	0.000	6.543	23.508	0.326	3.512	0.000	7.802	198.866	0.000	0.000	0.000	4.468	2.137	0.144	0.076
47	0.000	0.000	0.000	66.576	21.024	2.559	4.716	0.287	9.703	118.998	0.000	0.000	0.008	2.234	3.668	0.043	0.017
50	0.000	0.000	0.670	33.788	12.220	2.730	1.415	0.409	17.750	12.858	0.000	0.000	0.012	2.446	0.276	0.022	0.008
51	0.000	0.000	0.115	35.226	50.800	1.345	1.748	0.000	20.170	231.644	0.000	0.000	0.002	0.000	0.327	0.071	0.004
103	0.000	0.000	0.000	10.357	12.826	6.487	3.067	0.000	5.675	88.376	0.000	0.000	0.008	3.164	3.331	0.190	0.079
104	0.000	0.000	0.000	3.032	13.622	0.491	3.108	0.000	3.208	70.027	0.000	0.000	0.000	0.000	0.010	0.001	0.000
P2	0.000	0.001	0.186	59.611	20.566	0.783	2.623	0.000	13.882	148.307	0.000	0.000	0.003	9.896	8.456	0.497	0.482
P3	0.000	0.000	0.006	24.357	29.401	0.246	5.116	0.000	14.322	225.891	0.000	0.000	0.000	33.696	16.302	0.588	0.658

Table D.23 Measured dissolved metals in June, 2004, contd.

Well ID	Cu	Zn	Ga	As	Se	Rb	Sr	Mo	Ag	Cd	Cs	Ba	Tb	Tl	Pb	Bi	U
2	0.000	3.894	0.001	0.001	0.000	0.004	0.144	0.004	0.000	0.000	0.000	0.030	0.000	0.001	0.004	0.000	0.001
4	0.000	0.000	0.000	0.005	0.001	0.003	0.161	0.002	0.000	0.000	0.000	0.070	0.000	0.000	0.003	0.000	0.001
6	0.000	0.000	0.000	0.000	0.003	0.003	0.141	0.001	0.000	0.000	0.000	0.018	0.000	0.000	0.000	0.000	0.000
8	0.000	0.143	0.000	0.000	0.000	0.003	0.184	0.002	0.000	0.000	0.000	0.022	0.000	0.000	0.002	0.000	0.001
9	0.000	0.000	0.000	0.007	0.003	0.008	0.335	0.008	0.000	0.000	0.000	0.042	0.000	0.000	0.002	0.000	0.006
10	0.000	0.000	0.000	0.001	0.000	0.004	0.156	0.004	0.000	0.000	0.000	0.017	0.000	0.000	0.004	0.000	0.002
12	0.000	0.000	0.000	0.000	0.002	0.004	0.302	0.001	0.000	0.000	0.000	0.024	0.000	0.000	0.004	0.000	0.001
13	0.000	0.000	0.000	0.000	0.002	0.001	0.060	0.001	0.000	0.000	0.000	0.007	0.000	0.000	0.007	0.000	0.000
14	0.000	0.000	0.000	0.002	0.000	0.002	0.156	0.003	0.000	0.000	0.000	0.026	0.000	0.000	0.005	0.000	0.002
15	0.000	0.000	0.000	0.002	0.000	0.008	0.553	0.006	0.000	0.000	0.000	0.056	0.000	0.000	0.005	0.000	0.018
17	0.000	0.000	0.000	0.002	0.000	0.002	0.164	0.001	0.000	0.000	0.000	0.025	0.000	0.000	0.002	0.000	0.002
19	0.000	0.000	0.000	0.004	0.004	0.002	0.198	0.021	0.000	0.000	0.000	0.022	0.000	0.000	0.004	0.000	0.002
20	0.000	0.000	0.000	0.000	0.000	0.001	0.159	0.004	0.000	0.000	0.000	0.023	0.000	0.000	0.000	0.000	0.001
22	0.000	0.000	0.000	0.003	0.000	0.004	0.276	0.003	0.000	0.000	0.000	0.041	0.000	0.000	0.002	0.000	0.002
26	0.000	0.000	0.000	0.001	0.001	0.001	0.224	0.001	0.000	0.000	0.000	0.016	0.000	0.000	0.002	0.000	0.001
30	0.000	0.000	0.000	0.004	0.000	0.005	0.345	0.004	0.000	0.000	0.000	0.034	0.000	0.000	0.002	0.000	0.015
34	0.000	0.000	0.001	0.015	0.004	0.056	0.327	0.028	0.000	0.000	0.002	0.001	0.000	0.015	0.000	0.000	0.004
36	0.055	0.000	0.000	0.018	0.075	0.059	2.760	0.015	0.000	0.002	0.000	0.262	0.000	0.005	0.011	0.000	0.001
37	0.000	0.000	0.000	0.002	0.004	0.016	0.027	0.098	0.000	0.000	0.000	0.000	0.000	0.004	0.005	0.000	0.003
38	0.000	0.000	0.000	0.000	0.000	0.002	0.029	0.121	0.000	0.000	0.000	0.007	0.000	0.004	0.007	0.000	0.000
39	0.210	0.000	0.000	0.007	0.000	0.004	0.223	0.004	0.000	0.000	0.000	0.031	0.000	0.004	0.041	0.000	0.002
40	0.000	0.000	0.000	0.006	0.006	0.005	0.277	0.003	0.000	0.000	0.000	0.001	0.000	0.040	0.004	0.000	0.004
41	0.000	0.000	0.000	0.007	0.000	0.005	0.222	0.010	0.000	0.000	0.000	0.034	0.000	0.002	0.003	0.000	0.001
47	0.161	0.000	0.000	0.002	0.001	0.008	0.290	0.017	0.000	0.000	0.000	0.050	0.000	0.002	0.012	0.000	0.007
50	0.000	0.000	0.000	0.000	0.003	0.024	0.017	0.149	0.000	0.000	0.001	0.017	0.000	0.001	0.009	0.000	0.000
51	0.000	0.000	0.000	0.001	0.000	0.012	0.310	0.976	0.000	0.001	0.001	0.024	0.000	0.001	0.003	0.000	0.007
103	0.253	0.336	0.001	0.004	0.001	0.007	0.159	0.004	0.000	0.000	0.001	0.075	0.000	0.001	0.028	0.000	0.002
104	0.000	0.000	0.000	0.000	0.000	0.001	0.088	0.002	0.000	0.000	0.000	0.012	0.000	0.001	0.001	0.000	0.002
P2	0.000	2.184	0.001	0.002	0.009	0.004	0.342	0.002	0.002	0.001	0.001	0.029	0.000	0.001	0.004	0.000	0.002
P3	0.000	0.000	0.000	0.001	0.000	0.002	0.422	0.001	0.000	0.000	0.000	0.024	0.000	0.001	0.001	0.000	0.003

Table D.24 Measured organic compounds in September, 2007.

Well ID	Benzene	Toluene	Ethyl benzene	M&P-Xylene	O-Xylene	BTEX	F1-BTEX
Concentration (mg/L)							
1	0.000	0.000	0.000	0.000	0.000	0.000	0.000
2	0.000	0.000	0.000	0.000	0.000	0.000	0.051
4	0.077	0.065	0.170	0.349	0.134	0.794	1.477
6	0.326	0.404	0.140	0.752	0.435	2.057	3.041
8	0.400	1.276	0.144	0.728	0.396	2.945	3.769
8	0.400	1.275	0.144	0.728	0.396	2.944	3.769
9	0.129	0.438	0.163	1.696	0.647	3.073	5.241
11	2.860	2.853	0.213	2.121	1.441	9.487	14.201
12	0.378	0.156	0.070	0.500	0.193	1.297	1.675
13	0.124	1.011	0.324	2.399	0.939	4.796	7.800
14	0.000	0.000	0.000	0.000	0.000	0.000	0.000
15	0.134	0.270	0.111	0.433	0.261	1.209	1.385
16	0.473	1.639	0.247	1.612	0.683	4.654	7.160
17	0.080	0.156	0.073	0.363	0.152	0.824	1.012
18	0.000	0.000	0.000	0.000	0.000	0.000	0.000
19	0.071	0.079	0.000	0.027	0.140	0.317	0.060
20	0.000	0.080	0.000	0.000	0.000	0.080	0.000
21	0.082	0.129	0.074	0.362	0.331	0.978	1.459
22	0.000	0.000	0.000	0.000	0.000	0.000	0.000
23	0.000	0.075	0.071	0.195	0.121	0.462	0.325
26	0.294	0.178	0.000	0.403	0.252	1.127	1.329
29	0.204	0.067	0.000	0.183	0.100	0.554	0.384
30	0.166	0.065	0.000	0.275	0.144	0.651	0.471
33	0.051	0.815	0.075	0.827	0.511	2.278	3.770
34	0.000	0.000	0.074	0.000	0.130	0.204	0.092
35	0.000	0.000	0.000	0.000	0.000	0.000	0.000
36	0.000	0.000	0.000	0.000	0.079	0.079	0.009
37	0.000	0.000	0.000	0.000	0.000	0.000	0.000
38	0.000	0.000	0.000	0.000	0.000	0.000	0.000
39	0.000	0.000	0.000	0.000	0.000	0.000	0.028
40	0.000	0.000	0.000	0.000	0.000	0.000	0.000
41	0.000	0.000	0.000	0.000	0.000	0.000	0.054
43	0.242	0.384	0.108	0.776	0.451	1.961	2.650
44	0.104	0.135	0.000	0.514	0.362	1.114	1.789
46	0.091	0.091	0.096	0.577	0.327	1.182	2.460
47	0.000	0.000	0.000	0.000	0.000	0.000	0.000
50	0.000	0.000	0.000	0.000	0.081	0.081	0.024
51	0.000	0.000	0.000	0.000	0.000	0.000	0.000
103	0.072	0.069	0.160	0.395	0.452	1.148	1.862
104	0.000	0.000	0.000	0.000	0.000	0.000	0.000
106	0.000	0.000	0.000	0.000	0.077	0.077	0.033
P1	0.000	0.000	0.000	0.000	0.000	0.000	0.000
P2	0.000	0.000	0.000	0.000	0.000	0.000	0.000
P3	0.000	0.000	0.000	0.139	0.000	0.139	0.276
P4	0.000	0.000	0.000	0.000	0.128	0.128	0.107
P5	0.090	0.000	0.000	0.297	0.113	0.500	0.599

Table D.25 Measured major ions in September, 2007.

Well ID	Calcium	Potassium	Lithium	Magnesium	Sodium	NH4+ as N	Bromide	Chloride	Fluoride	Nitrate	Sulphate
Concentration (mg/L)											
1	88.406	4.735	0.000	14.883	3.072	0.000	0.000	0.000	1.539	0.000	197.889
2	89.046	3.250	0.000	8.353	3.447	0.000	0.000	0.000	1.156	0.000	166.914
4	120.923	2.499	0.000	16.111	10.500	0.000	0.000	0.560	0.469	0.000	185.334
6	126.763	3.480	0.000	15.964	5.797	0.000	0.000	2.155	1.080	0.000	299.996
8	123.814	2.378	0.000	17.551	10.745	1.456	0.000	1.290	0.746	0.000	266.435
9	178.883	5.769	0.000	21.999	5.857	0.000	0.000	1.104	1.074	0.000	426.614
11	573.171	8.446	0.000	74.091	30.250	0.000	0.000	11.657	0.448	0.000	1495.080
12	170.026	2.421	0.000	27.715	11.804	0.000	0.000	0.971	0.905	0.000	260.211
13	184.280	6.147	0.000	32.686	7.546	0.000	30.508	2.856	1.257	0.000	517.846
14	208.583	6.699	0.000	17.598	6.846	0.000	0.000	2.634	0.405	0.000	375.080
15	166.952	8.351	0.000	19.191	19.450	4.549	0.000	4.092	0.783	0.000	495.439
16	142.063	5.483	0.000	17.815	15.764	0.000	0.000	9.926	0.000	0.000	264.588
17	51.698	2.802	0.000	7.212	27.113	0.000	0.000	23.806	0.724	100.695	48.262
18	137.021	5.651	0.000	14.727	6.487	0.000	0.000	1.564	0.000	0.000	263.248
19	153.103	5.997	0.000	13.001	5.087	0.000	0.000	1.015	0.677	0.000	265.026
20	66.409	2.343	0.000	11.988	4.559	0.000	0.000	0.927	0.000	0.000	160.559
21	214.858	34.127	0.000	19.708	50.155	0.000	0.000	8.610	0.418	0.000	548.421
22	104.963	5.422	0.000	10.011	18.296	0.000	0.000	5.655	0.000	0.000	167.503
23	175.512	9.533	0.000	15.633	16.392	0.000	0.000	2.172	0.000	0.000	294.083
26	132.060	2.430	0.000	18.922	8.765	0.000	0.000	8.383	0.000	0.000	255.953
29	150.841	4.528	0.000	23.002	12.730	0.000	0.000	10.094	0.000	0.000	240.832

Table D.25 Measured major ions in September, 2007, contd.

Well ID	Calcium	Potassium	Lithium	Magnesium	Sodium	NH4+ as N	Bromide	Chloride	Fluoride	Nitrate	Sulphate
Concentration (mg/L)											
30	168.271	7.577	0.000	27.043	14.061	10.784	0.000	4.453	0.000	0.000	334.841
33	154.485	3.720	0.000	19.219	10.791	0.000	0.000	3.435	0.000	0.000	253.666
34	30.927	10.395	0.000	64.824	86.806	48.748	0.000	40.990	0.000	0.000	252.869
35	165.902	9.136	0.000	19.235	34.153	0.000	0.000	13.304	0.000	0.000	348.976
36	148.743	13.339	0.000	15.164	64.623	0.000	0.000	46.321	0.000	0.000	338.310
37	184.283	28.810	0.000	21.780	72.757	0.000	0.000	22.417	0.000	0.000	492.170
38	28.559	4.268	0.000	13.500	11.982	8.749	0.000	6.755	0.000	0.000	69.790
39	151.165	6.578	0.000	14.050	6.372	0.000	0.000	1.374	0.000	0.000	243.694
40	162.040	7.576	0.000	20.950	9.089	1.957	0.000	3.915	0.000	0.000	266.406
41	144.186	10.355	0.000	19.054	29.250	0.000	0.000	27.785	0.742	0.000	268.902
43	155.926	8.741	0.000	21.935	54.100	28.657	0.000	24.667	0.000	0.000	320.793
44	144.685	11.706	0.000	22.959	68.327	41.971	0.000	28.772	0.000	0.000	335.336
46	124.322	5.934	0.000	23.084	36.916	15.569	0.000	17.071	0.000	0.000	229.718
47	118.388	7.133	0.000	17.711	26.163	10.156	0.000	19.246	0.000	8.185	192.007
50	33.790	9.643	0.000	20.817	17.826	15.466	0.000	1.642	0.000	0.000	80.654
51	209.308	14.938	0.000	108.260	55.852	7.380	0.000	4.644	0.485	3.789	914.145
103	132.733	4.713	0.000	15.848	5.018	0.000	0.000	4.064	0.503	0.000	151.883
104	107.751	2.613	0.000	16.469	3.945	0.000	0.000	0.447	0.000	0.000	189.535
107	246.665	5.813	0.000	12.276	4.548	0.000	0.000	0.664	0.000	0.000	560.821
P1	143.174	5.572	0.000	22.016	27.184	5.051	0.000	2.588	1.277	0.000	538.290
P2	104.461	10.586	0.000	16.083	44.485	4.000	0.000	3.266	0.980	0.000	258.882
P3	131.598	10.239	0.000	12.692	27.734	3.831	0.000	1.659	1.079	0.000	299.538
P4	115.737	11.378	0.000	11.990	17.973	0.000	0.000	1.998	1.280	0.000	149.825
P5	129.017	5.356	0.000	34.810	39.104	0.000	0.000	7.912	0.909	0.000	90.912

Table D.26. Measured dissolved metals in September, 2007.

Well ID	Li	Be	B	Na	Mg	Al	Si	P	k	Ca	V
Concentration (mg/L)											
1	0.000	0.001	0.000	0.724	19.671	0.000	0.000	0.216	6.163	100.318	0.000
2	0.000	0.000	0.000	1.635	10.447	0.000	0.078	0.937	4.403	95.011	0.000
4	0.000	0.000	0.000	2.862	18.750	0.000	6.570	0.273	5.643	126.239	0.000
6	0.000	0.000	0.000	5.241	19.785	0.000	2.286	0.315	4.596	136.561	0.000
8	0.000	0.000	0.000	5.205	26.221	0.000	3.228	0.000	6.842	161.948	0.000
9	0.000	0.000	0.000	4.998	30.150	0.000	4.795	0.152	7.444	196.579	0.000
11	0.000	0.000	0.000	15.475	76.845	0.000	18.969	0.664	11.962	499.006	0.000
12	0.000	0.001	0.000	4.099	35.403	0.000	13.752	0.000	6.102	188.897	0.000
13	0.000	0.000	0.000	6.250	51.080	0.000	0.341	0.000	8.151	220.482	0.000
14	0.000	0.000	0.000	4.040	14.990	0.000	3.817	2.827	6.702	108.527	0.000
15	0.000	0.000	0.000	19.157	25.573	0.000	2.490	2.327	10.601	184.235	0.000
16	0.000	0.001	0.000	12.304	23.047	0.000	5.368	0.456	7.932	161.890	0.000
17	0.000	0.000	0.000	20.119	9.421	0.000	1.388	0.309	4.463	57.159	0.000
18	0.000	0.001	0.000	5.089	21.252	0.000	0.529	0.828	9.144	167.357	0.000
19	0.000	0.000	0.000	3.989	18.166	0.000	3.001	0.797	7.583	176.468	0.000
20	0.000	0.000	0.000	2.797	17.360	0.000	0.000	0.063	4.361	86.412	0.000
21	0.000	0.000	0.000	43.114	25.802	0.000	3.740	0.685	33.637	225.856	0.000
22	0.000	0.001	0.000	11.640	14.292	0.000	3.188	0.000	8.250	115.253	0.000
23	0.000	0.000	0.000	14.736	21.739	0.000	2.226	0.014	11.324	187.693	0.000
26	0.000	0.000	0.000	6.490	31.278	0.000	7.714	0.351	4.975	185.200	0.000
29	0.000	0.000	0.000	11.264	29.555	0.000	4.415	0.233	6.210	166.984	0.000
30	0.000	0.001	0.000	11.726	35.109	0.000	2.737	0.000	7.570	167.199	0.000
33	0.000	0.001	0.000	8.380	24.468	0.000	4.126	1.394	6.060	184.013	0.000
34	0.000	0.001	0.000	80.991	80.538	0.000	4.365	2.999	11.130	63.551	0.000
35	0.000	0.002	0.000	23.185	24.689	0.000	2.943	0.513	9.030	165.342	0.000
36	0.000	0.000	0.000	38.657	18.456	0.000	0.953	1.144	11.765	150.574	0.000
37	0.000	0.284	39.838	74.428	4.754	10.946	594.898	437.933	528.149	187.060	1.751
38	0.000	0.000	0.000	11.001	17.842	0.000	0.000	0.879	4.772	30.029	0.000
39	0.000	0.001	0.000	5.015	19.634	0.000	4.601	0.112	9.340	175.293	0.000
40	0.000	0.002	0.000	6.775	26.623	0.000	4.681	0.000	9.292	178.913	0.000
41	0.000	0.000	0.000	9.676	25.558	0.000	4.675	1.557	12.738	162.417	0.000
43	0.000	0.000	0.000	0.000	55.450	27.714	0.000	6.199	0.691	9.934	0.000
44	0.000	0.001	0.000	64.743	29.780	0.000	11.100	2.290	13.117	153.684	0.000
46	0.000	0.000	0.000	37.913	29.882	0.000	17.376	3.669	7.804	135.459	0.000
47	0.000	0.000	0.000	24.953	24.060	0.000	3.282	0.108	9.613	133.412	0.000
50	0.000	0.000	0.000	16.506	57.260	0.000	1.273	0.877	12.946	61.509	0.000
51	0.000	0.002	0.000	58.813	161.951	0.000	1.859	0.209	17.596	221.389	0.000
P1	0.000	0.000	0.000	27.518	38.428	0.000	0.000	0.341	9.357	192.998	0.000
P2	0.000	0.001	0.000	52.797	28.122	0.000	3.775	0.001	12.289	131.362	0.000
P3	0.000	0.000	0.000	26.670	16.349	0.000	8.816	0.297	12.316	143.277	0.000
P4	0.000	0.000	0.000	15.256	16.831	0.000	6.233	0.000	12.225	132.994	0.000
P5	0.000	0.000	0.000	37.917	38.212	0.000	15.041	2.973	7.340	123.820	0.000

Table D.26. Measured dissolved metals in September, 2007, contd.

Well ID	Cr	Fe	Mn	Ni	Co	Zn	Ga	As	Se	Rb	Sr
Concentration (mg/L)											
1	0.000	0.371	0.218	0.023	0.010	0.116	0.000	0.000	0.000	0.001	0.098
2	0.002	2.828	0.480	0.008	0.007	0.234	0.000	0.000	0.000	0.001	0.131
4	0.000	25.924	22.758	0.195	0.134	0.000	0.000	0.006	0.000	0.002	0.245
6	0.000	5.491	8.461	0.229	0.093	0.189	0.000	0.001	0.000	0.002	0.165
8	0.000	3.985	7.843	0.097	0.040	0.059	0.000	0.016	0.000	0.003	0.250
9	0.000	11.978	5.134	0.104	0.061	0.171	0.000	0.001	0.000	0.003	0.249
11	0.000	1.685	142.731	1.942	2.016	0.410	0.001	0.005	0.005	0.008	0.747
12	0.000	41.437	18.302	0.044	0.071	0.000	0.000	0.045	0.000	0.000	0.286
13	0.000	4.305	1.283	0.230	0.053	0.007	0.000	0.000	0.000	0.001	0.257
14	0.029	17.439	1.084	0.034	0.023	0.292	0.000	0.002	0.018	0.002	0.130
15	0.020	6.243	6.172	0.264	0.037	0.235	0.000	0.001	0.000	0.004	0.296
16	0.003	12.098	16.956	0.069	0.043	0.036	0.000	0.004	0.000	0.002	0.204
17	0.000	0.567	0.215	0.000	0.003	0.053	0.000	0.000	0.000	0.000	0.049
18	0.009	16.418	1.143	0.009	0.002	0.094	0.000	0.000	0.000	0.001	0.215
19	0.001	13.794	1.545	0.108	0.076	0.040	0.000	0.005	0.000	0.003	0.208
20	0.000	0.715	1.020	0.024	0.008	0.125	0.000	0.000	0.000	0.000	0.088
21	0.005	6.575	3.605	0.065	0.058	0.137	0.000	0.011	0.002	0.002	0.401
22	0.004	4.862	2.441	0.091	0.046	0.000	0.000	0.004	0.000	0.002	0.153
23	0.004	1.787	1.102	0.018	0.023	0.000	0.000	0.012	0.000	0.000	0.268
26	0.005	12.712	8.089	0.049	0.016	0.180	0.000	0.002	0.000	0.000	0.217
29	0.004	4.223	4.231	0.021	0.007	0.000	0.000	0.005	0.008	0.001	0.302
30	0.000	1.238	3.605	0.000	0.003	0.000	0.000	0.013	0.000	0.003	0.388
33	0.009	3.585	12.949	0.230	0.168	0.169	0.000	0.000	0.000	0.002	0.231
34	0.026	9.265	2.600	0.000	0.016	0.262	0.000	0.002	0.003	0.000	0.138
35	0.000	3.335	2.110	0.062	0.017	0.000	0.000	0.000	0.012	0.001	0.262
36	0.000	7.205	2.090	0.077	0.093	0.000	0.000	0.000	0.000	0.001	0.231
37	9.399	2245.334	1.150	0.000	0.036	62.675	0.077	1.061	26.275	0.076	1.749
38	0.013	5.121	0.124	0.000	0.001	0.000	0.000	0.000	0.000	0.002	0.035
39	0.004	10.325	2.914	0.000	0.008	0.000	0.000	0.010	0.000	0.005	0.199
40	0.000	12.478	3.972	0.001	0.008	0.000	0.000	0.004	0.000	0.005	0.212
41	0.008	17.075	2.856	0.040	0.041	0.108	0.000	0.004	0.000	0.009	0.201
43	0.005	2.651	16.672	1.464	0.063	0.066	0.000	0.000	0.000	0.006	0.232
44	0.041	22.243	12.638	1.323	0.164	0.143	0.000	0.004	0.000	0.007	0.280
46	0.036	56.460	15.557	1.333	0.828	0.162	0.000	0.025	0.000	0.004	0.189
47	0.002	1.145	3.720	0.062	0.031	0.000	0.000	0.000	0.000	0.004	0.241
50	0.000	15.526	1.746	0.000	0.022	0.000	0.000	0.002	0.000	0.009	0.075
51	0.003	15.706	2.422	0.045	0.017	0.000	0.000	0.000	0.000	0.003	0.446
P1	0.000	16.013	4.150	0.087	0.015	0.173	0.000	0.000	0.000	0.001	0.331
P2	0.000	0.966	3.812	0.235	0.119	0.019	0.000	0.000	0.007	0.001	0.265
P3	0.002	36.880	6.604	0.149	0.222	0.000	0.000	0.002	0.000	0.000	0.252
P4	0.000	15.547	4.623	0.060	0.073	0.000	0.000	0.005	0.000	0.004	0.262
P5	0.018	32.455	13.518	0.065	0.047	0.284	0.000	0.002	0.008	0.000	0.212

Table D.26. Measured dissolved metals in September, 2007, contd.

Well ID	Mo	Ag	Cd	In	Cs	Ba	Tb	Tl	Pb	U
Concentration (mg/L)										
1	0.001	0.000	0.000	0.000	0.000	0.000	0.000	0.000	0.000	0.011
2	0.003	0.000	0.000	0.000	0.000	0.000	0.000	0.000	0.000	0.002
4	0.006	0.000	0.000	0.000	0.000	0.027	0.000	0.000	0.000	0.008
6	0.000	0.000	0.001	0.000	0.000	0.000	0.000	0.000	0.000	0.003
8	0.003	0.000	0.000	0.000	0.000	0.000	0.000	0.000	0.000	0.010
9	0.002	0.000	0.000	0.000	0.000	0.000	0.000	0.000	0.000	0.003
11	0.004	0.000	0.002	0.000	0.000	0.071	0.000	0.000	0.000	0.012
12	0.003	0.000	0.000	0.000	0.000	0.063	0.000	0.000	0.000	0.014
13	0.000	0.000	0.000	0.000	0.000	0.000	0.000	0.000	0.000	0.010
14	0.001	0.000	0.000	0.000	0.000	0.000	0.000	0.000	0.000	0.002
15	0.005	0.001	0.001	0.000	0.000	0.000	0.000	0.000	0.000	0.002
16	0.002	0.000	0.000	0.000	0.000	0.000	0.000	0.000	0.000	0.005
17	0.000	0.000	0.000	0.000	0.000	0.000	0.000	0.000	0.000	0.001
18	0.003	0.000	0.000	0.000	0.000	0.000	0.000	0.000	0.000	0.001
19	0.002	0.000	0.000	0.000	0.000	0.000	0.000	0.000	0.000	0.004
20	0.000	0.000	0.000	0.000	0.000	0.000	0.000	0.000	0.000	0.000
21	0.004	0.000	0.000	0.000	0.000	0.000	0.000	0.000	0.065	0.007
22	0.003	0.000	0.000	0.000	0.000	0.000	0.000	0.000	0.065	0.003
23	0.003	0.000	0.000	0.000	0.000	0.000	0.000	0.000	0.000	0.005
26	0.001	0.000	0.000	0.000	0.000	0.000	0.000	0.000	0.000	0.002
29	0.002	0.000	0.000	0.000	0.000	0.000	0.000	0.000	0.000	0.007
30	0.004	0.000	0.000	0.000	0.000	0.000	0.000	0.000	0.000	0.008
33	0.001	0.000	0.000	0.000	0.000	0.000	0.000	0.000	0.000	0.002
34	0.027	0.000	0.000	0.000	0.000	0.000	0.000	0.000	0.000	0.002
35	0.004	0.000	0.000	0.000	0.000	0.000	0.000	0.000	0.000	0.003
36	0.025	0.000	0.000	0.000	0.000	0.000	0.000	0.000	0.000	0.003
37	0.262	0.092	0.898	0.000	0.024	1.166	0.000	0.004	0.000	0.008
38	0.060	0.000	0.000	0.000	0.000	0.000	0.000	0.000	0.000	0.000
39	0.001	0.000	0.000	0.000	0.000	0.000	0.000	0.000	0.000	0.003
40	0.001	0.000	0.000	0.000	0.000	0.000	0.000	0.000	0.000	0.001
41	0.004	0.000	0.000	0.000	0.000	0.000	0.000	0.000	0.000	0.003
43	0.000	0.000	0.000	0.000	0.000	0.000	0.000	0.000	0.000	0.002
44	0.005	0.000	0.000	0.000	0.000	0.000	0.000	0.000	0.000	0.004
46	0.001	0.000	0.000	0.000	0.000	0.001	0.000	0.000	0.000	0.005
47	0.006	0.000	0.000	0.000	0.000	0.000	0.000	0.000	0.000	0.007
50	0.063	0.000	0.000	0.000	0.000	0.000	0.000	0.000	0.000	0.000
51	0.160	0.000	0.000	0.000	0.000	0.000	0.000	0.000	0.000	0.041
P1	0.007	0.000	0.000	0.000	0.000	0.000	0.000	0.000	0.000	0.000
P2	0.003	0.000	0.000	0.000	0.000	0.000	0.000	0.000	0.000	0.003
P3	0.000	0.000	0.000	0.000	0.000	0.000	0.000	0.000	0.000	0.004
P4	0.003	0.000	0.000	0.000	0.000	0.000	0.000	0.000	0.000	0.005
P5	0.004	0.000	0.000	0.000	0.000	0.000	0.000	0.000	0.000	0.009

References

- Fingas, M., 2001. The basics of oil spill cleanup. Ed. J. Charles, Lewis Publishers, CRC Press LLC, London.
- Pichtel, J., 2007. Fundamentals of site remediation for metal and hydrocarbon-contaminated soils. 2nd Ed. The Scarecrow Press Inc., Toronto.
- Van Stempvoort D., Biggar K.W., Iwakun O., Bickerton G., Voralek J., 2006. Characterization of Fuel Spill Plumes in Fractured Rock at a Permafrost Site: Colomac Mine, NWT. 2005/2006 Program Progress Report, April 2006, National Water Research Institute and University of Alberta.
- Werner, E.R., 2000. Applications of Environmental Chemistry. Lewis Publishers, CRC Press LLC, London.

**APPENDIX E: SELECTED IMAGES OF THE BEDROCK CORES
AND WELL-BORE IMAGES**



Figure E.1 Bedrock core sample from monitoring well (MW) 48 at the camp area.



Figure E.2 Sample of bedrock core from MW 41 at the warehouse area.



Figure E.3 Rotary percussion drilling machine used for coring and installation of new monitoring wells (MWs) in 2007 at the site.



Figure E.4 Well-vu camera setup in MW 6 at the tank farm area.

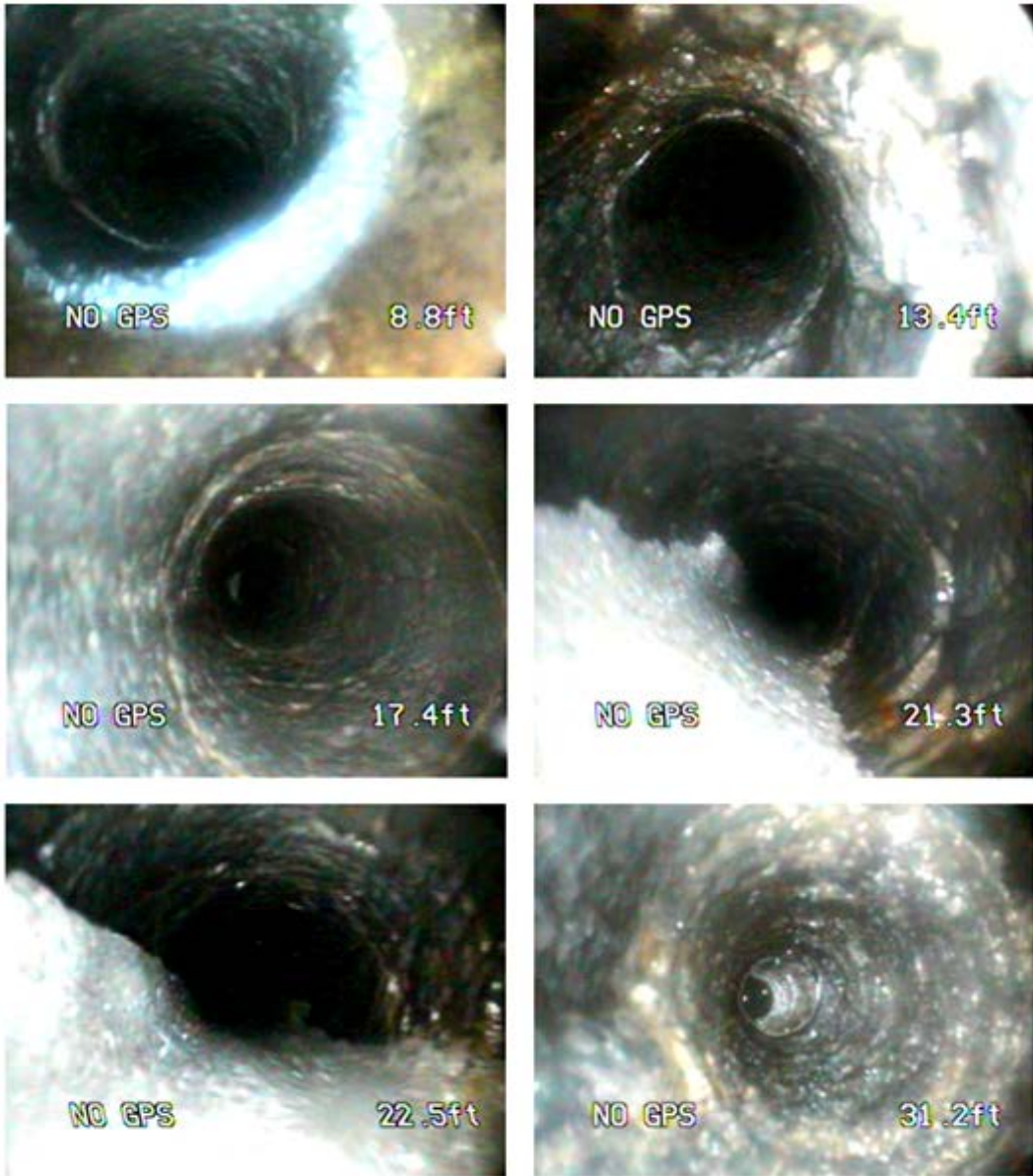


Figure E.5 Snapshots of well-bore from MW 26 north of the tank farm area

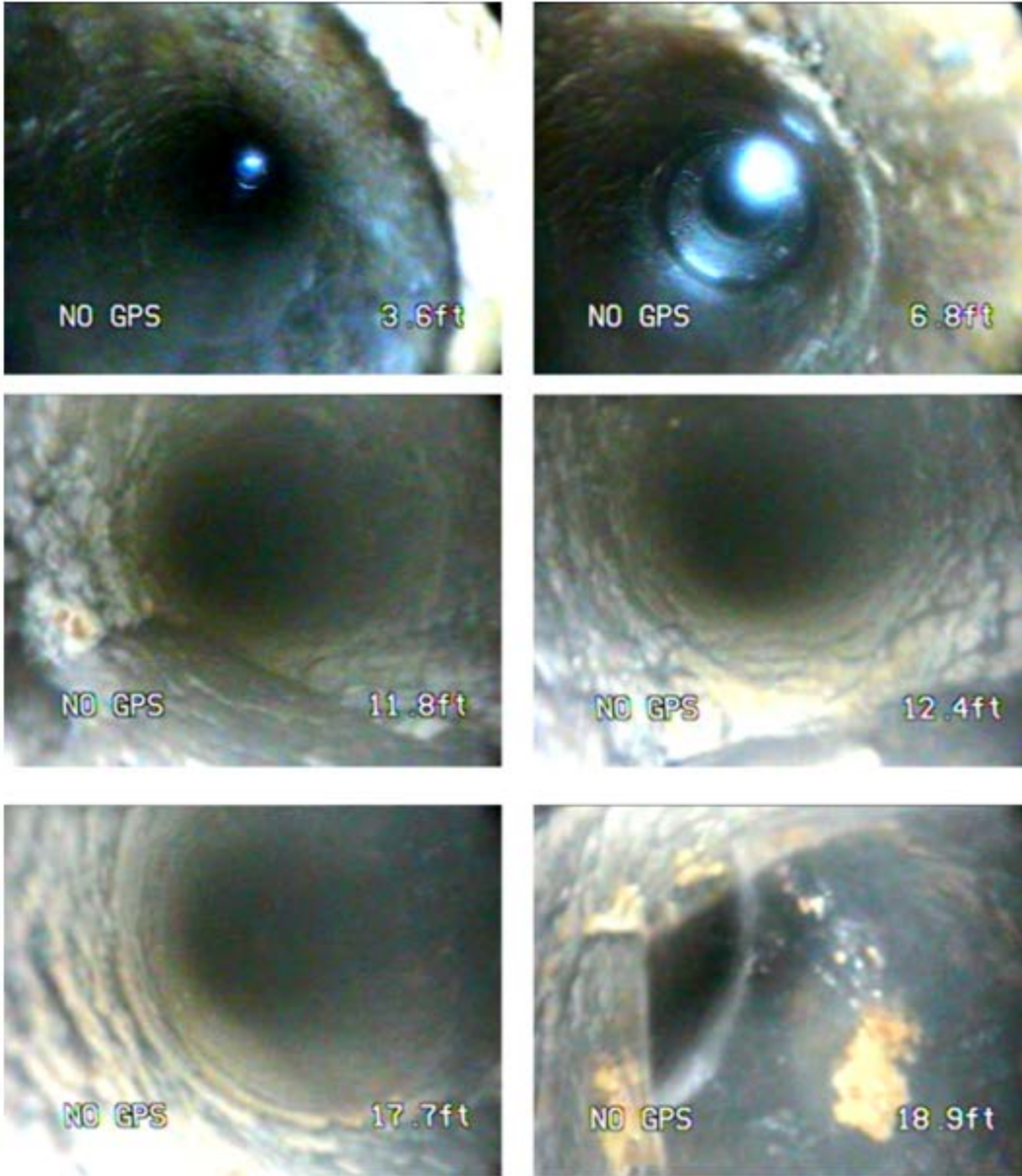


Figure E.6 Snapshots of well-bore from MW 04 at the tank farm area.

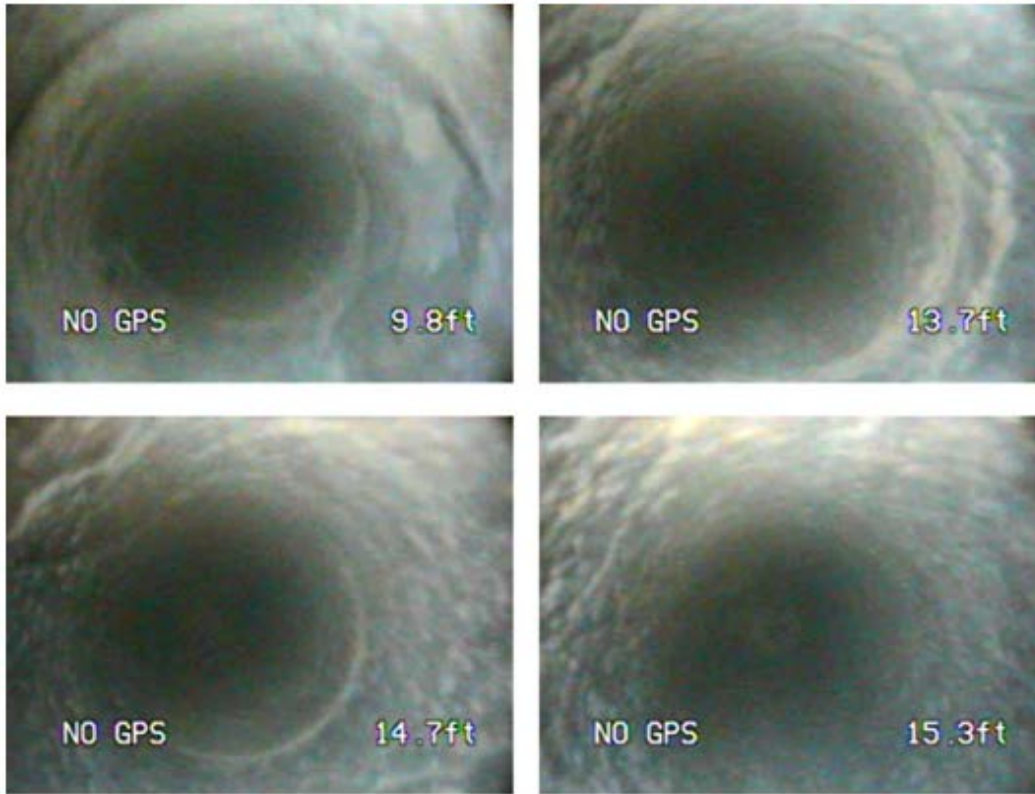


Figure E.7 Snapshots of well-bore from MW 08 at the tank farm area.

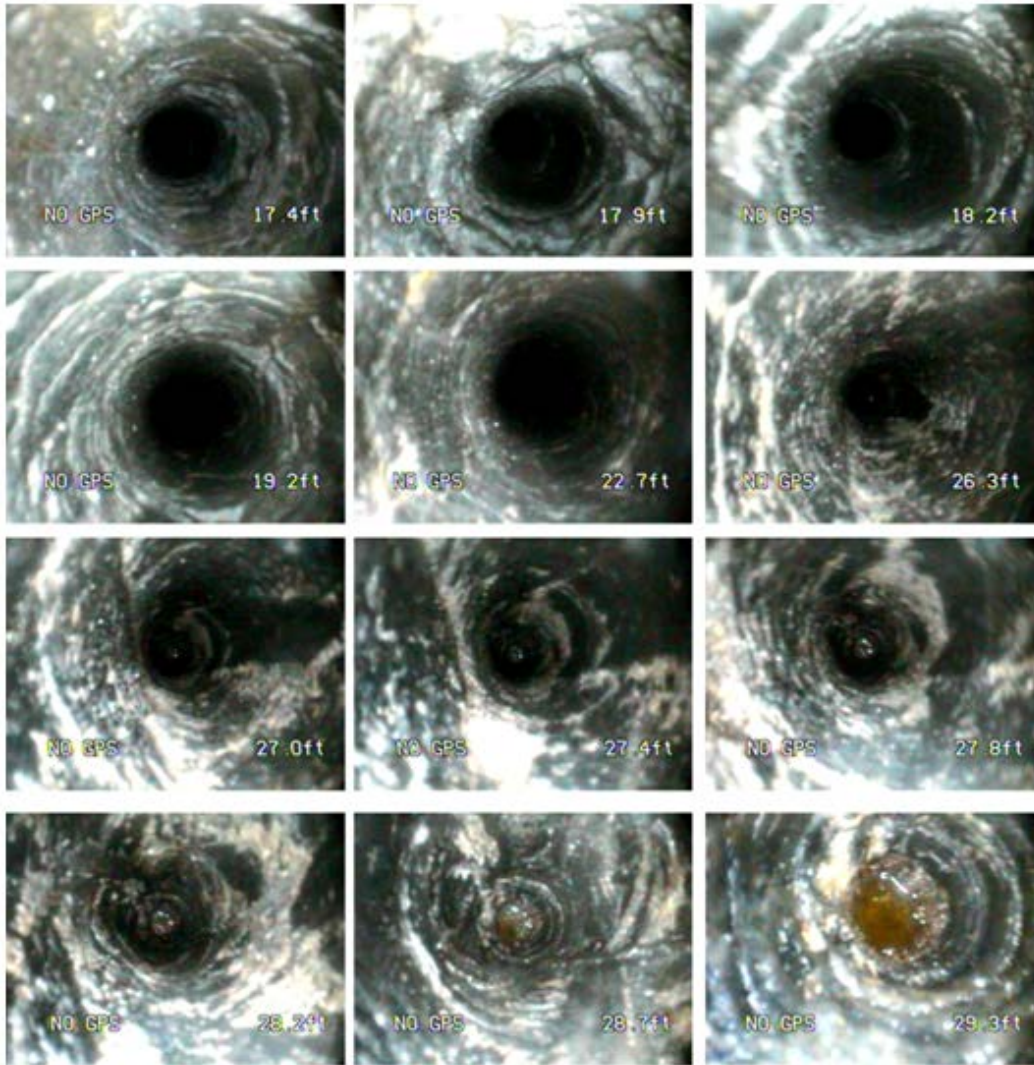


Figure E.8 Snapshots of well-bore from MW 11 east of the tank farm area, close to shoreline of Steeves Lake.

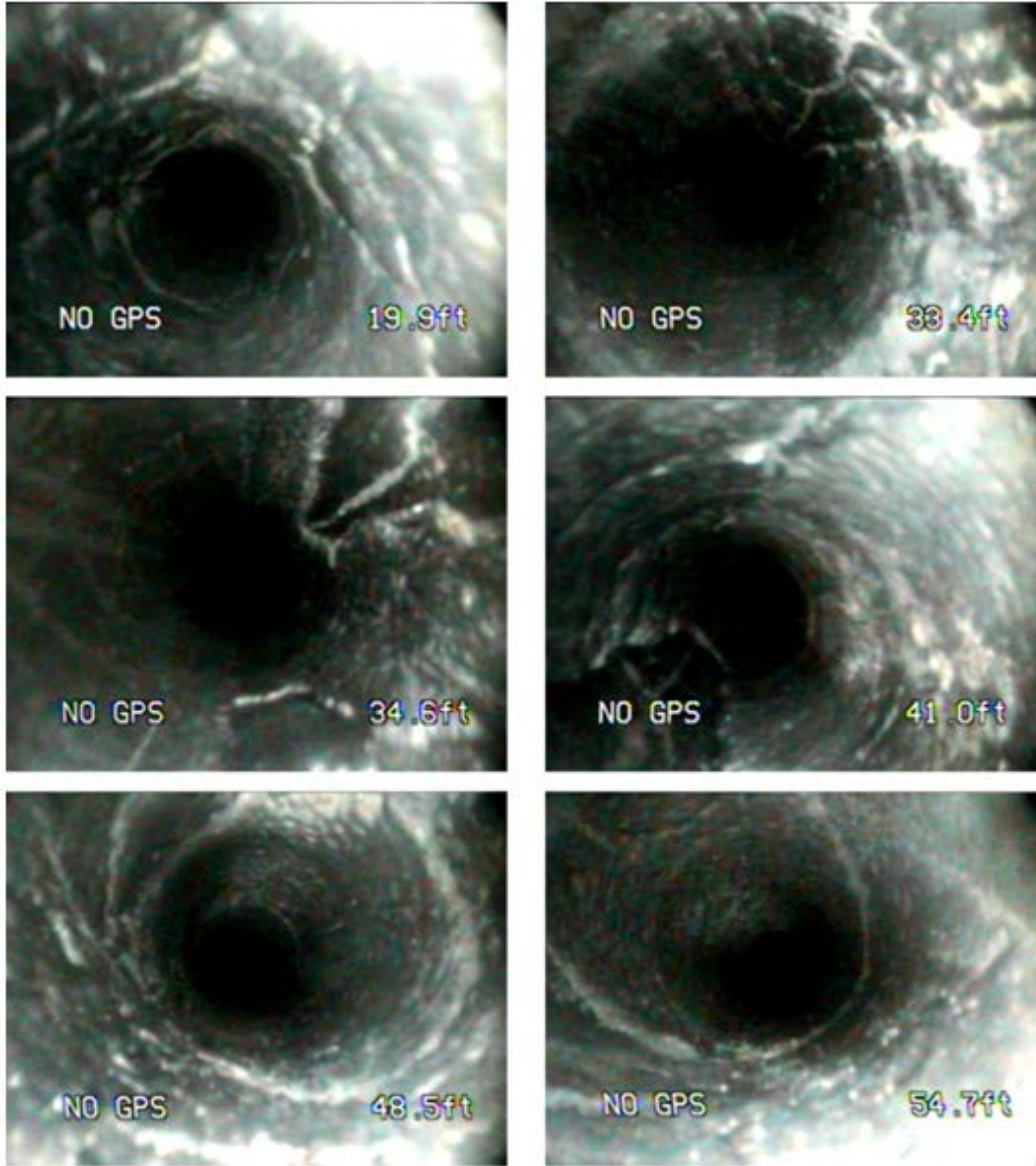


Figure E.9 Snapshots of well-bore from MW 27 at between the tank farm and shoreline of Steeves Lake.

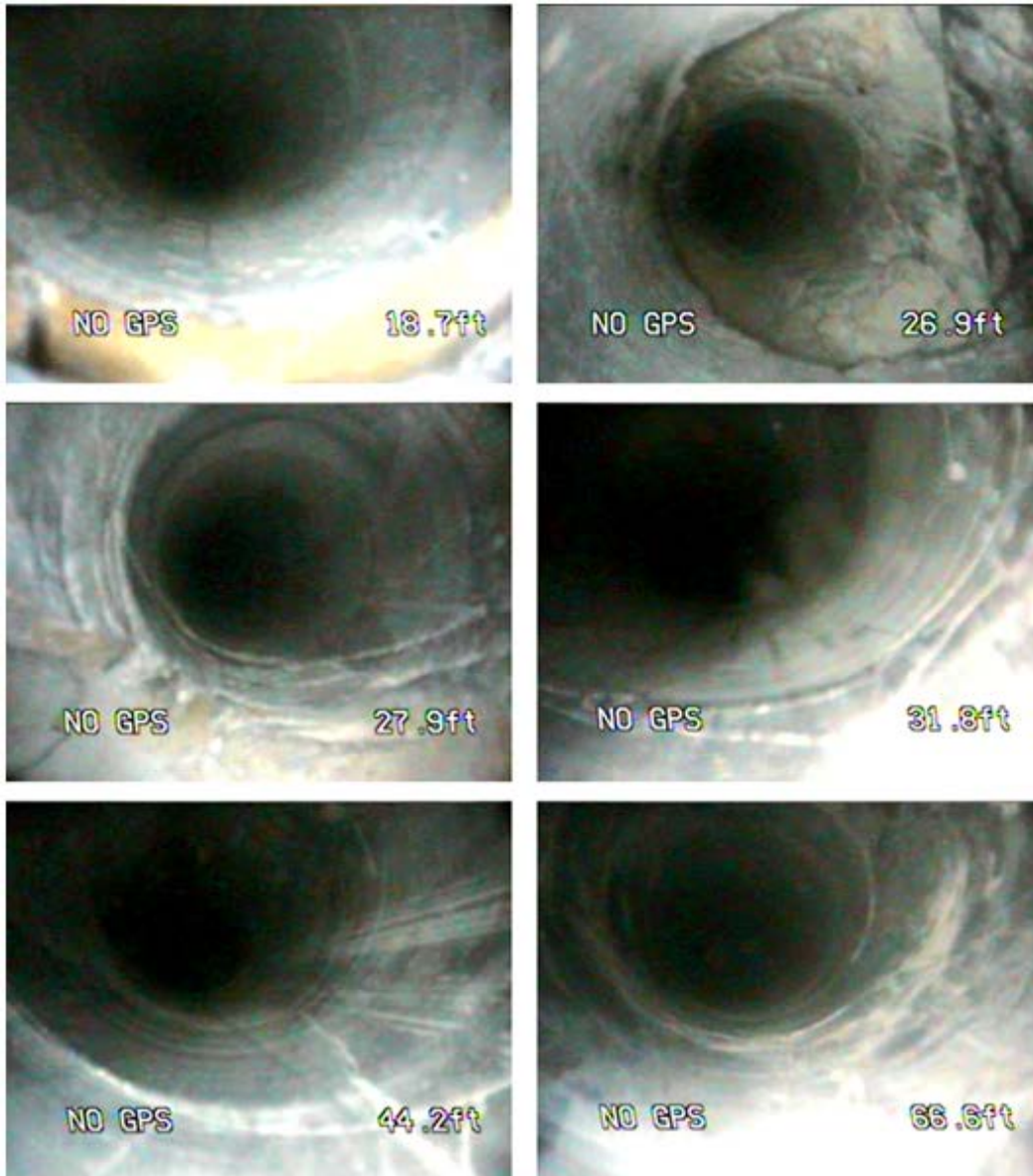


Figure E.10 Snapshots of well-bore from MW 41 at the warehouse area.

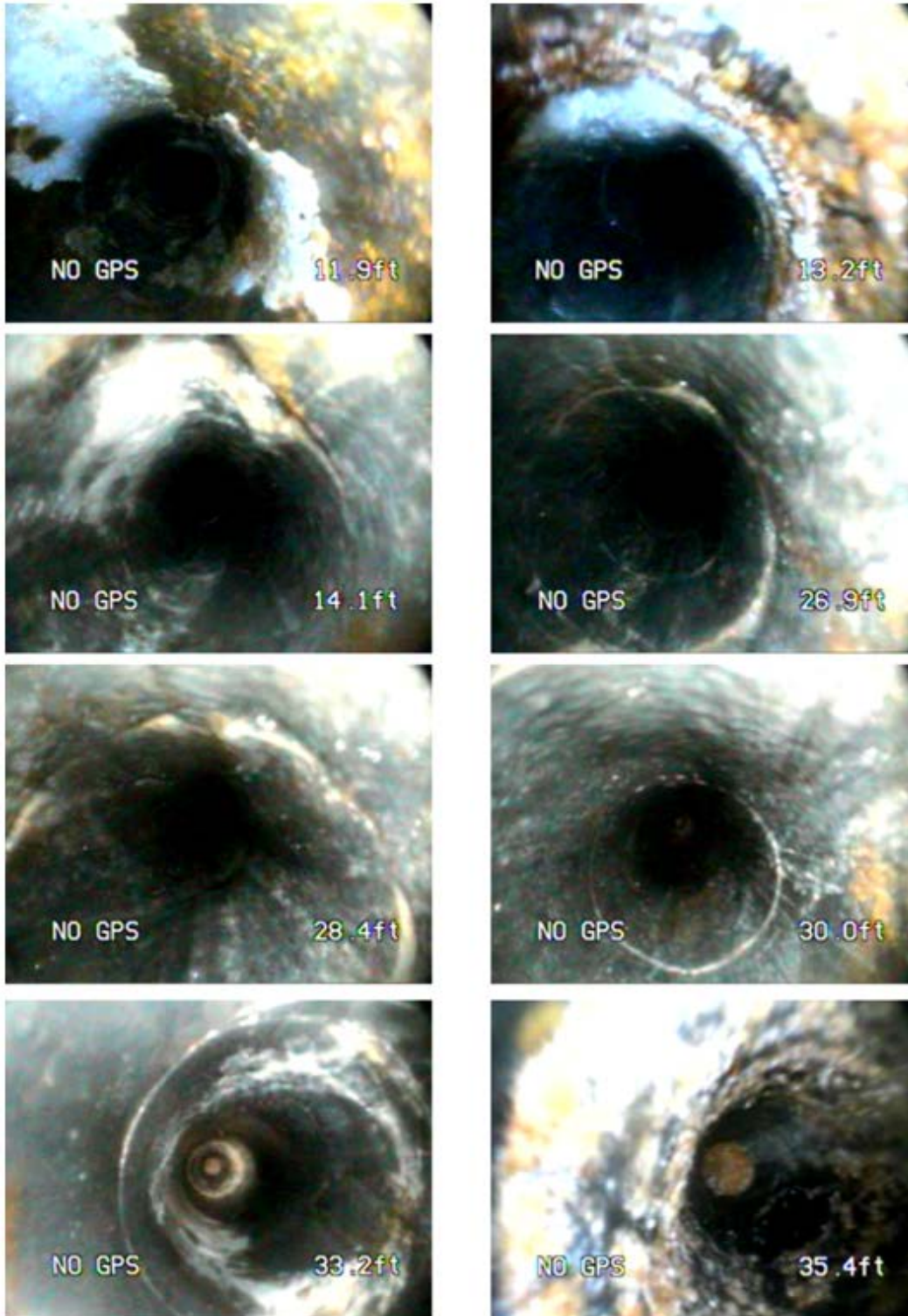


Figure E.11 Snapshots of well-bore from MW 44 at the tank farm area.

**APPENDIX F: SAMPLE CALCULATIONS AND PHREEQC DATA
FILES**

Kruskal-Wallis Test

Kruskal-Wallis test is a non-parametric statistical test developed as an alternative to F-test for comparing means of grouped data of independent observations. The advantage of the test over F-test is that it does not require normal distribution of the observations in each population or data sets. The procedure for performing the test for grouped data sets is outlined below:

1. Choose the level of significance (α) for the test.
2. Pool the grouped data sets and rank the parameters or observations (X_{ij}) in each data set from 1 to the total number of observations (N) in the pooled data. When two or more observations are equal, an average of the rank (R) is assigned to each of them. The data ranking must satisfy the condition below:

$$\text{Sum of rank} = \sum_{i=1}^{n_i} \sum_{j=1}^k R_{ij} = \frac{N(N+1)}{2} \quad \text{G.1}$$

Where R_{ij} is the rank of each observation (X_{ij}) for i ranging from 1..... n_i , and j ranging from 1..... k . The number of data sets or populations is k and n_i stands for the size of each data set.

3. Regroup the data sets and replace the parameters or observations with the rank (R) number.
4. Determine the test statistic (H) for the data sets using the equations below (Montgomery and Runger, 2003):

$$H = \frac{12}{N(N+1)} \left(\sum_{j=1}^k \frac{\left(\sum_{i=1}^{n_i} R_{ij} \right)^2}{n_i} \right) - 3(N+1) \quad \text{G.2}$$

Alternative equations when two or more observations are tied are:

$$H = \frac{1}{S^2} \left(\sum_{j=1}^k \frac{\left(\sum_{i=1}^{n_i} R_{ij} \right)^2}{n_i} - \frac{N(N+1)^2}{4} \right) \quad \text{G.3}$$

$$S^2 = \frac{1}{N+1} \left(\sum_{j=1}^k \sum_{i=1}^{n_i} R_{ij}^2 - \frac{N(N+1)^2}{4} \right)$$

5. Compare the test statistic (H) with the tabulated value in chi-square (χ^2) table for the chosen significant level (α) and degree of freedom ($\nu = k - 1$) for the test. If $H < H_{tabulated}$, the grouped data sets are not statistically different. However, if $H > H_{tabulated}$, the data sets are statistically different.

Sample analyses for the measured sulfate and BTEX compounds are given in Tables F.1 to F.5., and the results agree with the outputs of the STATSOFT STATISTICA® software used for the analyses. The chi-square table is given in Table F.6. For the test statistic (H), there is an equivalent probability such that $H > H_{tabulated}$ corresponds to $p < \alpha$ and vice versa. The probability values are calculated by the software program and reported in Chapter 5. The equations for the calculation of the equivalent probability to a test statistic are not given in most statistical textbooks and beyond the scope of this study.

Table F.1 Sulfate data used for the analyses.

Area	Sulfate	Rank	Area	Sulfate	Rank	Area	Sulfate	Rank
Powerhouse	71.2	2	Steeves lake	160.6	8	Tank farm	185.3	11
Powerhouse	72.2	3	Steeves lake	227.4	20	Tank farm	197.5	12
Powerhouse	90.9	4	Steeves lake	269.0	25	Tank farm	206.1	14
Powerhouse	149.8	7	Steeves lake	273.9	27	Tank farm	212.9	16
Powerhouse	162.5	9	Steeves lake	312.1	35	Tank farm	222.8	19
Powerhouse	164.4	10	Steeves lake	332.2	36	Tank farm	247.6	21
Powerhouse	212.4	15	Steeves lake	334.8	37	Tank farm	256.0	23
Powerhouse	219.7	17	Steeves lake	355.8	39	Tank farm	260.2	24
Powerhouse	419.1	50	Steeves lake	380.7	44	Tank farm	271.1	26
Powerhouse	489.7	55	Steeves lake	458.6	54	Tank farm	282.8	31
Powerhouse	538.3	57	Steeves lake	495.4	56	Tank farm	288.6	32
Powerhouse	686.0	60				Tank farm	296.5	33
Powerhouse	907.0	61				Tank farm	358.0	40
Powerhouse	1187.0	63				Tank farm	377.5	43
						Tank farm	431.3	52
						Tank farm	647.5	59
Area	Sulfate	Rank	Sulfate	Sulfate	Rank			
Upgradient	100.0	5	Warehouse	48.3	1			
Upgradient	108.0	6	Warehouse	205.0	13			
Upgradient	626.7	58	Warehouse	221.6	18			
Upgradient	914.1	62	Warehouse	248.6	22			
			Warehouse	276.9	28			
			Warehouse	279.8	29			
			Warehouse	281.9	30			
			Warehouse	304.9	34			
			Warehouse	348.9	38			
			Warehouse	371.7	41			
			Warehouse	375.1	42			
			Warehouse	386.0	45			
			Warehouse	389.2	46			
			Warehouse	392.1	47			
			Warehouse	394.0	48			
			Warehouse	411.6	49			
			Warehouse	429.9	51			
			Warehouse	440.4	53			

Table F.2 Kruskal-Wallis analyses for sulfate.

S/N	Powerhouse	Steeves lake	Tank farm	Upgradient	Warehouse	Rank (R)
1	2	8	11	5	1	
2	3	20	12	6	13	
3	4	25	14	58	18	
4	7	27	16	62	22	
5	9	35	19		28	
6	10	36	21		29	
7	15	37	23		30	
8	17	39	24		34	
9	50	44	26		38	
10	55	54	31		41	
11	57	56	32		42	
12	60		33		45	
13	61		40		46	
14	63		43		47	
15			52		48	
16			59		49	
17					51	
18					53	
Sum	413	381	456	131	635	2016
n	14	11	16	4	18	63
R ² /n	12183.50	13196.45	12996.00	4290.25	22401.39	65067.59
v	4	H _{tabulated}	9.488	α=5%	H	1.65355
Using Equation (G.3)						
S.N	Powerhouse	Steeves Lake	Tank farm	Upgradient	Warehouse	R ²
1	4	64	121	25	1	
2	9	400	144	36	169	
3	16	625	196	3364	324	
4	49	729	256	3844	484	
5	81	1225	361		784	
6	100	1296	441		841	
7	225	1369	529		900	
8	289	1521	576		1156	
9	2500	1936	676		1444	
10	3025	2916	961		1681	
11	3249	3136	1024		1764	
12	3600		1089		2025	
13	3721		1600		2116	
14	3969		1849		2209	
15			2704		2304	
16			3481		2401	
17					2601	
18					2809	
Sum	20837	15217	16008	7269	26013	85344
n	14	11	16	4	18	63
					S ²	336
v	4	H _{tabulated}	9.488	α=5%	H	1.65355

Table F.3 BTEX data used for the analyses.

Area	BTEX	Rank	Area	BTEX	Rank	Area	BTEX	Rank
Warehouse	0.000	10	Steeves lake	0.000	10	Tank farm	0.000	10
Warehouse	0.000	10	Steeves lake	0.030	22	Tank farm	0.000	10
Warehouse	0.000	10	Steeves lake	0.080	26	Tank farm	0.026	21
Warehouse	0.000	10	Steeves lake	0.300	38	Tank farm	0.050	24
Warehouse	0.000	10	Steeves lake	0.331	40	Tank farm	0.077	25
Warehouse	0.000	10	Steeves lake	0.405	48	Tank farm	0.154	32
Warehouse	0.013	20	Steeves lake	0.554	55	Tank farm	0.201	33
Warehouse	0.226	35	Steeves lake	0.651	60	Tank farm	0.370	42
Warehouse	0.317	39	Steeves lake	0.729	61	Tank farm	0.389	44
Warehouse	0.462	50	Steeves lake	1.209	72	Tank farm	0.396	47
Warehouse	0.563	56	Steeves lake	1.324	74	Tank farm	0.460	49
Warehouse	0.608	57	Steeves lake	1.939	82	Tank farm	0.496	51
Warehouse	0.619	58	Steeves lake	2.237	85	Tank farm	0.525	54
Warehouse	0.648	59	Steeves lake	2.260	86	Tank farm	0.780	62
Warehouse	0.785	63	Steeves lake	2.278	87	Tank farm	0.794	64
Warehouse	0.824	65	Steeves lake	4.218	94	Tank farm	1.114	68
Warehouse	0.978	66	Steeves lake	4.654	96	Tank farm	1.127	69
Warehouse	1.358	75	Steeves lake	4.961	98	Tank farm	1.148	70
Warehouse	1.361	76	Steeves lake	5.084	99	Tank farm	1.297	73
Warehouse	1.434	77	Steeves lake	9.487	104	Tank farm	1.961	83
Warehouse	1.508	78	Steeves lake	9.506	105	Tank farm	2.057	84
Warehouse	1.524	79	Upgradient	0.000	10	Tank farm	2.847	88
Warehouse	1.660	80	Upgradient	0.000	10	Tank farm	2.945	89
Warehouse	1.666	81	Upgradient	0.000	10	Tank farm	3.054	90
Warehouse	3.073	91	Upgradient	0.000	10	Tank farm	4.022	93
Warehouse	3.180	92	Upgradient	0.000	10	Tank farm	4.229	95
Warehouse	4.796	97	Upgradient	0.000	10	Tank farm	5.959	101
Warehouse	5.411	100	Upgradient	0.154	31	Tank farm	6.262	102
Warehouse	8.666	103	Powerhouse	0.000	10	Powerhouse	0.204	34
Warehouse	10.955	106	Powerhouse	0.000	10	Powerhouse	0.258	36
Warehouse	16.355	107	Powerhouse	0.000	10	Powerhouse	0.268	37
Warehouse	20.712	108	Powerhouse	0.031	23	Powerhouse	0.360	41
Camp area	0.000	10	Powerhouse	0.127	27	Powerhouse	0.388	43
Camp area	1.182	71	Powerhouse	0.128	28	Powerhouse	0.390	45
Powerhouse	0.503	53	Powerhouse	0.139	29	Powerhouse	0.393	46
Powerhouse	1.001	67	Powerhouse	0.144	30	Powerhouse	0.50035	52

Table F.4 Kruskal-Wallis analyses for BTEX using equation G.2.

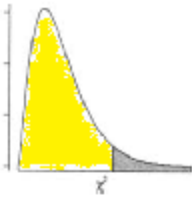
S/N	Camp area	Powerhouse	Steeves lake	Tank farm	Upgradient	Warehouse	Rank (R)
1	10	10	10	10	10	10	
2	71	10	22	10	10	10	
3		10	26	21	10	10	
4		23	38	24	10	10	
5		27	40	25	10	10	
6		28	48	32	10	10	
7		29	55	33	31	20	
8		30	60	42		35	
9		34	61	44		39	
10		36	72	47		50	
11		37	74	49		56	
12		41	82	51		57	
13		43	85	54		58	
14		45	86	62		59	
15		46	87	64		63	
16		52	94	68		65	
17		53	96	69		66	
18		67	98	70		75	
19			99	73		76	
20			104	83		77	
21			105	84		78	
22				88		79	
23				89		80	
24				90		81	
25				93		91	
26				95		92	
27				101		97	
28				102		100	
29						103	
30						106	
31						107	
32						108	
Sum	81	621	1442	1673	91	1978	5886
n	2	18	21	28	7	32	108
R ² /n	3280.50	21424.50	99017.33	99961.75	1183.00	122265.13	347132.21
v	5		H _{tabulated}	11.07	α=5%	H	26.855

Table F.5 Kruskal-Wallis analyses for BTEX using equation G.3.

S/N	Camp area	Powerhouse	Steeves Lake	Tank farm	Upgradient	Warehouse	
1	100	100	100	100	100	100	
2	5041	100	484	100	100	100	
3		100	676	441	100	100	
4		529	1444	576	100	100	
5		729	1600	625	100	100	
6		784	2304	1024	100	100	
7		841	3025	1089	961	400	
8		900	3600	1764		1225	
9		1156	3721	1936		1521	
10		1296	5184	2209		2500	
11		1369	5476	2401		3136	
12		1681	6724	2601		3249	
13		1849	7225	2916		3364	
14		2025	7396	3844		3481	
15		2116	7569	4096		3969	
16		2704	8836	4624		4225	
17		2809	9216	4761		4356	
18		4489	9604	4900		5625	
19			9801	5329		5776	
20			10816	6889		5929	
21			11025	7056		6084	
22				7744		6241	
23				7921		6400	
24				8100		6561	
25				8649		8281	
26				9025		8464	
27				10201		9409	
28				10404		10000	
29						10609	
30						11236	
31						11449	
32						11664	Sum
Sum	5141	25577	115826	121325	1561	155754	425184
n	2	18	21	28	7	32	108
R2/n	13214941	36343496	638841061	525705558	348103	758103391	1972556549
						S2	975.673
v	5		H _{tabulated}	11.07	α=5%	H	27.002

χ^2

Table F.6 Chi-square distribution table (after Stephens, 1998)



df	Area in the Right Tail under the Chi-square Distribution Curve									
	.995	.990	.975	.950	.900	.100	.050	.025	.010	.005
1	0.000	0.000	0.001	0.004	0.016	2.706	3.841	5.024	6.635	7.879
2	0.010	0.020	0.051	0.103	0.211	4.605	5.991	7.378	9.210	10.597
3	0.072	0.115	0.216	0.352	0.584	6.251	7.815	9.348	11.345	12.838
4	0.207	0.297	0.484	0.711	1.064	7.779	9.488	11.143	13.277	14.860
5	0.412	0.554	0.831	1.145	1.610	9.236	11.070	12.833	15.086	16.750
6	0.676	0.872	1.237	1.635	2.204	10.645	12.592	14.449	16.812	18.548
7	0.989	1.239	1.690	2.167	2.833	12.017	14.067	16.013	18.475	20.278
8	1.344	1.646	2.180	2.733	3.490	13.362	15.507	17.535	20.090	21.955
9	1.735	2.088	2.700	3.325	4.168	14.684	16.919	19.023	21.666	23.589
10	2.156	2.558	3.247	3.940	4.865	15.987	18.307	20.483	23.209	25.188
11	2.603	3.053	3.816	4.575	5.578	17.275	19.675	21.920	24.725	26.757
12	3.074	3.571	4.404	5.226	6.304	18.549	21.026	23.337	26.217	28.300
13	3.565	4.107	5.009	5.892	7.042	19.812	22.362	24.736	27.688	29.819
14	4.075	4.660	5.629	6.571	7.790	21.064	23.685	26.119	29.141	31.319
15	4.601	5.229	6.262	7.261	8.547	22.307	24.996	27.488	30.578	32.801
16	5.142	5.812	6.908	7.962	9.312	23.542	26.296	28.845	32.000	34.267
17	5.697	6.408	7.564	8.672	10.085	24.769	27.587	30.191	33.409	35.718
18	6.265	7.015	8.231	9.390	10.865	25.989	28.869	31.526	34.805	37.156
19	6.844	7.633	8.907	10.117	11.651	27.204	30.144	32.852	36.191	38.582
20	7.434	8.260	9.591	10.851	12.443	28.412	31.410	34.170	37.566	39.997
21	8.034	8.897	10.283	11.591	13.240	29.615	32.671	35.479	38.932	41.401
22	8.643	9.542	10.982	12.338	14.041	30.813	33.924	36.781	40.289	42.796
23	9.260	10.196	11.689	13.091	14.848	32.007	35.172	38.076	41.638	44.181
24	9.886	10.856	12.401	13.848	15.659	33.196	36.415	39.364	42.980	45.559
25	10.520	11.524	13.120	14.611	16.473	34.382	37.652	40.646	44.314	46.928
26	11.160	12.198	13.844	15.379	17.292	35.563	38.885	41.923	45.642	48.290
27	11.808	12.879	14.573	16.151	18.114	36.741	40.113	43.195	46.963	49.645
28	12.461	13.565	15.308	16.928	18.939	37.916	41.337	44.461	48.278	50.993
29	13.121	14.256	16.047	17.708	19.768	39.087	42.557	45.722	49.588	52.336
30	13.787	14.953	16.791	18.493	20.599	40.256	43.773	46.979	50.892	53.672
40	20.707	22.164	24.433	26.509	29.051	51.805	55.758	59.342	63.691	66.766
50	27.991	29.707	32.357	34.764	37.689	63.167	67.505	71.420	76.154	79.490
60	35.534	37.485	40.482	43.188	46.459	74.397	79.082	83.298	88.379	91.952
70	43.275	45.442	48.758	51.739	55.329	85.527	90.531	95.023	100.425	104.215
80	51.172	53.540	57.153	60.391	64.278	96.578	101.879	106.629	112.329	116.321

Sample of PHREEQC Input Data

```

1 TITLE Test 9.--Inverse modeling of Colomac mine site
2 SOLUTION_SPREAD
3   -units      mg/l
4 Number  pH   Si  Ca  Mg  Na  K   Alkalinity  S(6)   Cl  Fe  O(0)   pe
5 1    7.0 0.1 0.05  0.05  0.05  0.05  0.05  0.5 0.05  0.05  0.00  6.0 12
6 2    7.1 2.4 167 19.2  19.5  8.3 137 495.4  4.1 2.1  1.0 -1
7
8 INVERSE_MODELING 1
9   -solutions 1 2
10  -uncertainty 0.15
11  -range
12  -phases
13      Halite
14      Gypsum
15      CO2(g)
16      Pyrite
17      Albite
18      Sepiolite
19      Melanterite
20      Quartz
21      Dolomite
22      Calcite
23      Biotite
24      Plagioclase
25      Siderite
26  -balance
27      Ca      0.05      0.025
28
29 PHASES
30
31 Halite
32   NaCl = Na+ + Cl-
33   log_k  0.0
34
35 Biotite
36   KMg3AlSi3O10(OH)2 + 6H+ + 4H2O = K+ + 3Mg+2 + Al(OH)4- + 3H4SiO4
37   log_k  0.0
38
39 Plagioclase
40   Na0.62Ca0.38Al1.38Si2.62O8 + 5.52 H+ + 2.48H2O = \
41     0.62Na+ + 0.38Ca+2 + 1.38Al+3 + 2.62H4SiO4
42   log_k  0.0
43 END
44

```

Sample of PHREEQC output data

```

11363 Phase mole transfers:
11364     Halite      1.143e-04    9.676e-05    1.319e-04    NaCl
11365     Pyrite     2.322e-03    2.019e-03    2.589e-03    FeS2
11366     Albite     1.502e-03    1.212e-03    1.791e-03    NaAlSi3O8
11367     Melanterite -2.575e-04   -7.916e-04    5.313e-04    FeSO4:7H2O
11368     Quartz     -1.848e-03   -2.208e-03   -1.488e-03    SiO2
11369     Dolomite    2.731e-04   -5.930e-05    3.697e-04    CaMg(CO3)2
11370     Calcite     4.472e-03    4.227e-03    4.893e-03    CaCO3
11371     Biotite     2.112e-04    1.791e-04    2.432e-04    KMg3AlSi3O10(OH)2
11372     Plagioclase -1.241e-03   -1.474e-03   -1.008e-03    Na0.62Ca0.38Al1.38Si2.62O8
11373     Siderite    -2.027e-03   -2.507e-03   -1.754e-03    FeCO3
11374     O2(g)       7.971e-03    6.878e-03    8.938e-03    O2
11375
11376 Redox mole transfers:
11377     Fe(3)       -1.428e-10
11378     O(0)        1.625e-02
11379     S(-2)       4.644e-03
11380
11381 Sum of residuals (epsilons in documentation):      7.427e+00
11382 Sum of delta/uncertainty limit:                  7.427e+00
11383 Maximum fractional error in element concentration: 1.500e-01
11384 =====
11385
11386
11387 Summary of inverse modeling:
11388
11389     Number of models found: 121
11390     Number of minimal models found: 82
11391     Number of infeasible sets of phases saved: 411
11392     Number of calls to c11: 3645
11393 -----
11394 End of simulation.
11395 -----
11396
11397 -----
11398 Reading input data for simulation 2.
11399 -----
11400
11401 -----
11402 End of run.
11403 -----

```

References

Montgomery, D.C., Runger, G.C., 2003. Applied statistics and probability for engineers. 3rd Edition. John Wiley and Sons Inc., New York.

Stephens, L.J., 1998. Theory and problems of beginning statistics. Shaum's outline series, McGraw-Hill, New York.

APPENDIX G: SAMPLE IMAGES FROM LABORATORY TESTS



Figure G.1 Sample image of the saturated freezing cell filed with admixture of water and BAND-ADE Sawing fluid at 12% volume ratio with water. Fluorescein was added for coloring.

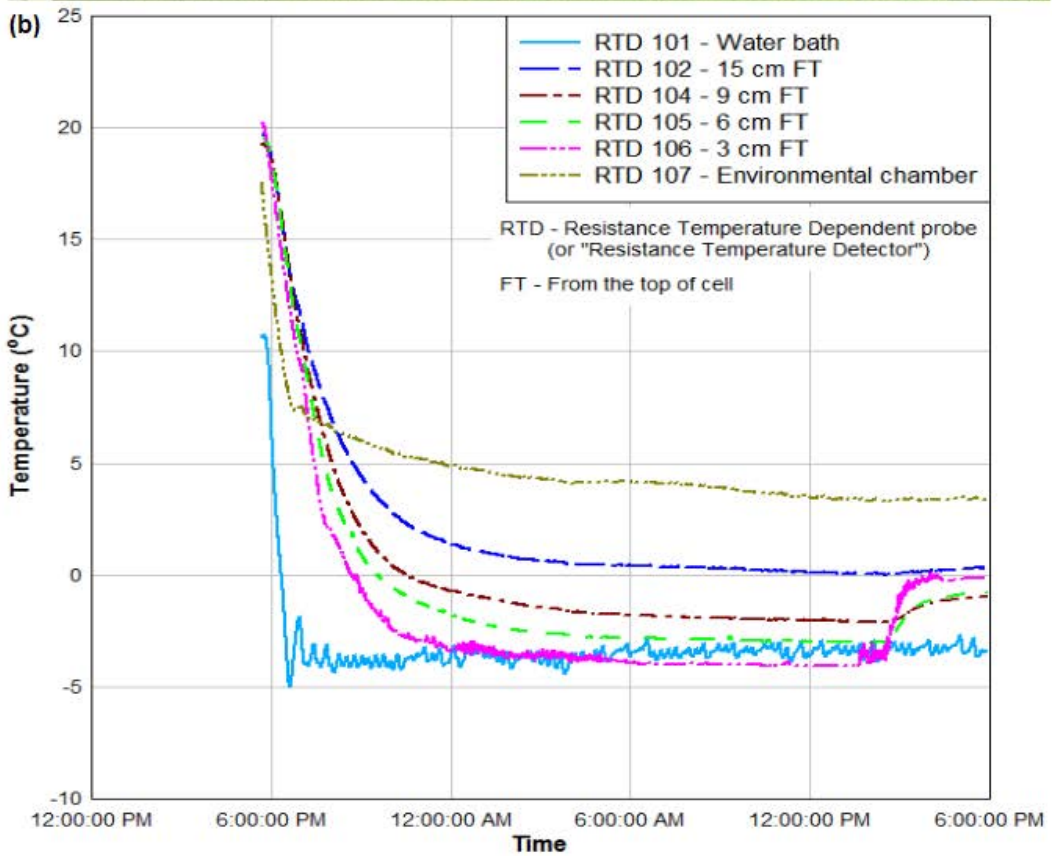
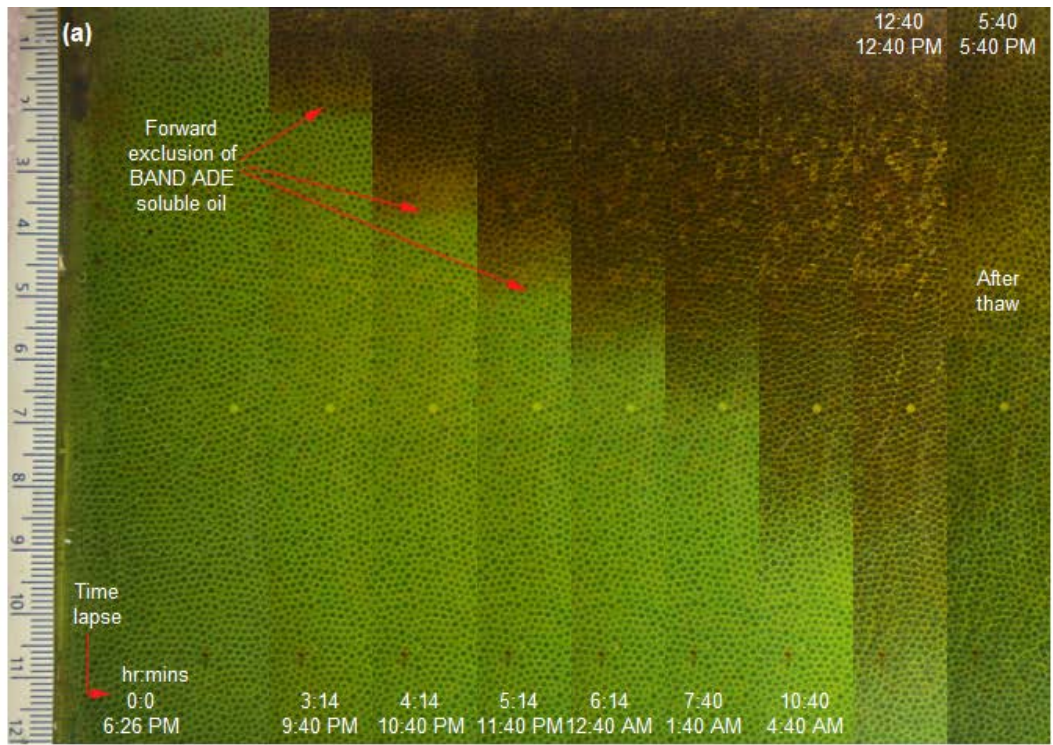


Figure G.2 Freezing test results using BAND ADE® soluble oil showing (a) cryogenic exclusion forward of freezing front and (b) temperature profile.

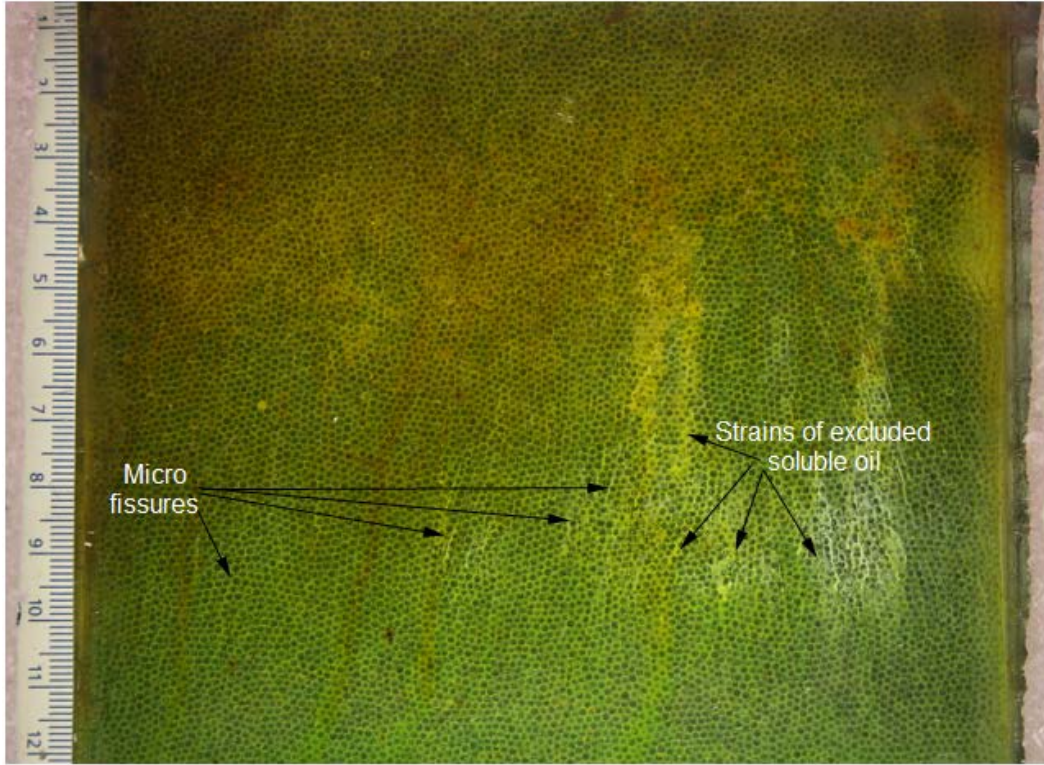


Figure G.3 Observed micro fissures in freezing experiment using BAND ADE® soluble oil after thaw.

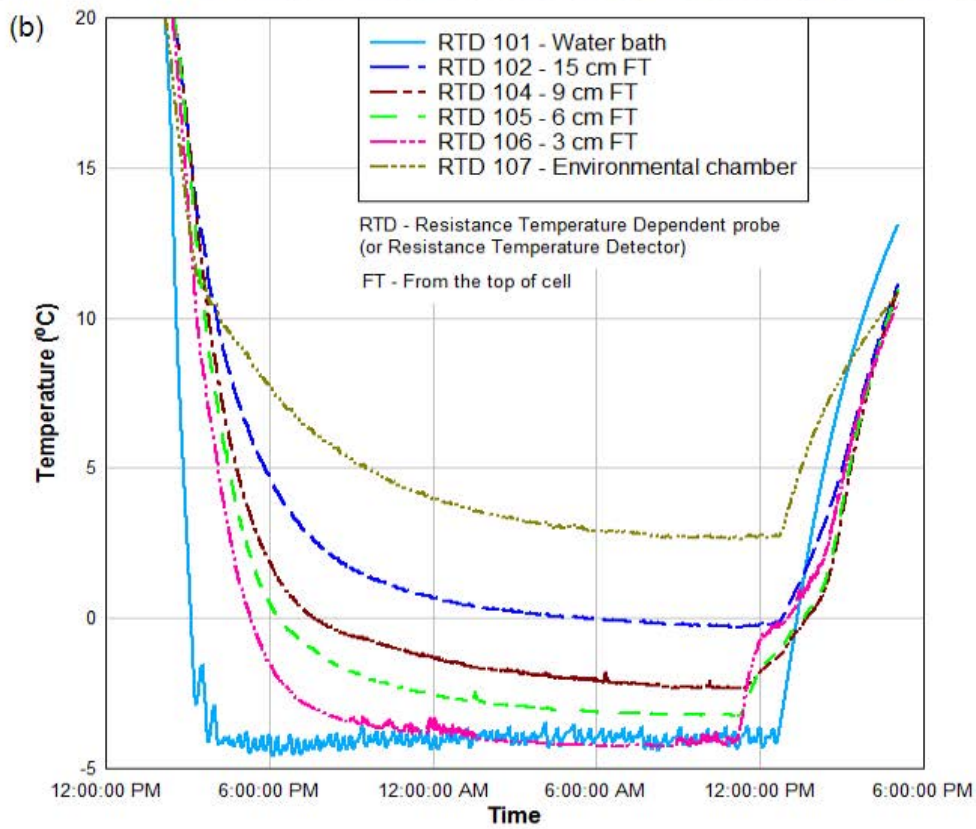
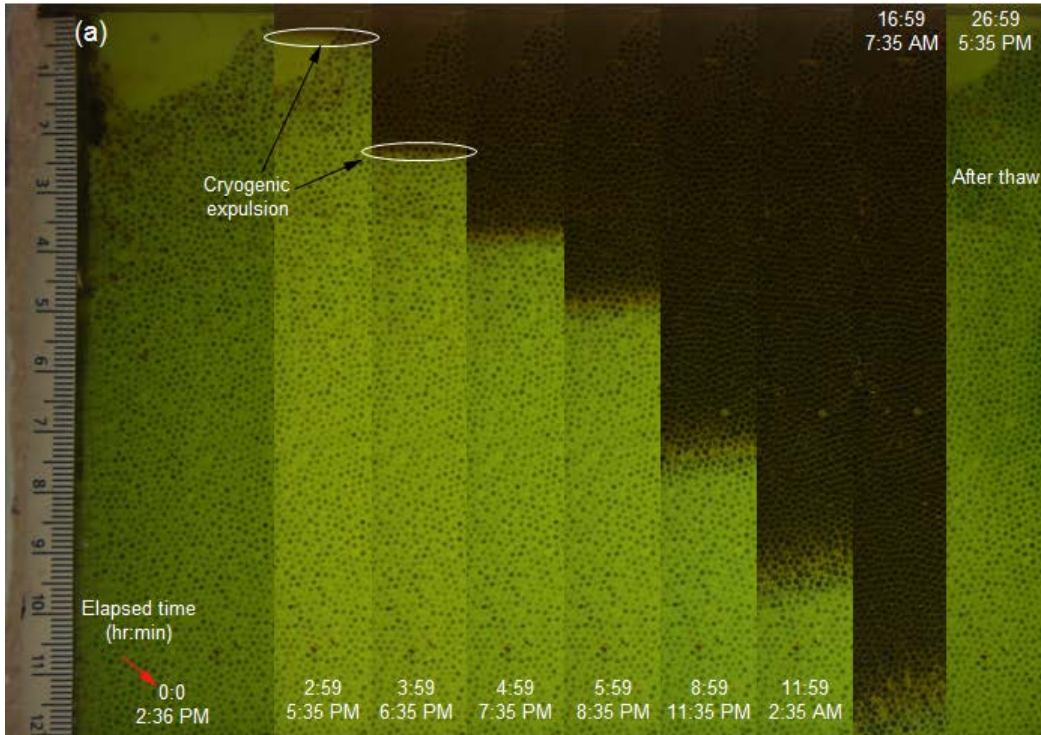


Figure G.4 Freezing test results using Mobilcut-102 at 2% volume ratio to water showing (a) cryogenic exclusion, and (b) temperature profile.

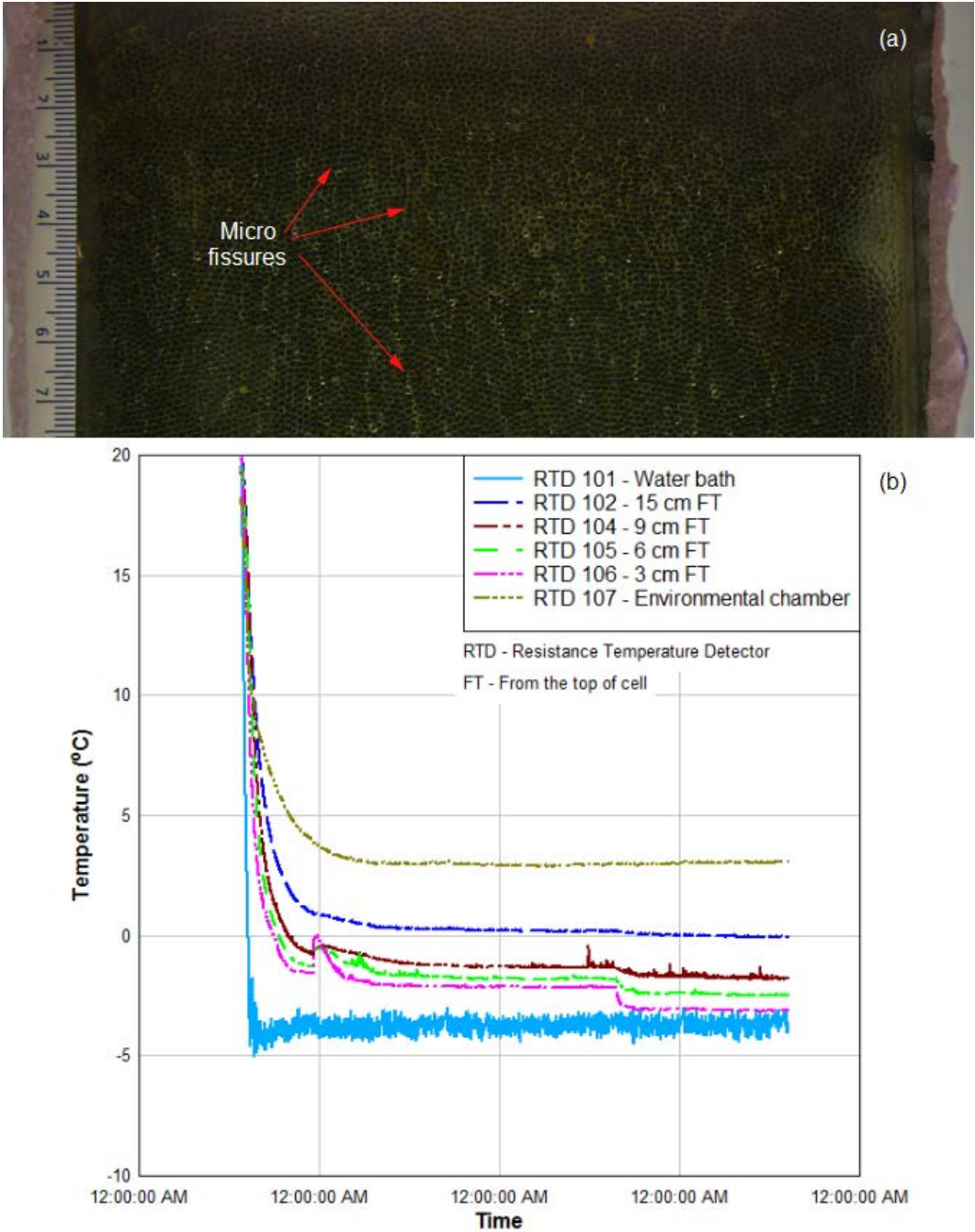


Figure G.5 Freezing test results using only fluorescein-water showing (a) micro fissures development, and (b) temperature profile.

Table G.1 Sample calculation using data used to plot Figure 7.8

Time (date hr:min)	RTD-102 (°C)	RTD-106 (°C)	Dt (hr:min)	DT/DX	Frost front "X" (mm)	Exclusion Front "E" mm)	DX/Dt (cm/day)	DT/Dt (°C/day)	DE/Dt (cm/day)
12/17/09 14:12	20.263	19.724		0.045					
12/17/09 15:12	16.085	15.217	1:00	0.072					
12/17/09 16:12	9.851	6.916	1:00	0.245					
12/17/09 16:22	9.141	5.911	0:10	0.269	3	0	43.2	11.628	
12/17/09 17:12	6.351	2.371	0:50	0.332	15	17	34.6	11.462	49.0
12/17/09 18:12	4.145	0.262	1:00	0.324	28	31	31.2	10.096	33.6
12/17/09 19:12	2.748	-0.608	1:00	0.280	39	45	26.4	7.383	33.6
12/17/09 20:12	1.884	-1.277	1:00	0.263	50	56	26.4	6.954	26.4
12/17/09 21:12	1.343	-1.304	1:00	0.221	58	66	19.2	4.235	24.0
12/17/09 22:12	0.971	-2.025	1:00	0.250	65	72	16.8	4.194	14.4
12/17/09 23:12	0.711	-2.291	1:00	0.250	72	81	16.8	4.203	21.6
12/18/09 0:12	0.548	-2.411	1:00	0.241	77	87	12.0	2.895	14.4
12/18/09 1:12	0.412	-2.300	1:00	0.226	82	93	12.0	2.712	14.4
12/18/09 2:12	0.311	-2.589	1:00	0.242	86	98	9.6	2.320	12.0
12/18/09 3:12	0.208	-2.743	1:00	0.246	90	103	9.6	2.361	12.0
12/18/09 4:12	0.095	-2.857	1:00	0.246	94	108	9.6	2.362	12.0
12/18/09 5:12	0.032	-2.865	1:00	0.241	97	112	7.2	1.738	9.6
12/18/09 6:12	-0.032	-2.923	1:00	0.241	99	116	4.8	1.156	9.6
12/18/09 7:12	-0.085	-2.923	1:00	0.237	102	119	7.2	1.703	7.2
12/18/09 8:12	-0.144	-3.029	1:00	0.240	105	120	7.2	1.731	2.4
12/18/09 9:12	-0.149	-3.021	1:00	0.239	106	121	2.4	0.574	2.4

Selected slides on the freezing test results

**APPENDIX H: LNAPL RECOVERY IN PERMAFROST
FRACTURED BEDROCK AT THE COLOMAC MINE SITE, NWT⁷**

⁷ Paper prepared for submission in Contaminants in Frozen Ground (CFG) conference, May 24 – 28 (2010), Kingston, Ontario

I.1 Introduction

Spills of fuels such as diesel and gasoline from storage tanks onsite are widespread problem leading to subsurface hydrocarbon contamination in mine sites and facilities where onsite fuel storage is crucial for smooth operations. These fuels are subset of light nonaqueous phase liquid (LNAPL) hydrocarbon because they are sparingly soluble in water and have specific gravities below unity. In this report, both diesel and gasoline are collectively referred to as LNAPL with the realization that LNAPL encompasses other petroleum products. According to Weiner (2000), less than 1% of spilled LNAPL are dissolved in the groundwater with the balance remaining as mobile or immobile phases. Consequently, much emphasis is laid on remediating or removing the balance as a precursor to treating the dissolved constituents in the groundwater. For free product hydrocarbon (or free product) to exist, the spilled LNAPL volume must be greater than the retention capacity of the LNAPL in the formation impacted by the spill. The free product constitute perpetual source of contamination in the formation. The immobile LNAPL phase included both trapped and adsorbed product, and contribute to time dependent desorption of hydrocarbon when awash by flowing groundwater. The desorbed concentration may be in excess of regulatory criteria even after recovery of the mobile LNAPL. Thus, it is imperative to remove as much LNAPL as possible from the formation wherever it occurred. The recovery of LNAPL in its different forms in the formation is termed LNAPL recovery, though the term is often used interchangeably with free product recovery.

LNAPL recovery using different remedial technologies such as multi-phase extraction (MPE) systems, petro-bailers, skimmer pumps, excavation, trenches, etc., have various degrees of successes to recover LNAPL from the formation in temperate regions. This paper presents a case study of the use of these remedial technologies at the abandoned Colomac mine site, which is located approximately 220 km northwest of Yellowknife in a discontinuous but widespread permafrost environment, in the Northwest Territories.

I.2 Site description

Colomac mine was an open pit gold mine site that operated between 1990 and 1997. The mine became insolvent in 1999, and subsequently closed and abandoned. Eventually, the site went into receivership by the Federal Government. At present, it is the responsibility of the Contaminants and Remediation Directorate (CARD) of Indian and Northern Affairs Canada (INAC) to clean up the site. Shown in Figure H.1 is the layout of the mine site where most of the fuel spills occurred. The mine site is located in Taiga shield ecozone, which consists of woodland and boreal forest in a discontinuous but widespread permafrost environment within the Indin Lake Supracrustal Belt (ILSB), and adjacent to Steeves Lake (DIAND, 2001; Shelton et al., 2000, Iwakun et al., 2008a). The ILSB contains metavolcanic and metasedimentary rocks subjected to greenschist to amphibolites metamorphism at 2.6 Ga (Morgan, 1990). The site was underlain by sand and gravel fill of varying thickness from zero to 4.6 m, with some peat towards the lake (Iwakun et al., 2010a). Fractured bedrock identified as Greywacke lay beneath the overburden soil at the site (Hearn, 1990; SEACOR, 2007). The upper section (~1.5 m) of the bedrock was highly fractured but competent at depth (> 7 m) with some localized fracturing (Iwakun et al., 2008a; Bickerton et al., 2007, EBA 2001). The fracture pattern of the bedrock was mostly sub-vertical and horizontal. The vertical inclination of the sub-vertical fractures ranged from 5° to 30° and that of the sub-horizontal ranged from 1° to 40° to the horizontal (Iwakun et al., 2010; SEACOR, 2007). Bedrock outcrop showing the fracture pattern at the site is shown in Figure H.2.

Over 50,000 L of spilled fuel occurred at the site between 1990 and 2003 as shown in Figure H.3. The fuel spills were chiefly Arctic diesel (P40 and P50) from leakage of one or more of the nine diesel tanks at the tank farm area, and accidental releases during transportation (via trucks and pipeline). Each of the diesel tanks had a capacity of 4.36 million liters. Other fuel types stored at the site were jet fuel and gasoline but most of the

recorded spills were the arctic diesel (Figure H.4). The diesel tanks were installed in 1989 at the tank farm area (Figure H.1), and removed in the summer of 2004 as part of the reclamation efforts at the site. Though the diesel tanks were placed over gravel fill lined with plastic membrane, compromise of the membrane resulted in subsurface contamination. The two major spills that occurred include 18,000 L in 1990 and 27,300 L in 1997. Both spills occurred in February of the respective years.

After the initial spill in 1990 via blind flange, in one of the diesel storage tanks at the tank farm area, the observed sheen of petroleum hydrocarbon (PHC) along the shoreline of Steeves Lake was approximately 1 km. This implied the liner system beneath the storage tanks at the tank farm had failed and subsurface migration of the spilled fuel had occurred. Different measures were taken after these spills to remediate the site and mitigate further migration of free product downgradient into the lake. Summary of these measures before the aggressive free product recovery efforts and further characterization of the site, which commenced in 2005, are summarized below:

1. Installation of a five-meter deep interceptor trench lined with corrugated pipe at the west berm of the tank farm in late 1990, as indicated in Figure H.4;
2. Placement of a skirted boom with an absorbent pads along the Shoreline of Steeves Lake, as shown in Figure H.4 when PHC sheen was observed in 1990/1991;
3. Site characterization, including installation of monitoring wells across the site, in 2000. The spatial locations of the monitoring wells are shown in Figure H.4;
4. Decommissioning of existing site fuel tanks and replacement of smaller capacity fuel tanks with Enviro Tanks in 2000;
5. Cleaning and demolishing of the main diesel tanks, coupled with purging of the underground piping system in 2004;

6. Replacement of the interceptor trench with a frozen soil barrier in 2004 to contain down-gradient migration of mobile phase PHC; and
7. Removal and biopile treatment of contaminated overburden soil from the tank farm area in 2005.

The continued persistence of free product at the site and continued seepage of free product along the shoreline of Steeves Lake in the summer period, despite these measures, necessitated further site characterization and aggressive recovery of free product at the site since 2005. After the first major spill in 1990, different studies were conducted at the site to understand the subsurface behavior of the spilled fuel, which is complicated by the presence of permafrost, and proffer practical remedial solutions.

I.3 Previous Assessments

Site assessment by O'Connor Associates (1990) using shallow vapor survey and test pit excavation following the initial release of 18000 L in February, 1990, found free product atop shallow water table (<2.2 m from the surface) at the tank farm area within the lowermost soil and uppermost bedrock. From the observed fracture pattern and hydrocarbon staining at the site, a soil and bedrock fracture-controlled groundwater flow system transporting free product to Steeves Lake was inferred.

Site inspection by EBA (1998) involving shallow soil sampling study and walk-over survey found active seepage of free product and surficial soil staining along the shoreline of Steeves Lake. This implied active subsurface movement of free product at the site.

EBA (2001) conducted hydrocarbon assessment at the site, which involved installation of 42 monitoring wells to delineate contamination extent at the site. The study concluded that considerable diesel-like liquid product source existed within the fractured bedrock at the site. The study also recommended a combined remedial strategy of pump-and-treat system and interceptor trench.

Whyte et al. (2001) evaluated the potential for bioremediation of fuel-contaminated soil at the site using microbial enumeration using viable plate counts and MPN analyses combined with molecular analysis (PCR and Colony hybridization) for hydrocarbon catabolic genes. Their study found that the site was amenable to bioremediation at low ambient summer temperatures because of cold-adapted microbes. The study also found that addition of fertilizers would enhance bioremediation of contaminated soils at the site.

Assessment of hydrocarbon product within the fractured bedrock by URS (2002) suggested that little quantity of free product exists within the fractured bedrock at the site because its fracture density is very low and primary porosity is insignificant. Furthermore, URS (2002) suggested that majority of the spilled product are limited to the soil-bedrock interface because the fractures were deemed too small to transmit or store significant amount of hydrocarbon. URS (2002) assumed that any product within the fractured bedrock were held by capillary suction (or tension) and used a computer program, BIOVENT, to prove that the free product at the site was essentially immobile and recovery of the spilled fuel by conventional pumping might not be feasible.

However, the assessment found that elevated concentrations of hydrocarbon existed in the soil at the shoreline of Steeves Lake above the CCME industrial land use guideline values. This implied that active fuel migration in both free and dissolved phase to Steeves Lake was ongoing. Nevertheless, hydrocarbon concentrations of the surface water in the lake were below the CCME guideline for the protection of freshwater aquatic life. URS (2002) opined that majority of the spilled product had migrated along the soil-bedrock interface.

The study by URS (2002) concluded that efficient recovery of free product might not be feasible based on existing technologies, and removal of all hydrocarbon-impacted bedrock was impractical. Thus, efforts should be steered towards the removal of contaminated soil, mitigation of dissolved phase migration by placing reactive barrier downgradient of contaminated

areas, the use of oxygen release compounds (ORC) downgradient of the site to promote biodegradation, and managing ensuing risks from the remedial strategies.

Hydrocarbon cleanup investigation by McNaughton (2002) suggested that attempts at free product recovery would be a “hit or miss” process due to heterogeneity and complex fracture pattern at the site. Furthermore, McNaughton (2002) stated that logistical and technological requirement for efficient free product recovery at the site would be expensive. Despite the complexity of fuel contamination at the site, McNaughton (2002) suggested that a “do nothing approach” was unacceptable because it sends the wrong message to other potential polluters in laying such precedence. The investigation proposed the use of a reactive barrier in addition to the use of ORC to promote biodegradation. Additionally, McNaughton (2002) proposed seeps excavation at the shoreline of Steeves Lake and permanently leaving the absorbent boom at the lake.

Hydrocarbon contamination evaluation by Biogenie (2004) recommended excavation of contaminated soil and biopile treatment to meet residential land use criteria, including the protection of groundwater for aquatic life pathway. In 2004, the Contaminated Site Office (CSO) of INAC adopted the use of interceptor trench or barrier wall for the groundwater treatment along with contaminated soil excavation and bioremediation at the site.

The ineffectiveness of the installed interceptor trench in 2004 in preventing continued migration of both free product and dissolved hydrocarbon plume towards Steeves Lake resulted in a joint study by the Geotechnical Centre at the University of Alberta (U of A) and Environment Canada (EC) in 2005 to characterize the hydrocarbon plume and determine its subsurface behavior at the site.

Tasks performed by the Geotechnical Centre at the University of Alberta in conjunction with Environment Canada included hydraulic tests using sets of packers, installation of additional monitoring wells (MWs) and

monitoring of depths to free product, water table, and bottom ice. Other concluded tasks involved installation of thermistor strings and monitoring thermal profile at the site, groundwater sampling, bedrock coring, borehole imaging, and free product recovery. These activities were discussed by Iwakun et al. (2008a, and 2010a), Bickerton et al. (2007), and Iwakun and Biggar (2007).

The study showed that significant free product exists at the northern part of the tank farm area around MW 12 and 26 and fuel contamination had penetrated the upper section (~ 7 m) of the fractured bedrock (Iwakun et al., 2008a; 2010a). Free product increased in MWs at the commencement of winter period at the tank farm area where most of the fuel spill occurred, and correlated inversely with the water table elevation and thermal profile at the site at 95% confidence limit (Iwakun et al. 2008b). The identified key mechanisms influencing migration of free product at the site were water table fluctuations and freezing induced displacements (Iwakun et al., 2008b; 2010a; and 2010b).

Iwakun and Biggar (2007) showed that efficient recovery of free product by the sole use of skimmer pump might not be feasible due to slow recharge of free product in the MWs after purging. The slow recharge of the free product in the MWs was due to natural discontinuity of the identified mechanisms contributing to its migration and accumulation. Furthermore, the study showed that active layer of thermal fluctuation was as deep as 15 m below the surface (Figure H.5) and the water table was as low as 13 m below the ground table in the winter period. As such, significant penetration and lateral migration of the spilled fuel into the bedrock have occurred at the site. The study explained that the ineffectiveness of the previously installed frozen core interceptor trench in 2004 was due to its placement within the active layer of both thermal and groundwater fluctuation, thus, not deep enough. The interceptor trench placed in 2004 was 5 m deep due to misconception that permafrost table was 4 m below the surface. Iwakun and Biggar (2008c) suggested that successful removal of free product at the site

might involve a combination of water table fluctuation, manipulation of formation temperature, use of surfactants, hydraulic gradient control, pumping from sump monitoring well, and volatile organic capture and treatment.

As a result of this characterization efforts and findings, Jacques Whitford AXYS Ltd. (JWA) was engaged by CARD to manage free product recovery efforts and petroleum impacted soil at the site among other objectives in 2007. To this end, JWA proposed and implemented different pilot scale studies involving different methods at the site.

I.4 Methodology

The methods employed for the LNAPL recovery efforts included the use of petro-bailers, single well multi-phase extraction (MPE) system, recovery trench, and blasting and excavation of the most impacted area of the site. Prior to the use of the MPE system north of the tank farm area, additional monitoring wells were installed at the site. Shown in Figure H.4 are the locations of the newly installed MWs and the excavated trench.

Petro-bailers were deployed in MWs P5, 15, 17, 21, and 44. Prior to the deployment of these petro-bailers, the conventional bailers were used to recover free product from the MWs across the site. Petro-bailer is a modified bailer with a hydrophobic filter intake at the upper end of the bailer, which serves as passive skimmer, and a weight at the bottom-tip to keep it submerged up to the hydrophobic filter section. The device is designed to accommodate fluctuations in water table.

A self-powered enhanced free product recovery (EFR) unit was used as an MPE system at the site. Shown in Figure H.6 is a typical layout of the EFR unit. MPE system is a modified soil vapor extraction (SVE) unit combined with a pump and treat system (USACE, 1999). It is designed to extract both free and dissolved phases of contaminants in addition to the removal of vapor phase and groundwater from the formation. The test involved recovery of air, hydrocarbon vapors, LNAPL, and groundwater,

using a 2-hp rotary lobe pump with an inlet air-liquid separator (JWA, 2009a; JWA, 2009b). Suction-pipe depths used during vacuuming process ranged from zero to 200 cm, below the water table in the MWs. The tested MWs were 15, 30, 40, 43, and 44 (Figure H.4). North of the tank farm around MWs 43 and 44, additional shallow (depth ~ 9 m) MWs were installed prior to deploying the EFR unit to test the radius of influence of the vacuum applied through the EFR unit.

A 4500 L holding tank at the back of the truck used for hauling the EFR unit served as temporary storage for extracted free product and water from the MWs. The mixture of the free product and water were transferred to an oil/water separator onsite. The recovered oil from the separator was put in a container for later use in the waste oil furnace onsite, while the groundwater was discharged at the site after treatment with an activated carbon. During the system operation, the hydrocarbon vapor concentrations, fluid recovery rates, liquid levels in MWs, and vacuum, were monitored. Furthermore, since the EFR system was designed to maximize recovery of free product at the site, the vapors generated through the system operation were discharged directly to the atmosphere.

In 2008, JWA installed a recovery trench up to 15 m below the ground surface by blasting and excavating the formation at the northern end of the tank farm area where considerable free product persists. Shown in Figure H.4 and Figure H.7 are the location and profile of the recovery trench. Before the installation of recovery wells in the trench, pooled hydrocarbon and water in the trench were pumped out to an aboveground treatment unit using a combination of vacuum trunk and rotary pump. Installation of the trench involved removal of approximately 726 m³ of overburden soil of which approximately 60% was deemed contaminated above 5000 mg/Kg from site screening. Then, two lift of depths 3 - 5 were blasted into the bedrock followed by a 7 m deep lift such that the final depth of the trench was 9 - 12 m below the bedrock surface and approximately 15 m from the ground surface at its deepest point (JWA, 2009b).

Prior to the installation of the recovery trench described above, a test involving evaluation of free product recharge in response to decrease in groundwater level was performed in MW 26. The test involved pumping of water at 8 m below the groundwater level at 0.625 L/min to create a cone of depression in the MW (with a total drawdown of 4m), and subsequent monitoring of accumulated free product in the MW resulting from lowering the groundwater level. Purged water from MW 26 was injected into nearby MW 42 northeast of it.

I.5 Results and Discussions

The use of conventional bailers and petro-bailers were effective in removing accumulated free product in the MWs across the site. However, low recharge of free product after bailing due to discontinuity of key mechanisms aiding LNAPL migration at the site as discussed by Iwakun et al. (2008b, and 2010a) limited their effectiveness. At the commencement of the winter period when free product accumulates atop frozen layer of ice on the water table in the MWs, petro-bailers are ineffective in removing free product like conventional bailers with bottom intake. Pumping test performed in MW 26 to evaluate LNAPL response to lowering the water table showed an increase in free product thickness from 197 mm to 465 mm during the six hours pumping period in the MW. This corroborated the findings by Iwakun et al. (2010a) that engineered fluctuation of the water table may enhance free product recovery at the site. This also showed that groundwater recharge caused remobilization of free product at the site as evidenced by the observed seepage of free product at the shoreline of Steeves Lake during the summer period in response to precipitation events. Additional 10 mm free product accumulated overnight when the MW was left overnight (~ 13 hrs).

Shown in Table H.1 are summary results from different configurations of the MPE system at the site. The MPE system was successful in recovering free product from the formation via hydraulic control of the groundwater, but inefficient in generating significant vacuum from the formation in all the

MWs tested. The reasons for the inefficient vacuum generation were due to the fracture pattern and slacked casing seal into the bedrock. Generally, the installed steel casings in all the MWs extended up to 1.5 m into the bedrock with a bentonite seal. The strains induced by blasting and excavation operations at the site might have loosened the casings. Additionally, the fracture pattern at the site is complex, and characterized by sub horizontal and vertical fractures. Thus, exposure of any of the interconnected fractures adjoining a MW to the atmosphere would result in the inability of vacuum to be generated from the formation in the MW. At the shoreline of Steeves Lake, the MWs produced higher yield of free product (e.g., MW 30 yielded approximately 111 L of free product in 2.3 hrs). Overall, approximately 804 L of free product were recovered from the MWs using the MPE system in combination with the bailers between 2007 and 2009 over the testing period.

The recovery trench yielded significant amount of free product at depths below 8 m from the ground surface. Approximately 5 cm of free product were recovered over an area of 64 m², amounting to 3200 L of free product. Significant volume of water of approximately 59,000 gallons, from two dewatering operations in September and October 2008, was removed from the formation. This was necessary in order to achieve the desired excavation depth of 15 m below the ground surface. The depth to water table at the start of excavation in August of 2008 was approximately 8 m below the ground surface. During the dewatering of 48,000 gallons in October 2008, approximately 0.15 m of ice had formed atop the water surface with approximately 3 cm of free product atop it (Figure H.8). This suggests that freezing process also played a role in mobilizing free product at the site as indicated by Iwakun et al. (2010a; 2010b). Other excavations around the warehouse in 2009 resulted in the recovery of over 700 L of LNAPL. The full report on these other excavation works are pending.

Between 2004 and 2007, approximately 1000 L of free product were recovered from the MWs using conventional bailers and pumps.

Furthermore, there appeared to be significant LNAPL trapped within the soil and bedrock matrix at the site. From site screening and the removal of approximately 726 m³ overburden soil during installation of the recovery trench, an estimated 3872 L of LNAPL was recovered from the soil. The LNAPL stains in the excavated rock were not accounted for because of the difficulty in estimating the concentration of total petroleum hydrocarbon in the rock matrix. All excavated soil and rock that were contaminated were transferred to the land treatment unit at the site. Shown in Table H.2 is the summary of LNAPL recovered from the MWs, recovery trench, and excavated soil from the recovery trench. Overall, over 8,000 L of LNAPL were recovered at the site from the use of bailers, MPE system, recovery trench, and other excavations since 2007. Because of these aggressive measures, the load of LNAPL in the formation has decreased significantly (e.g., over 16% of initial spilled fuel reduction). However, further assessment by JWA (2009c) showed that LNAPL persists at the site in both mobile and immobile phases.

I.6 Conclusions

A combination of remedial systems at the Colomac mine site, where spill of over 50,000 L of LNAPL occurred mostly as diesel and gasoline, resulted in the recovery of over 8,000 L of LNAPL including approximately 4,000 L of free product. The remedial scheme deployed at the site included recovery trench in combination with single well MPE system, bailers, and excavation of impacted soil. The findings showed that free product recovery through engineered fluctuation of the water table or hydraulic control was effective at the site. Additionally, the findings indicated that a significant portion of the spilled LNAPL in the formation was immobilized in the soil and rock matrixes. This is evidenced by the fact that excavation of the impacted soil alone accounted for over 50% of recovered LNAPL from the recovery trench only.

The MPE system showed significant promise in recovering free product at the site especially along the shoreline of Steeves Lake where over

110 L of free product were recovered in less than three hours in one of the monitoring wells. Petro-bailers and conventional bailers were only effective in removing accumulated free product in the MWs but limited by the very low recharge of free product after bailing. The seasonal nature of the identified key mechanisms (i.e., water table fluctuation and freezing induced processes) aiding LNAPL movement at the site contributed to its low recharge after bailing. The hydraulic control capability of the MPE system made it particularly effective at the site.

Furthermore, the recovery trench was the most effective measure in recovering LNAPL at the site. Approximately 3,200 L of free product were recovered from the recovery trench in less than two months, and an additional 3,872 L of LNAPL were removed due to the excavation of the contaminated soil. Despite the success achieved in recovering LNAPL at the site, significant LNAPL persists. It is impractical to remove all subsurface LNAPL contamination by such active measures. Thus, the remediation objectives at this site consist of removing LNAPL to its feasible extent from the formation, and reliance on natural attenuation for the remediation of those remaining, which might take a number of years to achieve remedial goal.

Table H.1 Summary of results from the multi-phase extraction (MPE) system (modified after JWA, 2009b).

Monitoring well	40	40	40	30	30	15	43	43
Suction tube depth below the groundwater level (m)	0.0	1.0	2.0	0.3	0.3	0.3	0.0	0.5 - 1.0
Vacuum (inch of water)	0	75	75	3	13	20	0	0
Hydraulic flow (lpm)	2	4.5 - 1.9	3.2 - 2.4	2.2	2.5	6	0.25	1.25 - 3.0
Pneumatic flow (cfm)	0	20 - 30	20 - 30	20	20	5 - 7	∞	∞
Hydraulic influence (m)	15 - 20	20	15 - 20	0	0	0	0	25
Pneumatic influence (m)	0	0	0	0	0	0	0	0
Free product recovery rate (mLpm)	0	16.2	24.3	800	800	120	30	0
Note: mLpm - milliliter per minute ∞ - infinity cfm - cubic feet per minute								

Table H.2 Summary of LNAPL recovered at the Colomac mine site from 2007 to 2009.

Type	LNAPL recovered (L)
Monitoring wells	804
Recovery trench	3200
Excavated soil from recovery trench*	3872
Excavation east of workshop	600
Excavation south of workshop	120
Total (L)	8596
* The reported value was estimated from the following: 1 Excavated volume = 726 m ³ 2 Ratio of contaminated volume from screening = 0.6 3 Density of solids = 1,600 kg/m ³ (assumed) 4 Average concentration of total petroleum hydrocarbon in the contaminated soil based on previous screening = 5,000 mg/kg 5 Average density of hydrocarbon = 0.9 kg/L 6 Total mass of petroleum hydrocarbon in soil = (726 x 0.6 x 1600 x 5000) / (0.9 x 1000000 mg/kg) = 3872 L	



Figure H.1 Layout of the Colomac mine site before demolition of the structure during reclamation.



Figure H.2 Bedrock outcrop and escarpment showing (1) sub-vertical fractures parallel to foliation, (2) sub-horizontal fractures, and (3) sub vertical fractures parallel to 1 and 2.

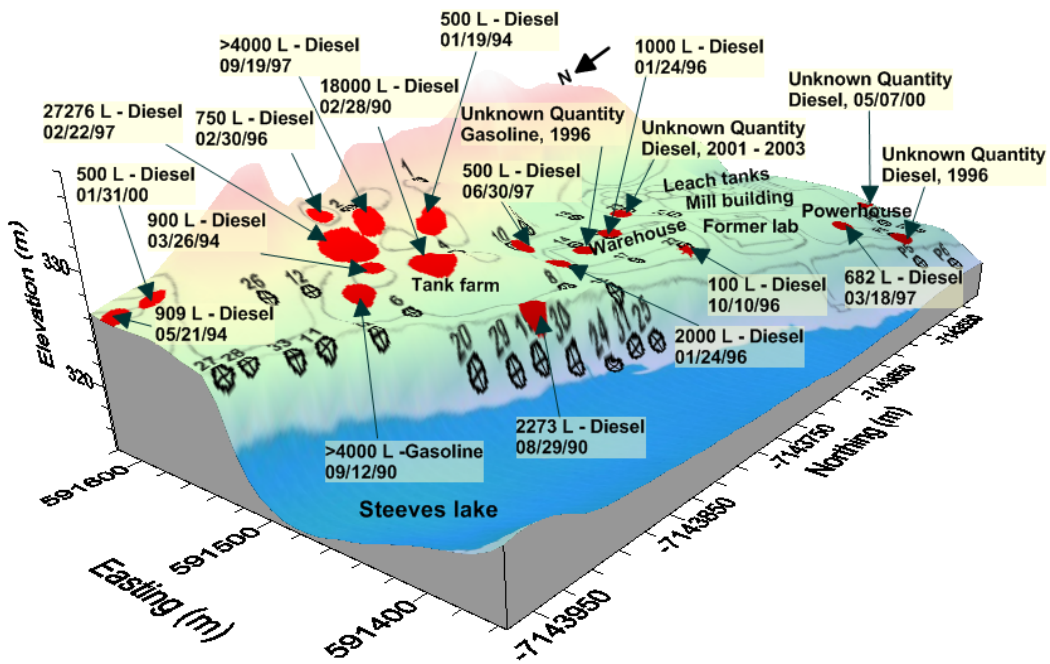


Figure H.3 Spill history at the Colomac mine site showing the date, spill quantity and type, and relative locations.

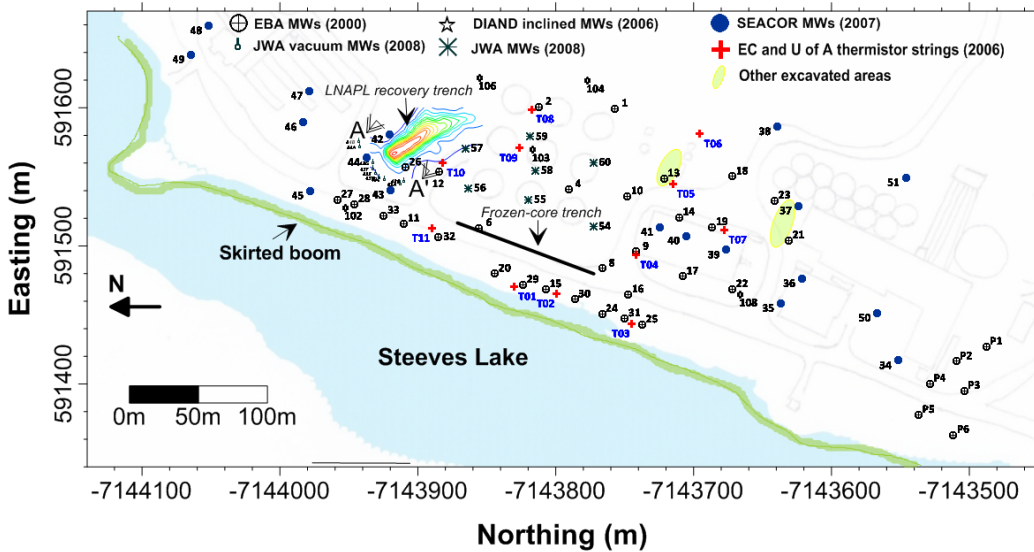


Figure H.4 Synthesized site plan showing the approximate locations of the monitoring wells (MWs), remedial measures, and installed thermistor string.

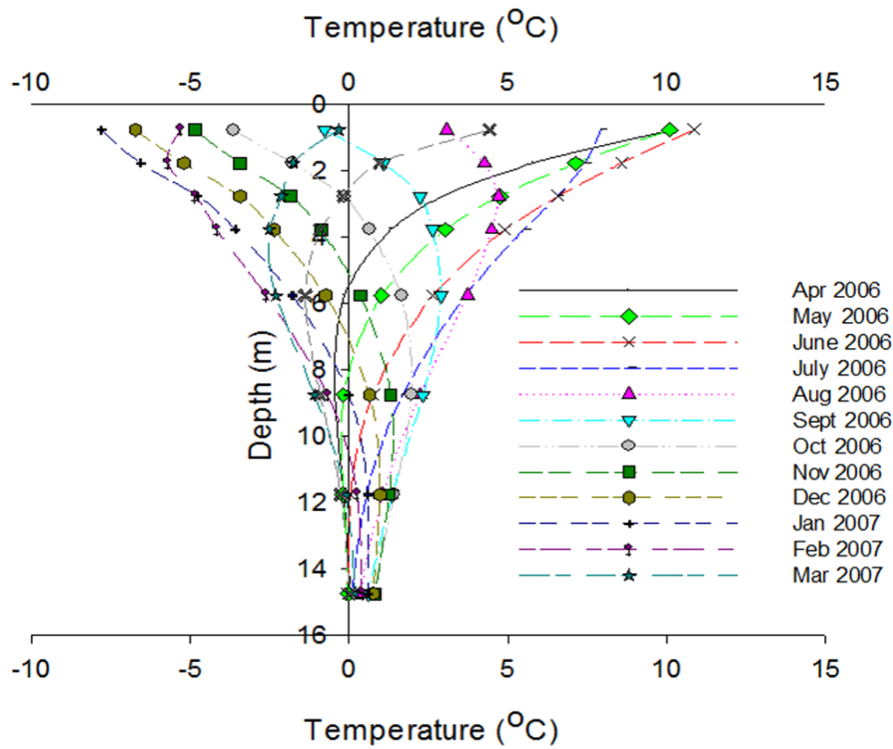


Figure H.5 Temperature profile with depth in MW 12 north of the tank farm where higher yield of free product persists.

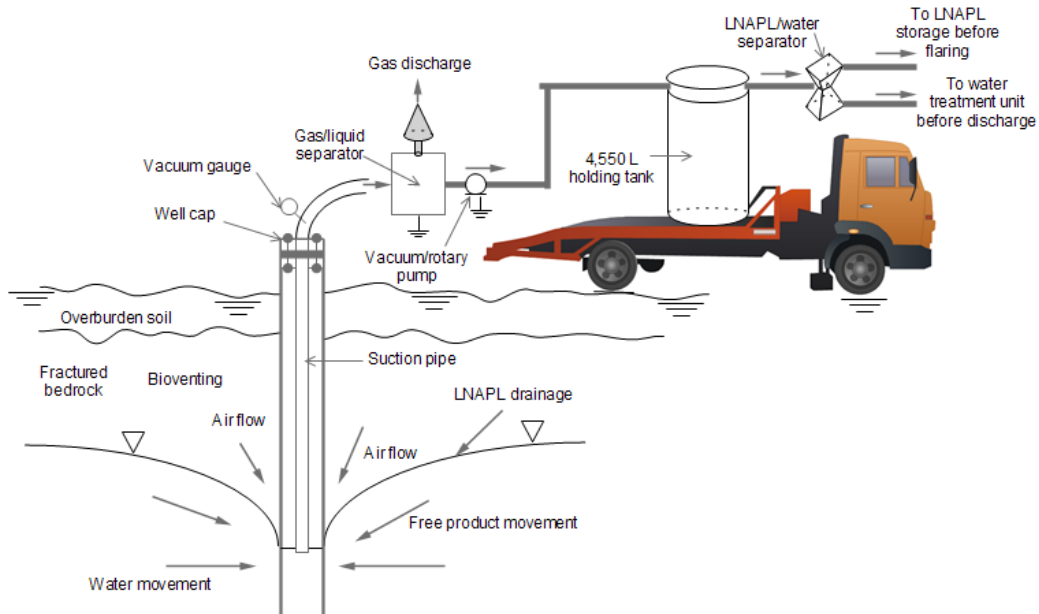


Figure H.6 Conceptual diagram of the layout of the deployed multi-phase extraction (MPE) system at Colomac mine site.

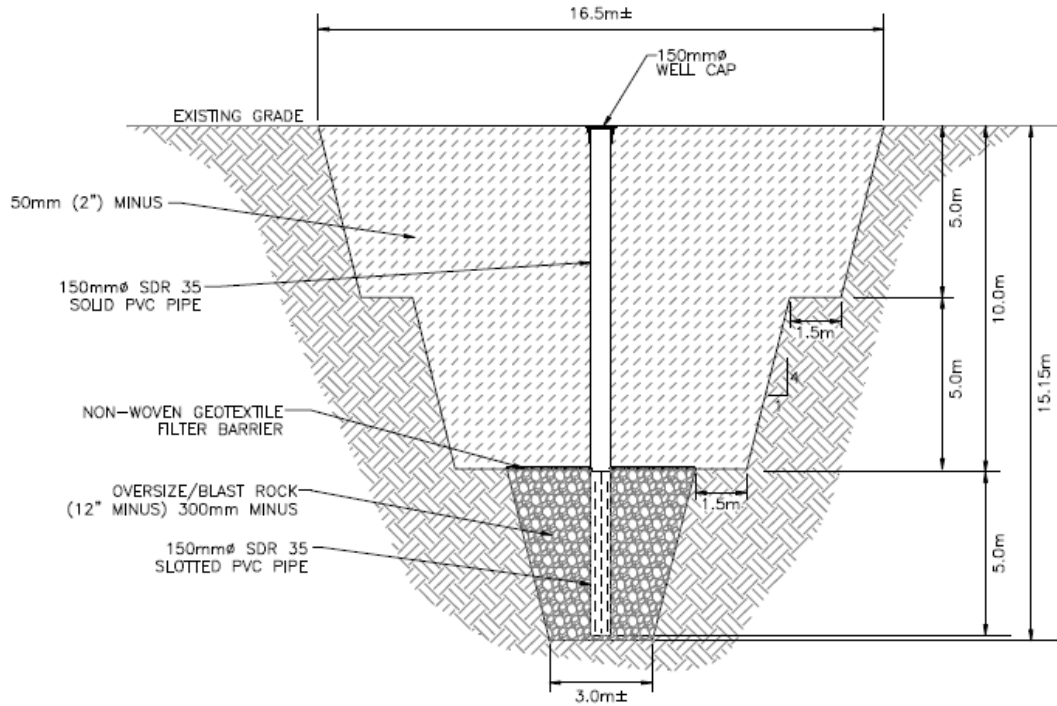


Figure H.7 Profile of the backfilled recovery trench through section A-A' (Figure 4) at the site (after JWA, 2009b).



Figure H.8 Northwest view of the recovery trench showing free product accumulation on ice (modified after JWA, 2009b).

References

- Bickerton, G., Van Stempvoort, D.R., Voralek, J., Biggar, K., 2007. Hydrocarbon setting of petroleum contamination at Colomac mine, NWT: A permafrost region of the Canadian Shield. Proceedings of the 60th Canadian Geotechnical Conference and the 8th Joint CGS/IAH-CNC Groundwater Conference, Ottawa.
- Biogenie S.R.D.C. Inc., 2004. Hydrocarbon contamination management. Phase I report – proposed remedial action plan. Report for Tli Cho Logistics and Northern Affairs Canada. 47 p. + appendices.
- DIAND - Department of Indian Affairs and Northern Development, 2001. Colomac mine abandonment and restoration plan, Department of Public Works AND Government Affairs, Canada. 551 p.
- EBA - Engineering Consultants Ltd., 2001. Hydrocarbon assessment, Lakefront and waste oil areas, Colomac Mine, NWT. Report to Deton 'Cho Corporation. Yellowknife, NT. 37 p. and appendices.
- EBA - Engineering Consultants Ltd., September 1998. Hydrocarbon Contamination Inspection Report, Diesel Tank Farm, Colomac Mine Site. Project 0701-9813465, report to Royal Oak Mines Inc., issued in draft only.
- Hearn, K., 1990. The Colomac deposit. Geological Survey of Canada Open File Report 2168, pp. 84–89.
- Iwakun, O., Biggar, K., 2007. Behavior of spilled petroleum hydrocarbon at Colomac mine site, NWT. Proceedings of the 60th Canadian Geotechnical Conference and the 8th Joint CGS/IAH-CNC Groundwater Conference, Ottawa, pp 2106-2114.
- Iwakun, O., Biggar, K., 2008c. Characterization of Fuel Spill Plumes in Fractured Rock at a Permafrost Site: Colomac Mine, NWT. Progress report submitted to Indian and Northern Affairs Commission (INAC), Yellowknife.
- Iwakun, O., Biggar, K., Segó, D., 2008b. Influence of temperature and groundwater fluctuation on LNAPL migration at Colomac mine site.

- Proceedings of Ninth international conference on permafrost, edited by Kaine, D. L., and Hinkel, K. M., 1:815-820.
- Iwakun, O., Biggar, K., Van Stempvoort, D., Bickerton, G., Voralek, J., 2008a. Fuel contamination characterization in permafrost fractured bedrock at the Colomac mine site, NWT. *Cold Regions Science and Technology*, 53(1):56-74.
- Iwakun, O., Biggar, K.W., Segó, D., 2010a. Estimation of actual LNAPL thickness in a fuel-contaminated mine site. *Cold Regions Science and Technology*, 60:212-220.
- Iwakun, O., Biggar, K.W., Segó, D., 2010b. Influence of cyclic freeze-thaw on the mobilization of LNAPL and soluble oil in a porous media. Submitted manuscript under revision in *Cold Regions Science and Technology*.
- Jacques Whitford AXYS Ltd., 2008. Management of remedial activities and free product hydrocarbon recovery: Colomac mine site. A summary report submitted to the Department of Indian Affairs and Northern Development, Contaminant and Remediation Directorate, Yellowknife, NWT. 590 p.
- Jacques Whitford AXYS Ltd., 2009a. Conceptual Design for hydrocarbon product remediation, Colomac mine, NT. Final report submitted to Indian and Northern Affairs Canada. Project no. 1027392.02. Yellowknife, 62 p.
- Jacques Whitford AXYS Ltd., 2009b. Multi phase extraction system pilot test report. Submitted to Indian and Northern Affairs Canada. Project no. 1027392.02. Yellowknife. 64 p.
- Jacques Whitford AXYS Ltd., 2009c. Management of remedial activities and free product hydrocarbon recovery: Colomac mine site. A summary report Submitted to the Department of Indian Affairs and Northern Development, Contaminant and Remediation Directorate, Yellowknife, NWT. 578 p.

- McNaughton, D. C., 2002. Colomac mine hydrocarbon cleanup Investigation options. A report submitted to Public Works and Government Services Canada. 7 p.
- Morgan, J., 1990. Gold deposits in the Indin Lake Supracrustal Belt. Geological Survey of Canada, Open File Report 2168, pp. 67– 83.
- O'Connor Associates, 1990; Petroleum leak at tank farm, Steeves Lake, Colomac Mine, NWT; Report to Colomac Mine Manager; October, 1990.
- SEACOR Environmental Inc., 2007. Environmental investigations of former Colomac mine, Draft report submitted to the Department of Indian Affairs and Northern Development (DIAND) Canada, Yellowknife, 115 p.
- Shelton, K. L., Costello, C. S., van Hees, E. H., 2000. Contrasting styles of Archaean greenstone gold deposition: Colomac gold mine, Canadian Northwest Territories. *Journal of geochemical exploration*, 69 – 70, pp. 303 – 307.
- URS Norecol Dames and Moore Inc., 2002. Assessment of hydrocarbons within fractured bedrock at the lakefront and waste oil areas and development of a remedial action plan, Colomac Mine, NWT. Report for Public Works & Government Services Canada. Vancouver, BC., 21 p. and appendices.
- USACE – US Army Corps of Engineer, 1999. Multi-phase extraction system, Engineer Manual, EM 110-1-4010. 286 P.
- Weiner, E. R., 2000. *Applications of environmental chemistry: A practical guide for environmental professionals*. CRC press LLC, Florida.
- Whyte, L.G., Dagenais, J., Labbe, D., Greer, C.W., 2001. Bioremediation treatability assessment of hydrocarbon contaminated soil from a NWT mine. National Research Council – Biotechnology Research Institute, submitted to Public Works and Government Services Canada. 18 p.